ProQuest LLC.
789 East Eisenhower Parkway
P.O. Box 1346
Ann Arbor, MI 48106 – 1346

An investigation into improving weld strengths during spot welding

Aravinthan Arumugam

A thesis submitted in partial fulfillment of the requirement of
The Nottingham Trent University for the degree of
Doctor of Philosophy

March 2003

ABSTRACT

Spot welding is a process that is widely used in industries worldwide. This project aims to research and develop a control system to improve the strengths of the spot welds. Conventional (pneumatic) spot welding systems do not lend themselves towards in-process control specifically controlling the forging force during welding. The importance of the forging force is that it is related to the dynamic resistance and hence to the rate of heating of the weld as has been shown in this work. The use of the forging force to control weld strengths was investigated by converting the electrode actuating system of a pneumatic spot welder to a motor driven servo system. This enabled the electrode forging force to be varied during welding. The control system was used to vary the forging force during welding by means of various preset force profiles in order to vary the heating during welding. The effects of the various force profiles to heat generation and weld growth were studied by using the dynamic resistance curve. The relationship between resistance and force enables the dynamic resistance to be used as an indicator for weld performance. Experiments were carried out to propose the force profile that will give the highest weld strength. Results obtained from this project shows that two changes in the characteristics of the force profile, viz, the delay time before ramping and the rate of ramping, affects the amount of heat supplied to the weld during welding which causes change in the weld strength. Statistically significant differences between average weld strengths due to the changes in these characteristics are presented. Forging force control was also found to produce stronger welds compared to the conventional electrode clamping force (ECF) condition, which was found to be statistically significant. It was also found possible to extend the weld lobe region of the electrode clamping force (ECF) condition by using forging force control, to produce improved weld strengths at the no weld and expulsion regions of the lobe. The profile that starts with a lower force and ends with a higher force with a longer ramping delay and slower ramping rate was the profile that produces the strongest weld strength among all the profiles tested. This profile with a welding current below the expulsion limit was suggested as the strategy to produce stronger welds at a faster rate.

Acknowledgement

The research presented in this thesis has occupied a very important part of my life and it wouldn't have been possible without the help of many people. Firstly I would like to thank my parents, who had supported and motivated me through the duration of this work. My heart full thanks goes to my supervisors Dr.K.Sivayoganathan, Dr.D.Al-Dabass and Dr.V.Balendran who had helped me a lot during the period of this project and also the time when I was writing this thesis. The time and contribution that they had put in to make this project successful even with their busy schedule are much appreciated. Special thanks to Dr.K.Sivayoganathan for teaching me what is research is all about. I am also greatful to all my friends especially Dr.Murugesan Sethu, Sureshkumar, Tan Chee Khoon and Kevin Davies for their help and support. Thanks guys!

Among the many people involved with the research work, I would like to thank in particular:

- All the members of the technical staff such as Mr. Jez Keeling, Mr. Rob Potter, Mr. Ralph James, Mr. Alan Tye and Miss Judith Keepling whom had helped me a lot during the period of this project
- Mr and Mrs. Corlett for all issues related with the availability of research materials
- Mr John Stanway of British Federal Ltd, Dudley for his contribution in proposing the idea of the carried out research

Table of contents

List of figures

List of Tables

Chapter 1

INTRODUCTION

1.1 The problem

Welding is a process in which materials of the same fundamental type or class are brought together and caused to join through the formation of chemical bonds under the combined action of heat and pressure (Messler 1993). The context material in this report refers to metals even though the welding is being used for certain polymers and ceramics. Looking around, it could be noticed that almost all metal components would have undergone some type of welding process besides mechanical attachment and fastenings. Some of the commonly used welding processes are arc welding, tungsten-inert-gas (TIG) welding, metallic-inert-gas (MIG), spot welding, soldering and laser welding.

This research project concentrates on a specific welding process; namely resistance spot welding (RSW). This process is widely used in sheet metal joining processes due to its inherent advantages of high speed, suitability for automation and inclusion in high-production rate assembly lines (Chang & Cho 1990). In spite of its simplicity, resistance spot welding is a complex thermo-physical process involving interactions between mechanical, electrical, thermal and metallurgical phenomena (Chang & Cho 1990). One of the major problems faced for many years by industries involving the spot welding process is maintaining the consistency of the weld strength after a certain amount of production time.

Weld strength was found to change due to improper control of the welding parameters and inherent process variations such as electrode deformation and wear, work-piece surface contamination and coating and poor fit-up of work-piece (Arumugam 2000). Any or all of these reduce weld strength, demand production of more welds than are needed and increase in production cost.

Due to the above-mentioned problems, various studies had been carried by many researchers to get an in-depth understanding of the resistance spot welding and how the inherent process parameters and variations can affect weld strength. Further researches were also carried on finding ways to minimize or eliminate these errors and variations by means of stringent control of the parameters.

1.2 The Research

The studies carried out on the resistance spot welding can be divided into 3 main areas: -

1.2.1 Weld development and welding parameters

Weld development was pointed out to be a function of sheet thickness, welding current and weld time (Gould 1987). Experiments to understand the shape of the welding lobe by measuring the static and dynamic resistance showed that current and resistance change continuously during the heating and melting of materials (Dickinson 1981). Study on the effect of electrode deformation on weld strength suggested that welding schedule with higher current and shorter time is the most appropriate schedule to give a lower electrode deformation and higher strength (Arumugam 2000). All the above stated studies were carried out on the welding parameters and the knowledge on the effect of the parameters to weld properties were obtained.

1.2.2 Modelling of the welding process

Some researchers used numerical and finite element modelling to study the spot welding process. Most researchers developed a two-dimensional axisymmetric model of the electrodes and sheet metal as shown in figure 1.1. Two different meshes were used in the model i.e. finer meshes at the end of the electrode and work piece (region of interest) and coarser meshes at the upper region of the electrode. Sufficiently refined meshes were used at the region of interest for the determination of the temperature and stress at that region. Because of the heat conduction to the water-cooling channel at the upper region of the electrode, coarser meshes were used without

sacrificing solution accuracy. Joule heating will be included in this model to study the weld development during the process (Archer 1960)(Greenwood 1961). Another model was developed which took into account temperature dependent material properties, energy generation due to joule heating and contact resistance at the sheet interface (Funk & Rice 1967). Further improved

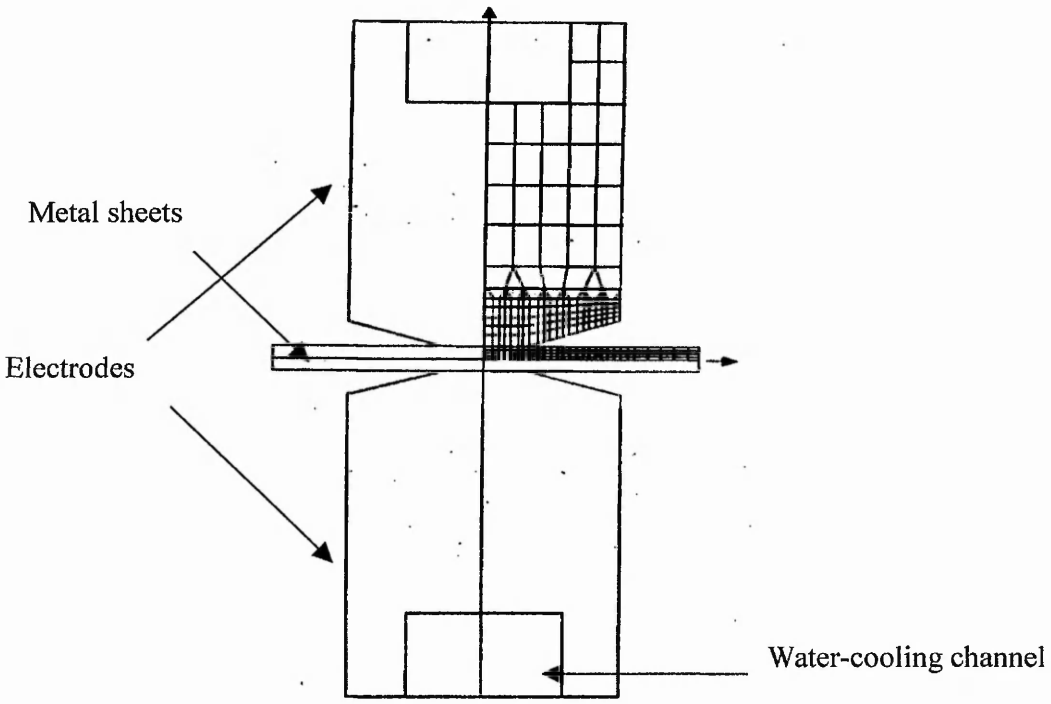

Figure 1.1 – Resistance spot welding axisymmetric model

models were developed which took into account electrode geometry and latent heat of fusion (melting) (Gould 1987)(Nied 1984). The latest work shows the development of a 3-D finite difference electrical-thermal model for joints with dissimilar materials (mild steel and stainless steel) (Chunsheng et al. 2002). This model also took into account the contact resistance, heat generation, latent heat of fusion (melting) and the temperature dependent material properties for both mild steel and stainless steel. These models were used for thermal analysis that provides the temperature distributions showing the characteristic isotherms of an elliptical shaped weld. Through these models the weld diameter, weld penetration and heat generation for certain welding parameters that consists of current, time, force and electrode diameter can be predicted (Gupta & Amitava 1998).

Since spot welding is a non-linear process and consists of a number of parameters, developing r eliable mathematical models to control the weld strength was not possible. Most models include some assumptions that simplify the complexity of the process and that may be adjusted to fit the model to the actual welding data. Therefore these models are more suited for off-line simulations than an on-line estimation and control (Zhongdian et al. 1997). In order to control weld strength, all the variations during welding process need to be identified and controlled on-line at real-time rather than depending on some developed models. With this aim, many researchers ventured into the field of developing control systems for the spot welding process.

1.2.3 Application of control systems in the spot welding process

The importance of controls for resistance welding was brought to the attention of the industry with the announcement of a new $13.6 million research Advance Technology Program (ATP) from the National Institute of Standards and Technology (NIST) (Irving 1996). Irving also reported that resistance-welding controls are a $1.1 billion-per-year industry. Most welding controllers have weld monitoring techniques based on measurable process parameters such as electrode displacement caused by thermal expansion arising from weld formation, electrical signal derived from the welding current and voltage waveform and acoustic emission or ultrasonic signal (Brown et al. 1998). Artificial neural networks (ANN), fuzzy logic, proportional-integral-derivative (PID) algorithms and adaptive systems have been used for monitoring and control of spot welding.

A microprocessor based control system using proportional plus integral (PI) control algorithm was developed (Chang et al. 1989). This controller was used to compensate the variation in weld strength due to electrode wear by means of tracking a desired electrode movement curve. A similar microprocessor based electrode movement controller using just the proportional algorithm was also developed to control the weld expansion (Cho & Chun 1985). In both these controllers, the signal generated by the control algorithm was used to drive the silicon-

controlled-rectifier (SCR) in order to control the welding current. An adaptive control system was developed using the same electrode displacement tracking method as both the controllers above (Haefner et al. 1991). However in this adaptive control system, the gains are changed in real time depending on the process variations unlike both the P and PI based controllers where the gains are preset. Messler (1996) reported that none of these systems was adequate for most production environments due to their limitations. Firstly each controller can only be used for a specific weld joint and becomes useless when the material type or joint geometry is changed. Secondly the affect of electrode force to displacement curve was not considered in these systems.

A back propagation neural network with heat and time as the inputs and electrode displacement as the output was developed (Jou et al. 1998). The output signal from the neural network is then fed into a fuzzy controller to control the thyristor-firing angle to adjust the heat supplied to the weld to produce good welds. Another back propagation neural network with dynamic resistance as input and weld diameter as the output of the network was developed, to predict weld diameter based on changes in dynamic resistance (Brown et al. 1998). A fuzzy controller was developed to produce current reference model based on dynamic resistance as the input. Change in dynamic resistance was studied and inference rule was developed to produce current reference model (Chen et al. 1998). Most of the work using ANN was purely for process monitoring rather than process controlling. All developed back propagation neural network as shown in figure 1.2 or auto-associative neural network use either dynamic resistance curves or electrode displacement as the inputs to the network and weld diameter and weld strength as the outputs of the network. The networks were trained with various training patterns and tested with a number test patterns in order to evaluate weld strength on-line (Javed & Sanders 1991)(Zhongdian et al. 1997)(Li et al. 2000)(Sohn & Bae 2000)(Dilthey & Dickersbach 1999)(Xihua et al. 1998).

As discussed above, all the controllers developed use the welding current as the control parameter in order to control weld strength based on either electrode displacement or dynamic resistance curves. The secondary current is controlled by controlling the firing angle of the silicon-controlled-rectifier (SCR), which is in the primary circuit of the welding machine (Stanway 1992). The electrode force is another important parameter that is often neglected as a

control parameter (Hirsch 1993). That is because all the above-mentioned studies were carried out on spot welding machines, which were actuated using pneumatic systems. The open-loop characteristic of the pneumatic cylinder means that the electrode force could not be used as a control parameter (Slavick 1999). Mechanical pressure switch, differential pressure transducers and electronic air regulators have been used to create a closed loop for electrode force control (Hirsch 1993). But the high inertia and friction in the pneumatic cylinder causes electrodes could not be controlled at faster speed to follow weld expansion therefore causing expulsion to occur (Arasuna 1999). Thus in order to apply the electrode force as another control parameter, the system used to apply the electrode force needs to be converted into a closed loop system and the electrodes should be controlled at high speed.

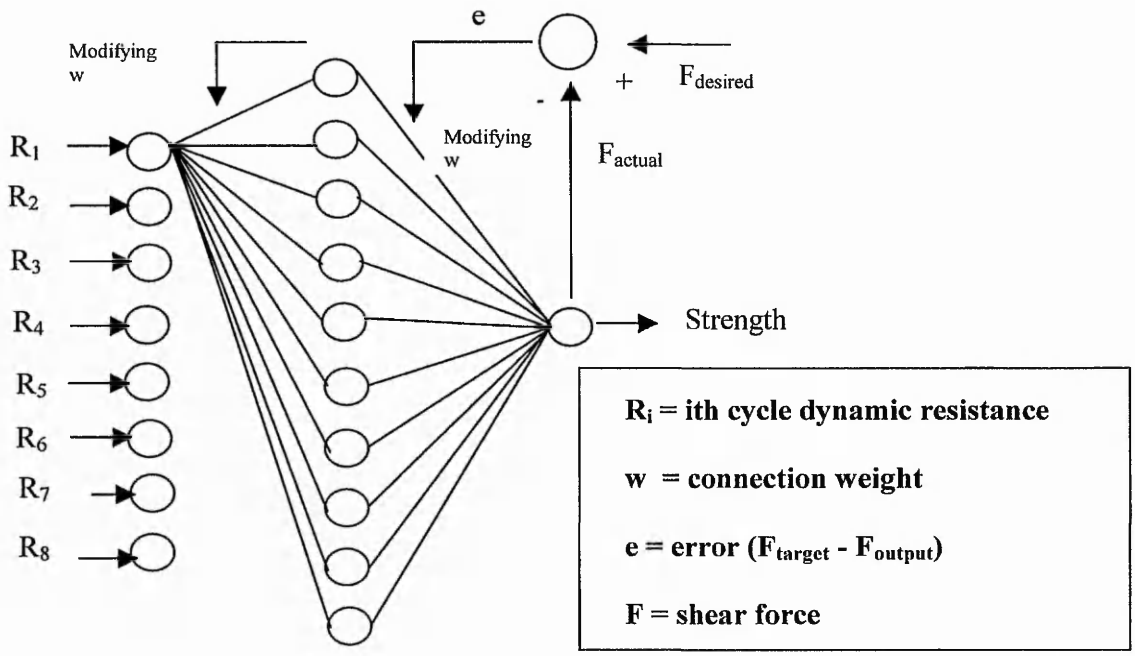

Figure 1.2 – Back propagation architecture

Figure 1.2 shows only one neuron connection for clarity. All the other neurons have a similar connection to connect the input neuron to the output neuron.

1.3 The Proposed Research

Since this project was initiated with the interest to solve the problem faced by the industries in controlling weld strength on-line, the area of developing a controller for the spot welding process was chosen as the area of interest. The literature review above shows that most work has been carried out on the monitoring of the spot welding process while only a small number of papers have concentrated on the control of the spot welding process. Also, all the control systems developed so far are based on current control and there are no indications on work done so far on the control of forging force during welding in real-time to control weld expansion.

In this research, a prototype model of a servo controlled spot welding machine will be developed where the electrode force will be actuated electrically using a servomotor rather than the pneumatic cylinder. The use of the servomotor creates a closed-loop system whereby a feedback from the supplied forging force can be obtained and used for control. The ability to control the electrodes at high speed can also be achieved by using the servo system due to the inherent lower inertia. A small number of companies such as Obara UK [Online](www.obara.co.uk) and Milco [Online](www.milcomgf.com) have gone into manufacturing servo spot welding machines recently. Companies like Toyota and Honda in Japan have replaced their air gun armoured spot welding robots with electric servo gun ones, and are presently updating their overseas factories (Yagi 2002). The use of these machines is mainly due to the other advantages such as easier control of the squeeze force, less noise pollution, variable stroke length and faster welding process. Yagi (2002) had reported that with the servo spot welding machine, total welding time would only be 0.34 – 0.44 seconds (17-22 cycles) compared to 0.6 – 0.9 seconds (30-45 cycles) using pneumatic spot welding machine. However there are no indications from these companies on the control of the forging force during the welding process. Investigation on the possibility of controlling the forging force during welding and the effect on weld strength will be the novelty of this project.

Force profiles, which consist of a series of forces, will be supplied to the servo system during the welding cycle and the electrode movement will be controlled to follow the supplied

profile. The objective of this research was to investigate the ability of the force control to control weld strength and also maintain the consistency of weld strength within a tighter strength envelope. Force control systems will be developed to control the squeeze force during the squeeze cycle and the forging force during weld cycle. Various force profiles will be supplied to the developed control system during welding and how these force profiles effect weld strength will be studied.

1.3.1 Aim and objectives

Aims - To investigate and develop a control system using a servomechanism to achieve improved weld strengths.

Objectives – a) Investigate the effect of welding parameters on weld strength
b) Investigate the ability to monitor weld development using various weld development monitoring techniques
c) Develop a prototype model of a servo controlled spot welding machine
d) Investigate the ability to control weld development during welding by controlling the forging force.
e) Study different force profiles and proposes the improved force profile to achieve higher weld strengths.

1.4 Organisation of the thesis

The current chapter 1 explains the problems in the spot welding process. A brief literature review on the various work carried out in the spot welding process was presented in this chapter. Finally the proposed research and the aims of this research were introduced.

Chapter 2 gives an introduction to the spot welding process, the spot welding machine and the various types of electrodes. This chapter also explains the development of the weld during

welding and points out certain factors, which affect weld development. Types of weld defects are also looked and reasons for these defects are specified.

Chapter 3 introduces the equipment and instrumentation used in the experiments that were discussed in this thesis. This chapter also describes the fusion zone and the heat-affected zone, which develops during spot welding and explains briefly the changes in the structure of the parent material at these regions during welding. Finally the various types of testing methods are presented and how these methods affect the measured weld strength are explained.

Chapter 4 presents the design, fabrication and assembly of the servo actuated spot welding machine. This chapter also compares the previous pneumatic system and explains how the new servo system would replace the old system. The developed PID control for force control and position control will also be discussed at the final part of this chapter.

Chapter 5 discusses the various experiments carried out for system performance evaluation. The three developed control systems were tested and the results of the tests are discussed. Various force profiles were also used to test the force control during weld cycle.

Chapter 6 explains the study carried out to investigate the changes in the fusion zone due to changes in the welding parameters using metallographic methods. It also deals with the various preliminary experiments that were carried out to study the changes in the weld strength to changes in the various spot welding parameters. This chapter also discusses the various weld development monitoring methods used to study weld development

Chapter 7 investigates the change in the dynamic resistance curves and weld strength with the use of various force profiles to change the forging forces during welding. This chapter discusses how the used force profiles change the dynamic resistance during welding and finally conclude the changes in strength due to change in dynamic resistance.

Chapter 8 presents the proposed force profiles that were developed based on the studies on various force profiles characteristics, which would guarantee high strength welds. Comparisons

made on the forging force controlled and electrode clamping force conditions during welding based on the changes in the dynamic resistance curves and achieved weld strength are also discussed in this chapter. Finally the use of these force profiles to modify the lower welding lobe and to avoid expulsion is also presented.

Chapter 9 covers the conclusions of this project and discusses the proposed further work.

Chapter 2

SPOT WELDING – A REVIEW

In this chapter, the introduction to the spot welding process is given. Various aspects of this welding process such as the welding parameters, welding cycle, heat generation during welding and the equipment and materials used in this process i.e. the spot welding machine and electrode, are explained. Later the weld growth is discussed and the factors that govern weld growth during welding are explained. Finally the types of weld defects and the phenomenon that cause weld defects are investigated.

2.1 Historical Background of Resistance Spot Welding

Resistance spot welding is a process of joining two or more metal parts by fusion at discrete spots at the sheet interface. The invention of resistance welding is generally attributed to Professor Elihu Tompson of Massachusetts in 1877 (Milner 1968). He was demonstrating the discharge of a battery of Leyden jars through a multiple-turn primary of a transformer to obtain high current - low voltage pulse through a single turn secondary when he inadvertently brought the ends of the secondary coil into contact and found that they welded together. Ten years later Thompson designed an equipment suitable for commercial application and patented the process, which came to be known as resistance butt-welding and is now used for the joining of wires, strips and pipes. In this process, the ends of the material to be joined are butted together and a current passed through them; the metal in the vicinity of the joint attains a high temperature, due to resistance heating, at which it can be forged (Milner 1968).

A few years after the invention of butt-welding, a resistance heating method was invented for the joining of sheet metal. The sheets were overlapped and placed between two water-cooled copper electrodes and a pulse of current, passed between the electrodes produced a fused nugget at the interface between the sheets, joining them together. This is resistance spot welding, a process, which because of economy, ease and rapidity of operation

with the comparatively small amount of damage it causes to the surface, has largely replaced riveting for the joining of sheet metals (Milner 1968).

2.2 The Principle of Resistance Spot Welding

Resistance spot welding is probably the most common type of resistance welding. It is widely used by most of the manufacturing industries such as the automobile industry, aircraft industry and furniture industry (Cary 1989). Figure 2.1 shows the principle of the spot welding process. The sheets that are to be joined are placed on the lower electrode, then the upper electrode is moved down to squeeze the sheets. Pressure is applied on the electrodes to bring both the sheet metals into contact. Current is then turned on which flows through the electrodes. Resistance to current flow through the metal sheets generates heat. The temperature rises at the sheet interface till the melting point of the metal is reached. The metal will then fuse and a weld will be formed. The current is then switched off and the weld is allowed to cool down slowly to solidify under pressure, till it has adequate strength to hold the welded parts together.

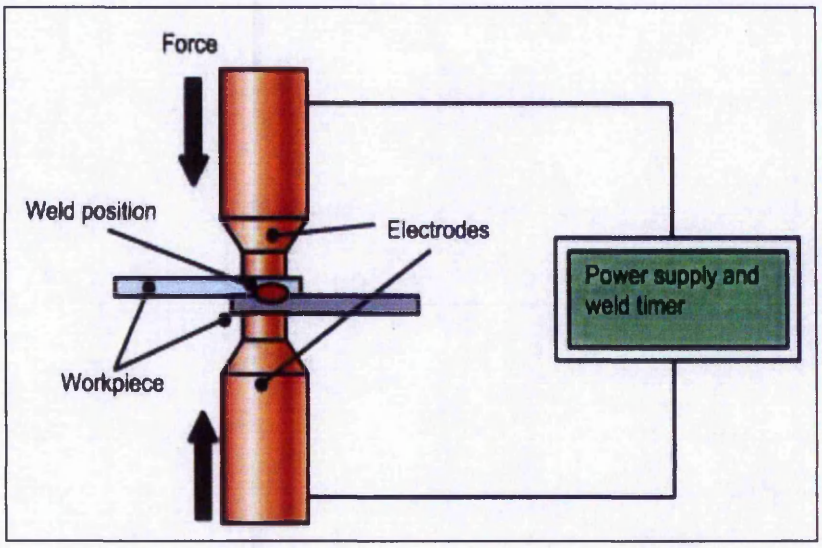

Figure 2.1 – Schematic diagram of the spot welding process

2.3 The welding parameters

The 3 main welding parameters that affect weld strength in spot welding are: -

a) current
b) force
c) time

These parameters are dependent of each other. When welding time is reduced, the welding current is increased and vice versa. Increase in electrode force requires an increase in welding current since it results in a decrease in interface resistance. Other variables that affect the weld strength are electrode deformation, gap between sheets, misalignment of sheets and material surface condition (Arumugam 2000).

2.4 Weld cycle

The spot welding consists of three cycles: -

a) Squeeze cycle
b) Weld cycle
c) Hold cycle

Squeeze cycle is the time for the electrodes to apply the required force to the metal sheets in order to bring them in contact at the area to be welded. Weld cycle is the time for the current to be turned on and the metals fused and the weld is formed at the interface between the sheets. Hold cycle is the time during which the current is turned off and the weld is allowed to cool and solidify under electrode force. Figure 2.2 shows the spot welding cycles, with force and current variations during the 3 cycles.

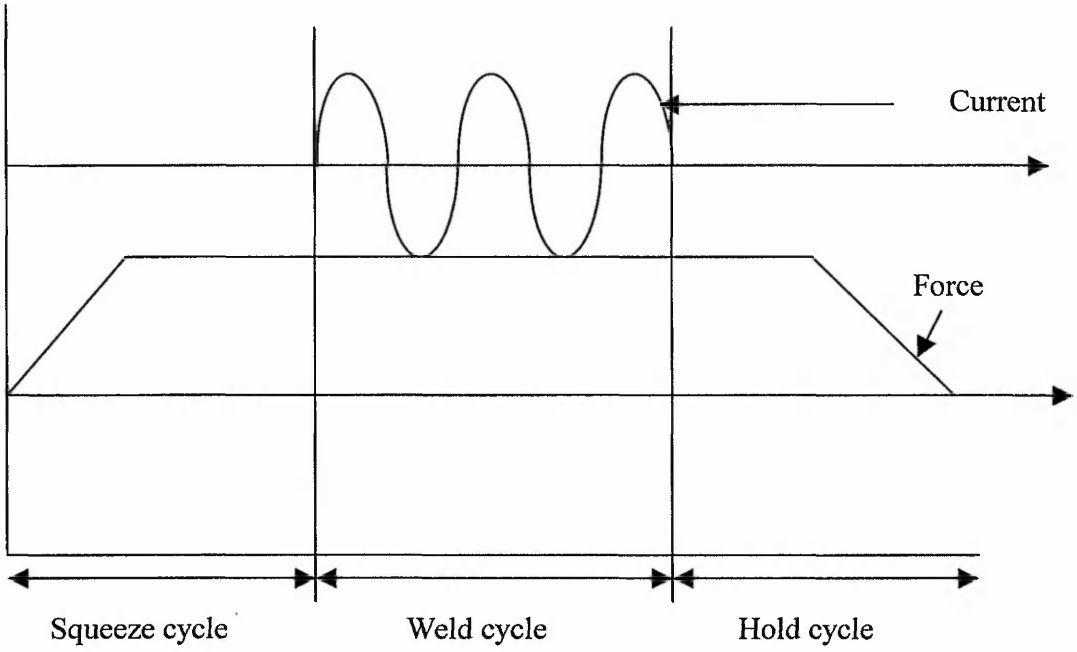

Figure 2.2 – Spot welding cycle

2.5 Heat generation for resistance spot welding

The heat input for weld formation at any given instant in time is given by the formula (Messler et al. 1995): -

$$\mathbf{Q = I^2 . R . t} \text{ ----------(2.1)}$$

where Q is the heat supplied in Joules, I is the current in amperes, R is resistance at the sheet interface and t is the time of current flow in seconds.

Resistance R is the summation of the contact resistance and the bulk resistance of material. There are, in effect, at least seven resistances connected in series for any one weld that account for the temperature distribution in the welded joints. For a one thickness joint these are: -

1. Resistance of the upper electrode
2. Contact resistance between upper electrode and upper sheet
3. Resistance of the upper sheet metal itself
4. Contact resistance of the surface interface of the upper and lower sheets at the location of the weld formation. This is the highest resistance and therefore the point of the greatest heat generation
5. The static resistance of the lower sheet
6. Contact resistance between lower electrode and lower sheet
7. Resistance of the lower electrode

Figure 2.3 shows the temperature distribution at various locations due to variation in resistance during the spot welding process (AWS 1980). Heat is most rapidly developed at point 4 because of the high contact resistance at that location. The heat generated at points 2 and 6, which is lower than at 4 are rapidly dissipated into the contacting water-cooled electrodes 1 and 7.

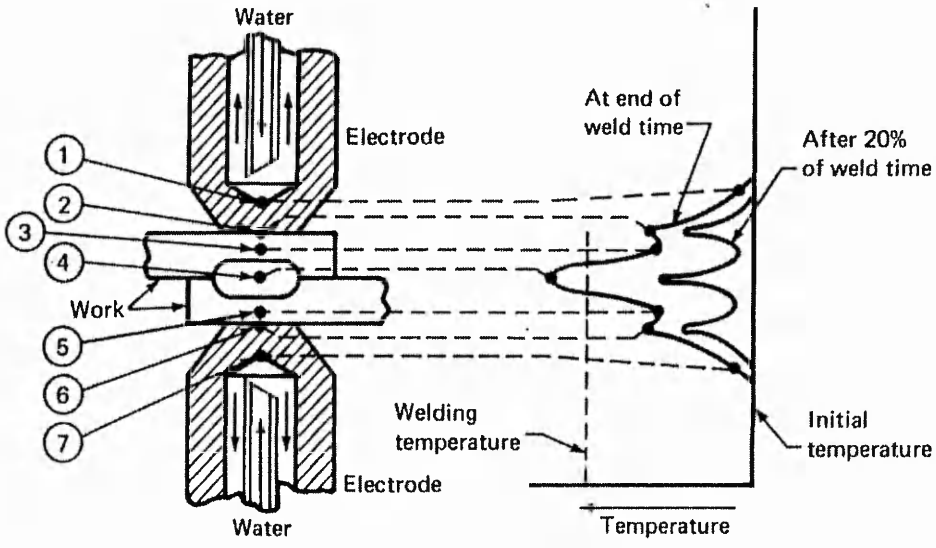

Figure 2.3 – Temperature distribution during spot welding (AWS 1980)

2.5.1 Effect of welding current on heating

The quantity of heat generated is proportional to the square of the current as seen in the heat equation above. Hence current must be controlled very accurately (Cullison 1993). If the current density is low, melting may not occur or a fully developed weld will not be obtained at a certain preset time due to insufficient supplied heat. If the current density is high, a rapid increase in temperature occurs at the sheet interface due to the high rate of heat generation, causing weld expulsion to occur.

2.5.2 Effect of welding time on heating

To a first approximation, the heat input is proportional to time. Sufficient time should be given to produce a fully developed weld. The welding time should be such that the heat generated is enough for proper fusion but not so great that it will cause weld expulsion due to ejection of molten metal from the weld region. To a certain extent, a good quality weld could be achieved with a proper co-ordination between current and time. Since heat transfer is a function of time, the development of a proper weld size requires a definite length of time regardless of the amperage (Guendouze 1995).

2.5.3 Effect of electrode force on heating

The force is exerted on the weld by the electrodes. A lower force will cause the resistance at the interface to increase and in turn increase heat generation and vice versa. Effect of force on the heat input will be explained in detail in the Section 2.8.

2.5.4 Effect of work piece surface condition on heating

In order to obtain the highest quality of spot welds, the resistance at the work piece surfaces that contact the electrodes must be kept to a minimum. Resistance at the work piece surfaces increase because of presence of dirt, scale, rust and oxide film. Reduction in this resistance can be achieved by cleaning the work piece surfaces. If the work piece surfaces that

contact the electrodes have too high a contact resistance, the temperature rise at these surfaces is almost as fast as at the faying surface. The surfaces of the work pieces are not smooth on a micron scale and a firm metal-to-metal contact may be secured by an increase in electrode force, thus reducing the electrical resistance (Vogler & Sheppard 1993). Removal of foreign substances from the work piece surfaces also reduces electrode pickup and consequently increases electrode life.

2.6 Spot welding machine

At present there are mainly 3 types of spot welding machines available in the market. These are the rocker arm type, the press type and the portable type. The rocker arm, which is the simplest and low cost, is so called because of the rocker movement of the upper arm. The movement of the upper arm transmits electrode force and current during welding. Three methods of operation are pneumatic, electric and manual. The travel path of the upper electrode is an arc about the fulcrum of the upper arm. The press type is the most recommended for many spot welding applications. The moveable welding head travels in a straight line and pneumatic or hydraulic cylinder is used to exert force. Figure 2.4 shows example of a press type spot welding machine. The portable types are widely used in the car industry. They are normally fitted to the arms of the spot welding robots. The small guns use a hand -operated lever to apply force to the electrode manually. Bigger units, especially those used for welding bigger components, are fitted with pneumatic and hydraulic cylinders to allow higher forces to be used.

Even though the designs of the spot welding machines vary, they all have the same 3 principal elements:

a) an electrical circuit consisting of a welding transformer and a secondary circuit including electrodes which conduct the welding current to the work
b) a mechanical system consisting of machine frame and associated mechanisms (pneumatics, hydraulics or manual) to apply the welding force.
c) control equipment to initiate and time the duration of current flow. It can also control the current magnitude as well as the sequence and time of the welding cycle.

Figure 2.5 shows a general schematic diagram of the spot welding machine.

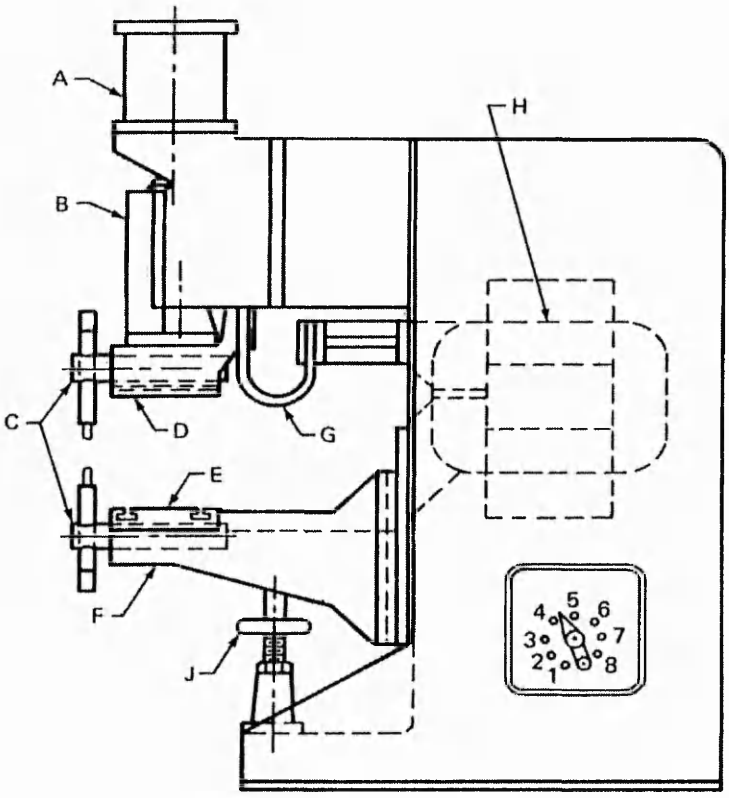

A - Air or hydraulic cylinder
B - Ram
C - Spot welding attachment
D - Upper platen
E - Lower platen
F - Knee
G - Flexible conductor
H - Transformer secondary
J - Knee support

Figure 2.4 – Press type spot welding machine (AWS 1980)

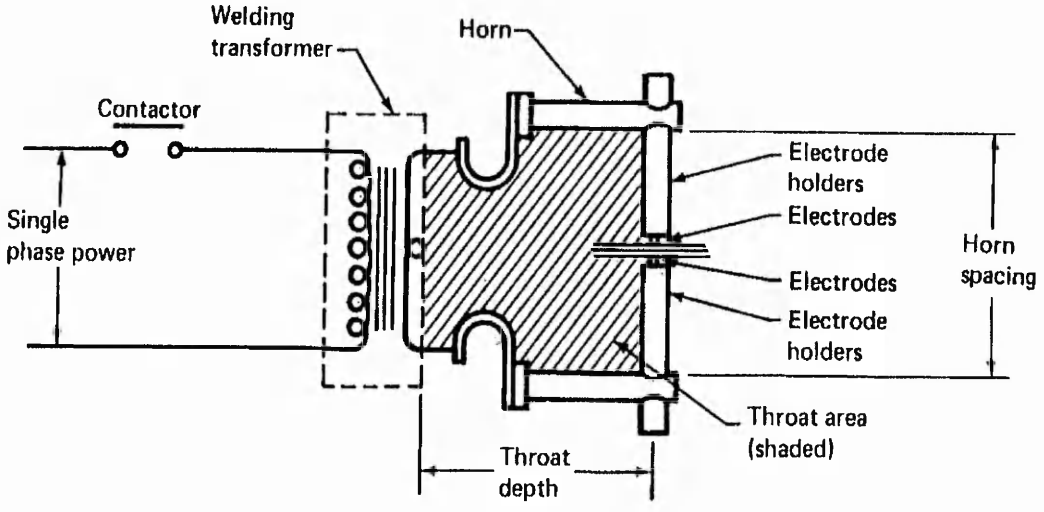

Figure 2.5 – Schematic diagram of a spot welding machine(AWS 1980)

2.6.1 Principle of operation of a press type machine

The principle of operation is as follows: -

a) Air is passed into the top of the cylinder to provide electrode force
b) Head descends and force is built up on the work piece
c) Weld timer closes the main contactor and current begins to flow
d) When the weld timer has completed its cycle, the main contactor will open
e) The head returns to its initial position and the cycle is completed.

2.6.2 The pneumatic system of the spot welding machine

The pneumatic system that will be discussed here is of the British Federal's Stronghold spot welding machine that was used in this project. Figure 2.6 shows the schematic diagram of the Stronghold's pneumatic system.

The pneumatic system that actuates the electrode consists of two separate cylinders; a small diameter low force cylinder and a normal size weld cylinder with joined piston rods connected directly to the ram as shown in figure 2.6. The ram is connected to the upper arm of the welding machine, which is connected to the electrode holder. The weld cylinder is single acting and air is supplied from the weld pressure regulator and a valve. The low force cylinder is double acting with piston rods at both ends. When line pressure is applied to both sides of the piston in the low force cylinder, the cylinder has a small net trust downwards since the area above the piston is slightly greater than below. This trust together with the weight of the ram, electrode holder and stake causes the head to descend and air is pushed from below, through a flow control to above the piston.

When the ram moves far enough to operate the limit switch, the timer is activated. This timer initiates another air valve to create a clamping force during welding due to the air pressure build-up in the weld cylinder. The clamping force is normally preset by means of the air regulator. When the timer is deactivated after welding is over, the air from the weld cylinder is sent to the bottom of the low force cylinder. This causes a higher air pressure buildup at the bottom to push the piston upward, which in turn will cause the ram to ascend.

The ascending of the ram will move the movable electrode upwards away from the fixed electrode.

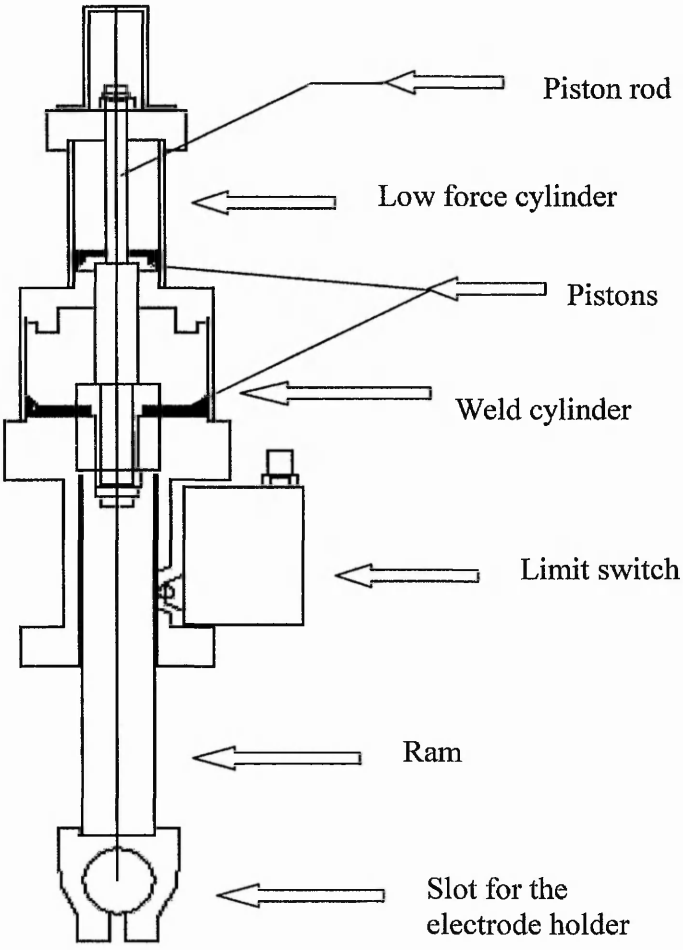

Figure 2.6 – The Stronghold's pneumatic system

2.7 Electrode

Electrodes play an important role in the spot welding process. They are specifically designed to keep the workpieces in intimate contact, and supply them with current, which will be transformed to heat, generated by resistance to current. The main requirements of a spot welding electrode are (a) high electrical conductivity and (b) high thermal conductivity (Kalpakjian 1995). Without these properties, too much heat is likely to be generated at the points where the electrodes make contact with the work piece, resulting in electrode tip pick-

up and sticking of the electrodes to the work pieces. Most electrodes for spot welding are made of low resistance copper alloy. Electrodes are hollow to facilitate the passage of water for cooling. Cooling is an essential phase of spot welding since the heat needs to be dissipated as quickly as possible from the weld area.

2.7.1 Functions of electrodes

Electrodes in resistance spot welding perform four major functions (Guendouze 1995): -

a) conduct welding current to the work
b) transmit the force needed to the work and determine the welding pressure in the welding area
c) water flow inside the electrodes dissipates the heat from the weld zone. Therefore electrodes prevent heat concentration and fusion between the electrode and the work piece surface
d) assure good contact and alignment of the work.

2.7.2 Electrode materials

Materials for spot welding electrodes should have high thermal and electrical conductivities and low contact resistance to prevent burning of the work piece surface or alloying of the electrode face with the work piece. Electrode materials should also have adequate strength to resist deformation at operating pressures and temperatures. Since the electrodes are subjected to high current, force and temperature, the electrode tips slowly loose their original shape. This phenomenon is known as mushrooming. Electrode materials have been classified by Resistance Welder Manufacturer's Association (RWMA) into two composition groups - copper-base alloys and refractory-metal composition (ASME 1971). These classifications cover a wide range of resistance spot welding electrode materials to meet most application. Electrodes of several copper alloys with satisfactory physical and mechanical properties are available commercially. The choice of a suitable alloy for any application is based on the compromise of its electrical and thermal properties with its mechanical qualities.

Electrodes selected for aluminium welding should have high conductivity at the expense of high compressive strength to minimise electrode sticking to the work. Electrodes for welding stainless steel, on the other hand, should sacrifice high conductivity to obtain good compressive strength to withstand the required electrode force (AWS 1980).

2.7.3 Electrode design

Many factors affect the design of electrodes; such as accessibility of the weld area, composition and thickness of the parts being welded and finished surface requirements. Electrode design involves four structural features of the electrode: face, shank, attachment and provision for cooling.

Face of the electrode is that portion which contacts the work. Electrode face geometry determines the current and pressure densities in the weld zone. Figure 2.7 shows the standard types of electrode face shapes available commercially. Shank of the electrode must have sufficient cross-sectional area to support the electrode force and carry the welding current. The shank may be straight as seen in figure 2.7 or bent. The method of attaching the shank end to the holder is usually one of the three general types: tapered, threaded or straight-shank. Spot welding electrodes should have an internal cooling passage extended close to the welding face. This passage should be designed to accommodate a water inlet tube and provide for water out around the tube. The tube should be positioned to direct the cooling water against the tip of the electrode.

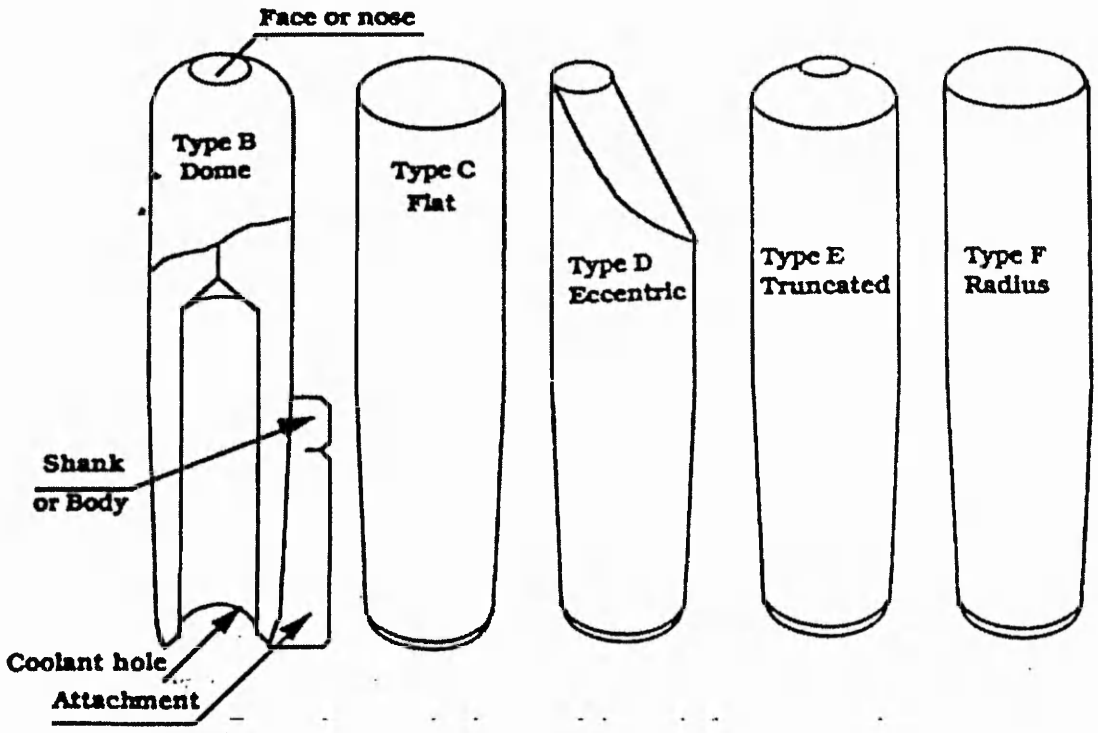

Figure 2.7 – Standard types electrode faces or nose shapes (Kalpakjian 1995)

2.8 Weld formation

This section details the weld formation and the factors that affect weld formation.

2.8.1 Contact resistance

Changes in contact resistance in between the workpieces that need to be welded govern the weld growth. Surface asperities between the two sheets' contact surfaces cause the true contact area between the two contacting surfaces to be really small. When force is applied through the electrode face, the contact points between the contacting surfaces collapse and flatten as the local yield stress is exceeded causing plastic deformation to occur at the contact area. Further increase in contact force causes the number of asperities that comes in contact between the two surfaces to increase causing the area of contact to increase (Xu et al. 1999). This increase in contact area will decrease the electrical contact resistance between the two contacting surfaces. Analysis (Greenwood 1966) shows that the contact resistance (R_C) between two clean, uncoated surfaces is given by: -

$$R_C = (\rho_1 + \rho_2)\left[\frac{1}{4na} + \frac{1}{4\alpha}\right]; \quad \text{where } \alpha = \frac{3\pi}{16n^2}\left[\Sigma\Sigma(1/s_y)\right] \text{ ------(2.2)}$$

where ρ_1 and ρ_2 - bulk resistivities of the contacting work pieces, n - number of contacting asperities, a - average radius of the contacting asperities and s_y - distance between contacts.

The dependence of unit area contact resistance (R_{CA}), units Ohms/m^2, on force, temperature and material yield strength is given by the formula (Babu et al. 1998):-

$$R_{CA} = \left[\frac{(\rho_1 + \rho_2)}{\sqrt{\eta}}\left[\Psi\left\{\frac{\sigma_{YS}}{P}\right\}^{-1/2} + \theta\right]\right] \text{ -------- (2.3)}$$

where A_E - area of electrode tip, $\eta = (n/A_E)$ is the contacting asperity density (m^{-2}), P - force, σ_{YS} - yield strength of material and ψ and θ are constants. Based on this formula, with the variation of η with P and σ_{YS} derived empirically, it was found that at ambient temperature and low applied force, the number of contacting asperities will be small and the contact resistance will be relatively high. Then as the applied force increases, the number of contacting asperities will rapidly increase resulting in a decrease in contact resistance. Finally the rate of increase of η will slow as the true contact area approaches the apparent contact area.

The contact resistance monotonically decreases with increasing temperature due to drop in yield strength. It was noted that the yield strength of the asperities decreases with increase in temperature and then approaches zero at the melting point (Babu et al. 1998). At low temperatures, bulk resistance is low but contact resistance is high because of relative difficulty of deforming the contact asperities. At high temperatures, contact resistance becomes negligible when melting starts to occur and yield strength of asperities drops to zero but bulk resistivity will be relatively high. Thus varying the contact resistance, which is a function of current and force can vary weld growth.

2.8.2 Weld growth

Weld growth in spot welding consists up to 4 stages (Gould 1987)

a) An incubation period where no weld is observed
b) A period of very rapid weld growth
c) A period where weld growth rate progressively decreases
d) Expulsion.

Temperature change in the weld due to heating is given by the formula (Gould 1987): -

$$\Delta T = \frac{I^2 R}{2K}\left(\frac{A}{\Delta x}\left(\frac{(\Delta x)^2}{\alpha \Delta t} + 1\right)\right)^{-1} \quad \text{------ (2.4)}$$

where ΔT - total temperature rise, I - current, R - material resistivity, K- thermal conductivity, A - electrode face area, Δx - sheet thickness, Δt - welding time and α - thermal diffusivity. The temperature rise (ΔT) is proportional to current (I) and inversely proportional to thermal conductivity. Temperature rise decreases with increase in electrode face area and sheet thickness. The reason is that when the electrode face area increases, current density reduces, resulting in reduced energy input and the change in temperature rise reduces. Similarly with thicker material, more heat is needed to produce a weld and with high thermal conductivity, as heat is easily conducted away from the weld, causing temperature change to reduce. The formula also shows that change in temperature increases with increase in weld time.

The weld forms as a toroid about the centreline of the sheet thickness. The toroid is formed as a result of highly stressed region around the contact area, which will constrain the weld when it is developing (Browne et al. 1995). A molten pool will be created within the toroid due to melting and the molten region will spread rapidly towards the centre and form an elliptic shaped weld. The force created by the weld expansion should be less than the force of the toroid supplied by the electrode in order to contain the molten weld (Zhang 1999). If the force from the weld exceeds the toroid force, molten metal will be ejected out of the weld region causing expulsion to occur as in figure 2.8. As explained in section 2.8.1, the weld growth is initiated by the interface contact resistance, which decreases to zero at the melting

point. Later Joule heating will dominate weld growth for longer times (Wei & Ho 1990). The examination of temperature gradient shows that the mean temperature gradient along the thickness is 3 times greater than along the radial direction (Arefin & Khan 1999). As the weld approaches the electrode/work piece interface, heat flow along the thickness escapes through the electrode to the water, rapidly causing the penetration rate to decrease. However the radial growth rate will increase since the heat flow in the radial direction contributes to the increase in weld diameter.

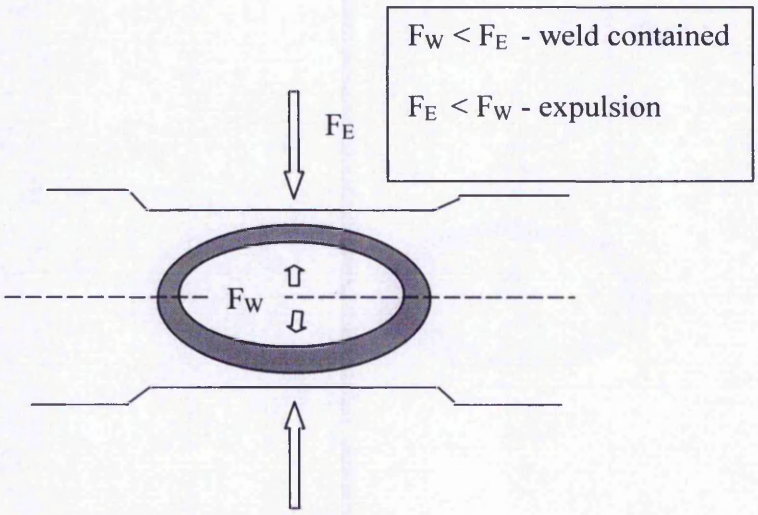

Figure 2.8 – Weld growth

2.8.3 Weld size

The size of the weld must meet the requirement of the appropriate specifications or the design criteria (Guendouze 1995). There is a maximum limit to the weld size of a spot weld. This limitation is based more on the economics and practical limitations of producing a weld than on the laws of heat generation and dissipation that limit the minimum size of weld. The maximum weld size cannot be specified in general terms. Each user should establish this limit in accordance with the design requirements and prevailing shop practises.

2.8.4 Weld penetration

Penetration is the depth to which the weld extends into the work pieces that are in contact with the electrodes. Penetration into the base metal is ordinarily permitted to vary from 20% to 80% of the thickness of the outer piece (AWS 1980). If the depth of penetration exceeds 80% of the thickness, this will result in expulsion, excessive indentation and rapid electrode wear. Also if penetration is less than 20%, the weld is said to be cold because the

heat generated in the weld zone is too small and normal variations in the welding current, time and electrode force will cause undesirable changes in the weld strength. Another author had also suggested that the acceptable weld penetration should be equal to 0.6-0.7 times total joint/ sheet metal thickness (Jou 2003) for similar sheet thickness. For dissimilar thickness of workpieces, the depth of penetration into the thicker piece needs to be equal to that in the thinner piece (ASME 1971).

2.8.5 Sheet separation

Sheet separation occurs at the work piece surface interface due to expansion and contraction of the weld and the forging effect of the electrodes on the molten weld (Tang et al. 2000). The amount of separation varies with the thickness of the assembly, increasing with greater thickness. Excessive sheet separation results from the same causes as surface indentation to which it is related. Improperly dressed electrode faces act as punches under high electrode force. This tends to decrease the joint thickness, upset the weld radially , and force the sheets up around the electrodes (Guendouze 1995)

Figure 2.9 shows the features of the spot weld that were explained above.

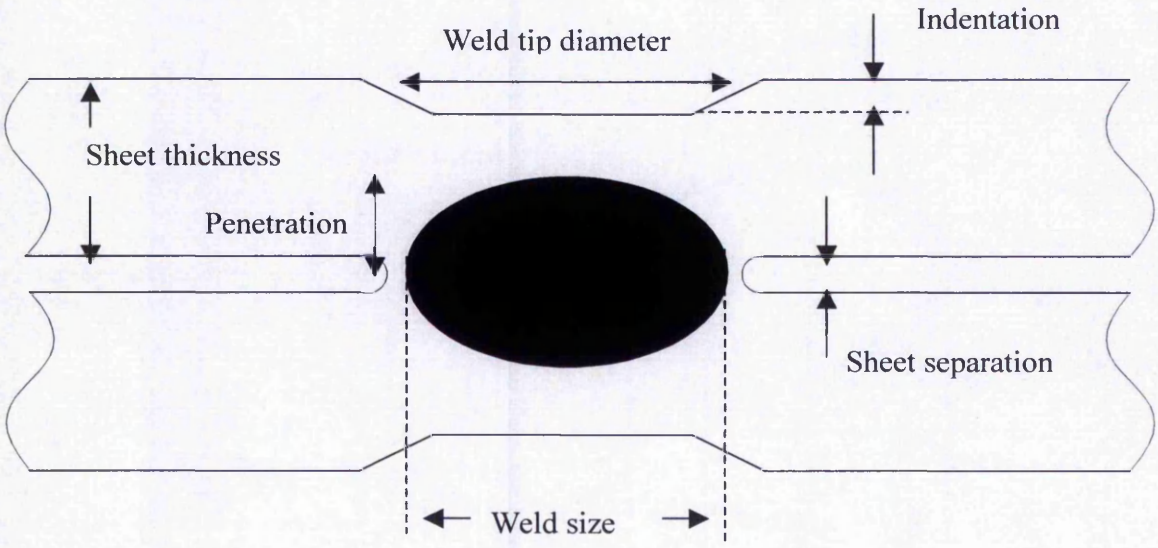

Figure 2.9 - Features of a spot weld

2.9 Weld defects

Inconsistency in weld strength seems to be a major problem faced by industries (Greitmann 1998). In industries like the automobile industry, an automobile assembly requires between 7000 and 12000 welding spots depending on the size of the vehicle (Dickinson 1981). It is also reported that the car industries in United States spend an estimated $400 to $600 million per year in testing spot welds (Rexroth 2003). Therefore, this issue is a serious matter in the automobile industries.

It has been pointed out that the inconsistency in weld strength is due to improper control of the critical parameters (Guendouze 1995). A satisfactory strength is the results of using correct weld settings and maintaining them for the duration of a particular production run. Factors such as current, time and electrode force need to be controlled properly. Even if these primary factors were kept under control, there are various secondary factors such as primary line voltage variations, electrode deformation, workpiece surface conditions and effects of current shunting that will affect the weld strength. A good weld or normal weld should have a diameter of $4 - 5\sqrt{t}$ where t = sheet thickness in millimetres and the electrode indentation should be 10% of the sheet thickness (AWS 1984).

Table 2.1 shows the important weld defects and their causes: -

2.9.1 Phenomena causing weld defects

a) Expulsion

Expulsion is influenced by many factors of electrical, mechanical, thermal and metallurgical nature. Several theories or hypotheses on the causes of expulsion have been proposed. It was believed that electrode causes expulsion because the molten metal from the weld is squeezed out by the electrodes. Excessive current density or energy input was also considered to be the reason for expulsion (Zhang 1999). Another theory of expulsion is that it happens when force from the weld expansion exceeds the force from the electrodes as shown in figure 2.8 (Zhang et al. 2000). Expulsion happens at either the faying surface or the electrode/work piece interfaces. Expulsion on the faying surface may severely affect the surface quality and

Defects	Causes
Spatter between sheets	a) Squeeze time too short b) Electrode force too low c) Welding current too high d) Electrode tip diameter too small e) Impurities on sheet steel surfaces
Weld nugget too small	a) Welding current too low a) Weld time too short b) Electrode force too high c) Electrode tip deformation
Gap between work piece sheets	a) Poor fit b) Electrode force too high c) Weld time too long
Burned material on work piece surface	a) Welding current too high b) Electrode force too low c) Work piece sheet not clean d) Electrode tip not clean e) Unsuitable electrode material
Higher electrode indentation	a) Unsuitable electrode force b) Current is too high c) Weld time is too long d) Electrode tip diameter is too small
Expulsion on sheets	a) Squeeze time too short b) Electrode tip diameter is too small c) Current is too high d) Impurities on surfaces of the sheets

Table 2.1 – Weld defects

electrode life, but not the strength of the weld if it is limited to the surface. Meanwhile expulsion at the faying surface is undesirable in terms of weld quality because it involves loss of molten metal from the weld during welding (Zhang et al. 2000). Figure 2.10 shows traces of expulsion at the faying surface. Comparison made between welds with expulsion and without expulsion show that welds with expulsion have slightly smaller weld diameters, less penetration, wider heat-affected-zone (HAZ) and larger electrode indentation (Zhang 1999). The same study showed that welds with expulsion have lower strength than the ones without expulsion. Even though expulsion was suggested to occur when the radius of the growing

weld exceeds the compressive force of the electrodes, poor electrode conditions, electrode misalignment and work piece conditions are also pointed as other reasons for expulsion to occur (Browne et al. 1995).

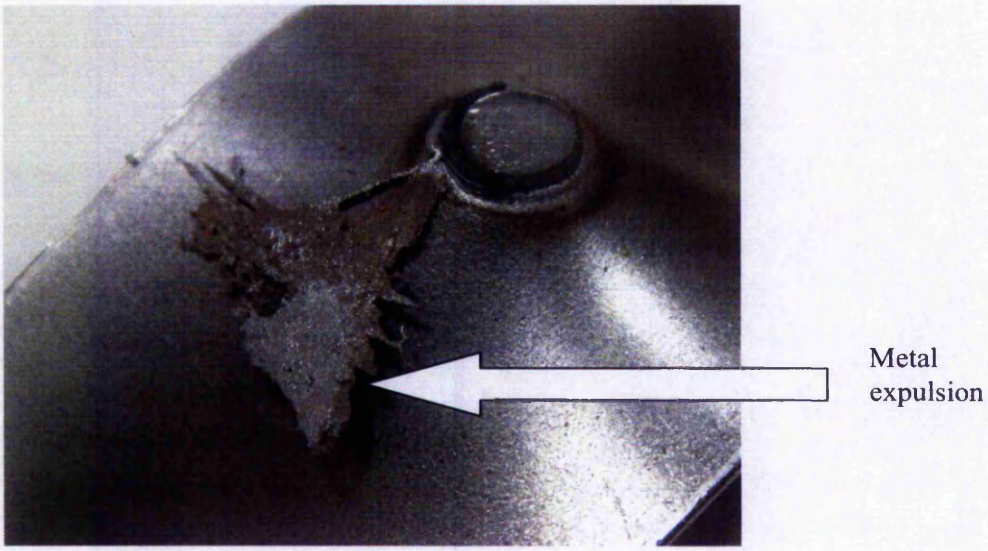

Figure 2.10 – Expulsion at faying surface

b) Electrode deformation/mushrooming

Electrode deformation is a cause for weld defects. Electrode deformation is a phenomenon where degradation occurs at the tip of the copper electrode due to repeated loading imposed on the electrode tip and development of high temperature at the electrode tip ($\approx 500^0$C)(Holliday et al. 1995). Electrode life is defined as the number of welds that can be made, without tip dressing, before the weld size falls below an acceptable level due to electrode deformation. A low electrode life can limit the rate of production that can be achieved in a fixed period due to the need for frequent electrode dressing and/or electrode changing operations. Interaction between the electrode face and work piece under high pressure and temperature condition results in the increase in electrode face diameter (Dong et al. 1998). This results in decreased current density flowing through the increased area, decreased heat supplied to produce weld and in turn decreasing the size of the weld formed. Increase in electrode tip diameter occurs due to concentration of high stress at the periphery of the electrode tip compared to the centre of the electrode during joule heating. This

concentration of high stress causes plastic deformation to occur at the tip periphery as the number of welds increase (Dong 1997).

c) Current shunting

The spacing between neighbouring spot welds is another factor that produces weld defect especially in a smaller weld. Shunting occurs when two or more spot welds are made very close to each other. When the first weld is made, all the welding current flows directly from the upper electrode and through the work piece to the lower electrode by the normal and most direct route. However when a subsequent weld is made, a part of the welding current flows through the work material between the electrodes, and the remainder of the current travels through the metal to the second weld. When the distance between the first and second spot weld is great enough, the resistance of the path through the first weld, compared to that directly through the work material will be high and the shunting effect will be neglected. However, if the distance to the first spot weld is too short then a significant portion of the welding current will be shunted through the first weld. It is not advisable to attempt to form spot welds closer together than three times the diameter of the electrode (British Standards 1993). The reduction in welding current due to shunting through previous weld is shown in figure 2.11

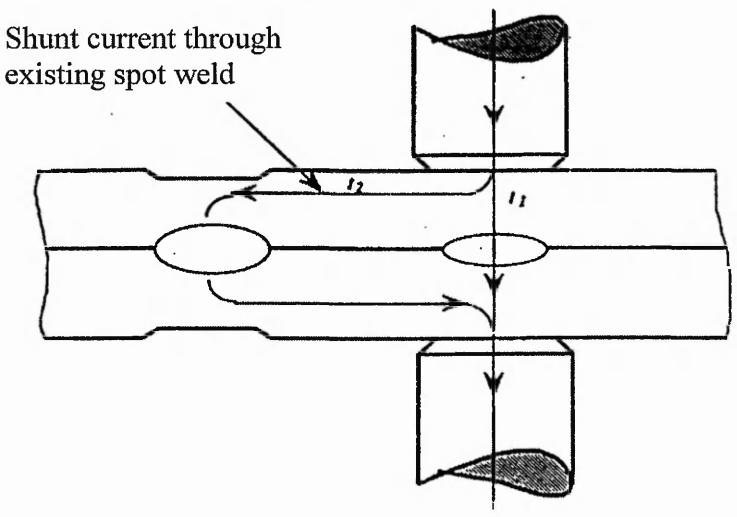

Figure 2.11 – Shunting effect (British Standards 1993)

2.10 Summary of chapter

The spot welding process that is used to join metal sheets through discrete fusion at the sheets' interfaces was introduced in this chapter. The three important parameters of the spot-welding process namely the current, time and force and how the change in these parameters can affect the heat generation during welding were explained. The heat generation for weld development was found to increase with the increase in welding current and weld time. As in the case of the welding force, heat generated during welding was found to reduce with increase in force. The role of the contact resistance between sheets in the weld growth and how the contact resistance changes with change in force and temperature were described. The contact resistance reduces during heating and becomes zero during melting of material. Finally the various spot welding defects and the cause of these defects such as expulsion, electrode mushrooming and current shunting were presented. The next chapter will look into the metallurgical aspects of the spot weld and the testing methods to measure weld strength.

Chapter 3

SPOT WELDING INSTRUMENTATION, WELD METALLURGY AND TESTING METHODS

This chapter presents the equipment and instrumentations used in this project and discusses briefly the metallurgical changes, which take place at the weld during the spot welding process. In this chapter also, the various weld strength testing methods will be looked at and a comparison will be made on the ability of each of the testing methods to measure the spot weld strength.

3.1 Equipment and instrumentation

3.1.1 Spot welding machine

A 75kVA Stronghold spot welding machine shown in figure 3.1, manufactured by British Federal Ltd was used for all the experiments in this project. The WS2000 welding control was fitted to this machine. The StarChive programming software developed by British Federal Ltd was used to program the welding schedule that will be used during welding process. The programmed weld schedule is then fed into the weld timer by means of an RS485-to-RS232 converter.

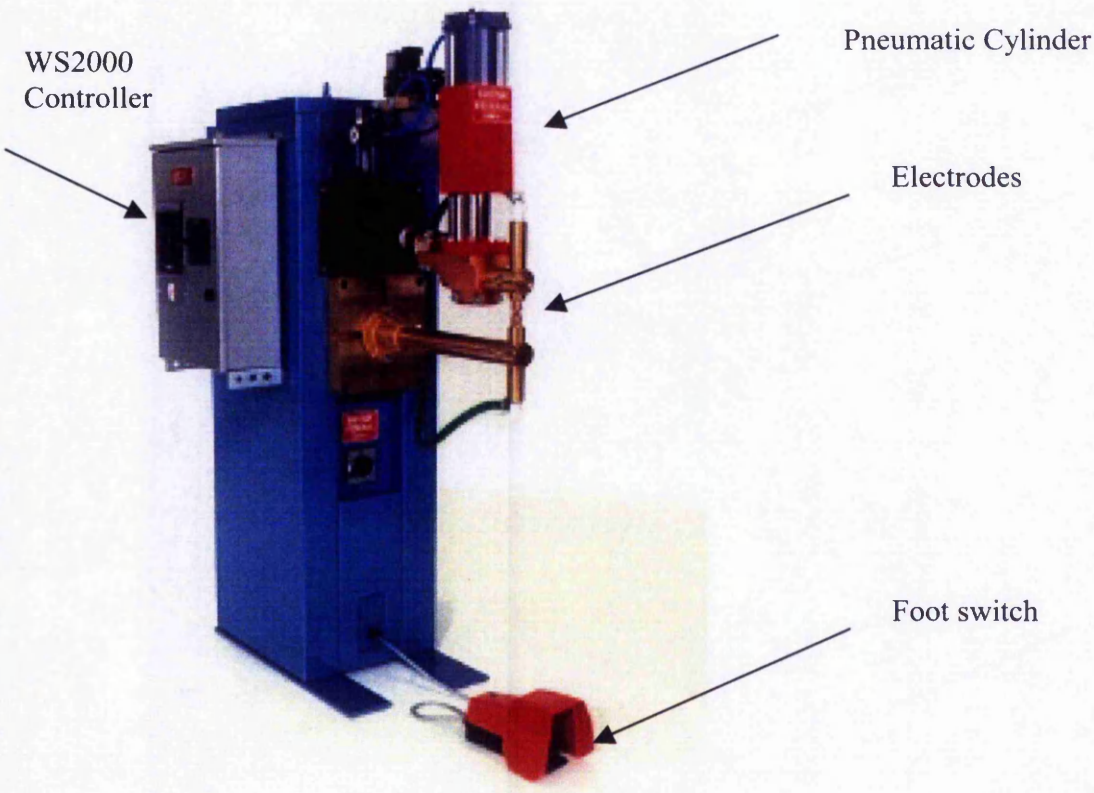

Figure 3.1 – Stronghold spot welding machine

3.1.2 Electrodes

British Federal Ltd's water cooled CuCr Zr electrodes with tip diameters of 5mm, 6mm 8mm and 10mm (nominal) were used for various experiments in this project.

3.1.3 Sheet metals

Low carbon steel (BS1449) was used for these experiments. The dimensions of the sheets used were 170mm x 35mm with 1mm and 2mm thicknesses.

3.1.4 Pressure gauge

A pressure gauge with a range of 1-10 bar was fitted to the machine and the pneumatic cylinder was used to actuate the electrode. The required electrode force is supplied by setting the required cylinder pressure in the pressure gauge.

3.1.5 Current probe

A LEM~flex current probe as shown in figure 3.2 was fitted to the secondary circuit of the spot welding machine. A signal conditioner was used to convert the measured current into an equivalent voltage reading. The voltage value is sent to the computer for analysis through an analogue-to-digital converter (ADC) card. The conversion factor for the probe is 1V = 3000A. A power supply was used to calibrate the current probe. Table 3.1 shows the programmed current in the StarChive program and the current measured by the current probe after been converted to an amperage value based on the conversion given above. 5 repetitions were made for each programmed welding current.

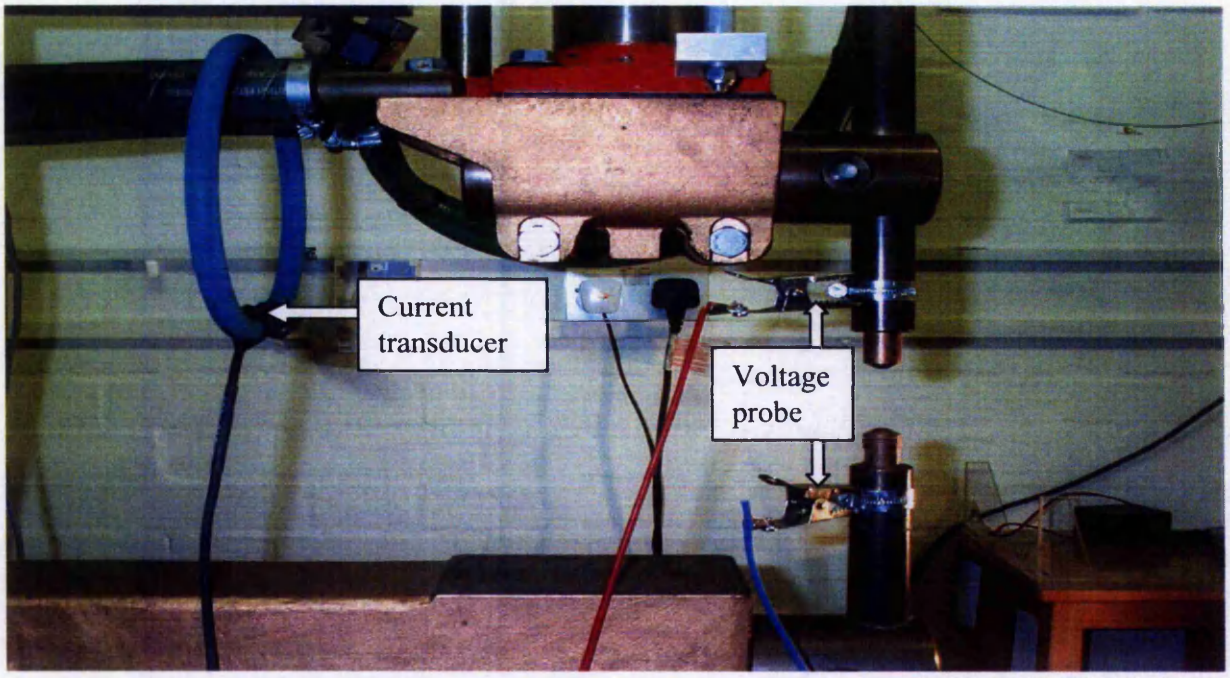

Figure 3.2 – The current transducer and voltage probe

Current programmed in StarChive (A)	Current measured by the current probe (A) Conversion factor 1V = 3000A					Average current (A)	Standard deviation
3000	3090	3100	3075	3089	3108	3092.4	12.46
4000	4250	4189	4265	4177	4258	4227.8	41.46
5000	5350	5299	5210	5340	5285	5296.8	55.62
6000	6289	6350	6254	6330	6389	6322.4	52.55
7000	7320	7389	7330	7289	7293	7324.2	40.19

Table 3.1 – Difference between the programmed and measured current values

Table 3.1 shows the difference between the programmed current value in the StarChive program and the measured current value using the current probe. Even though there is a difference between these two values, figure 3.3 shows that both these variables have a linear relationship.

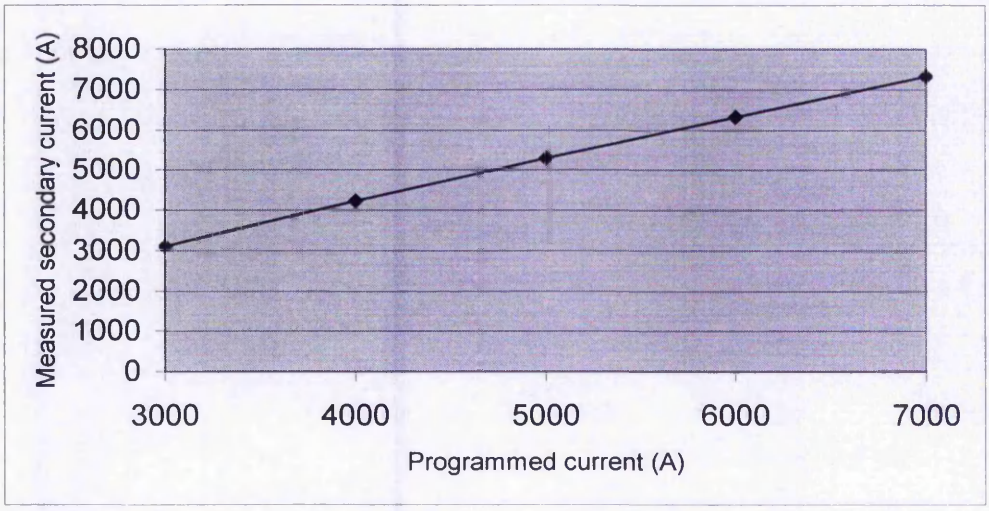

Figure 3.3 - Relationship between the programmed and measured secondary current

3.1.6 Voltage probe

An in-house built voltage probe as shown in figure 3.2 that consists of two crocodile clips and connection cable was used to measure the secondary voltage by clipping the crocodile clips to both the welding electrodes.

3.1.7 Linear-variable-differential-transformer (LVDT)

RDPElectronic's LVDT as shown in figure 3.4, model D5 with ±1mm range was fitted to the upper movable arm of the spot welding machine in order to measure the electrode displacement due to weld growth/expansion. A plunger that was connected to the upper electrode holder was used to transmit the movement of the upper electrode to the LVDT. A signal conditioner was then used to output a voltage signal proportional to the displacement of the armature in the LVDT. The conversion was 0.2mm = 2V. The LVDT was calibrated using the LVDT calibration jig where the armature core mid-position was set to zero and the full stroke was set to 1mm.

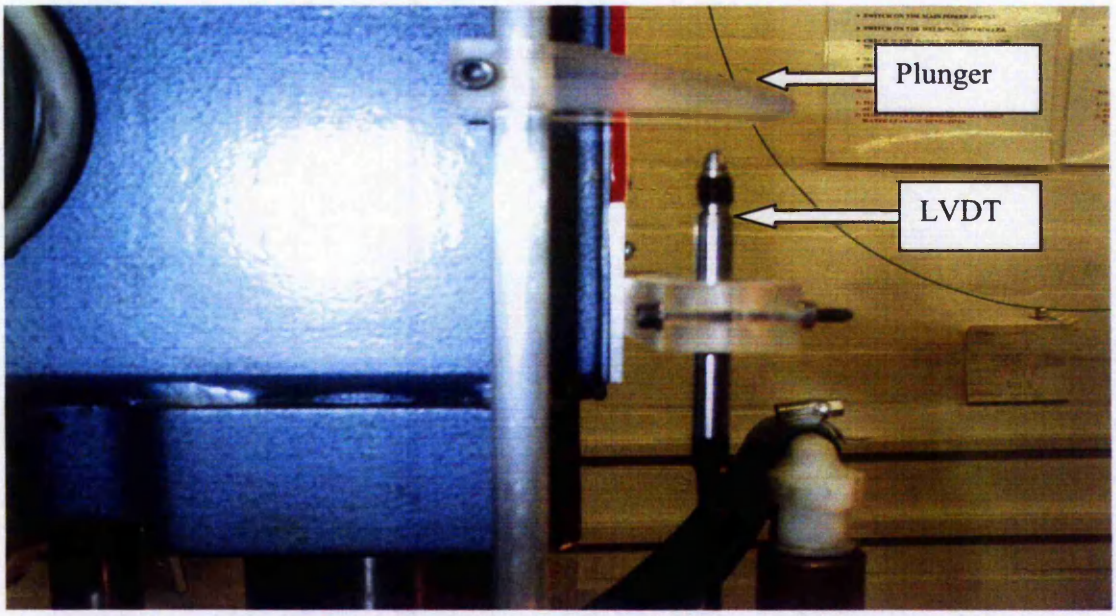

Figure 3.4 – Linear-variable-differential-transformer (LVDT) fitted to the machine

3.1.8 Piezoelectric sensor

Kistler's piezoelectric sensor (9232A) shown in figure 3.5 was fitted to the body of the spot welding machine in order to have an indirect force measurement during welding process. The piezoelectric sensor senses the slight bending of the arm of the spot welding machine due to the applied electrode force. Depending on the bending of the arm, an equivalent charge signal is produced by the sensor. This charge is converted into a proportional voltage signal by a charge amplifier (5855A). A load cell that was placed in between the electrodes was used to calibrate the charge amplifier so that both the devices read the similar force reading when a force is applied on the load cell.

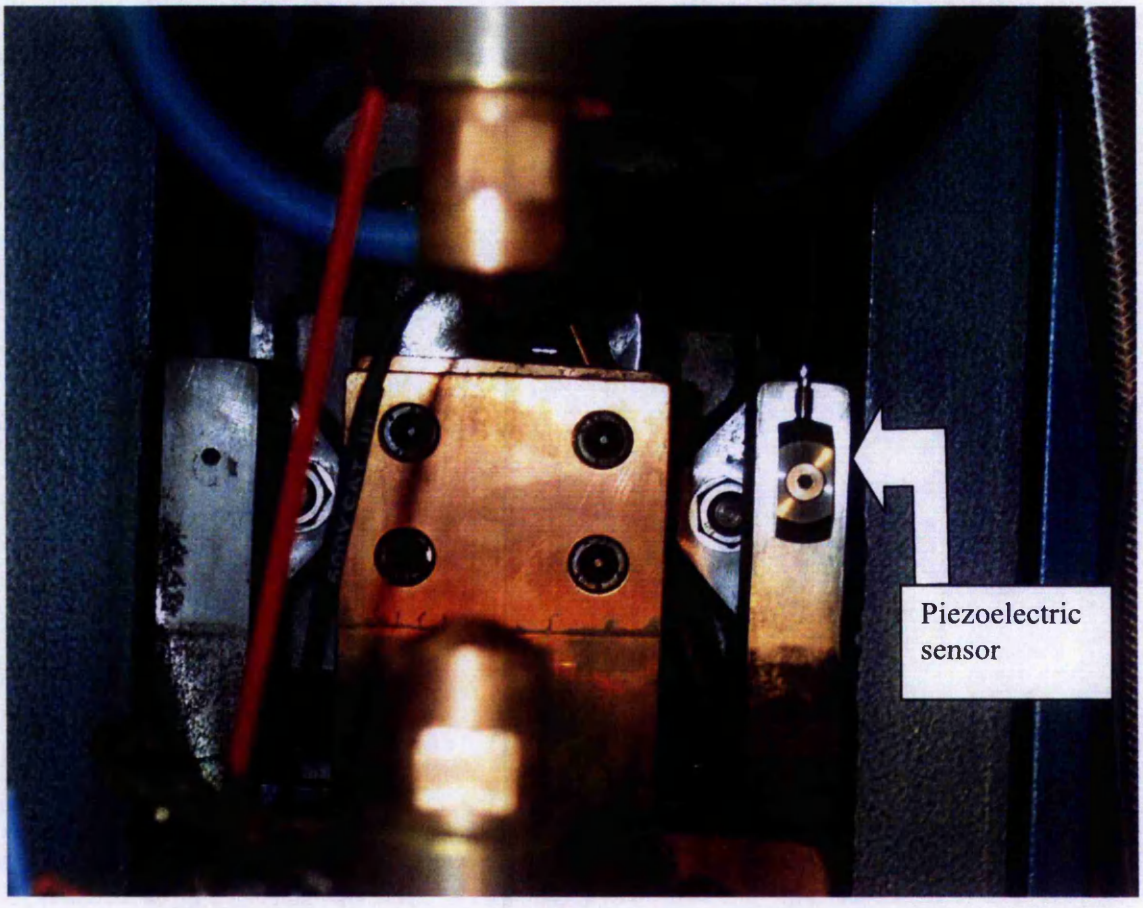

Figure 3.5 – Piezoelectric sensor fitted to machine body

Table 3.2 shows the results of the calibration of the piezoelectric sensor. Five different electrode forces were applied on the load cell that was placed between the electrodes. The sensitivity of the charge amplifier was adjusted based on the load cell reading to convert the input charge from the sensor to voltage between the range of 0V to 10V which is equivalent to 0kN to 10kN. 5 repetitions were taken for each force.

Load cell reading (kN)	Piezoelectric sensor reading (kN)					Average reading (kN)	Standard deviation
2.00	1.62	1.68	1.65	1.68	1.64	1.65	0.026
3.00	2.64	2.62	2.61	2.57	2.58	2.60	0.029
4.00	3.58	3.58	3.54	3.50	3.59	3.59	0.038
5.00	4.55	4.53	4.59	4.60	4.57	4.57	0.029
6.00	5.42	5.46	5.43	5.48	5.47	5.45	0.026

Table 3.2 - Difference between load cell and piezoelectric sensor readings

The differences in both the readings might be due to the thickness of the load cell, which was loaded in between the electrodes and due the position at which the piezoelectric sensor was fitted to measure indirectly the applied electrode force.

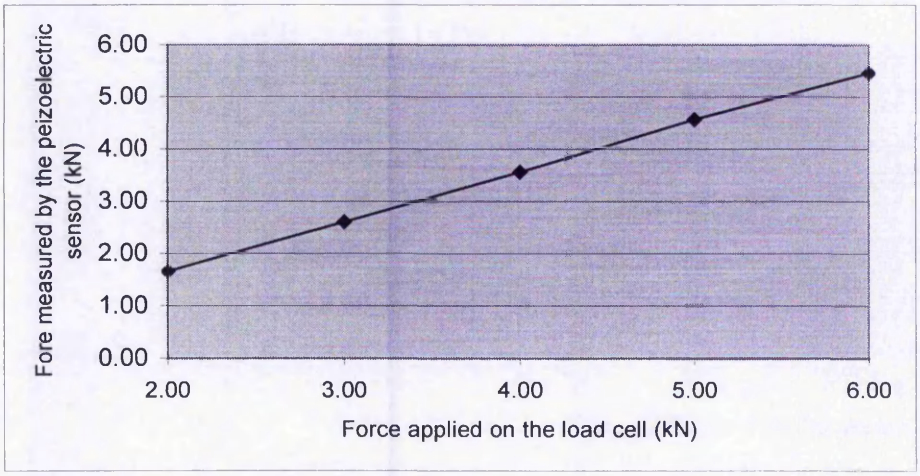

Figure 3.6 – Relationship between the reading from the load cell and the piezoelectric sensor

However figure 3.6 shows a linear relationship between the force measurements from the load cell and the piezoelectric sensor.

3.1.9 Analogue-to-digital converter (ADC)

ComputerBoard's 12bit, 8 channels, CIO-DAS801 analogue-to-digital card was used to digitize all the voltage signals from the current transducer, voltage probe, piezoelectric sensor and the LVDT for measurement and analysis purposes.

3.2 Spot Weld Metallurgy

A spot weld consists of two distinct zones i.e. the fusion zone (FZ) and the heat-affected-zone (HAZ)(Easterling 1992). These 2 zones correlate with various transformations on appropriate equilibrium phase diagram, adjusted for non-equilibrium heating and cooling effects on transformation temperatures and micro constituents. Figure 3.7 shows the fusion zone and the heat-affected-zone for a spot weld.

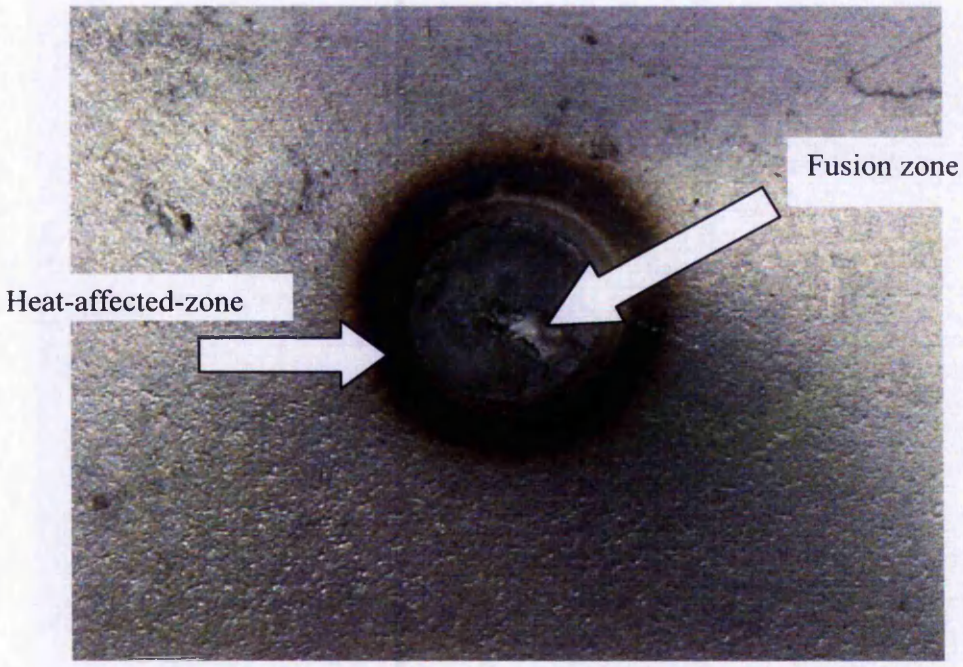

Figure 3.7 – The fusion zone and heat-affected-zone

3.2.1 Fusion zone (FZ)

The fusion zone (or weld) is the portion of the weld that completely melts during welding when heated by the welding thermal cycle to above the material's melting point. It is important to the properties of the final weld because it has undergone melting and solidification and so may be quite different in structure and properties to the base material. To understand the microstructural changes that occur in the fusion zone, the phase diagram of the material used to make the weld needs to be considered. The phase diagram of any material is the graphical method of illustrating the relationship between the composition, temperature and structure of the material. Figure 3.8 shows the phase diagram for carbon steel (Fe-C).

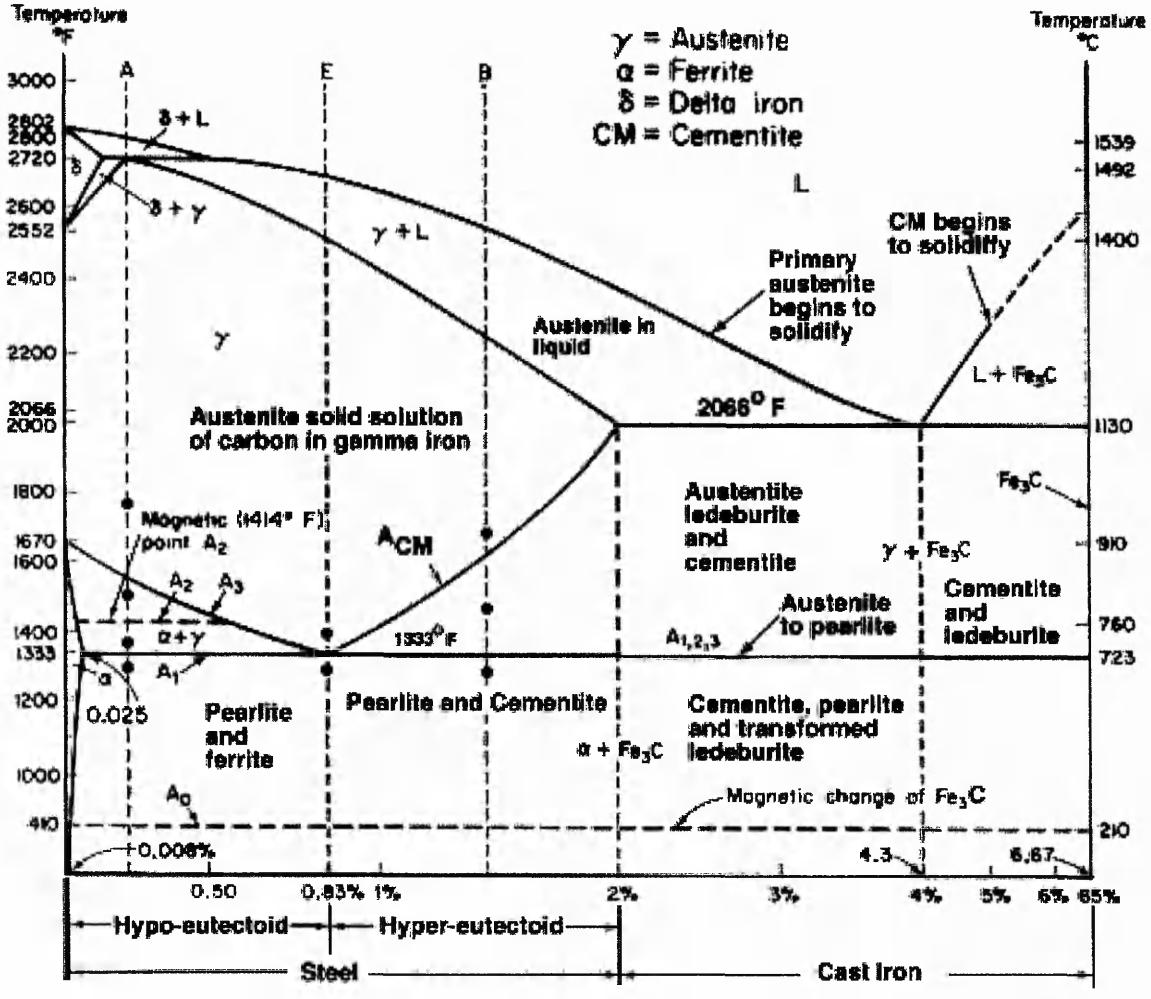

Figure 3.8– Fe-C phase diagram for carbon steel (Smallman 1992)

When carbon steel with 0.15% carbon content (mild steel) is heated above its melting p oint (1500°C) during the weld thermal cycle, liquid solution of carbon in iron will be formed. During solidification, as the temperature decreases a phase mixture of δ-ferrite and liquid is formed. There is a peritectic reaction at ~1493^{0}C where the mixture of δ-ferrite and liquid starts to transform to austenite (γ). Below this temperature, the steel is completely solid and below ~1450 ^{0} C the structure will be a uniform austenite (γ). As this uniform austenite continues to cool till it reaches the upper critical point of this steel(≈890°C), some of the austenite will begin to transform to ferrite (α). Ferrite generally forms as small new crystals at the grain boundaries of the austenite. At 723°C (lower critical temperature), the structure will consist of a mixture of austenite and ferrite. Below 723°C, the remaining austenite transforms into a eutectoid, which is a mixture of ferrite and cementite known as pearlite. As the steel cools to room temperature no further important changes will take place in the weld structure.

The final structure of the fusion zone may consist of the mixture of ferrite-pearlite or bainite or martensite depending on how fast the fusion zone was cooled. Very slow to moderately slow cooling rate will produce a mixture of ferrite and pearlite. Faster cooling rate will form bainite and a very fast cooling rate will form martensite. They are all very different in structure and properties. Fusion zone grain structure has a strong influence on the mechanical properties of the weld (David & Vitek 1989). The presence of martensite and bainite will lead to very high hardness in the fusion zone (Santella et al. 1998).

3.2.2 Heat-affected-zone (HAZ)

The heat-affected-zone is the region that undergoes changes in the microstructure due to the heating during the weld cycle but no melting occurs in this region. The heat affected zone lies outside the fusion zone (FZ). As the distance from the centre of the weld increases, the heat-affected zone begins where the temperature of the weld cycle is just below the melting point of the base material and extends to a point where the temperature is high enough to cause some change in the microstructure of the base material.

Figure 3.9 shows the micro-structural changes in the heat affected zone for a mild steel (0.3%C) based on a Fe-C phase diagram(Messler 1993). The heat affected zone consists of partially grain refined (point 3), grain refined (point 2) and grain coarsened (point1) regions corresponding to just above the A_1, just above the A_3 and well above A_3 respectively. Upon cooling the partially refined region (point 3) decomposes into very fine grains of pearlite and ferrite. In the grain refined (point 2), a non-uniform distribution of ferrite and pearlite will be formed during cooling. In the grain-coarsened region (point 1), due to rapid cooling rate compared to the other regions and a larger grain size of austenite, martensite will be formed. Although the HAZ of mild steel consists of both fine and coarse grains, its average grain size is smaller than the coarse columnar grains of the fusion zone.

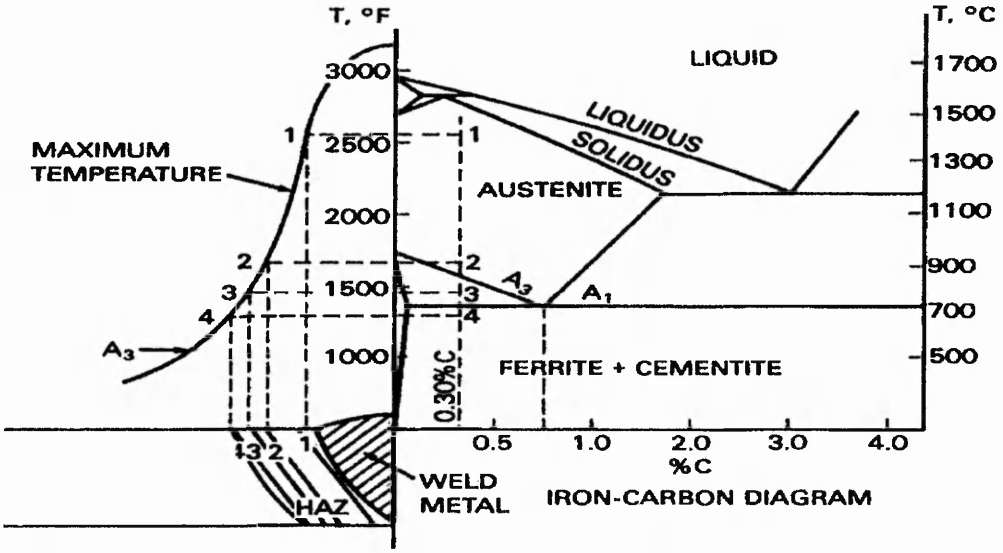

Figure 3.9 – Microstructural changes in the heat-affected zone (Messler 1993)

3.3 Weld testing methods

Various weld-testing methods have been investigated to study the various failure modes of the spot weld.

3.3.1 Loading and failure modes

Defining the centre of the spot weld as the origin of the local coordinate system and the axis that is perpendicular to the surface of the spot weld as the local coordinate x_3, the local coordinates x_1 and x_2 would be in the plane of the mid-surface of the weld and parallel to the surface of the weld. Figure 3.10 shows the local forces (f_1 , f_2 and f_3) and the local moments (m_1 , m_2 and m_3). The in-plane shear forces $f_1$and f_2 can be combined into resultant shear force f_s and the local peel moments m_1 and m_2 can be combined into one local resultant bending moment m_b. After combination there are four generalized loading components applied to each spot weld in its local coordinate system: the shear force f_s, the normal force f_n , the bending moment m_b and the in-plane torque m_t as shown in figure 3.11 (Wung 2001a).

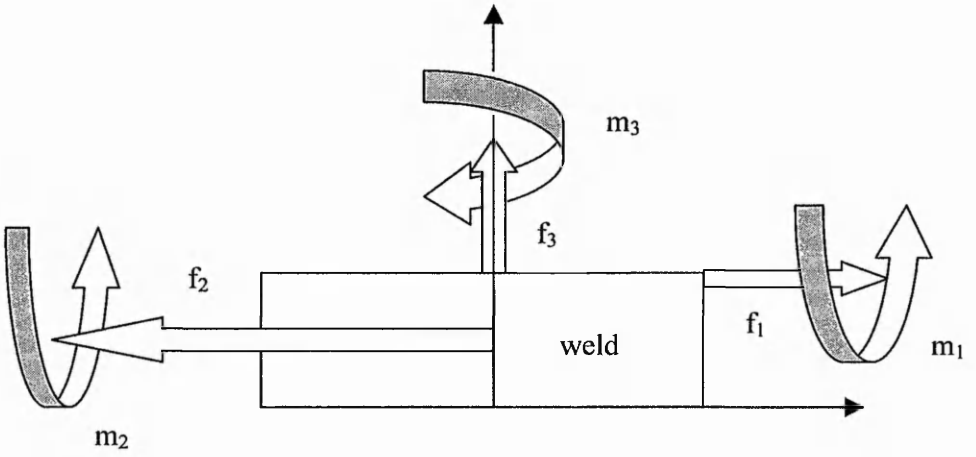

Figure 3.10 – The local forces and moments on a spot weld (Wung 2001a)

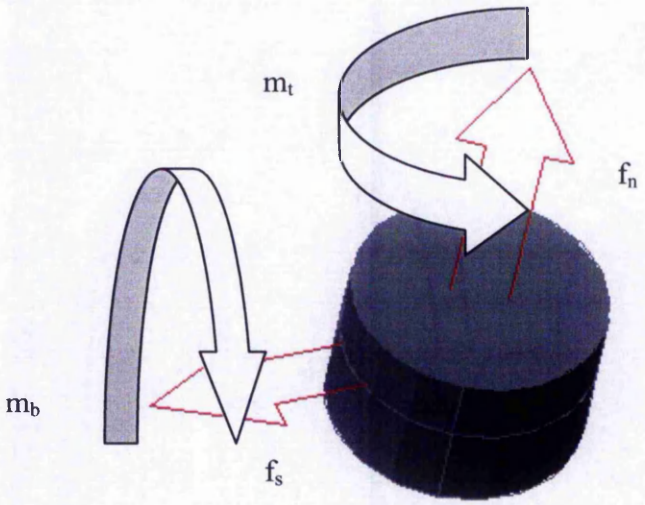

Figure 3.11– The loading components on a spot weld

It is assumed that there exists a criterion that governs the failure of a spot weld under combined static loading as shown in the equation below (Wung, 2001b): -

$$\left(\frac{f_s}{F_s}\right)^{\alpha} + \left(\frac{m_b}{M_b}\right)^{\gamma} + \left(\frac{f_n}{F_n}\right)^{\mu} + \left(\frac{m_t}{M_t}\right)^{\beta} = 1 \quad \text{---------- (3.1)}$$

In this equation, s, b, n, and t represent the four independent failure modes – tensile shear, peel bending, normal pull and in-plane torsion respectively. The denominators represent the spot weld strengths of the four independent failure modes respectively and the numerators represent the applied loads on the corresponding failure modes, respectively. The symbols α, γ, μ and β are constants. For any single loading regardless of the values of the constants, this equation would satisfy the failure conditions as long as the numerator is equal to the denominator. This means that when the applied load reaches the strength of the spot weld, the spot weld will fail for each single mode.

3.3.2 Testing methods for each failure mode

3.3.2.1 Shear test

Figure 3.12 shows the test coupon used to determine the shear strength of a spot weld. The test coupon is prepared such that both the sheets that need to be welded are placed overlapping each other at an equal distance from the edges of both the overlapping sides. According to the British Standards (British Standards 1993), for a sheet thickness of 1mm, the overlap length is 35mm. However this overlap length was found to differ for the same thickness among different professional organisation such as American National Standards Institute (ANSI), American Welding Society (AWS) and International Organization of Standards (ISO) (Zhou et al. 1999). The sheets were pulled apart using the Monsanto tensometer machine as shown in figure 3.13. When the sheets are pulled apart symmetrically along the centre of the weld, the shear force f_s, will cause an in-plane shear failure to occur. However due to this pulling, an out-of-plane warping will also occur causing the sheets of the overlapping part to bend as in figure 3.14. To avoid this, a u-shape guide plate was designed and installed around the spot weld, so that a pure in-plane shear is achieved.

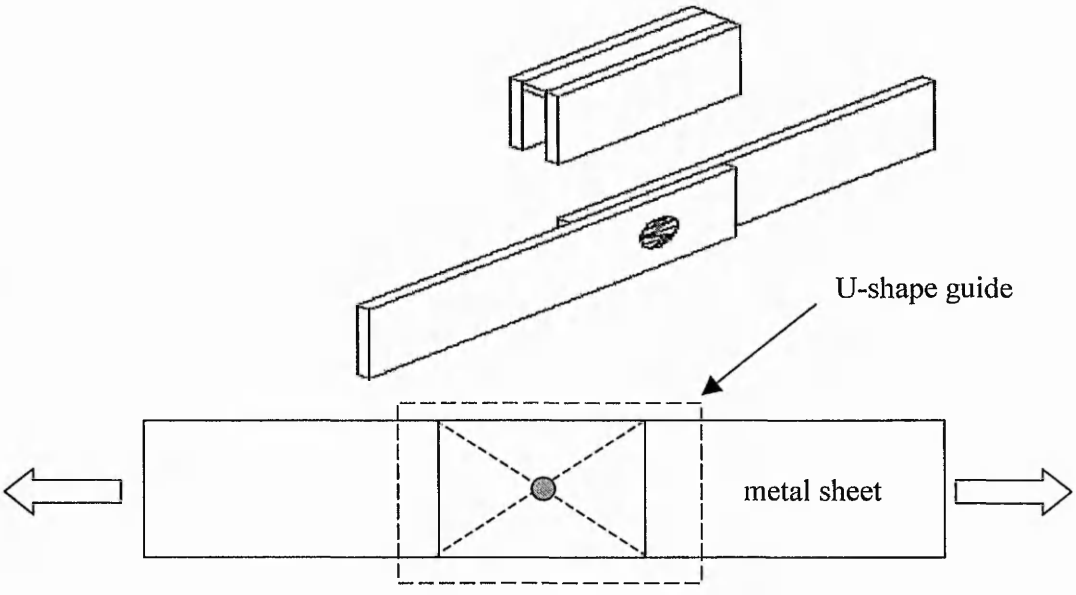

Figure 3.12 - Shear test specimen

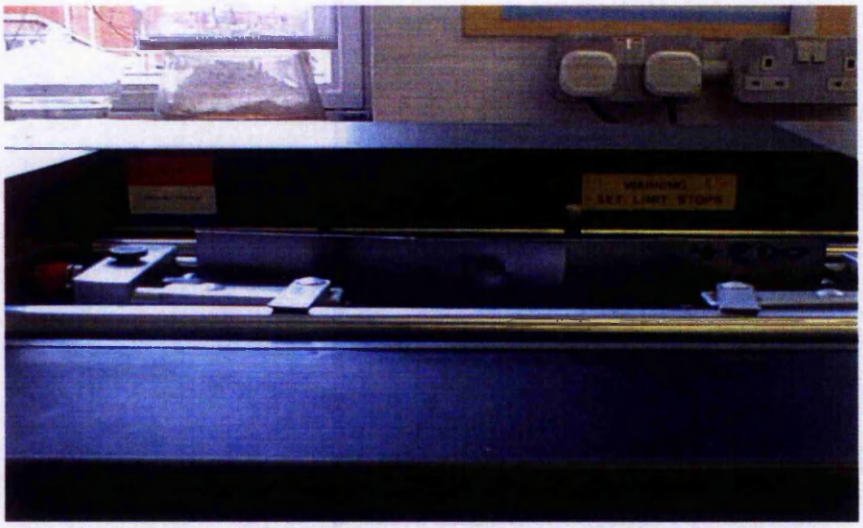

Figure 3.13- The shear test specimen fitted in the Monsanto tensometer machine

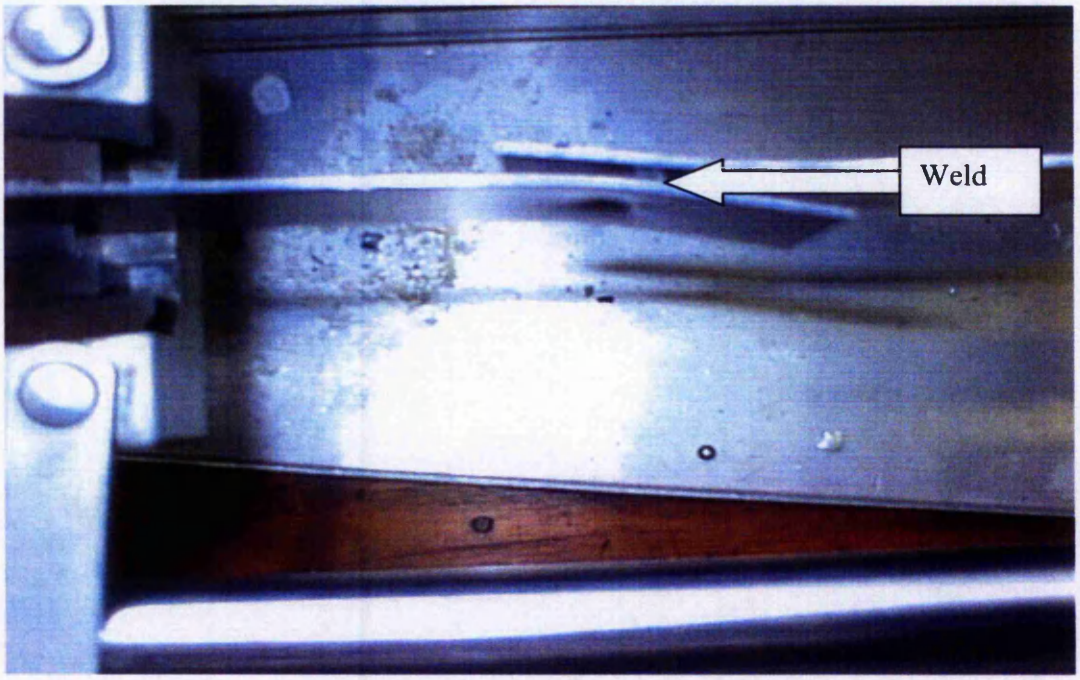

Figure 3.14 – Sheets bending due to out-of-plane warping

3.3.2.2 Peel test

Figure 3.15 shows a triangular coupon used to determine the peel strength of a spot weld. When the test coupon is pulled apart as shown by the white arrows, both the sheets edges will bend losing the right angle between the peeling portion and the pulling portion. To avoid this, 2 triangular blocks were placed at both sides of the peeling portion so that the bending of the pulling portion is constrained and peeling at the weld area due to moment m_b only occurs.

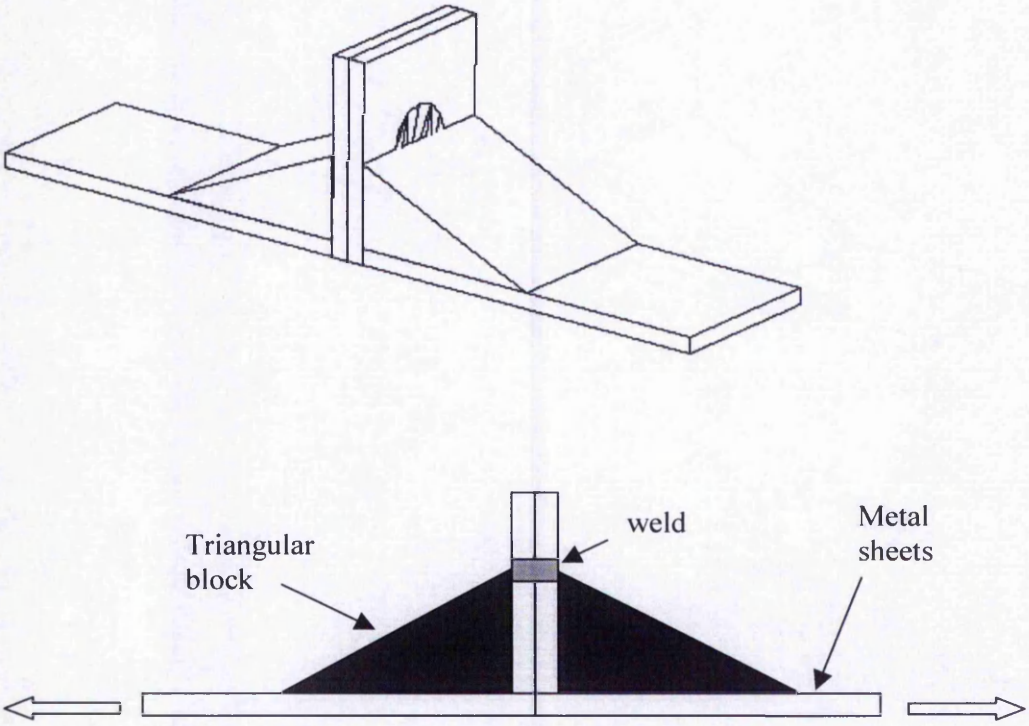

Figure 3.15 - Peel test specimen

3.3.2.3 Normal pull / Cross tension test

A cross-tension test specimen, as shown in figure 3.16, was used for this test. The testing jig designed for this test according to the British Standards (British Standards 1993), as shown in

figure 3.17 enables the pulling force (f_n) to be applied exactly normal to the weld. The edges of the sheets are constrained from bending due to the applied force using washers, which are tightly fixed to the sheet edges by means of nuts and bolts.

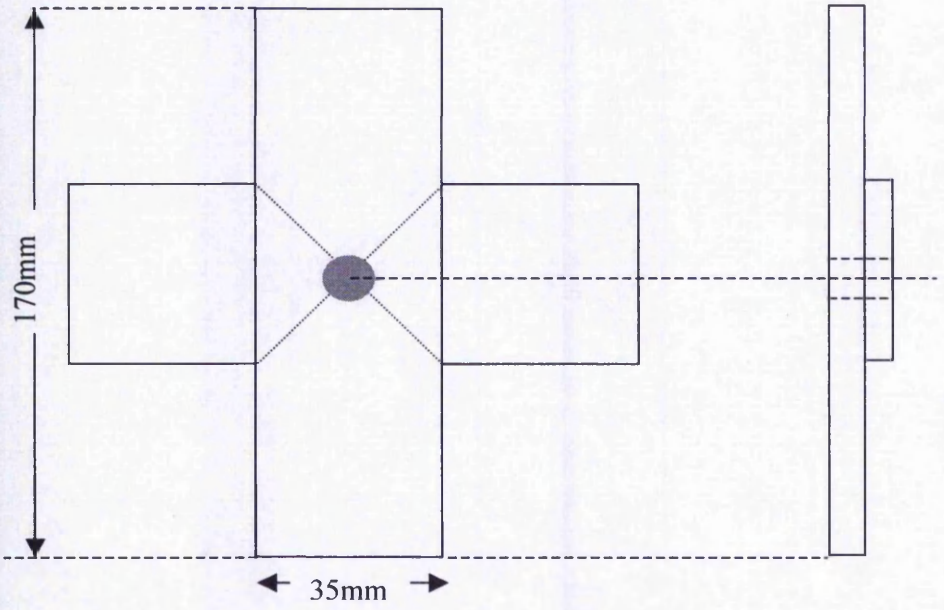

Figure 3.16 – Cross-tension test specimen

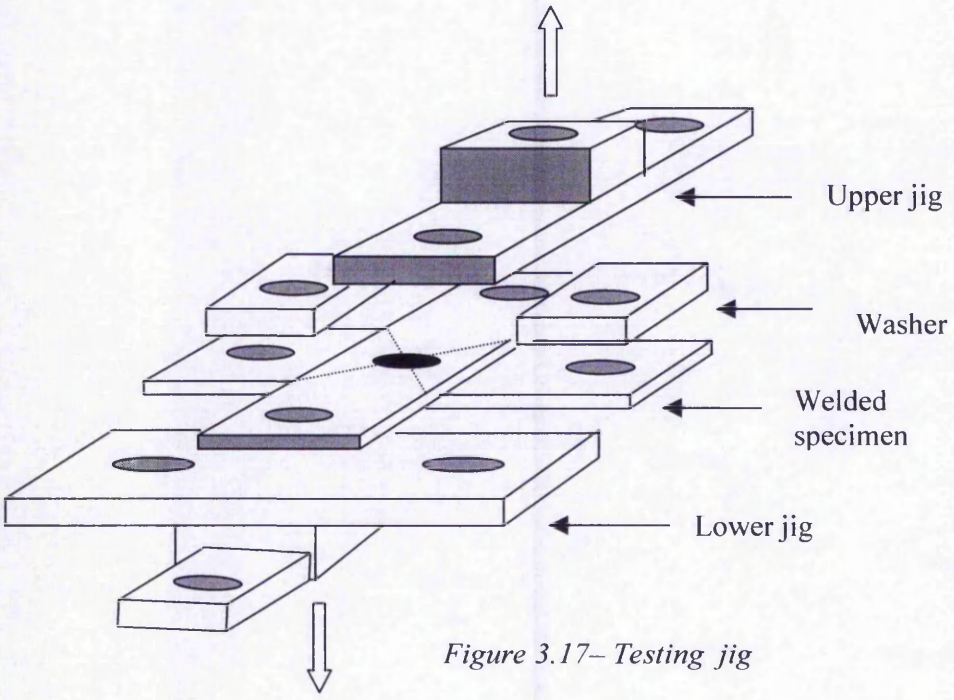

Figure 3.17– Testing jig

Figure 3.18 below shows the cross-tension specimen and the testing jig fitted the testing machine.

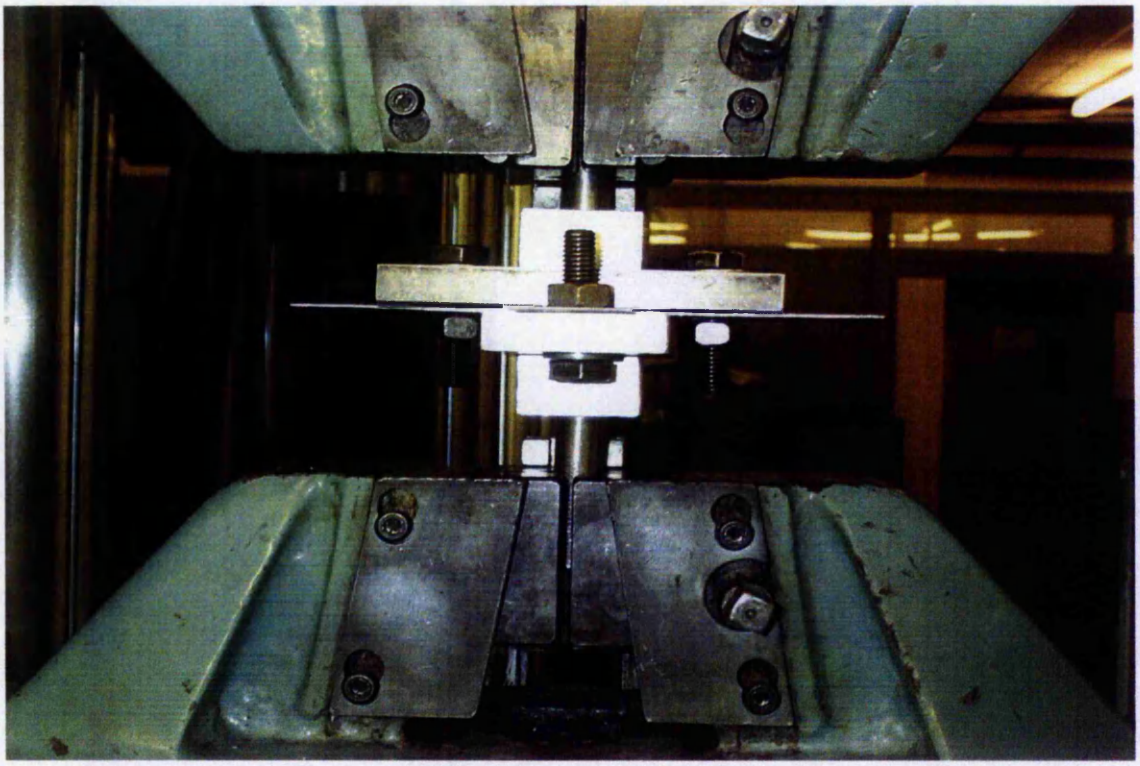

Figure 3.18 – Cross tension testing jig fitted to testing machine (without washers)

3.3.2.4 Rotation test

Wung (Wung 2001a) had used a scissors test coupon to determine the in-plane rotation strength due to an in-plane torque m_t. This testing was not carried out in this research due to the unavailability of suitable testing equipment.

3.3.3 Comparison between the testing methods

The shear test, peel test and normal test were chosen to evaluate the accuracy of each testing method to measure the spot weld strength. As already discussed in section 3.3.1, each of these testing method represents the failure of the spot weld at various planes in the

coordinate system. The two welding schedules as shown in table 3.3 were used in this experiment. The welding schedules were chosen such that a strong weld and a weaker weld will be produced. Electrodes with 5 mm tip diameter and mild steel sheets with 1mm thick were used. 60 welds were made with both the welding schedules with 10 repetitions for each testing method and each welding schedule.

	Current (A)	Weld time (cycle)	Force (kN)
Schedule 1	9000	15	4
Schedule 2	8000	10	4

Table 3.3 – Welding schedules for weld testing methods experiment

3.3.3.1 Results

Table 3.4 shows the summary of the results obtained from this experiment

	Shear test		Normal test		Peel test	
	A.F (kN)	Std.dev	A.F (kN)	Std.dev	A.F (kN)	Std.dev
Schedule 1	6.903	0.156	3.217	0.167	0.961	0.209
Schedule 2	2.921	0.239	1.725	0.219	0.441	0.243

Std.dev – standard deviation A.F – average force

Table 3.4 – Results of the testing methods

The load-elongation diagram obtained for all three testing methods is as shown in figure 3.19 below: -

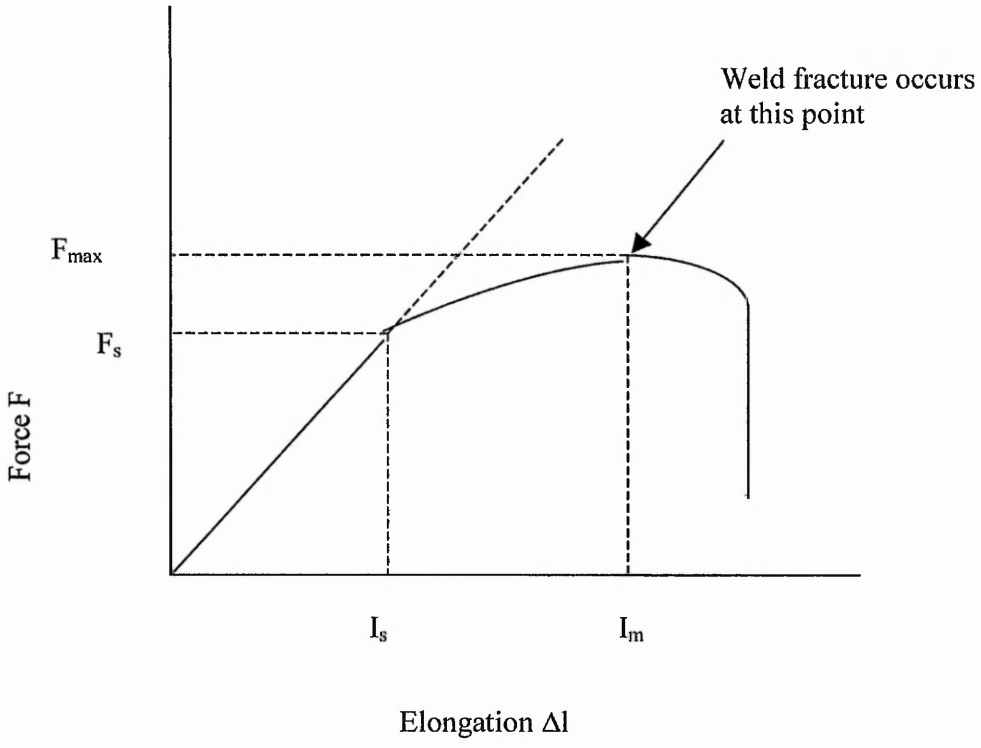

Figure 3.19 – Load-elongation diagram

F_{max} = Maximum force

F_s = Yield force

I_m = Elongation at maximum force

I_s = Elongation at yield force

The F_{max} recorded in these experiments are taken as the maximum strength of the weld as explained in the equation in section 3.3.1.

3.3.2.4 Discussion of the results

The results on the three different testing methods (shear, normal and peel) for two different welding schedules show that shear test gives a higher force value for weld fracture followed by the normal test and finally the peel test. As explained in equation 3.1 in section 3.3.1, the applied load, which causes the weld to fail, is the strength of the weld. The experiment above gives 3 different weld strength values for the same welding schedules due to the fracture of the weld in 3 different planes.

Two different weld failures were noticed during the shear test. The U-shape guide fitted around the weld helped to make sure that only the in-plane shear occurs. When the weld is stronger then the parent material (schedule 1), shearing did not occur in the middle of the weld but around the vicinity of the heat-affected-zone as shown in figure 3.20. A study showed that the metallurgical structure of the weld is maintained before and after the shear test, indicating that no shear deformation occurs at the weld (Wung 2000b). However for a weaker weld (schedule 2), the shearing force causes the weld to fracture at the sheets' interface i.e. middle of the weld.

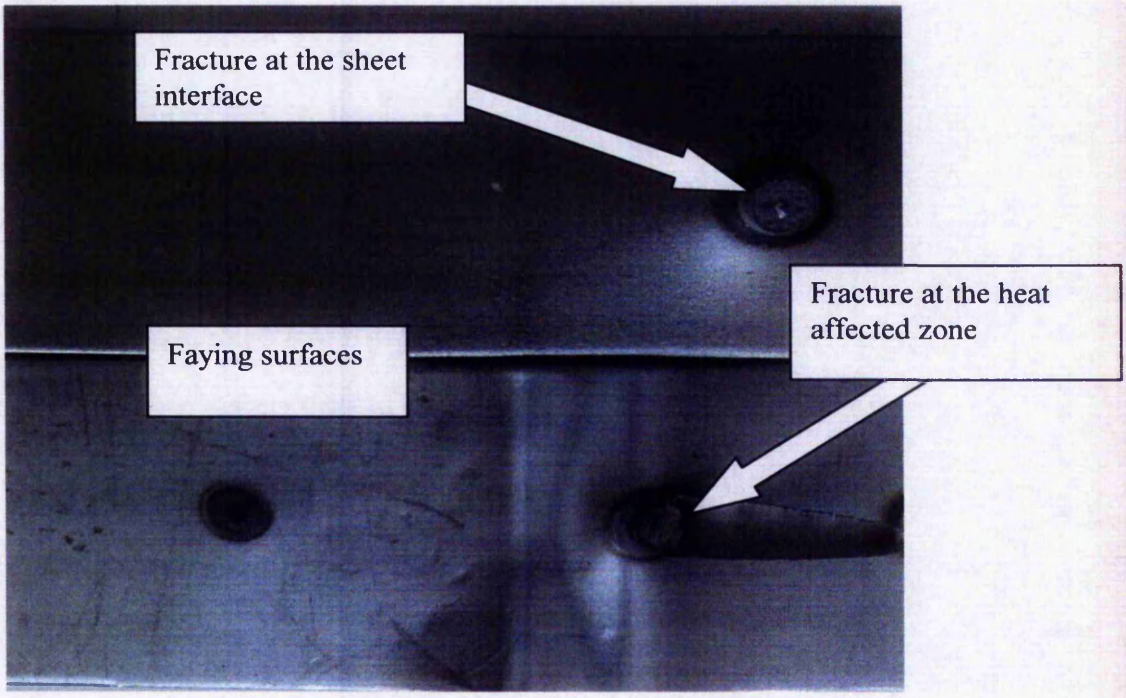

Figure 3.20– Spot weld failures due to shear testing

When the normal force around the spot weld is uniformly distributed, a force will pull the sheets away from each other uniformly. This is the principle of the normal pull test. As for the shear test, two different weld failures were noticed during the normal test. A stronger weld (schedule 1) will cause a weld button to be pulled out due to the normal pull as shown in figure 3.21. The compressive stress around the weld periphery was found to be high due to application of electrode force (Tsai et al. 1999). This highly stressed area will tear off due to shear between the weld area and heat-affected-zone area causing the weld to be pulled out from one sheet, leaving a hole in between the heat-affected-zone of that sheet. The other failure is the radial failure in the middle of the weld at the faying surface due to the weld being weaker than the parent material as shown in figure 3.21.

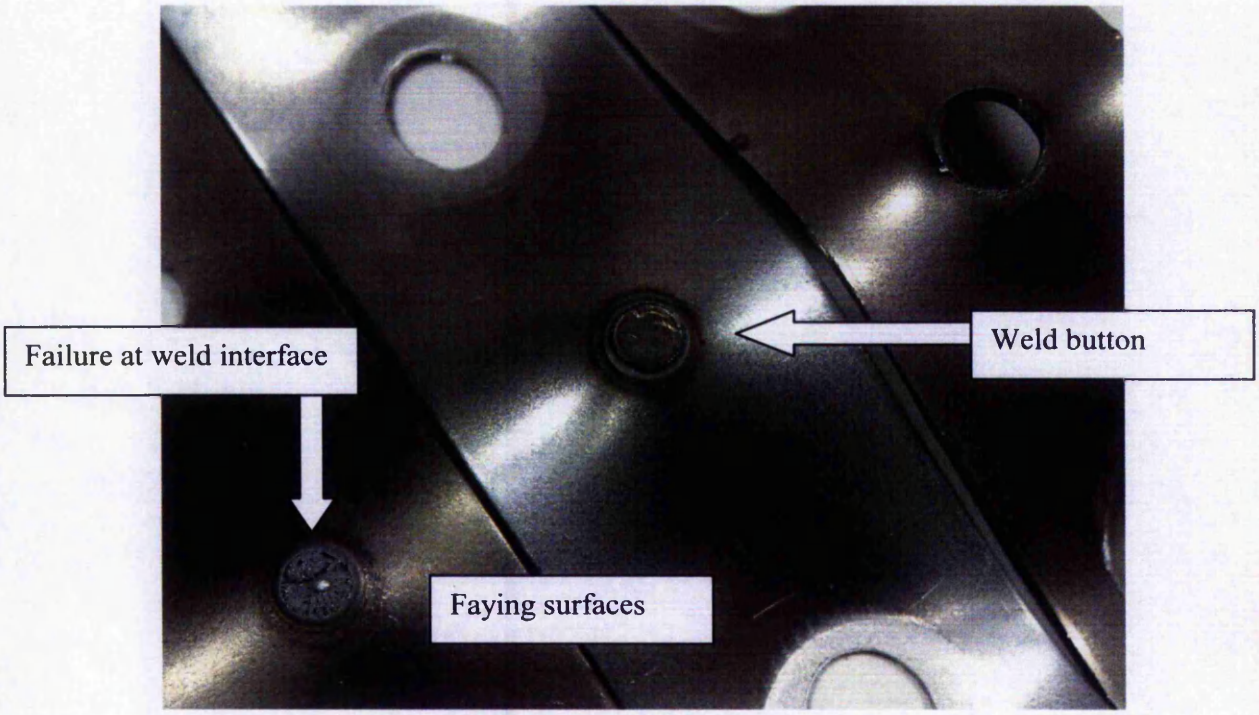

Figure 3.21– Spot weld failures due to normal/cross tension testing

When the normal force around the spot weld is non-uniformly distributed, one side of the weld will experience tension due to the sheets being pulled apart and the other side of the weld

will experience compression since the sheets have been welded together. This phenomenon will cause peeling of the metal sheet to occur from the tension side of the weld to the compression side. Again as for the shear test, tearing was noticed at the heat-affected-zone for weld made from schedule 1. As such, accurate weld diameters are found hard to be measured from peel test specimens (Guendouze 1995). Failure in the middle of the weld was again noticed for the weld made from schedule 2 similar to the other tests.

The failure of weld at the heat-affected-zone points out that the shear test and peel test are not the most reliable method of testing welds. Peel testing is still the preferred method used to check the quality of the weld and to measure the nugget size in some automotive companies (Gould 1987). However peel testing has the drawback of inaccuracy in weld diameter measurement since the failure occurs in the heat-affected-zone. Therefore since normal or cross tension testing has failure occurring around the weld surface rather than the heat-affected-zone, this experiment concludes that normal test would be the reliable weld testing method of all the present existing destructive testing methods.

3.4 Summary of the chapter

The spot welding equipments and the various instruments that will be used in the experiments in the following chapters were introduced in this chapter. This chapter also describes the metallurgical aspects of the 2 zones of the spot weld; the fusion zone and heat-affected-zone. The fusion zone, which is equivalent to the weld, undergoes melting and solidification during welding has a final structure of either a mixture of ferrite-pearlite or bainite or martensite. The heat-affected-zone, which undergoes changes in the microstructure due to the heating during weld cycle without any melting occurring at this zone, has a smaller grain size compared to the final coarse columnar grains of the fusion zone.

Study on the loading and failure of a spot welding indicates that the weld fails due to 4 different loading modes; the shear force f_s, the normal force f_n , the bending moment m_b and the in-plane torque m_t . 3 different tests were developed to study the failure of the spot weld due to shear force, normal force and bending moment. The tests were called shear test, normal or cross tension test and peel test respectively. The experiment on all these 3 different testing methods

shows 3 different weld strengths to be achieved due to the weld fracture occurring at 3 different planes. The result of the experiment indicates that the cross tension or normal test would be the reliable method for testing spot welds because the failure occurs around the weld surface rather than the heat-affected-zone as in case of the shear test and peel test.

Chapter 4

THE SERVO CONTROLLED SPOT WELDING MACHINE – SYSTEM DEVELOPMENT

This chapter deals with the design and manufacturing aspects of the servo spot welding machine. An introduction to the motion control system and explanation on how the system was used to develop the servo controlled spot welding machine will also be given. Finally the developed force control during squeeze cycle and weld cycle together with position control will be discussed.

4.1 Mechanical design and component fabrication

The development of the servo controlled spot welding machine begun by modifying a Stronghold spot welding machine that was used for this investigation. The pneumatic system (section 2.6.2) that actuates the welding electrode on the spot welding machine was removed and replaced by an electrical servo controlled system.

4.1.1 Drawbacks of the pneumatic actuation systems

This modification of the electrode actuating system was undertaken due to overcome the inherent drawbacks in the pneumatic actuating system listed below: -

- Open-loop characteristics of the pneumatic cylinder with no feedback to control cylinder and hence the electrode force. Proportional valves have been used to send analogue signals to vary the air pressure but with little success (Slavick 1999).

- The use of the pneumatic cylinder also meant that the electrode stroke could not be varied without manual set up. Hence the use of the spot welding machine will be limited to only few components or designs.
- The impact of the electrode when it comes in contact with the sheets which needs to be welded could cause damage to the electrode tip and the sheet surface.
- The use of pneumatic cylinders create a noisy environment in the production line

Replacing the pneumatic actuation system with the servo actuation system could solve all the above stated drawbacks of the pneumatic system used to control the electrodes on the spot welding machine. The comparison of the pneumatic system with the electrical servo system is shown in table 4.1 below. The design and fabrication of a servo actuated spot welding machine is presented later in this chapter.

4.1.2 Comparisons between pneumatic welding machine and servo system welding machine

The differences of the pneumatic system and servo system spot welding machine are as below (Slavick 1999): -

	Pneumatic system spot welding machine	Servo system spot welding machine
Force control type	Open loop	Close loop
Ability for quicker force change during welding	No	Yes
Soft touch capability	Yes (add-on equipment required)	Yes
Feedback device	Proximity switch, pressure switch and limit switch	Encoder
Communication rate	>8ms	250μs
Electrode stroke	Fixed	Variable

Table 4.1 – Comparison between the pneumatic system and servo system spot welding machines

4.1.3 Design of the mechanical assembly for the servo actuation system

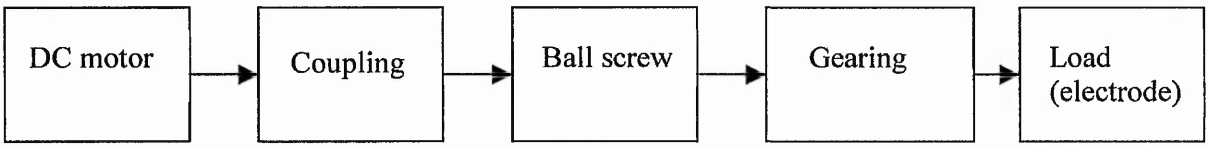

Figure 4.1 – Schematic diagram showing the components in the mechanical assembly of the servo controlled electrode actuation system

Figure 4.1 shows the schematic diagram, which consists of the main components in the assembly of the electrode actuation system in the servo spot welding machine.

A ball screw was used to convert the rotary motion of the servomotor to a linear motion so that the electrode could be actuated up and down. The ball screw assembly consists of two parts: - the screw and a nut as shown in figure 4.2. The ball screw assembly works without direct contact between screw and nut thread. Recirculating balls fill the grooves cut into the screw and nut. The balls are the medium through which the internal and external grooves engage. As the screw spins in a rotary motion, the rolling action of the balls moves the nut in a linear motion. Other than the ability of the ball screw to convert rotary motion to linear motion, the ball screw was also used due to its high efficiency. Ball screw has an efficiency of 90% because of the rolling contact between screw and nut. This rolling contact instead of the sliding contact in the conventional screws reduces friction between the screw and nut hence increases efficiency. The other important reason for using ball screw in this design was also to eliminate backlash. Ball screws have an almost near zero backlash due to the preloading of the balls against the screw grooves. Below are the advantages of the ball screw that was considered in the design of the servo spot welding machine (Anon 2002): -

a) High efficiency – 90%
b) Near zero backlash elimination

c) Low starting torque – due to rolling ball contact, ball screw needs only a small starting force to overcome its starting friction.

d) Less noise during operation

e) Unlike the pneumatic actuators, ball screw used in an actuator has no leakage hence energy saving and also has a good repeatability.

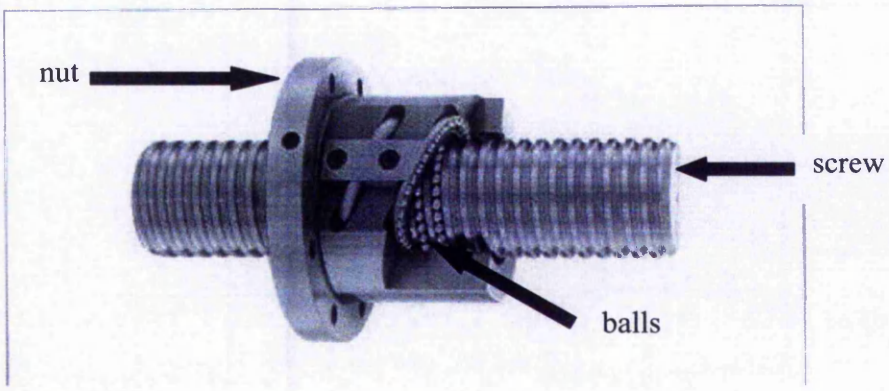

Figure 4.2 – Components of the ball screw (Anon 2002)

Harmonic drive gears where used for speed reduction. Harmonic gear assembly consists of 3 parts: - a) wave generator b) flexspline and c) circular spline as in figure 4.3 (Anon 2000a).

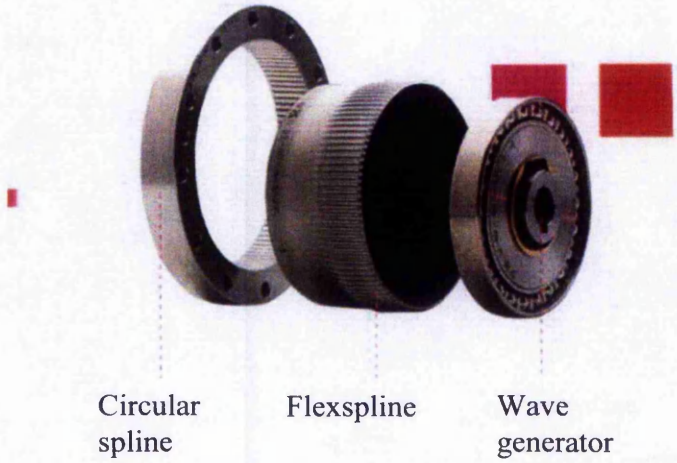

Figure 4.3 – Harmonic drive components (Anon 2000a)

The wave generator is a thin race ball bearing fitted onto an elliptical plug serving as a high efficiency torque converter. The flexspline is a flexible steel cylinder with external teeth and a flanged mounting ring. The circular spline is a solid steel ring with internal teeth.

The harmonic gear was chosen for the design because being a compact component; it simplified the whole design of the mechanical system. The design was found to become quite complicated when other gearing systems like the pulley system or the worm-and-wheel system were considered. The inherent advantages of the harmonic gear are the major reason why this gearing system was chosen. The advantages of this gearing system are as follows: -

a) zero backlash – these gears may operate with essentially zero backlash between mating teeth because of the natural gear preload
b) high efficiency – operating efficiency up to 85%
c) high torque capacity

The ratio of the harmonic gear used in this design is 50:1.

The ram that was connected to the piston rod in the pneumatic system as, explained in section 2.6.2 will be connected to the nut of the ball screw in the new system. The rotation of the ball screw will cause linear movement of the nut that, in turn will move the ram upward and downward depending on the direction of rotation of the ball screw. This movement of the ram will move the moveable electrode towards or away from the fixed electrode. The ball screw is connected to the motor by means of an Oldham flexible coupling. Figure 4.4 shows the mechanical design of the servo spot welding system. A thrust and a deep groove bearing was also used in the design to withstand the backward thrust of the ballscrew due to sheet metal expansion during welding and to reduce friction during rotation of ballscrew. Table 4.2 shows the list of components used in the mechanical design of the servo actuation system and their descriptions.

Component	Description
Ballscrew and nut	A 16mm diameter SKF ballscrew with 5mm lead was used. The dynamic load and static load of the ballscrew are 732kg for 1x 10^6 rev and 1247kg respectively. The nut has got 2 channels for ball rotations.
Thrust and deep grove bearing	A thrust bearing with dynamic and static load capacity of 5070N and 2240N respectively was used. The deep groove bearing used has a dynamic load capacity of 11200N and static load of 12200N
Oldham flexible coupling	A coupling with a torque disc having a breaking torque of 53Nm was used to connect the motor shaft and ball screw
Harmonic drive	Harmonic drive with a gear ratio of 50 was used

Table 4.2 – Components of the mechanical design for the servo actuation system

The design as in figure 4.4 consists of 3 separate housings, which houses all the above stated components. The housing (3) is the cylinder that houses the nut (10), screw (8) and the ram (figure 4.5), which carries the electrode. This cylinder is the weld cylinder in the pneumatic system. The screw is inserted into the ram, which is actually a hollow cylinder. The nut is connected to the ram by means of a sleeve (9). The next housing (2) is fitted to the top of the first housing and connected to the machine by means of 4 threaded bars (6) and nuts. This housing houses the thrust and deep groove bearings (7) and the end of the screw that is fitted through the bearings. The last housing (1) houses the connection of the harmonic drive shaft (5) and screw by means the flexible coupling (4). The assembly of the motor and the harmonic drive is fitted to the top of this housing.

All the three housings are fabricated in steel and the entire fabrication process of the mechanical design was carried out in-house in the department's workshop.

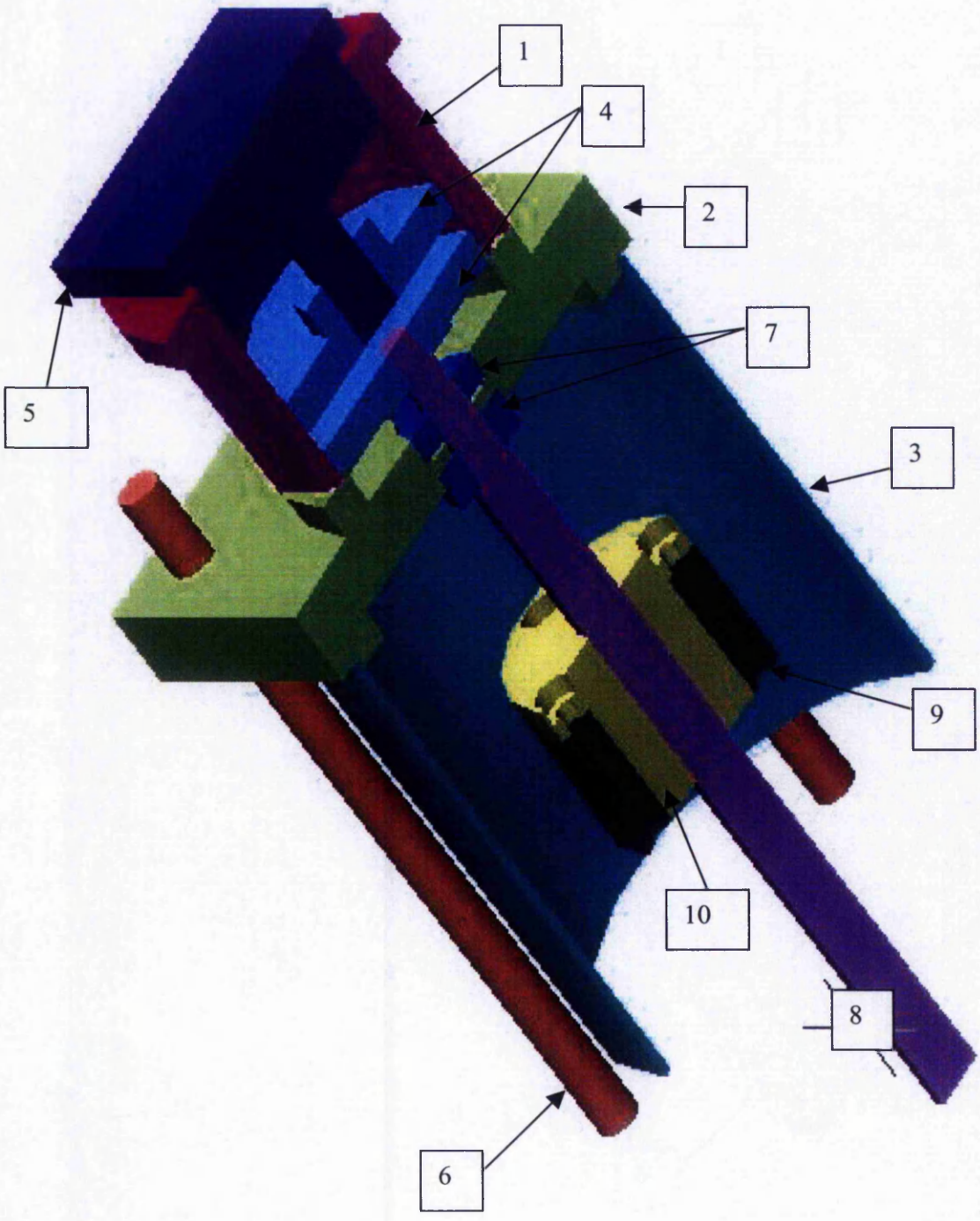

Figure 4.4 - Mechanical design for the servo electrode actuation system

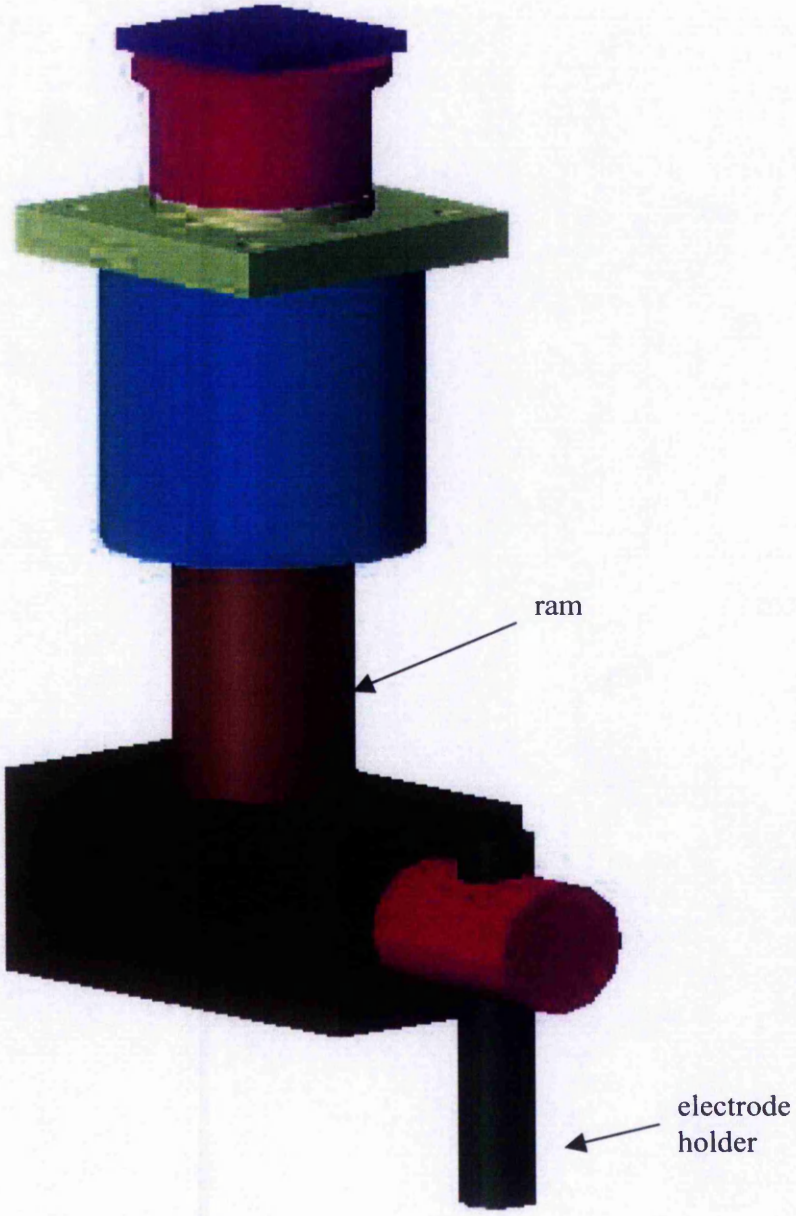

Figure 4.5 – 3-D model of the servo electrode actuation system

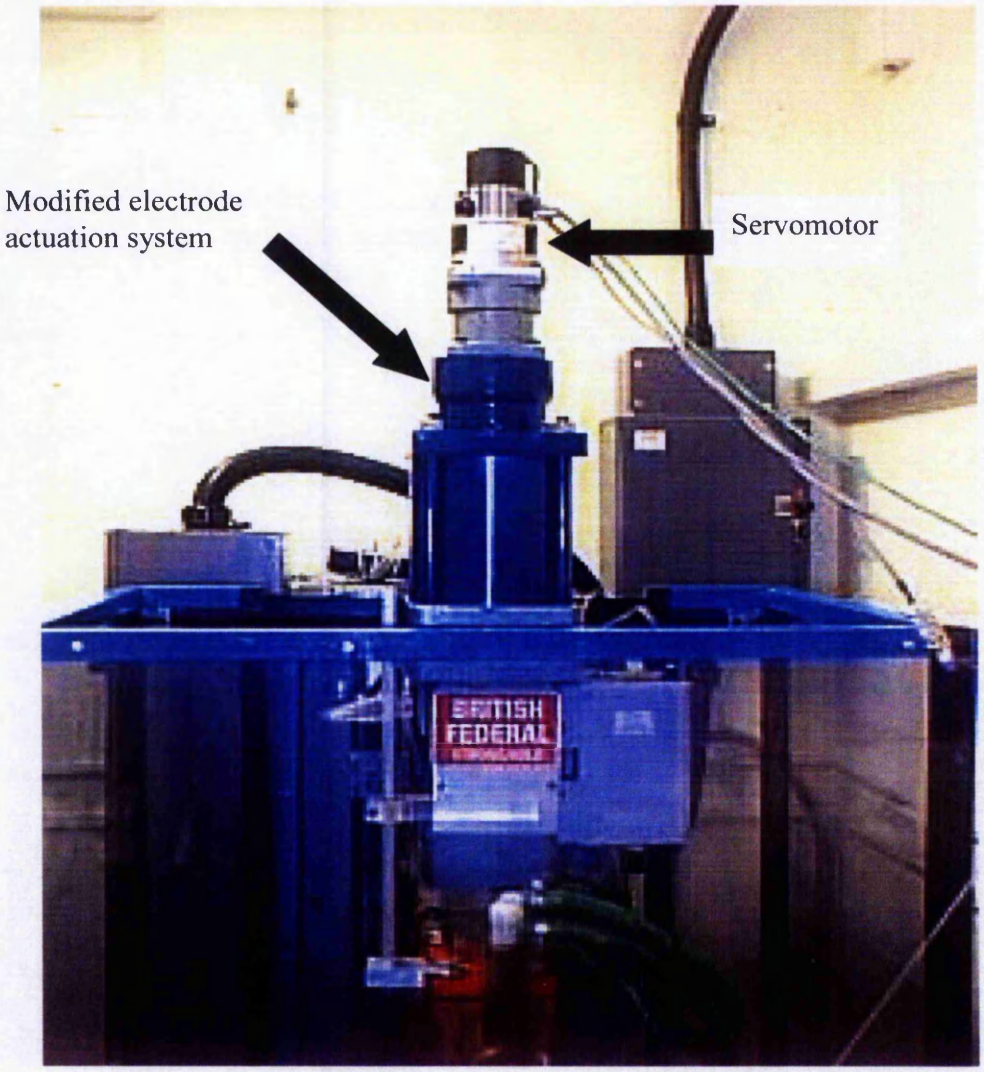

Figure 4.6 – Fabricated housing fixed to machine to develop a servo spot welding machine

Figure 4.6 shows the fabricated housings assembly in blue fixed to the spot welding machine with a servomotor connected at the top of the assembly. Once the mechanical design and fabrication of the newly developed spot welding machine was completed, the functioning of the design to create a closed loop system was developed by means of the motion control technology.

4.2 Introduction to the servo motion control system

Motion control technology is used in industrial processes to move a specific load in a controlled fashion. These systems can use pneumatics, hydraulics or electromechanical actuation technology. Figure 4.7 shows the graphical representation of a typical motion control system (Anon 1993).

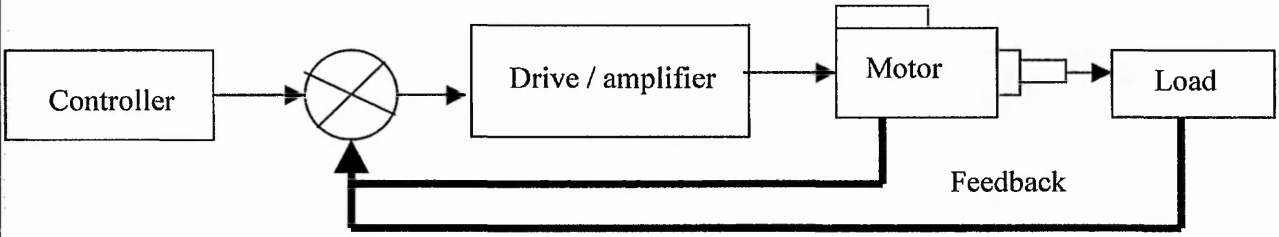

Figure 4.7 – Servo motion control system

The motion control system consists of four important elements: -

a) motor
b) drive / amplifier
c) controller
d) feedback devices

4.2.1 Servomotor

Usually a DC brush motor, a brushless motor or a stepper motor is used in the motion control system. The motor needs to be fitted with some kind of feedback device unless it is a stepper motor.

4.2.2 D rive / amplifier

In t he a mplifier, a n input v oltage u sually in t he range of +/- 1 0volts can represent the desired motor velocity. Full forward velocity is represented by +10V and full reverse velocity by –10V. 0V represents the stationary condition and intermediate voltages represent speeds in proportion to the voltage. The various adjustments needed to tune an analogue drive are usually made by means of potentiometers or computer controls.

4.2.3 Co ntroller

The controllers in the servo system can be developed based on proportional-integral-derivative (PID) control system, programmable logic control (PLC) control system or fuzzy logic/neural network control system. These control systems are normally used to control the position, velocity and/or acceleration of the motor in a certain desired fashion in order to move the attached load. Feedback signals from the load and the motor are sent to the controller where error signals are generated based on the comparison between the feedback and reference signals. These error signals from the controller are then sent as low energy signals in the range of +/- 10V to the amplifier. The amplifier converts these low-energy signals into high-energy signals in order to drive the motor.

4.2.4 Feedback devices

The back of the DC servomotors are normally fitted with feedback devices such as tachometers, optical encoders or resolvers. These feedback devices give the speed and position of the motor as feedbacks to the controllers. For the system developed in this project, the piezoelectric sensor discussed in section 3.1.7 was also used as a feedback device. The signal from the sensor will be sent to the controller to control the motor torque.

4.2.5 Incorporation of the motion control technology to the new system

As mentioned in section 1.11, in order to use the welding force as a control parameter the existing pneumatic system needs to be converted into a closed loop system so that the force can be varied in real time during weld formation. The electrode needs to be actuated at higher speed in order to have a better follow-up with the weld expansion during welding. Therefore the servo motion control system would be used where the electrode will be actuated electrically rather than the conventional pneumatic system in order to achieve a faster movement of the electrode and to investigate the possibility of achieving a better electrode follow-up with weld expansion.

4.2.6 The servo control system components

Referring to figure 4.7, the load in this case would be exerted by the electrode, which is actuated by means of the motor. The servo system was developed using a 3000rpm DC brushed servomotor and Harmonic Drive's DC servo amplifier (HS-250-3). The motor is fitted with an incremental encoder with a resolution of 2000 pulses per revolution. The optical encoder generates a pulse for a given increment of shaft rotation. Total shaft angular rotation is determined by counting the encoder output pulses.

Initially the NextMove motion controller (Anon 1999) was used to drive the servomotor and develop the servo-loop. The NextMove is a PC bus motion controller with a 32bit digital signal processor (DSP) from Texas Instruments. This motion controller card is an industrial standard architecture (ISA) card with 8 axes of control – four closed loop servo and four stepper motors. The +/- 10V signal to drive the servomotor was supplied from the card to the amplifier through a break-out board. The encoder signal from the servomotor is also sent as a feedback signal to the controller through the same break-out board. The figure 4.8 shows the schematic diagram of the servo system connections.

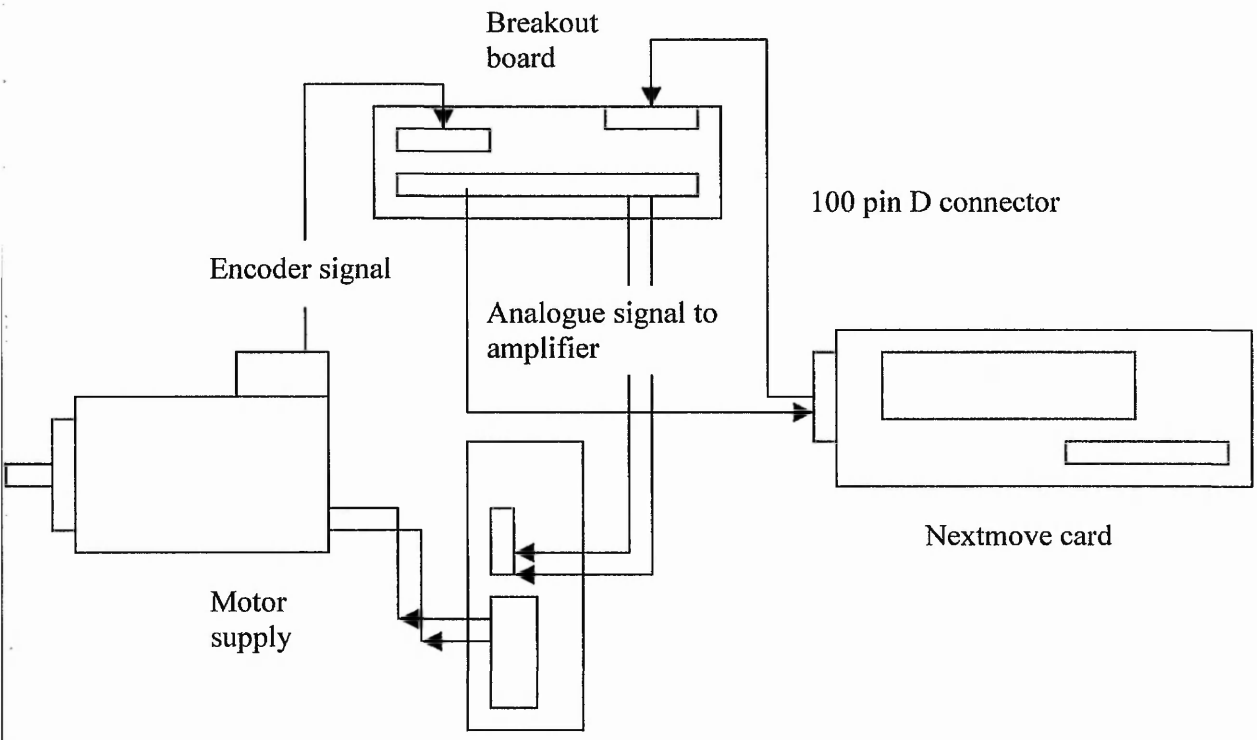

Figure 4.8 – Servo system connections using the NextMove motion controller

Mint programming language (Anon 1999) was used to program motion profiles to the NextMove card in order to drive the motor. The Mint software can be used for position control, speed control and torque control. Integrated software 'oscilloscope' with the NextMove workbench acquires and plots motion profiles in real time for commissioning of the servo system. Some of the important MINT programming keywords used to create motions are as follows: -

1) JOG – provides straightforward speed control of an axis. If JOG = 30, the motor will jog at 30 revs/sec.

2) MOVEA and MOVER - provides absolute and incremental positional movements respectively. MOVEA = 200:GO will cause the controller to move the axis to an absolute

position of 200 counts from zero. MOVER = 200:GO will move the axis further 200 counts relative to the current position make total movement of 400 counts.

3) SPEED – set the slew speed of positional moves. If SPEED = 20 MOVE = 200, the motor will have a constant speed of 20units/sec for 200 positional counts.

4) ACCEL and DECEL – set the acceleration and deceleration rate of an axis. If SCALE = 2000 ACCEL = 500, the acceleration rate will be 500 x 2000 counts/sec^2. Similarly if DECEL = 500, the deceleration rate will be 500 x 2000 counts/sec^2.

The control system can be tuned by changing the values of the system gains like proportional gain, derivative gain and integral gain. The servo loop time is 2ms.

Even though the NextMove has the ability to create motion profiles, the card that was used was very old and does not support some of these additional features. The cost to upgrade the card was found to be very expensive and time consuming. Therefore using digital-to-analogue converter card (DAC) to supply current to the motor, an encoder card to read the encoder pulses and a computer program based servo motion control system was looked at as another alternative.

Computerboard's DAC card (CIO-DAS1602) was used to drive the motor by sending analogue signal through a breakout board to the amplifier and finally to the motor as in the case of the NextMove motion controller. A computer program written in C was used to send digital signals where any given digital value will be converted to the equivalent current value and sent through the amplifier to drive the motor. The digital values of the board have a range from 0 to 4095. The output voltage range can be set to bipolar (± 10V, ± 5 V, ± 2.5V or ± 1.25V) or unipolar (0-10V, 0-5V, 0-2.5V or 0-1.25V). If output range is set as bipolar ±10V, 0 will be equivalent to –10V, 2048 will be equivalent to 0V and 4095 will be equivalent to = +10V. If output range is set as bipolar ±5V, 0 will be equivalent to –5V, 2048 will be equivalent to 0V and 4095 will be equivalent to = +5V. Similarly is unipolar 10V is selected, 0 will be equivalent 0V, 2048 will be equivalent to 5V and 4095 will be equivalent to 10V. All the intermediate digital

values will be converted to their equivalent voltage values based on these conversions. Figure 4.9 shows the digital values and their equivalent voltages for bipolar ± 10V setting.

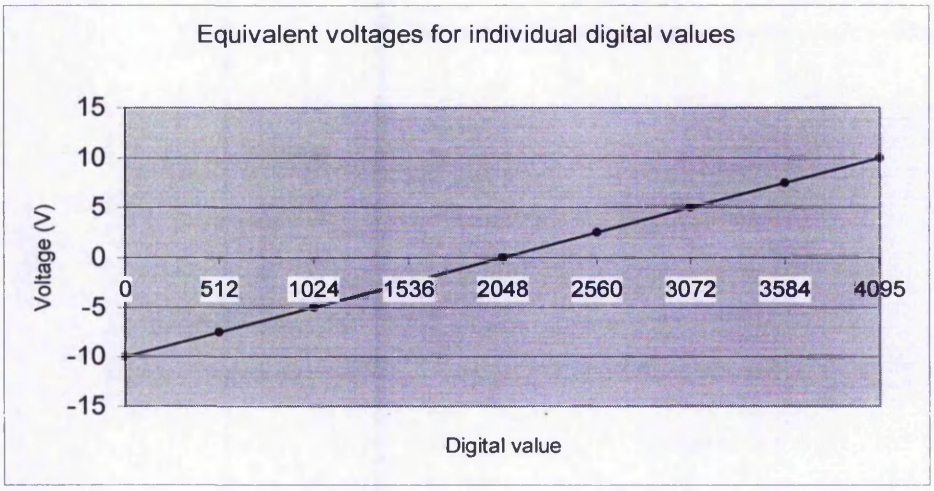

Figure 4.9– Digital values and their equivalent voltages values for ±10V output setting

Deva Electronic Controls Ltd's 3-axis incremental encoder interface card (DEVA001) was used to read the encoder pulses. The encoder card is based around the Texas THCT12316 chip which may be programmed to operate in any of the following modes: - a) incremental encoder position measurement, b) up/down counter, c) pulse width measurement or d) frequency measurement (Anon 1997). Since there was noise disturbance when the motor is running at a certain speed, which caused the encoder signal could not be read, a filtering circuit had to be made to filter this unwanted noise. A 74LS14 Smitth trigger chip with 600pF capacitors connected in series at the input and output of the chip for both channels A and B of the encoder signal enables the noise to be filtered out and a 'clean' pulse to be sent to the encoder card. This was clarified by connecting the outputs from the channels to an oscilloscope to view the encoder pulses that are sent to the card.

A proportional-integral-derivative (PID) based control system was developed using Borland C program. Among all kinds of feedback controllers, PID controller is the most widely used, due to its simplicity and effectiveness (Sun 2001). The controller is based on the equation:-

$$c(t) = K_p . e + K_I \int_0^t e\,dt + K_D . de/dt \text{ ----------(4.1)}$$

where K_P , K_I and K_D are the proportional , integral and derivative gains respectively, e is the error signal and c is the output of the system as a function of time, t .

The proportional gain gives the output signal of the system based on the error signal. The larger the proportional gain, the larger the output signal caused by the error signal. This usually improves the response speed of the system i.e. smaller rise time (Dorf 1995). A larger proportional gain also reduces the steady state error. However, a larger proportional gain increases the overshoot. If the gain is too large, it might also cause instability of system.

The proportional gain itself cannot eliminate the steady state error. The integral gain is introduced to eliminate the steady-state error, with the proper selection of the gain. It does so by accumulating the error over a certain period of time (Kuo 1995).

The derivative gain responds to the rate of change of the error. It can be viewed as additional damping to the system. It reduces overshoot and slows down the initial response of the system. However, it has no effect on the steady state error (Kuo 1995).

This developed PID control system with all the other components mentioned above forms the servo system of the servo spot welding machine. The servo system was then used to create the position control and electrode force control during squeeze and weld cycles. These would be discussed in the following sections.

4.3 The control system

Two types of control systems were developed for the servo spot welding machine; force control system and position control system. The force control system consists of force control during squeeze cycle and force control during weld cycle. The position control was used only to

bring the electrode from the home position to a preset position closer to the sheet metal before the force control takes over. Figure 4.10 shows the servo control system connection of the newly developed spot welding machine.

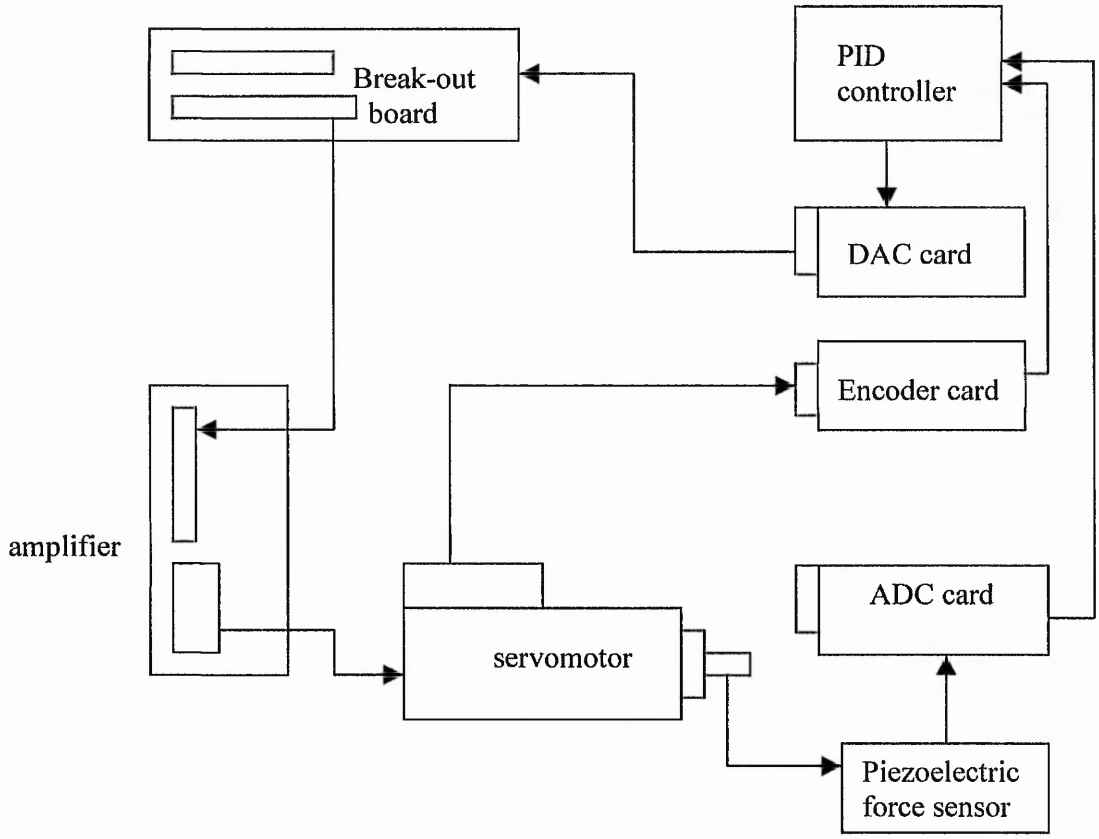

Figure 4.10 – Schematic diagram of the servo control system

The PID controller will calculate the output signal needed to drive the servomotor based on the input signal from either the encoder or the piezoelectric force sensor, and this output signal, which is in the form of digital value, will be converted to the equivalent voltage value by the digital-to-analogue converter (DAC) card. This voltage will be sent to the Harmonic Drive's servo amplifier through a break-out board that in turn will drive the servomotor. The feedback signals that can either be the incremental encoder signal or the force signal depending on the type of control will be sent through the encoder card or the analogue-to-digital converter (ADC) card respectively to the PID controller. A software timer interrupt was used to set the servo loop to

either 5ms or 10ms. Appendix A gives the experiment carried out to test the software timer interrupt.

4.3.1 Position Control

A proportional-integral-derivative (PID) position control was developed to drive the electrode from a home position to a preset position closer to the metal sheets, which are to be welded before the force control during squeeze cycle starts. As already mentioned in sections 4.1.3 and 4.2.5, the resolution of the encoder used in the servo system is 2000 pulses/rev and the ballscrew pitch is 5mm/rev. Also the gear ratio was also given as 50. Therefore for each revolution of the motor shaft, the encoder will generate 2000 pulses. However with a gear ratio of 50, the shaft of the harmonic drive will rotate 1 revolution for each 100000 pulses from the encoder. The relationship is as follows: -

1 revolution of motor shaft = 2000 pulses (encoder); for gear ratio of 50:-
50 revolution of motor shaft = 100000 pulses (encoder) = 1 revolution of harmonic gear
therefore when harmonic drive shaft is coupled to the ballscrew: -
1 revolution of harmonic gear = 100000 pulses (encoder) = 5mm linear movement of nut

The control loop is generated every 5ms by the software timer interrupt. Five milliseconds control loop time was chosen because this is the minimum time required by the control system to receive the input signal from the encoder, go through the control algorithm, output the required current to the motor and get ready for the next interrupt to occur. Any time lower than this causes the whole system to 'crash' due to the inability of the system to cope with the faster interrupt time. The desired distance that the electrode needs to move is specified by means of total encoder pulses. The Deva encoder interface card that was explained in section 4.2.6 counts the encoder pulses and is read by using a computer program. For example if the electrode needs to move 30mm from home position downward towards the metal sheets, the desired position (P_D) is given as (30/5)*100000 = 600000 encoder pulses. Whenever the interrupt is generated, the current encoder position (P) is read and the error that is equivalent to ($P_D - P$) is computed. The change in encoder position for every 5ms, dP/dt and integration of the error with time $\int e.dt$ were also

computed. These terms were multiplied with the proportional, derivative and integral terms respectively and added together to calculate the change in the digital value.

This calculated change in digital value is then used to compute the new motor current value, which will be used to drive the motor to the desired position. The encoder position is measured to determine if the position is within the preset threshold. If the encoder position is outside of the threshold, the control wait for the next interrupt and the whole control routine mentioned above is repeated. However if the encoder position is within the threshold, the interrupt is stopped and the control loop is terminated. Figure 4.11 shows the position control flowchart as discussed above.

4.3.2 Force control during squeeze cycle

The squeeze cycle is the term used in the pneumatic system for the time taken for the clamping force to attain the preset force before welding occurs. The time for the squeeze cycle is normally programmed arbitrarily by the operator depending on experience or previous records. An incorrect squeeze time setting can affect the weld quality to a certain extent. If the squeeze time is too short, electrode force will be too low at the beginning of the heat cycle, causing metal expulsion, poor surface appearance and low electrode life. If the squeeze time is too long, fewer welds will be produced for a certain production period (Hirsch 1998). The inherent open-loop characteristic of the pneumatic system causes the force at the electrode tip to be an immeasurable parameter. Leakage in the airline system or friction in the pneumatic system would cause the required force at the electrode tip not to be attained before the squeeze time finishes and the weld cycle starts. To avoid this problem, a differential pressure transducer, which measures the difference in air pressure at the top and bottom of the cylinder or an electronic air regulator were used to start the weld only when the maximum force had been attained (Hirsch 1993). However the squeeze time recommended for a good quality weld in a pneumatic system is between 0.4sec (20 cycles) to 0.6sec (30 cycle)(Anon 2000b). With the servo system, the same amount of forces can be attained in less than 0.4sec as reported by Yagi(2002). This would cause the time needed to make a weld to reduce which in turn would reduce production time as mentioned in section 1.3.

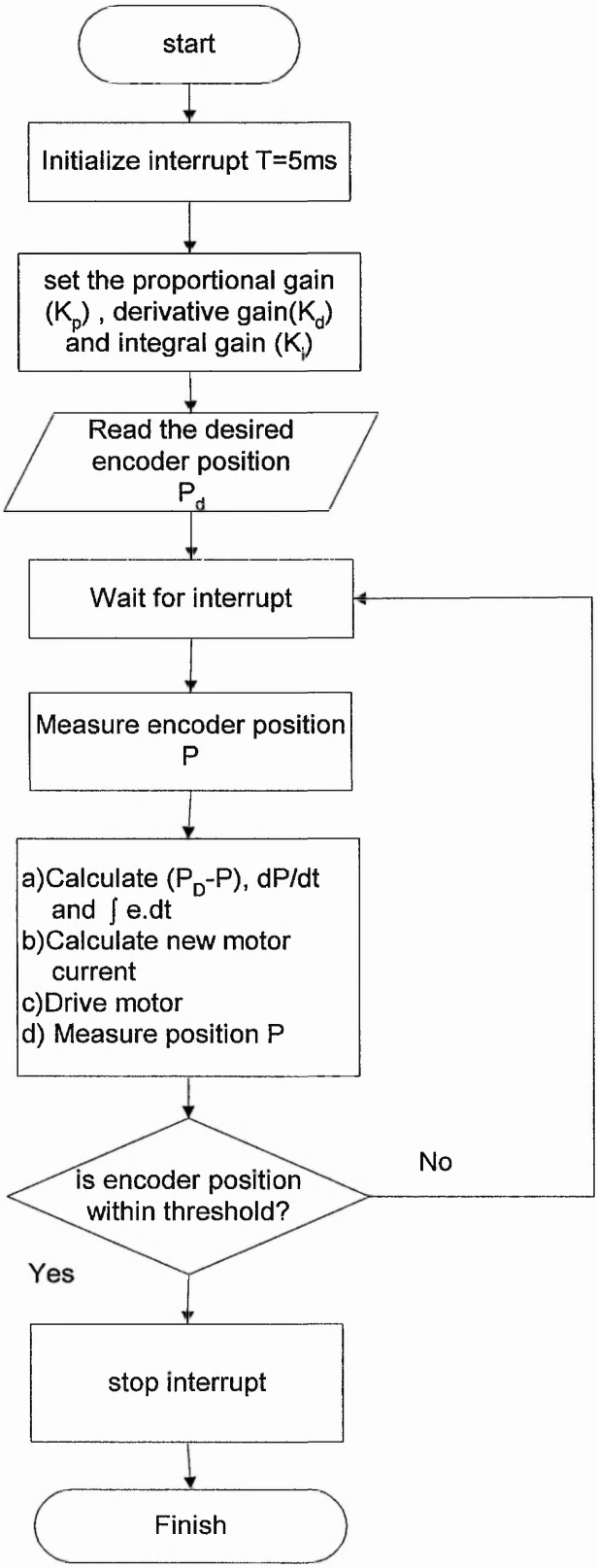

Figure 4.11 – Flowchart of the position control

Bringing the motor to a stall condition generates the clamping force during squeeze cycle. The force control during squeeze cycle for the servo spot welding machine was developed based on the feedback signal from the piezoelectric sensor, which was attached to the lower arm of the machine. The control loop occurs every 5ms, which is governed by the software timer interrupt. Five milliseconds control loop time was chosen because this is the minimum time required by the control system to receive the input signal from the piezoelectric sensor, go through the control algorithm, output the required current to the motor and get ready for the next interrupt to occur. Figure 4.12 shows the flowchart of the squeeze cycle control.

The required force (F_d) is given at the beginning of the control loop. At every interrupt event the force (F) from the piezoelectric sensor is read. The error, which is the difference between desired force and current force ($F_d - F$) and the rate of change in force (dF/dt) will be calculated. These two values are multiplied with the proportional gain (K_p) and derivative gain(K_d) respectively to calculate the change in digital value . In order to increase the clamping force, the digital value needs to be reduced. Reduction in digital value would increase the applied current for motor rotation because the voltage that is sent to the amplifier is increased as shown in figure 4.8. Hence the change in digital value will be subtracted from the current digital value to increase the current supplied to the motor and also the force during squeeze time. The force is measured again to check if the desired force is achieved. If the force is not attained, the control loop will wait for the next interrupt to be generated and the whole control routine mentioned above is repeated. If the force value is achieved, the interrupt is stopped and the control loop is terminated.

Till this stage, the servo system is acting similar to the conventional pneumatic system where the required squeeze force is applied during the spot welding squeeze cycle in both the systems. However as already been described, the pneumatic system does not have the ability to control the forging force during the weld cycle. The change in the forging force during weld cycle for the pneumatic system is process dependent. With the use of the servo system the following force control in the next section (section 4.3.3) will be used to control the forging force during weld cycle. In order to reproduce the welding process of the conventional pneumatic system with the use of this servo system, a condition called the electrode clamping force (ECF) condition was created.

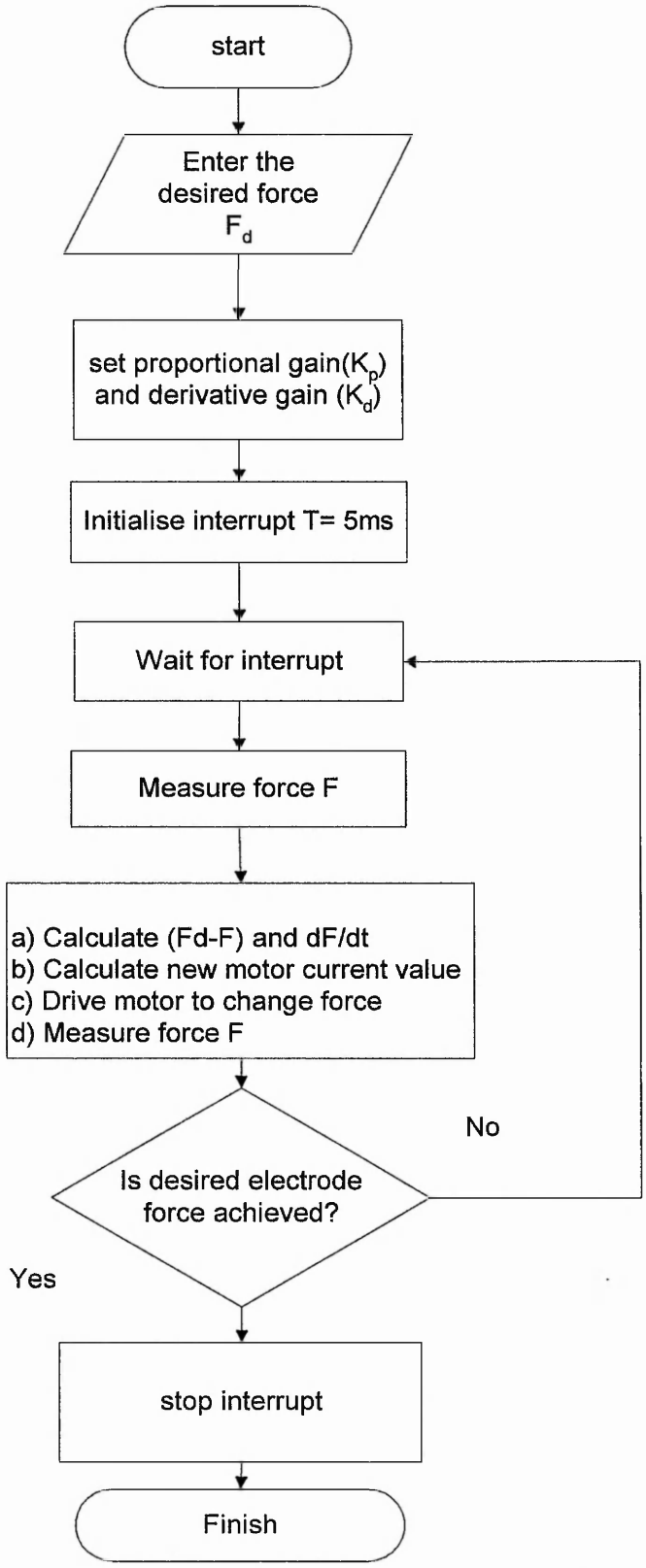

Figure 4.12 – Flowchart for the force control during squeeze cycle

The squeeze force control described in this section will be used to apply the required squeeze force during the ECF condition but the forging force control during weld cycle will not be applied. The change in forging force during the ECF condition will be process dependent as in the case of the pneumatic system.

4.3.3 Force control during weld cycle

The ability of the servo-controlled system to have a better follow-up with weld expansion during welding compared to the pneumatic system, allows the force to be changed dynamically during the process. The force control during welding was developed to enable the electrode to vary the applied force during welding based on a given force profile. The supplied force profile consists of the desired force values for every 10ms for the entire welding period. This interrupt based system would control the current supplied, to change the motor torque to this desired force every 10ms i.e. for every half cycle of the total weld time.

Figure 4.13 shows the force control structure during weld cycle. The control structure starts with the initialization of the interrupt and setting of the interrupt counter to 0. When the 10ms software timer interrupt is generated, a 400-iteration loop is initiated. The time for 400 iterations, measured using the Zen Timer [Online] (http://archive.devx.com), was found to be 8ms before the next interrupt is generated at the end of every 10ms. Within the 8ms, computation will be carried out to bring the measured force to/closer to the desired force in the profile. Since the card has a sampling rate of 10MHz, this 400 iteration was within the capability of the system to change the force according to the desired force.

Within the 400 iterations, are two control loops, which will increase or reduce electrode force. During every iteration, force (F) is measured by means of the piezoelectric sensor. This force is compared with the desired force ($F_d(t)$) in the force profile for the respective time and the error is calculated. If the error is positive (measured force less than desired force) the control loop which, increases motor torque is executed to increase the force and if the error is negative (measured force greater than desired force) the loop which reduces motor torque is executed to reduce the force. Even if computation is done within the 400 iterations , current to the motor is

only sent every 5 iterations (0.1ms). The inertia of the motor and the friction in the whole system might affect the ability of the motor to react for each 400 iterations. Hence a delay of 5 iterations was given for the motor torque to be changed depending on the supplied current before the control system sends the next current signal to the motor.

During the 400 iteration times, the electrode force is brought closer to the desired force before the control comes out of the loop and wait for the next interrupt to be generated. When the interrupt is generated, the interrupt counter is incremented by one and control loops undergo 400 iterations again. However when the interrupt counter becomes N/10, where N is the total weld time is ms, the interrupt is stopped and control loop is terminated.

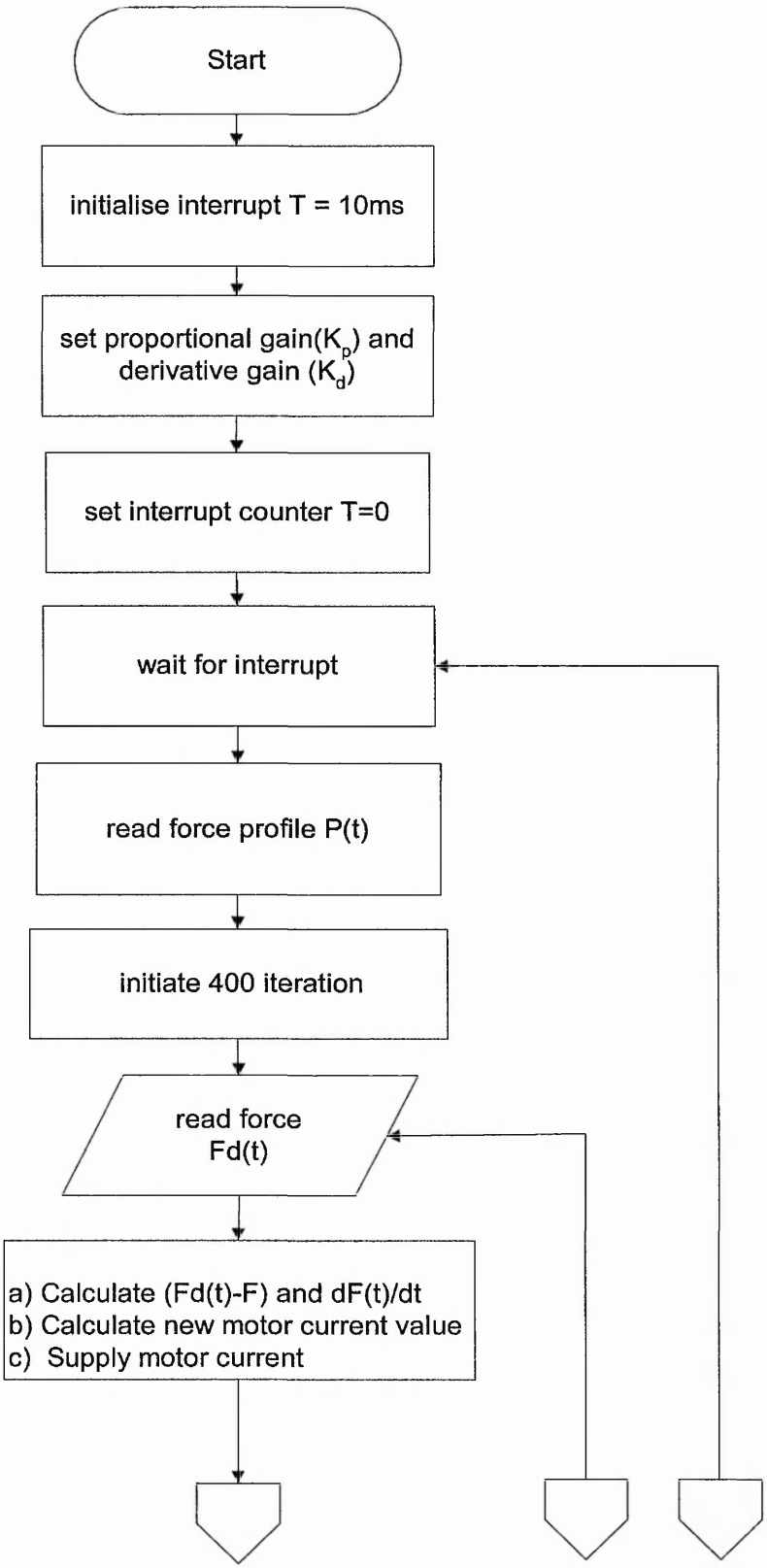
Start
initialise interrupt T = 10ms
set proportional gain(K_p) and derivative gain (K_d)
set interrupt counter T=0
wait for interrupt
read force profile P(t)
initiate 400 iteration
read force Fd(t)
a) Calculate (Fd(t)-F) and dF(t)/dt
b) Calculate new motor current value
c) Supply motor current

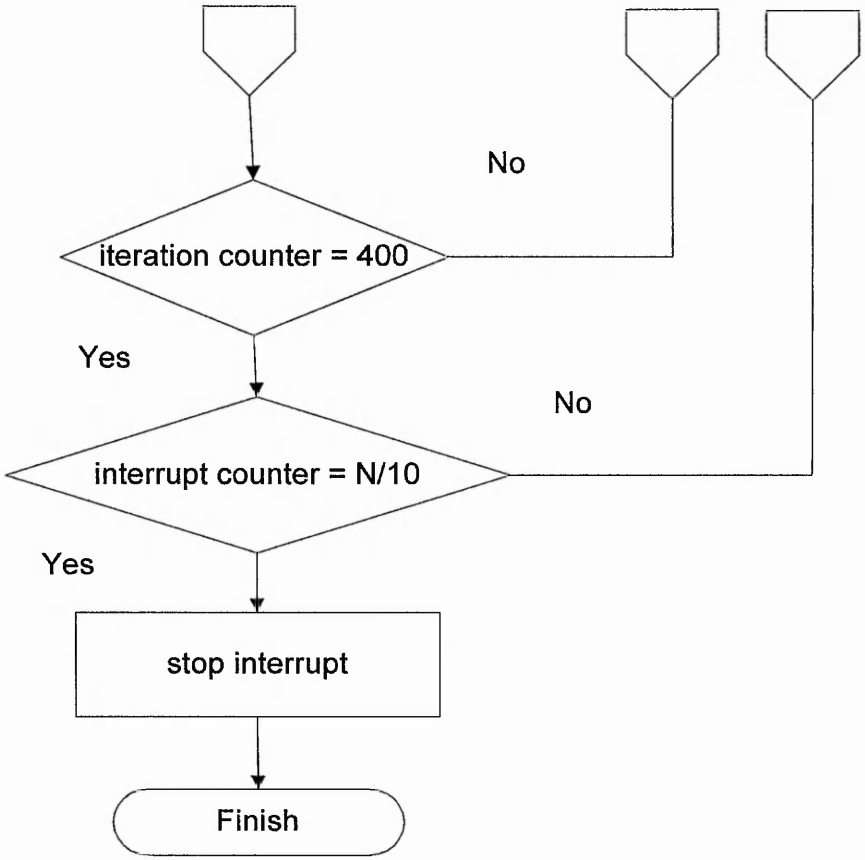

Figure 4.13 – Flowchart for force control during weld cycle

4.4 Summary of chapter

The development of the servo actuated spot welding machine is presented in this chapter. An introduction to the servo motion control system was given and the servo system components for the spot-welding machine were explained. Details on the mechanical design and fabrication of the mechanical assembly were also given. The parts of the mechanical assembly were listed. Finally the software development of the force and position control to control the force exerted by the spot welding electrode during squeeze and weld cycle and position of the electrode movement were discussed. The next chapter with look into the system evaluation of this newly developed servo spot welding system.

Chapter 5

SERVO CONTROLLED SPOT WELDING MACHINE – SYSTEM EVALUATION

This chapter deals with the evaluation of the control system for the newly developed servo actuated spot welding machine. As discussed in the previous chapter, the three control systems developed are force control during squeeze cycle, force control during weld cycle and electrode position control. The ability of the system to achieve the required force and position, the time taken to achieve the desired force and position, percentage overshoot and the steady state error of the system would be some of the parameters which will be taken into consideration during the evaluation of these there control systems.

5.1 Evaluation of the position control system

The position control was developed to drive the motor from the home position to a predetermined position closer to the metals sheets at a faster speed and then reduce the speed when the electrode is about to come into contact with the sheets to create a 'soft touch' effect. Unlike the pneumatic system, where the electrode stroke length had to be adjusted manually off-line, the developed position control will enable automatic adjustment of the electrode stroke length on-line. This variable electrode stroke length will allow the spot welding machine to be used for welding various designs of work pieces in the production line unlike the pneumatic system, where manual adjustments had to be made for each design, which is a time consuming process.

As stated in section 4.3.1, the desired position where the electrode needs to move is given in terms of encoder pulses, where 100000 encoder pulses is equivalent to 5mm of linear movement of the electrode.

The control system was tested with different desired positions for the electrode to move from the home position. When the movable electrode is at the home position, the distance between the electrode and a 2mm thickness sheet metal is 40mm or 800000 encoder counts as shown in figure 5.1. The home position was fixed using a limit switch, which stops the motor when the limit switch is activated. Figures 5.2, 5.3 and 5.4 below show the results of the evaluation of this system.

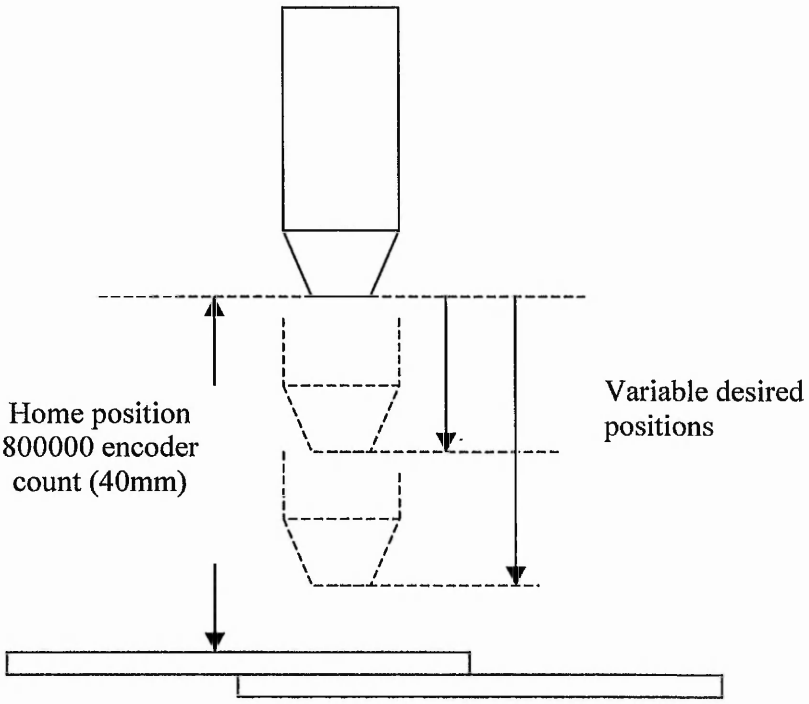

Figure 5.1 – Movement of electrode from home position to desired position

Results show that the position control is able to drive the motor to move the electrode from the home position to the desired position before the electrode comes in contact with the metal sheets. The encoder position has negative polarity, which shows that the motor is rotating in the opposite direction in order to move the electrode downwards towards the fixed electrode and metal sheets.

Figure 5.2 shows the electrode movement, based on encoder counts, for a distance of 600000 encoder counts (30mm) from home position. The average overshoot based on 3 repetitions is about 0.5mm or 10000 encoder counts and standard deviation of 0.021mm. The average steady state error is 8 encoder counts or 0.0004mm and a standard deviation of 0.00002mm.

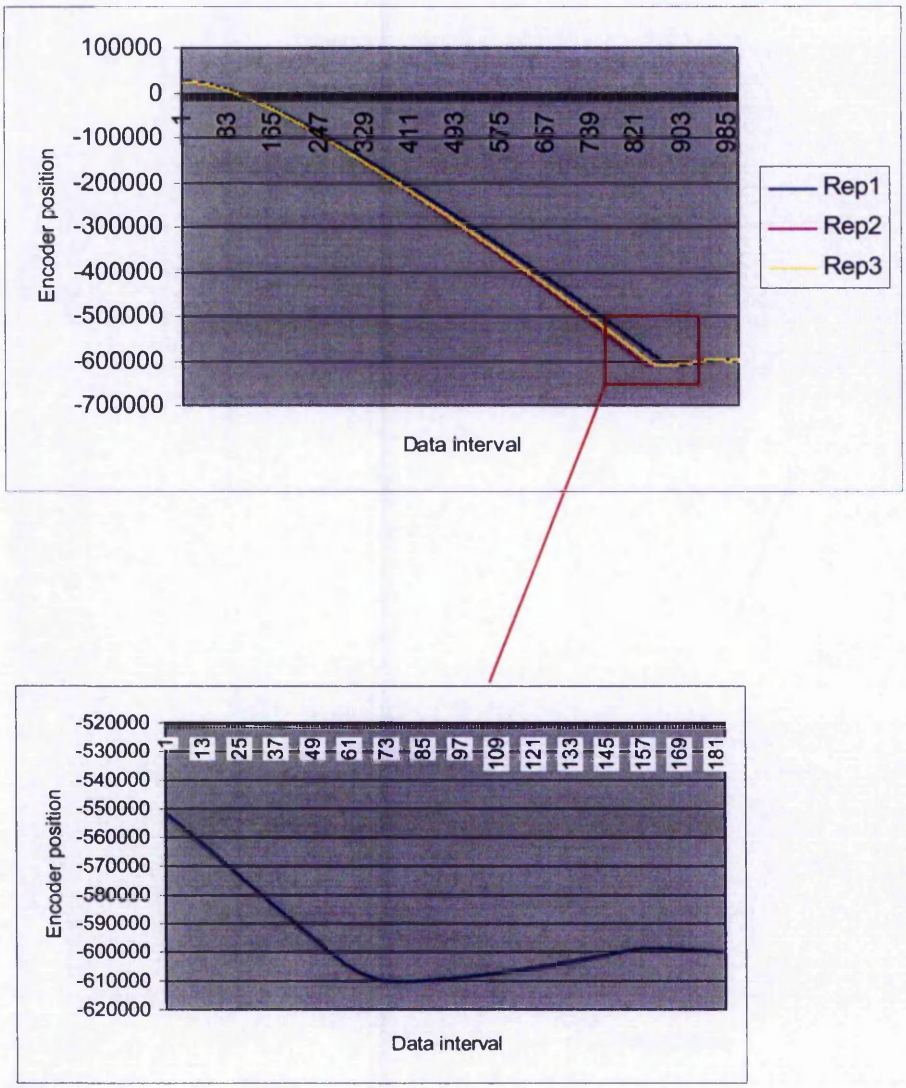

Figure 5.2 – Linear movement of electrode for 600000 encoder counts (30mm)

Figure 5.3 shows the electrode movement for a distance of 450000 encoder counts (22.5mm) from home position. The average overshoot based on repetitions is about 0.4mm or 8000 encoder

counts with a standard deviation of 0.024mm and the steady state error is 5 encoder counts or 0.00025mm with a standard deviation of 0.000019mm.

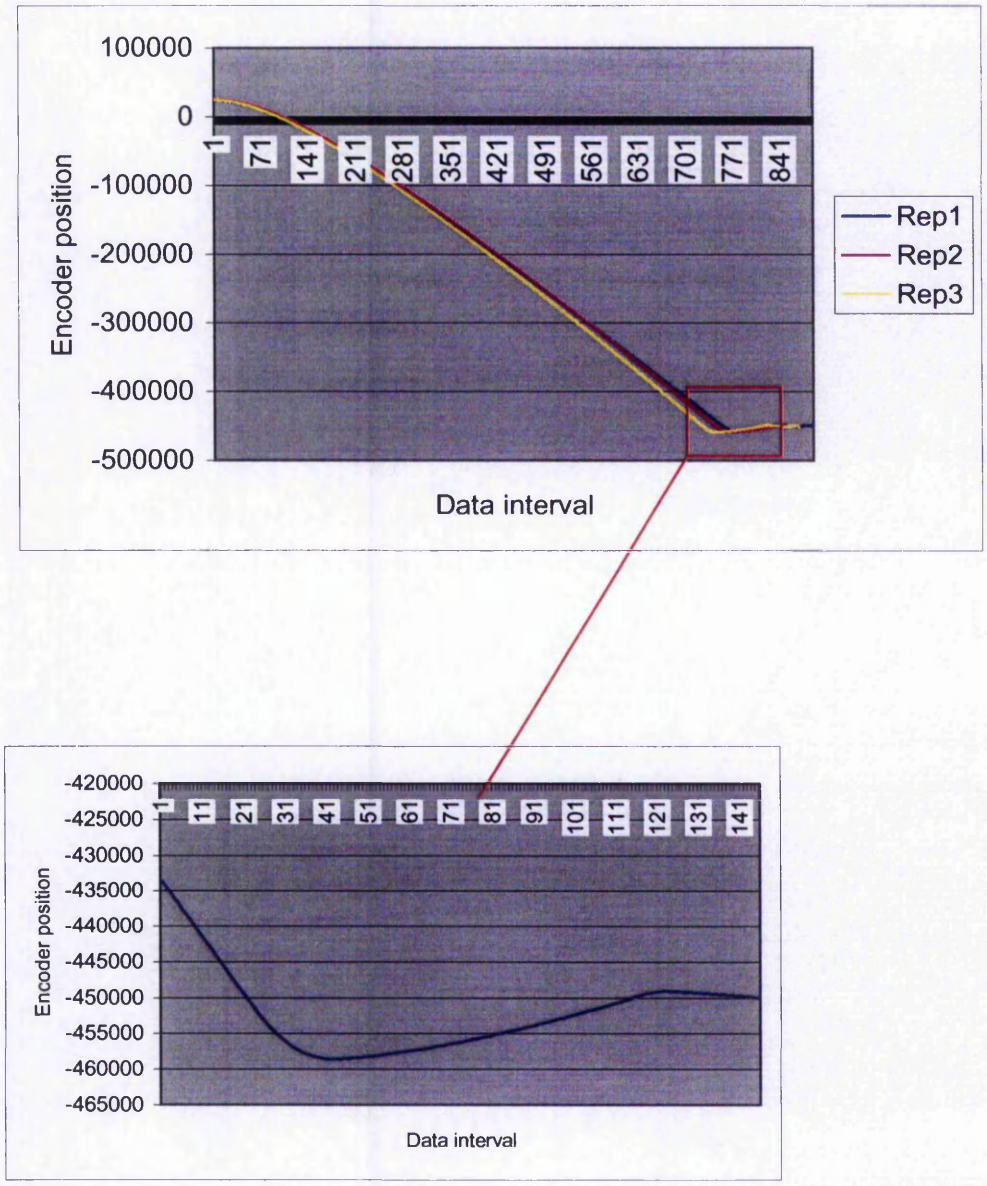

Figure 5.3 – Linear movement of electrode for 450000 encoder counts (22.5mm)

Similarly figure 5.4 shows the electrode movement for a distance of 550000 encoder counts (27.5mm) towards the fixed electrode. The average overshoot for 3 repetitions is 0.7mm or 14000

encoder counts and the standard deviation is 0.018mm. The achieved steady state error is about 6 encoder counts or 0.0003mm in average with a standard deviation of 0.000015mm.

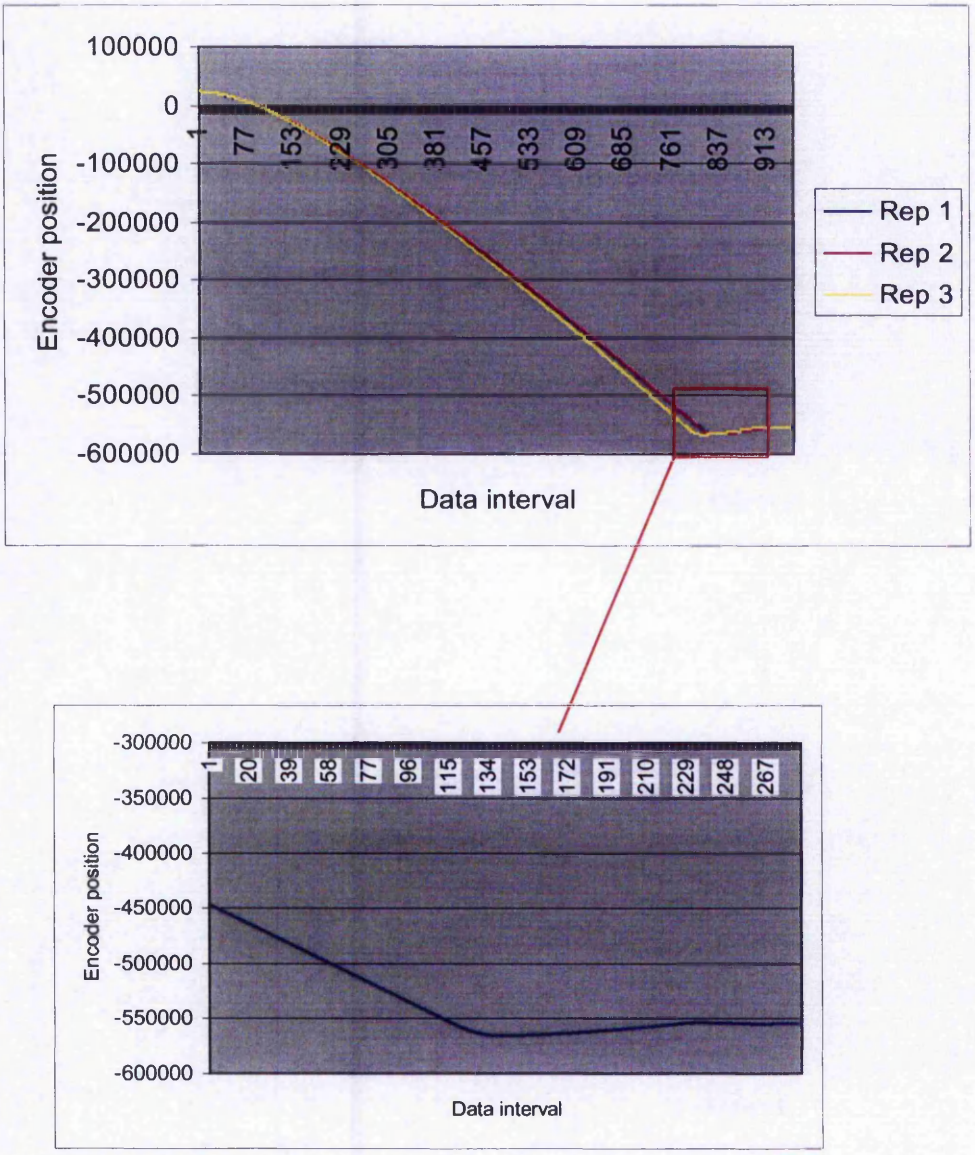

Figure 5.4 – Linear movement of electrode for 550000 encoder counts (27.5mm)

The evaluation of the position control for various others desired encoder positions and the system's repeatability study based on 3 repetitions for each encoder position is given in appendix B.

5.2 Evaluation of the force control system during squeeze cycle

As mentioned in section 4.3.2, the feedback signal from the piezoelectric sensor (figure 3.5) is sent to the controller in order to increase and decrease the motor torque to achieve the required force. Initially the motor is driven so that the movable electrode moves from the home position to a certain predetermined position nearer to the sheets, which are to be welded, by means of the position control explained in section 5.1. The motor is then driven slowly till the electrode comes into contact with the metal sheets and achieves stalled condition. The reason for driving the motor slowly when the electrode approaches the sheets is to create a 'soft touch' when the contact occurs. Electrode of the pneumatic system impacts the metal sheets with a hammering effect due to their high speed (Tang 2000). This would cause damage to the electrode tip and also surface of the metal sheets. Stall condition is achieved due to the inability of the motor to rotate further since the torque produced by the motor is smaller than the resistance torque of the metal sheet. The force control is then initiated to further change the motor torque in order to achieve the desired squeeze force before weld starts.

Figure 5.5 shows 3 repetitions of the force control used to achieve a squeeze force of 2.5kN during squeeze cycle. The force increases when the electrode comes in contact with the metal sheets and then becomes constant when the motor achieves the stall condition.

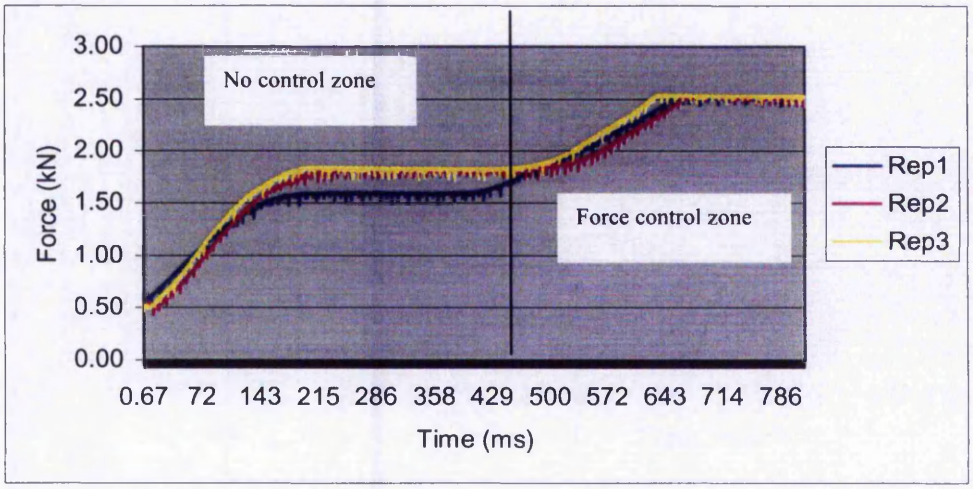

Figure 5.5 – Squeeze force of 2.5kN achieved through force control

As seen in figure 5.5, the force is between 1.5kN to 2.0kN during the stall condition. The force achieved during stall condition may vary because there is no control occurring till the motor reaches stall condition. Once the motor has reached the stall condition, the force control is initiated, which increases the motor torque based on the feedback from the piezoelectric sensor to raise the electrode force to the desired force of 2.5kN. The average rise time based on the 3 repetitions of figure 5.5 is approximately 205ms or 10cycles. The percentage overshoot is 0% and the steady state error is 0.02kN.

Figure 5.6 shows the force control used to achieve four different desired squeeze forces. The rise time was found to increase when the desired force increases. However the percentage overshoot is 0% and the average steady state error is 0.03kN. Using a higher current to drive the motor towards the sheets will cause the force achieved during the stall condition to be greater than the desired force. The motor will then be driven in the opposite direction to reduce the motor torque, which results in achieving the desired stall condition. As shown in figure 5.7, the forces when the motor achieves stall condition are greater than the desired forces. The control system will send current with an opposite polarity to reverse the motor hence the electrode will move upwards, reducing the applied force to the desired force. The average time taken by the control system to reduce the force to the desired force is about 164ms or 8.2 cycles. Again the percentage overshoot of the force is 0% with a 0.02kN steady state error.

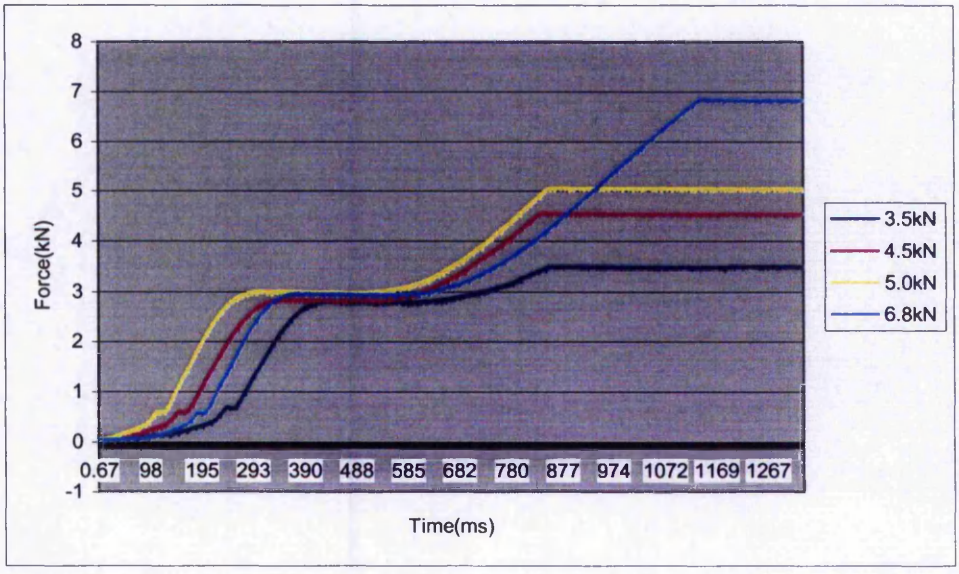

Figure 5.6 – Various squeeze forces achieved through force control

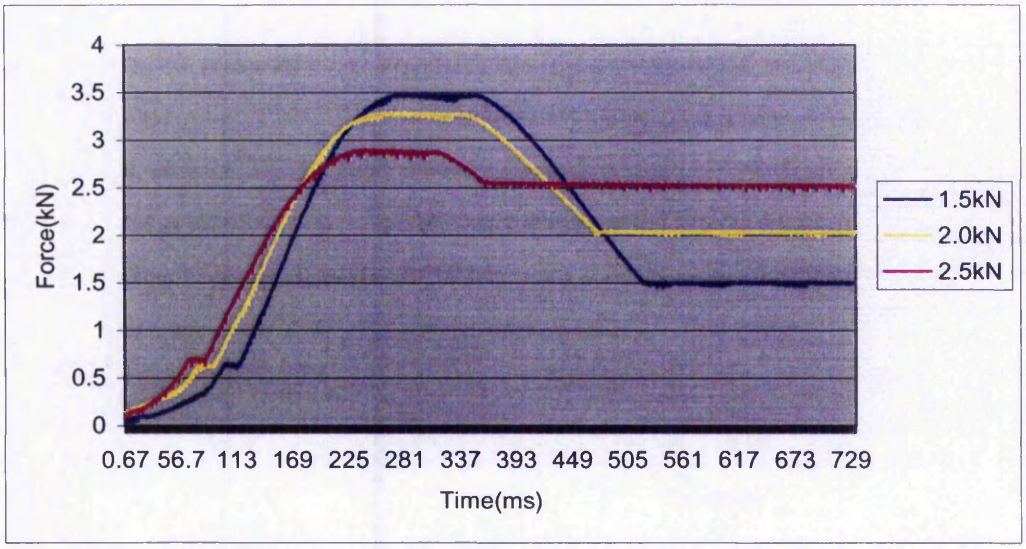

Figure 5.7 – Force control reducing the force to the desired force

The evaluation of the force control during squeeze cycle shows that the control system is able to drive the motor effectively so that the desired force is achieved before weld starts. The evaluation of the system's repeatability can be seen in appendix B. This developed force control during squeeze cycle will guarantee a constant desired force to be achieved at all times during the squeeze cycle unlike the pneumatic system where the desired force during squeeze cycle may vary due to leakage in the airline system or system friction.

5.3 Evaluation of the force control system during weld cycle

The evaluation of the force control system during the weld cycle is the most important of the three different control systems since development of this control system is the main aim of this project and no such work has been discussed in the literature at the time of writing this thesis. Similar to the force control during squeeze cycle, the feedback signal from the piezoelectric sensor is the input to the system and the output would be the amount of current needed to drive the motor. A force control is needed to change the applied force at a certain period in time or for a certain amount of period in time during the welding process. The force control is activated by

giving a preset force profile and the servomotor is driven in such a manner that the applied force during welding follows the given force profile.

The system was first evaluated by giving a step input and a ramp input. Figures 5.8 and 5.9 show the response of the system to these inputs. Based on figure 5.8, it was noticed that with a proportional gain of K_p = 800, the system has a rise time (T_r) of 180ms and peak time (T_p) of 250ms. The percentage overshoot (PO) of the system was measured based on the formula (Dorf 1995):-

$$\mathbf{PO = \frac{M_{pt} - f_v}{f_v} \times 100\%} \quad \text{----------} \quad \mathbf{(5.1)}$$

where M_{pt} = peak value of the force response

f_v = final value of the force response

Hence $PO = \frac{2.96 - 2.5}{2.5} \times 100 = 18.4\%$

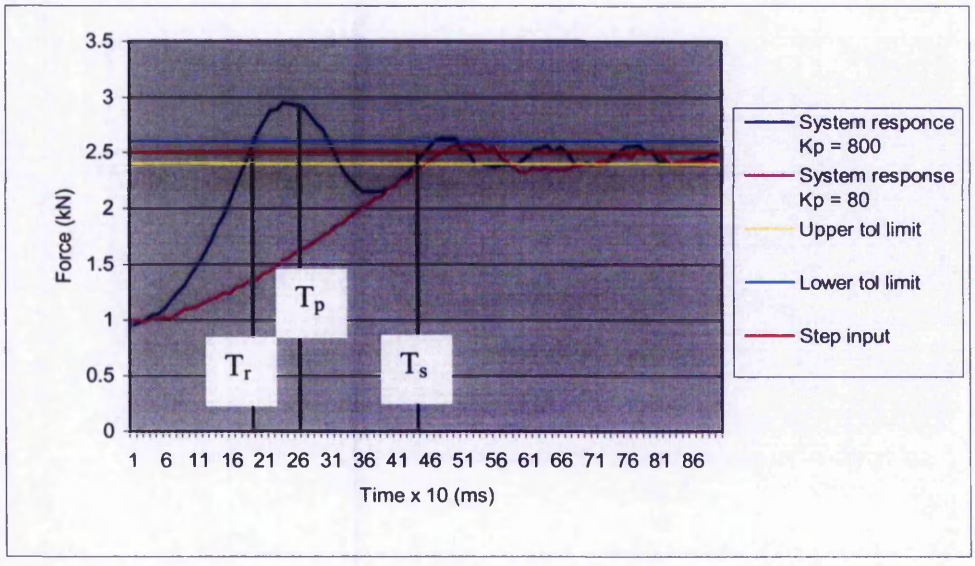

Figure 5.8 – System response to a step input

The settling time T_s that, is defined as the time required for the system to settle within certain tolerance limits is 430ms and the steady state error is 0.05kN. With a proportional gain of Kp = 80, the system overshoot is eliminated but the rise time had increased to 430ms. Figure 5.8 also indicates the underdamped and overdamped cases of the system depending on the value of K_p gain applied.

Figure 5.9 shows the response of the system to a ramp input. It could be seen from the figure that the control is able to follow the given input very closely.

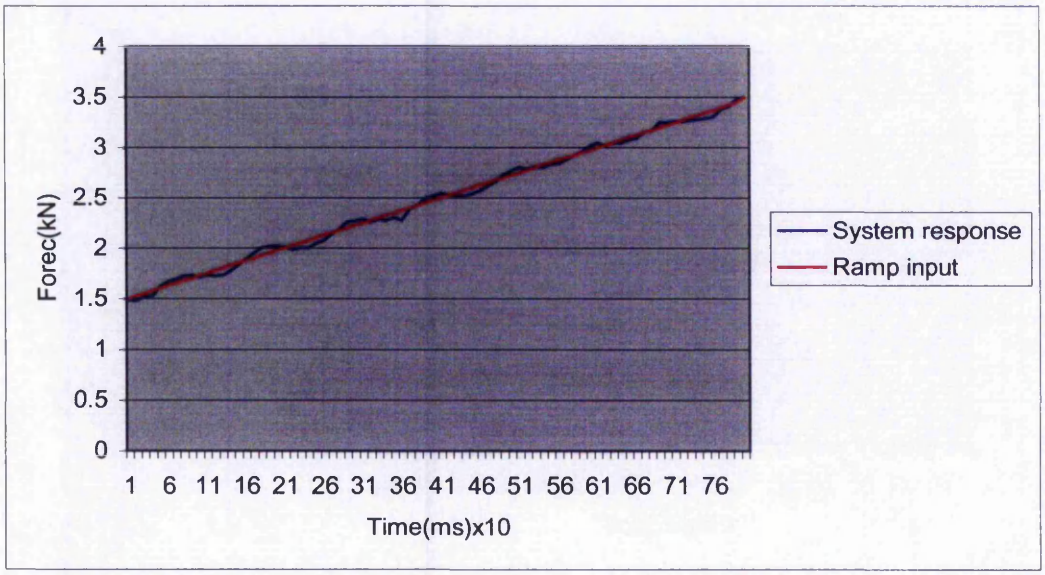

Figure 5.9– System response to a ramp input

5.3.1 The force profile

The force profile is a function of time (f(t)). In this project, the force profile consists of a series of force values for each half cycle (10ms) throughout the entire weld time. 4 different types of force profiles as shown in the figure 5.10 were used to test the force system without doing a weld. The force profiles are shown with an offset between each for reasons of clarity and are for a weld time of 800ms (40 cycles).

Profile A is a varying force profile from 1.5kN to 2.5kN. A 1.5kN force is applied during the squeeze cycle and the force is ramped up to 2.5kN after 100ms (5th cycle) of the weld time. The force takes 200ms to ramp up to 2.5kN and reaches the 2.5kN force during the 300th ms (15th cycle). The force is maintained constant at 2.5kN till the end of the weld time.

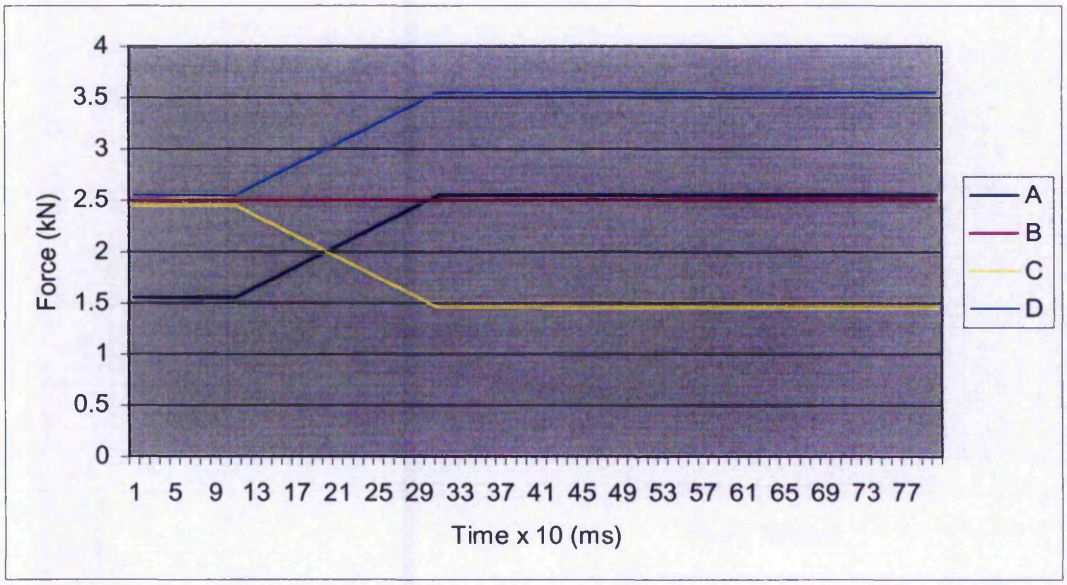

Figure 5.10- The force profiles

Profile B is a constant force profile of 2.5kN. The motor torque will be controlled throughout the weld time so that a constant force of 2.5kN is applied for the entire 800ms.

Profile C is a varying force profile from 2.5kN to 1.5kN. A squeeze force of 2.5kN is applied during the squeeze cycle and the force is ramped down to 1.5kN after 100ms (5th cycle) of the total weld time. The force takes 200ms to reach 1.5kN and achieves the 1.5kN after 300ms (15 cycles). The force is maintained constant at 1.5kN till the end of the weld time.

Profile D is a varying force profile from 2.5kN to 3.5kN. The applied squeeze force of 2.5kN is applied and ramped up to 3.5kN after 100ms(5th cycle). The force reaches 3.5kN on the 300th ms after ramping for 200ms. The force is maintained constant at 3.5kN till end of the weld time.

5.3.2 Hypothesis of resistance change due to the force profiles

These profiles were chosen with the intention of varying the dynamic resistance during welding. The hypothesis on the change in dynamic resistance for each chosen profile is described below.

Profile A is chosen to apply a preset force, which is less than the desired force at the start of the welding cycle. Force is then increased to the desired force in the middle of the welding cycle and maintained constant till the end of the weld cycle. The resistance is estimated to be higher at the start of the welding cycle due to the applied low force and then reduces when the high force is applied.

Profile B which is a constant force profile will be used so that the applied force is maintained constant and equal to the preset force during welding. This will avoid the increase in force during welding. The dynamic resistance is expected to increase at the start of welding process and then drop when the area for current flow increases due to weld growth.

Profile C will apply a preset force equivalent to the desired force at the start of the welding cycle. At the middle of the welding cycle force is reduced to a lower force and maintained at that force till the end of weld cycle. This profile is estimated to create a lower resistance due to the higher force applied at the beginning and increases later in the middle of the weld cycle when the force is reduced.

Finally profile D will apply a preset force equivalent to the desired force at the start of the welding cycle. The force is increased to a higher force during the middle of the weld cycle and maintained at this force till the end of the weld time. This profile was chosen so that the resistance reduces when the force in increased during the welding cycle.

Based on the hypotheses discussed above, it is expected that profile A will produce the strongest weld of all, due to the initial lower force of this profile that will increase the contact resistance and the amount of heat generation. With this high heat, melting will occur faster and weld will start to grow earlier. Since the total cycle time is 40 cycles, the weld has sufficient time to fully develop. The weakest weld was assumed to be produced by profile D since this profile has a higher initial force compared to A that would reduce the contact resistance. Reduction of contact resistance would decrease the amount of heat generated for weld development. Also when compared with B and C, profile D ends with the highest force hence the drop in resistance would be greater in this profile compared to B and C.

5.3.3 System response to force profiles

The figures 5.11 to 5.14 show that the force control is able to follow the given force profiles within the set tolerance band. A tolerance band of ± 0.2kN was given for each profile to compensate for the fluctuation in the force value due to the noise generated from the motor amplifier. This was solved partially by adding a low-pass filter at the digital input channel of the acquisition board. The low pass filter was tested by using the constant force profile as shown in figures 5.15 and 5.16.

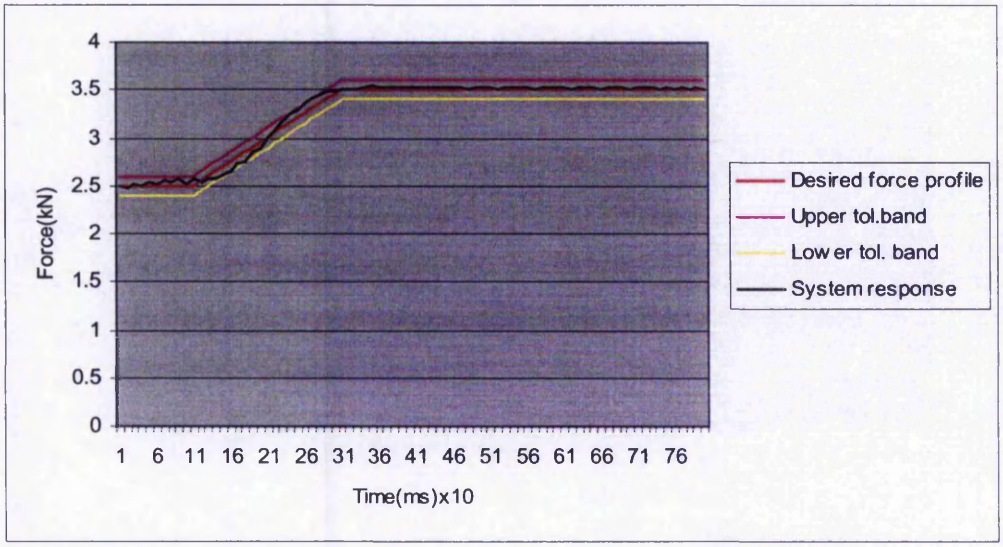

Figure 5.11 – System response to 2.5kN-3.5kN force profile

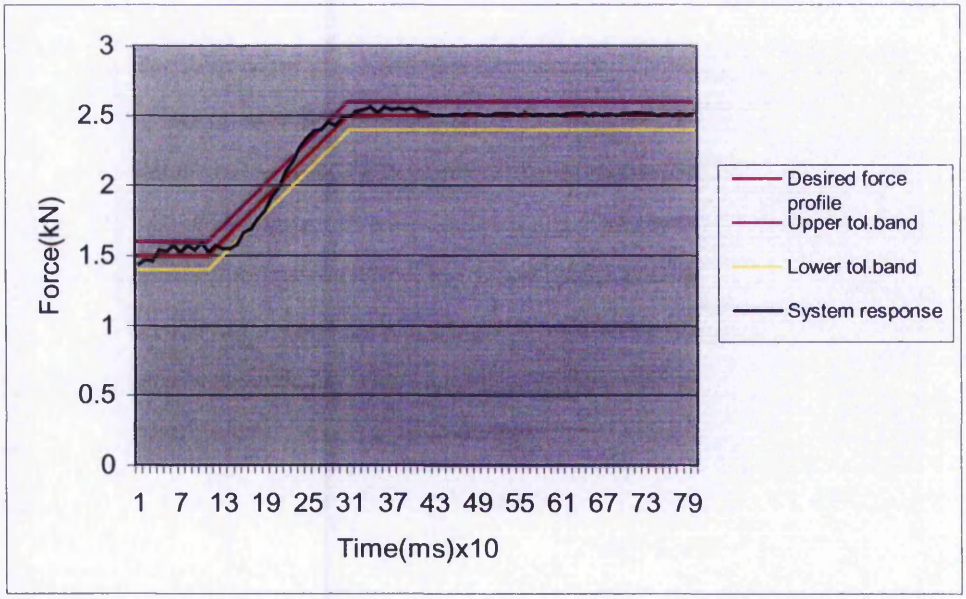

Figure 5.12 – System response to 1.5kN - 2.5kN force profile

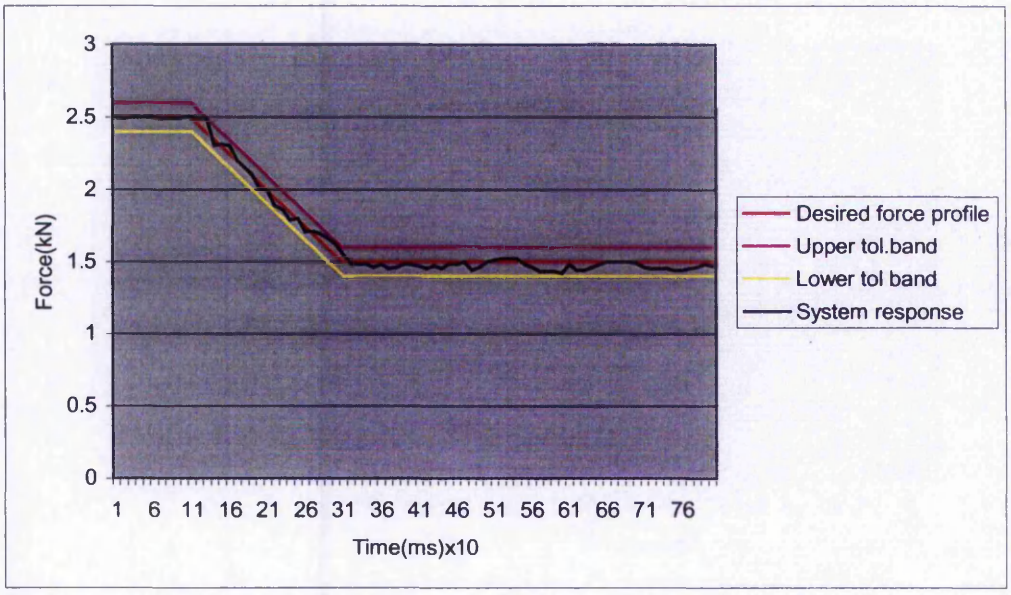

Figure 5.13 – System response to 2.5kN – 1.5kN force profile

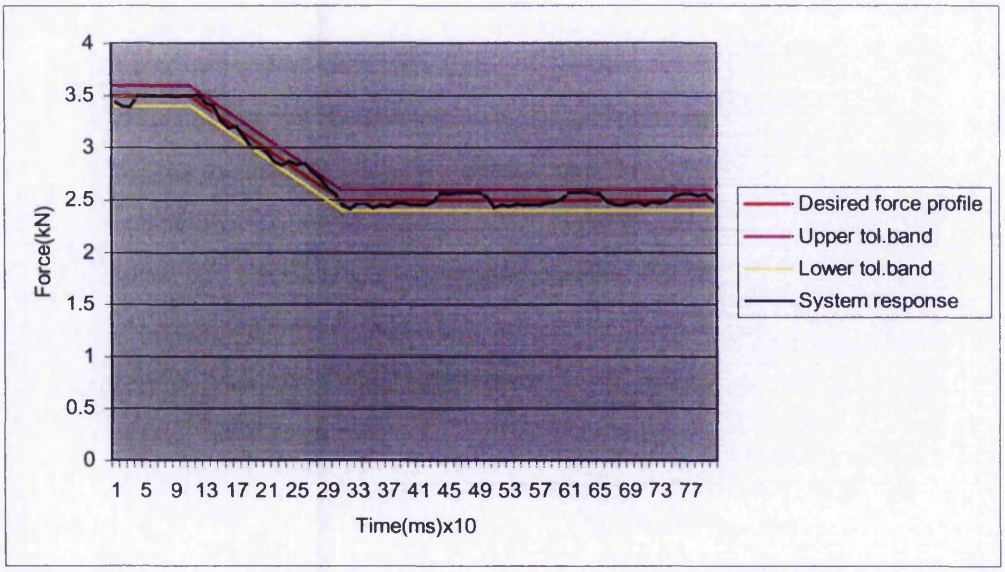

Figure 5.14 – System response to 3.5kN – 2.5kN force profile

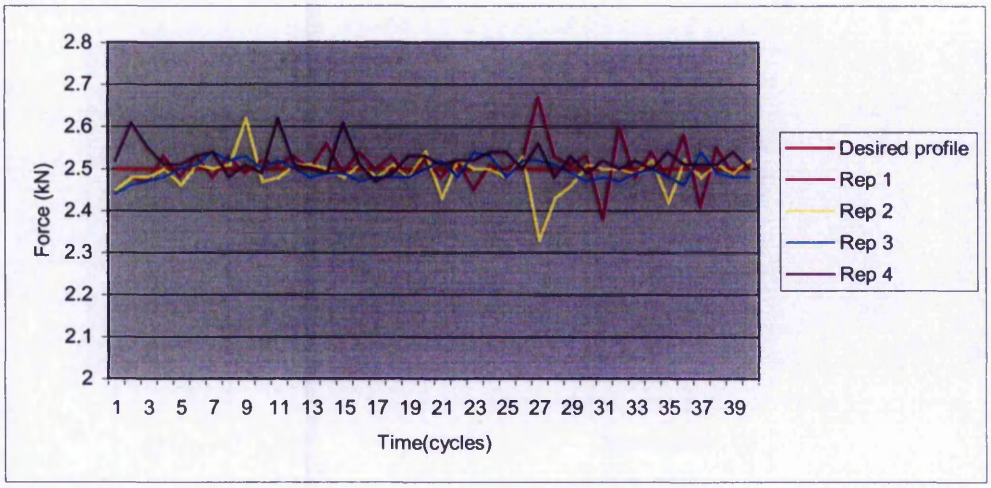

Figure 5.15– Fluctuation in force before adding a low pass filter

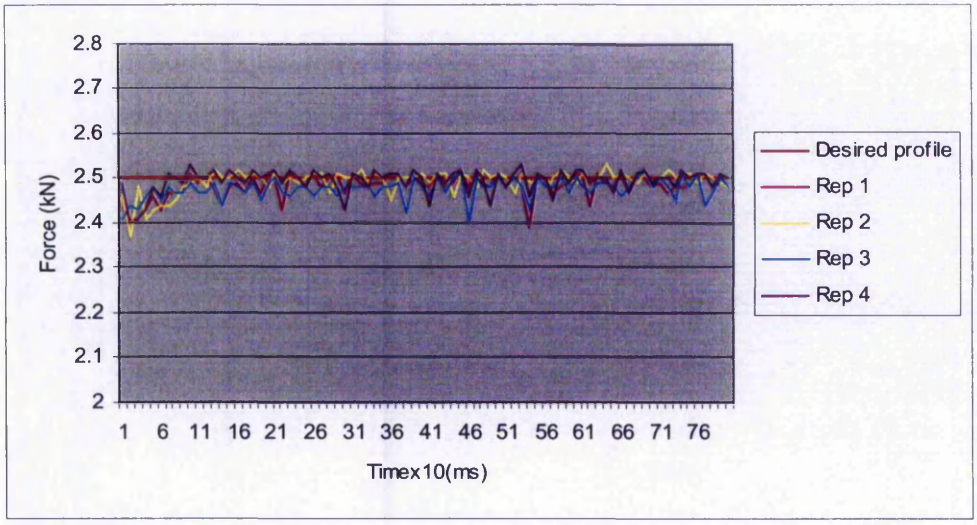

Figure 5.16 – Fluctuation in the force after adding a low pass filter

According to figures 5.11-5.14, it can be seen that the controller is able to follow the given force profiles within the set tolerance band of ± 0.2kN. Repeatability study on the system response to force profiles in figure 5.10 will be discussed in appendix B

5.4 Summary of the chapter

This chapter presents the system evaluation on the developed servo spot welding machine. The force control during squeeze cycle shows that the desired squeeze force is achieved with a steady state error of 0.02kN. Development of the control system would guarantee that the desired force with minimal error is always achieved before the weld starts. The force control during weld cycle was tested by giving a few force profiles, which will be used during welding in chapters 7 and 8. In this chapter the system response to these profiles was tested without doing a weld. Results of these evaluation show that the force control is able the follow the given profile within the given ± 0.2kN tolerance band. The developed position control that drives the electrode closer to the metal sheet was found to able to drive the motor so that the electrode travels to the desired position with error of less than 0.0004mm.

Chapter 6

Preliminary Experiments On Resistance Spot Welding

This chapter presents the metallography studies on the spot weld for different welding currents and weld times. Next, experiments were carried out on the welding parameters to study the effect of the various parameters on weld strength. The changes in weld strength due to changes in current, weld time and force will be extensively looked at and discussed. Later in this chapter, the different weld growth-monitoring methods used in the industries will be introduced. The dynamic resistance curve, electrode displacement curve and force profile during weld cycle were used to monitor the weld development. The experiments that were carried out on these monitoring methods, the results and analysis to show changes in weld strength due to variations in the weld parameters will be explained.

6.1 M etallography study of spot weld

Standard metallographic methods were used to investigate the effect of change in the welding parameters on the size of the fusion zone that was discussed in section 3.2.1 in chapter 3. These results are presented below. The fusion zone is equivalent to the weld diameter.

6.1.1 Metallographic preparation of the specimens

6.1.1.1 Specimen mounting

The welds that need to be inspected using the metallograhic method are first sectioned in the middle of the welds using a hacksaw. This will expose the welds, which need to be inspected. These specimens are then mounted in Lucite by heating the plastic under a pressure of 2 bars for 14 minutes and cooling for 5 minutes.

6.1.1.2 Grinding and polishing of specimen

A grinding operation is then carried out on these specimens to eliminate the scratches caused by the hacksaw cutting. Wet grinding using different grades of silicon carbide papers is carried out. Grinding is started with the 120-grit size paper, which is a coarse grade then to the 240-grit size, 800-grit size and finally the finest grade, which is the 1200- grit size paper. The grinding operation is carried out till the weld surfaces are smooth and free of scratches. Then diamond-polishing operation is carried out where the surfaces of the welds are polished with a diamond paste of 1-micron grit size. Glycerol is used instead of water for lubrication. Polishing is carried till a mirror-like surface is obtained. The specimens are then rinsed with methanol and dried under the hot air dryer.

6.1.1.3 Specimens etching

The etching operation is the last step in the preparation of the specimen for metallographic examination. The etching solution (etchant) is very effective in revealing the fusion zone or the weld solidification structure. The type of etchant used is 2%-nital, which has a composition of 2ml nitric acid and 98ml methanol. The specimens were immersed in the etchant for 10 seconds and then dried under the hot air dryer. Now the specimens are ready to be viewed under the microscope.

6.1.2 Change in the fusion zone due to change in welding current

3 different welding currents of 7000A, 9000A and 11000A were used in this experiment. The squeeze time, weld time and hold time were programmed into the Starchive program as 600ms (30 cycles), 300ms (15 cycles) and 200ms (10 cycles) respectively. The electrode force was maintained constant at 5kN. Table 6.1 shows the heat generated calculated using equation 6.1 below and the measured fusion zone diameter for the 3 different welding currents. The diameter of the fusion zone is measured using the program that was used to capture the weld macrograph photos.

$$Q = k \cdot I^2 \cdot T \cdot \sum_{i=0}^{i=t} R_i \quad \text{----------} \quad (6.1)$$

Where Q = heat generated (kJ), k = heat loss factor, I = current (kA), T = time for current flow for each half cycle (sec), R = resistance (ohms), t = total resistance values

The value for R was calculated by summing all the individual resistance values in a dynamic resistance curve. The individual resistance values were computed by dividing the voltage in the voltage waveform with the respective peak current in the current. This will be discussed in detail in section 6.3 later. The value of k was assumed to be equal to 1.

Sample No.	Current (kA)	Heat generation (kJ)	Fusion zone diameter (mm)
A	7000	1.53	4.2
B	9000	1.89	5.4
C	11000	2.05	6.8

Table 6.1 – Heat generation and measured fusion zone diameters for 3 different welding currents

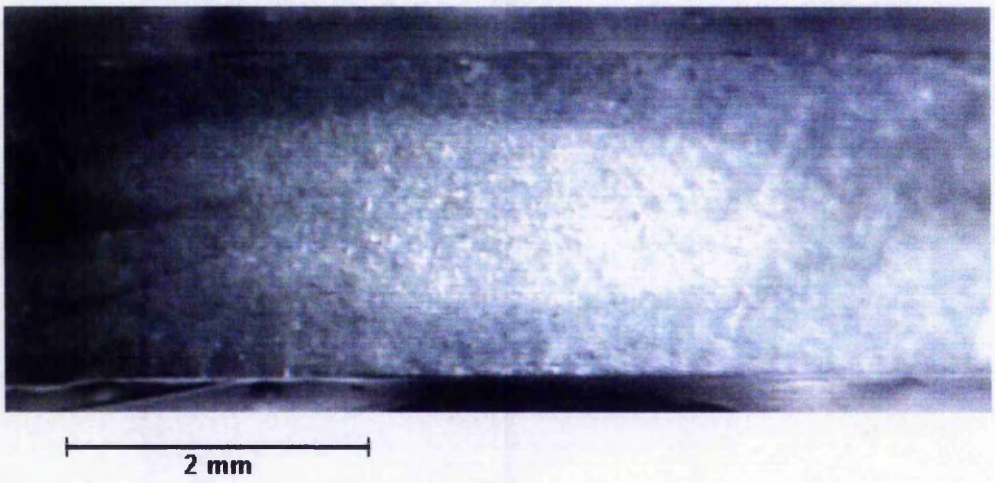

Figure 6.1 – Sample A with 7000A current

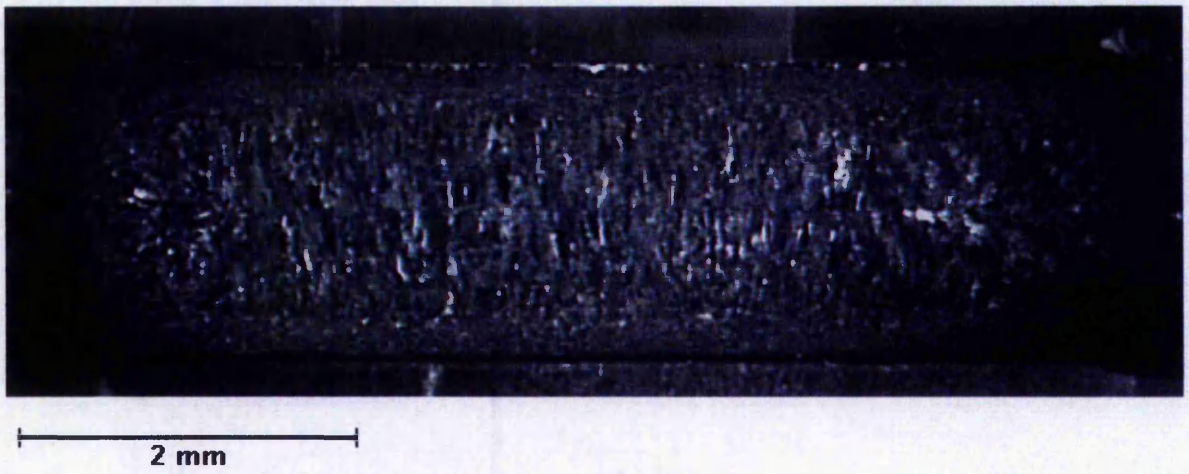

Figure 6.2 – Sample B with 9000A current

Figure 6.3 – Sample C with 11000A current

6.1.3 Changes in the fusion zone due to changes in weld time

3 different weld times of 140ms (7 cycles), 200ms (10 cycles) and 300ms (15 cycles) were used in this experiment. The squeeze time, hold time and welding current was programmed into the Starchive program as 600ms (30 cycles), 200ms (10 cycles) and 9000A respectively. The electrode force was maintained constant at 5kN. Table 6.2 shows the heat generated calculated using equation 6.1 above and the measured fusion zone diameter for the 3 different weld times.

Sample No.	Weld time (ms)	Heat generation (kJ)	Fusion zone diameter (mm)
D	140	1.56	4.0
E	200	1.96	5.8
F	300	2.35	6.7

Table 6.2 – Heat generation and measured fusion zone diameters for 3 different weld time

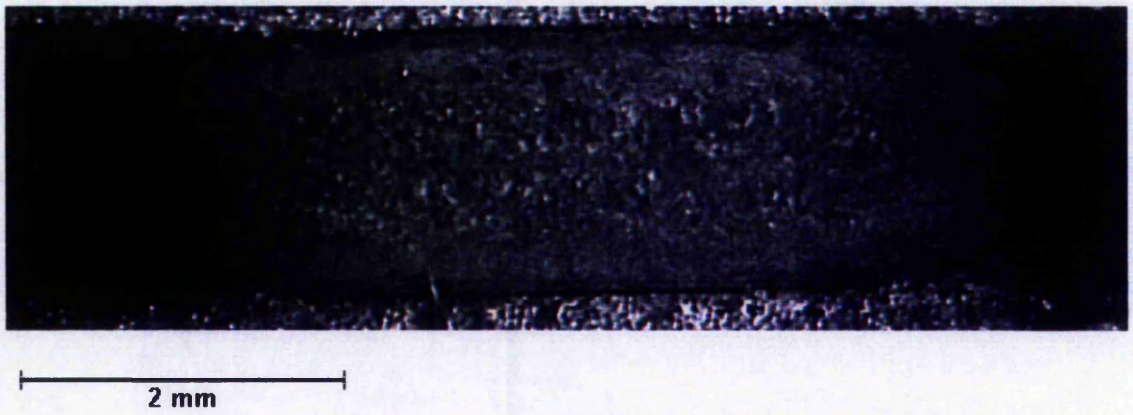

Figure 6.4 – Sample D with 140ms weld time

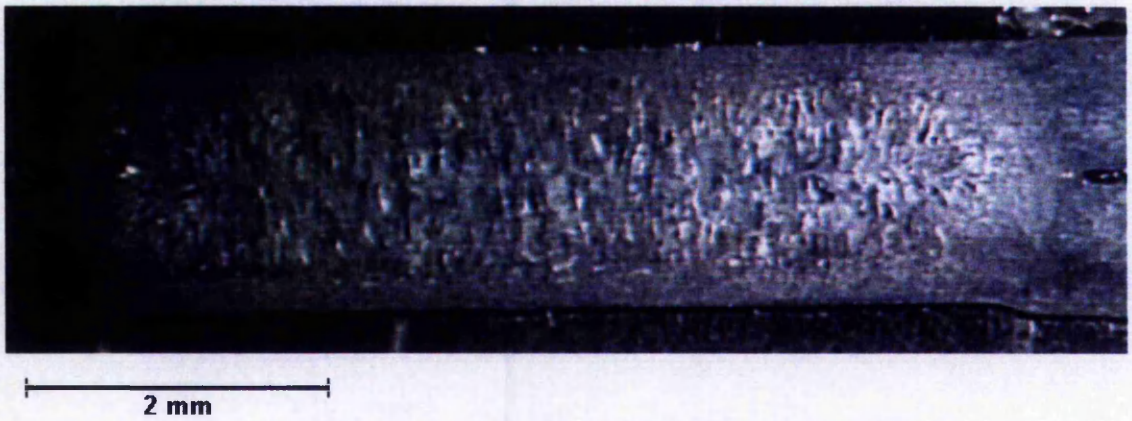

Figure 6.5 – Sample E with 200ms weld time

Figure 6.6 – Sample F with 300ms weld time

6.1.4 Discussion on the metallography study

The specimens for the metallographic study were made using 1mm thickness steel sheets and spot welds were made using two 6 mm diameter electrodes. The welding schedules as in sections 6.1.2 and 6.1.3 were used and the specimens were prepared as discussed in section 6.1.1. Section 6.1.2 shows the macrostructural images of the changes in the size of the fusion zone due to change in the welding current as in table 6.1. Figure 6.1 shows the macrostructure for sample A, which is made with 7000A. Since the current is not sufficient to produce a weld but enough to initiate melting, a small fusion zone was obtained. Figures 6.2 and 6.3 show the macrostructures for sample B and C respectively. Fusion zones having coarse dendritic structures were noticed. The dendritic structures were formed due to the rapid directional solidification of the molten metal (Oldland et al. 1989).

Encircling the fusion zones are brighter regions with grain sizes smaller than the dendritic structures of the fusion zones. These are the heat-affected-zones (HAZ) where the austenite is partially transformed into martensite that is developed with rapid cooling from above the A_1 transformation point as seen in section 3.2.2 in chapter 3. The fusion zone in figure 6.2 measures about 5.4mm in diameter and fusion zone in figure 6.3 measures about 6.8mm in diameter. Table

6.1 also shows that the heat generated for weld growth increase with the increase in current. The heat generated increased from 1.53kJ to 2.05kJ when the welding current is increased from 7000A to 11000A. This increase in heat generation would increase the size of the fusion zone for a certain weld time (Gould 1987). This shows that when the welding current increases, the increase in heat generated would lead to the increase in the size of the fusion zone. Since the fusion zone refers to the weld diameter, it can be concluded that weld diameter increases with increase in current. Section 6.1.3 shows the macrostructural images of the changes in the fusion zone size due to changes in the welding cycle as in table 6.2. Figures 6.4, 6.5 and 6.6 show the fusion zones for 140ms, 200ms and 300ms respectively. The fusion zone for 140ms measures about 4mm, fusion zone for 200ms measures about 5.8mm and the fusion zone for 300ms measures about 6.7mm. Table 6.2 also shows that the heat generated during welding increase with the increase in weld time. The heat generated increase from 1.56kJ to 2.35kJ when the weld time was increased from 140ms to 300ms. The heat generated would increase for the same welding current if the weld time was increased (Gould 1987). This shows that the fusion zone increases in size when the weld time was increased with the welding current maintained constant. Therefore it can be concluded again that the weld diameter increases with the increase in weld time.

6.2 Experiments on the welding parameters

In order to support the conclusions in section 6.1, a study on the contribution of the weld parameters to weld strength was carried out. The experiments were to study the following: -

a) effect of welding current on weld strength
b) effect of weld time* on weld strength
c) effect of welding force on weld strength

*weld time is defined as number of cycles with 1 cycle = 0.02 seconds

The electrode tip diameter was monitored throughout these experiments to avoid the possibility of changes in the tip diameter due to electrode deformation. The electrode tips were machined to the original diameter once significant diameter changes were detected.

6.2.1 Effect of welding current and weld time on weld strength

6 welding currents were used for this experiment that are in the range from 4000A to 6000A as shown in table 6.3. The range of welding time used is from 80ms (4 cycles) to 160ms (8 cycles). The squeeze time and hold time were programmed in the Starchive program as 600ms (30 cycles) and 200ms (10 cycles) respectively. The electrode force is maintained constant at 0.5kN. Mild steel sheets with 1mm thickness and 5mm tip diameter electrodes were used for this experiment.

Table 6.3 shows the welding schedules used for the experiments together with the results obtained as average, standard deviations of the weld strengths and a 95% confidence interval of the average using the t test. 10 repetitions were made for each welding schedule. The normal testing method discussed in section 3.3.2.3 was used to measure the weld strength.

Current \ Time		80ms	100ms	120ms	140ms	160ms
4000A	A.S (kN)	3.43	3.82	4.41	4.45	4.5
	S.D (kN)	0.48	0.60	0.24	0.21	0.22
	95%C.I(kN)	2.94<μ<3.92	3.20<μ<4.44	4.16<μ<4.66	4.23<μ<4.67	4.27<μ<4.73
4400A	A.S (kN)	3.57	3.84	4.47	4.50	4.87
	S.D (kN)	0.19	0.21	0.14	0.21	0.23
	95%C.I(kN)	3.37<μ<3.77	3.62<μ<4.06	4.33<μ<4.61	4.28<μ4.72	4.63<μ<5.11
4800A	A.S (kN)	3.58	4.28	4.55	4.67	4.93
	S.D (kN)	0.23	0.22	0.1	0.22	0.19
	95%C.I(kN)	3.34<μ<3.82	4.05<μ<4.51	4.45<μ<4.65	4.44<μ<4.90	4.73<μ<5.13

5200A	A.S (kN)	4.14	4.54	4.68	5.00	5.51
	S.D (kN)	0.14	0.2	0.2	0.2	0.09
	95%C.I(kN)	4.00<μ<4.28	4.33<μ<4.75	4.47<μ<4.86	4.79<μ<5.21	5.41<μ<5.60
5600A	A.S (kN)	4.20	4.74	5.00	5.13	4.80
	S.D (kN)	0.21	0.12	0.08	0.1	0.14
	95%C.I(kN)	3.98<μ<4.42	4.62<μ<4.86	4.92<μ<5.08	5.03<μ<5.23	4.66<μ<4.94
6000A	A.S (kN)	4.75	4.84	5.12	5.40	4.63
	S.D (kN)	0.20	0.22	0.21	0.19	0.15
	95%C.I(kN)	4.54<μ<5.00	4.61<μ<5.10	4.90<μ<5.34	5.20<μ<5.60	4.48<μ<4.78

A.S – average strength S.D – standard deviation 95% C.I – 95% confidence interval

μ – population mean

Table 6.3 – Results for the effect of welding current and weld time on weld strength

6.2.1.1 Discussion on the effect of welding current on weld strength

Figure 6.7 shows that the strength of the weld increases as the current is increased while keeping the force and weld time constant. At high current, the heat supplied to the weld is sufficient for the weld to achieve full growth within the selected weld time. This will cause a fully-grown and stronger weld to be produced (Tsai et al. 1992). For the same time, at lower current, undersize and brittle welds are formed because of insufficient heat supplied. This in turn will produce weaker welds with lower strength. This study can be related to the metallographic study in section 6.1.2, which shows that weld diameter, increases with increase in current. Increasing the current from 9000A to 11000A causes the weld diameter to increase from 5.4mm to 6.8mm. Further increase in current will reduce weld strength due to occurrence of expulsion as discussed in section 2.9.1. Sparks were created during expulsion of molten metal from the weld zone. Traces of expulsion as seen in figure 2.10 are noticeable when the weld is destructively tested. Loss of material during expulsion causes voids and porosity in the weld (Zhang 1999). This can cause drop in the achieved weld strength as seen during 5600A and 6000A and 8 cycles

weld time. A similar result to this experiment was described by other studies (Han & Orozco 1989).

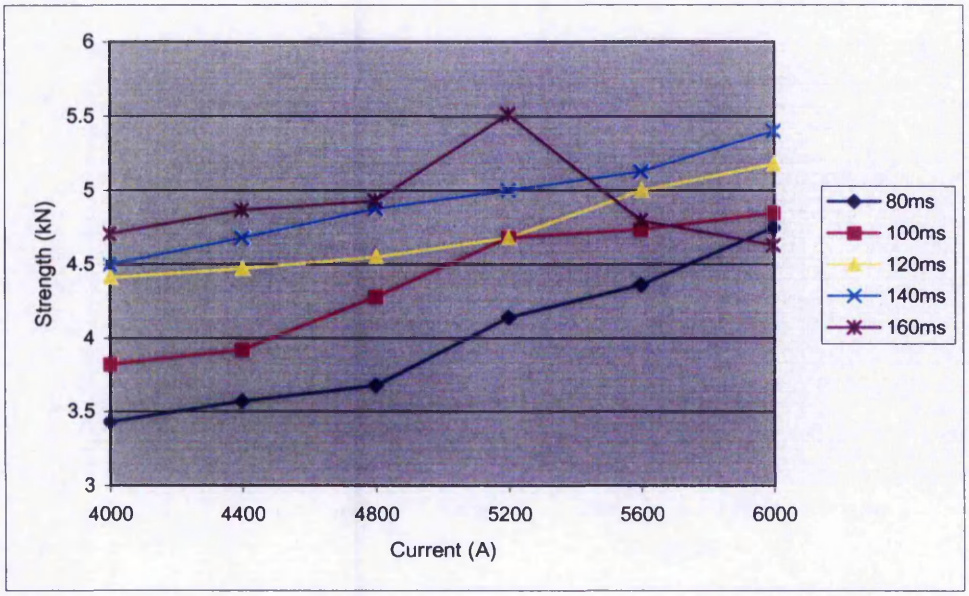

Figure 6.7 – Changes in strength due to changes in current and time

The t-test was used to test the significance of the difference between two means/averages (μ) based on equation 6.2.

$$t = \frac{\bar{x}_1 - \bar{x}_2}{\left[\frac{(n_1 - 1)s^2_1 + (n_2 - 1)s^2_2}{n_1 + n_2 - 2} \cdot \left[\frac{1}{n_1} + \frac{1}{n_2}\right]\right]^{1/2}} \quad \text{--- (6.2)}$$

where n_1 and n_2 = number of sample from two populations, $\bar{x}_1$ and $\bar{x}_2$ = means of the two populations and s^2_1 and s^2_2 = variances of the two populations. For example if n1 = n2 =10, if t is either $\leq -t_{0.005}$ or $\geq t_{0.005}$, where $t_{0.005} = 2.861$ is the value for a 99% confidence interval with degree of freedom of 20-1=19, then the null hypothesis of no difference between the means is rejected and the difference between the means is said to be significant (Freund 1992a) .

T tests were carried out on 3 different pairs of welding currents as shown in table 6.4 below using equation 6.2 above. The tests were carried out for 3 different weld times to determine the significant differences between the mean strength values.

Weld cycles	Test samples	t values at 99% confidence interval
80ms	4000A and 5200A	-5.903
	5200A and 6000A	11.174
	6000A and 4000A	11.350
120ms	4000A and 5200A	-3.865
	5200A and 6000A	6.785
	6000A and 4000A	9.952
160ms	4000A and 5200A	-19.001
	5200A and 6000A	-22.142
	6000A and 4000A	2.183

Table 6.4 – T test results for the differences between average weld strengths for 3 welding currents

The tests were carried out on the 4000A and 5200A with 80ms welding time, 5200A and 6000A with 80ms welding time and finally 4000A and 6000A with 80ms welding time. The calculated t values are either $\leq t_{0.005} = -2.861$ and $\geq t_{0.005} = 2.861$ for 99% confidence interval. Hence the null hypotheses is rejected and mean strengths between the 3 welding currents show significant differences between them. The test was repeated with the same welding currents but with 120ms weld time. The calculated t values are either $\leq t_{0.005} = -2.861$ or $\geq t_{0.005} = 2.861$ for 99% confidence interval. Again the means show significant differences between them. Finally the test was repeated with 160ms weld time. The last t value was found to agree with the null hypothesis since it is smaller than 2.861 even though the two tested welding current of 4000A and 6000A are wider apart between each other. This lack of significant difference between the means is due to expulsion caused by high current and longer welding time, which reduced the weld strength for 6000A closer to the weld strength for 4000A as seen in figure 6.2. This test concludes that the weld strength increases with increase in welding current, except during occurrence of expulsion, with significant difference between means.

6.2.1.2 Discussion on the effect of weld time on weld strength

Figure 6.7 also shows that the weld strength increases as the weld time increases. The weld will continue to grow in size for the constant current when the time is increased. The growth of the weld will cause the weld strength to increase as the weld becomes fully developed. Cho (1989) indicated that the weld diameter and penetration increases as weld time increases at constant current and force. This was proved through the metallographic study in section 6.1.3. However with a longer weld time, overheating will occur causing expulsion and the weld strength will drop as seen for 160ms weld time

Welding current	Test samples	t values at 99% confidence interval
4000A	80ms and 120ms	-8.167
	120ms and 160ms	1.225
	160ms and 80ms	9.063
4800A	80ms and 120ms	-17.296
	120ms and 160ms	7.915
	160ms and 80ms	20.237
5200A	80ms and 120ms	-9.892
	120ms and 160ms	16.923
	160ms and 80ms	19.924
6000A	80ms and 120ms	-5.705
	120ms and 160ms	-8.491
	160ms and 80ms	-2.146

Table 6.5 – T test results for the differences between average weld strengths for 3 weld times

T tests based on equation 6.2 were carried out on mean strengths of the 80ms and 120ms welding time with 4000A current, 120ms and 160ms welding time with 4000A current and finally 160ms and 80ms with 4000A current. The t test results are presented in table 6.5. The second t value shows insignificant difference between means because $t=1.225 < t_{0.005}= 2.861$.

However the other t values show significant differences between means because the t values are either $\leq t_{0.005}$= -2.861 or $\geq t_{0.005}$ 2.861 for 99% confidence interval. The tests were later repeated with 4800A current. The calculated t values show significant differences between means because all these values reject the null hypothesis. The test was repeated with the same welding time but with 5200A current. The calculated t values are either $\leq t_{0.005}$= -2.861 or $\geq t_{0.005}$ = 2.861, which again indicate significant differences between means. Finally the test was carried out with 6000A current. T values show that the last t value was found to agree with the null hypothesis since it is greater than –2.861 even though the two tested welding current of 4000A and 6000A are wider apart between each other. This lack of significant difference between means are due to expulsion caused by high current and longer welding time, which reduced the weld strength as seen in figure 6.7. This test concludes that the weld strength increases with increase in welding time, except during occurrence of expulsion, with significant difference between means.

6.2.2 Effect of welding force on weld strength

The same welding currents used in the previous experiment were also used in this experiment. 4 different electrode forces of 0.6kN, 1.2kN, 2.4kN and 3.6kN were used. The squeeze time, weld time and hold time was programmed in the Starchive as 600ms (30 cycles), 140ms (7 cycles) and 200ms (10 cycles) respectively. 1mm thick mild steel sheets and 5mm tip diameter electrodes were used for this experiment.

Table 6.6 shows the welding schedules used for the experiment together with the results obtained as average, standard deviations and a 95% confidence interval of the average strength using the t test. 10 repetitions were made for each welding schedule. The normal testing method discussed in section 3.3.2.3 was used to measure the weld strength.

Current	Force	0.6 kN	1.2 kN	2.4kN	3.6kN
4000A	A.S (kN)	4.35	4.12	x	x
	S.D (kN)	0.20	0.13	x	x
	95%C.I(kN)	4.14<μ<4.56	4.00<μ<4.25	x	x
4400A	A.S (kN)	4.50	4.36	x	x
	S.D (kN)	0.10	0.12	x	x
	95%C.I(kN)	4.40<μ<4.60	4.24<μ<4.48	x	x
4800A	A.S (kN)	4.78	4.67	2.56	x
	S.D (kN)	0.21	0.21	0.36	x
	95%C.I(kN)	4.56<μ<5.00	4.45<μ<4.89	2.19<μ<2.93	x
5200A	A.S (kN)	5.21	5.00	3.62	2.18
	S.D (kN)	0.13	0.20	0.29	0.48
	95%C.I(kN)	5.08<μ<5.34	4.79<μ<5.21	3.32<μ<3.92	1.69<μ<2.67
5600A	A.S (kN)	5.24	5.13	3.93	2.78
	S.D (kN)	0.10	0.22	0.30	0.41
	95%C.I(kN)	5.14<μ<5.34	4.90<μ<5.36	3.62<μ<4.34	2.38<μ<3.20
6000A	A.S (kN)	4.60	5.40	3.78	3.10
	S.D (kN)	0.22	0.18	0.39	0.48
	95%C.I(kN)	4.37<μ<4.83	5.21<μ<5.59	3.39<μ<4.18	2.61<μ<3.59

A.S– average strength S.D – standard deviation 95% C.I – 95% confidence interval

x- no weld μ – population mean

Table 6.6 – Results for the effect of welding force on weld strength

6.2.2.1 Discussion on the effect of welding force on weld strength

Weld strength reduces when forged with a higher welding force. As discussed in section 2.8.1, increase in welding force will reduce the contact resistance causing less heat to be

supplied for weld formation (Murakawa et al. 1997)(Sari et al. 2002). At 3.6kN, since the contact resistance was too low, no weld was produced at lower currents (4000A-4800A). In this case, higher welding current (5200A-6000A) need to be supplied in order to produce a weld. A similar observation applies for the force of 2.4kN. At 0.6kN and 6000A, weld strength tends to deteriorate as in figure 6.8. A lower force will cause the contact resistance to increase and more heat is supplied for weld development. In addition to this, the use of high current will cause overheating to occur for the same amount of time and leads to the occurrence of expulsion.

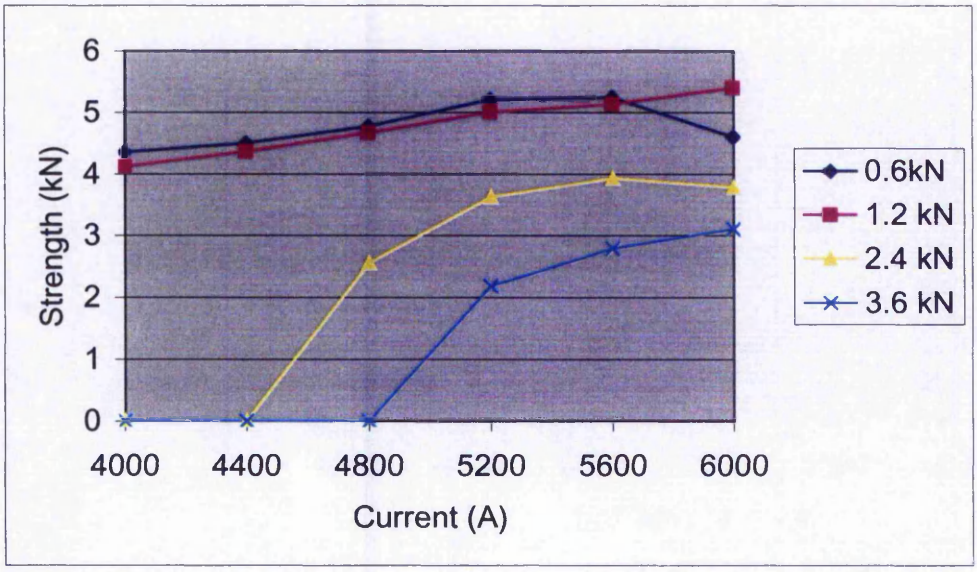

Figure 6.8 – Change in strength due to change in force

T tests based on equation 6.2 were carried out to test the significant differences between mean strengths as given in table 6.7. First test was carried out on the 0.6kN and 1.2kN welding forces with 4000A current. The t value which is greater than $t_{0.005}$= 2.861 shows significant difference between means. The next test was carried out on 0.6kN and 1.2kN, 1.2kN and 2.4kN

Welding current	Test samples	t values at 99% confidence interval
4000A	0.6kN and 1.2kN	4.312
4800A	0.6kN and 1.2kN	2.656
	1.2kN and 2.4kN	-22.641
	2.4kN and 0.6kN	-23.821
5600A	0.6kN and 1.2kN	2.306
	1.2kN and 2.4kN	-11.425
	2.4kN and 3.6kN	10.123
	3.6kN and 0.6kN	21.655

Table 6.7 – T test results for the differences between average weld strengths for 4 welding forces

and 0.6kN and 2.4kN at 4800A welding current. The second and third calculated t values rejects the null hypothesis when tested with 99% confidence interval because all the values are $\leq t_{0.005} = -2.861$. Hence these values show that the mean strengths for the welding forces have significant differences between them. However the first t value t=2.656 shows the means difference between 0.6kN and 1.2kN is less significant when tested 99% confidence intervals because this value is smaller than $t_{0.005} = 2.861$. However when tested with 95% confidence interval, it rejects the null hypothesis because the t value is greater than $t_{0.025} = 2.093$. Finally the test was carried out on the four pairs of forces of 0.6kN and 1.2kN, 1.2kN and 2.4kN, 2.4kN and 3.6kN and finally 3.6kN and 0.6kN with 5600A current. The calculated t values shown significant differences between means when tested with 95% confidence interval because these values are either $\leq t_{0.025} = -2.093$ or $\geq t_{0.025} = 2.093$. However when tested with 99% confidence interval, the t=2.306 shows the means difference between 0.6kN and 1.2kN is less significant because this value is smaller than $t_{0.005} = 2.861$. Hence it can be concluded that the weld strength decreases with increase in the forging force with significant difference between means at 95% confidence interval for different welding forces.

6.2.3 Investigation on the weld lobe curve of the servo spot welding machine

The weld lobe curve is a graphical representation of ranges of welding variables over which acceptable spot welds are formed on a specific material welded with a pre-selected electrode force (Dickinson & Franklin 1980). Figure 6.9 shows a typical spot weld lobe curve. The lobe is determined by making spot welds using different combinations of weld time and welding current. Welds made with currents and/or times exceeding the upper curve experience expulsion and are therefore considered unacceptable. Welds made with currents and times below the lower curve have insufficient size weld/no weld and therefore are unacceptable. Only welds made with currents and weld times lying within the lobe area are acceptable.

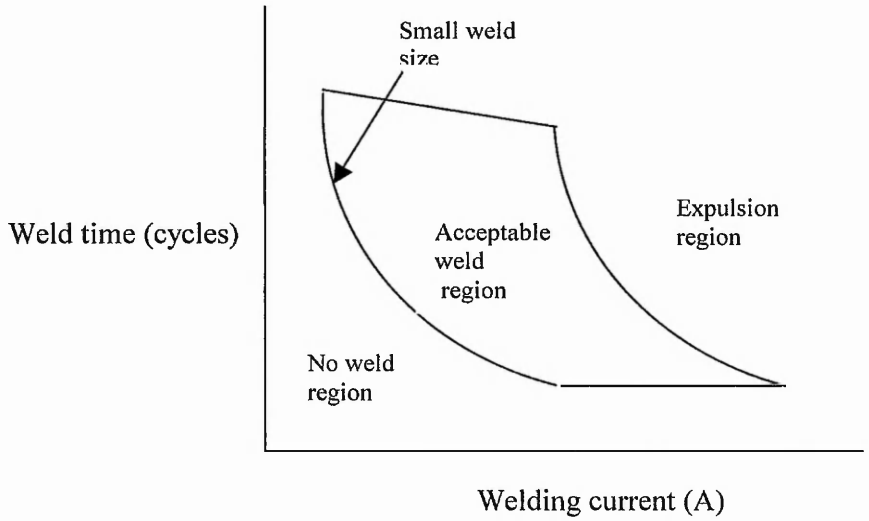

Figure 6.9 – Typical spot weld lobe curve

Experiments were carried out to determine the weld lobe of the servo spot welding machine by using various combinations of currents and weld times with pre-selected electrode forces ranging from 1.5kN to 7.5kN for the ECF condition described in section 4.3.2. The maximum force that can be produced from the developed spot welding machine without exceeding the couplings breaking torque of 50Nm is 7.5kN. A certain amount of force of approximately 0.5kN to 1.0kN will always be applied when the electrode comes into stall

condition depending on the speed at which the electrode is brought in contact with the steel sheets before the force control during squeeze cycle is activated. Hence the lowest force that could be supplied from the force control would range from 1.0kN to 1.5kN. Mild steel sheets with thickness of 2mm each and electrodes with tip diameters of 6mm were used in these experiments.

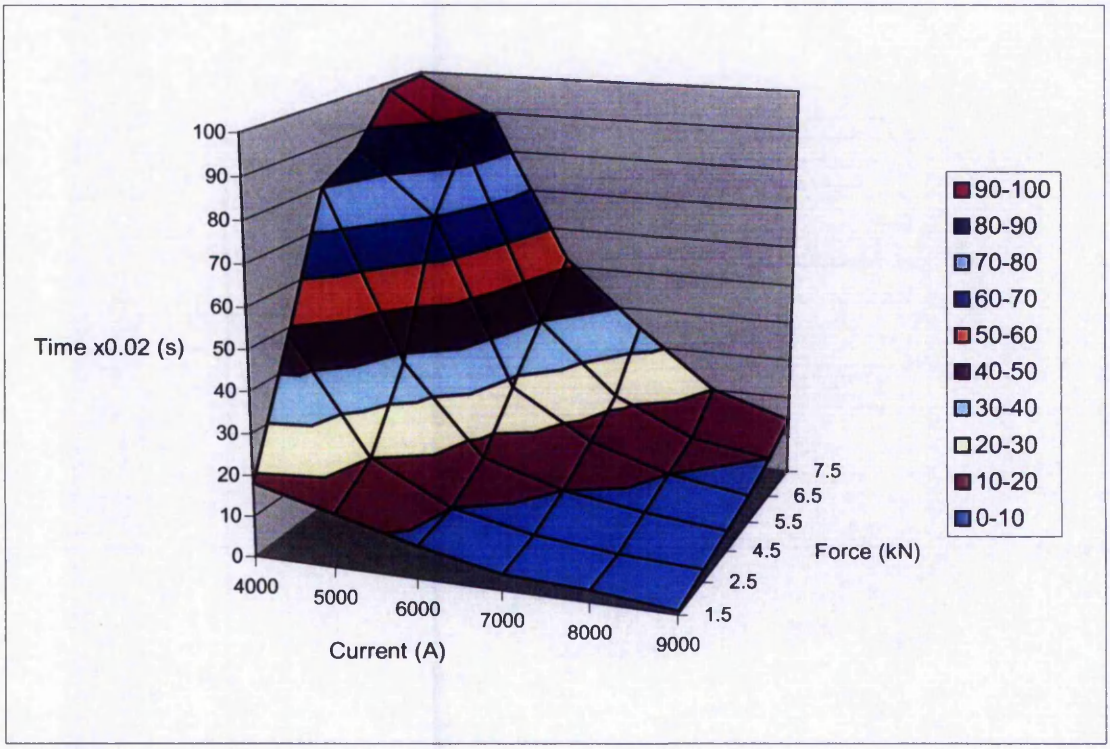

Figure 6.10– Lower weld curve for 2mm thick sheets under electrode clamping force condition

Figure 6.10 shows the lower weld curve where weld starts to develop due to the heat generated by the selected welding schedule. The lower weld curve of the servo spot welding machine shows that at 1.5kN force and 4000A current, weld starts to develop after about 360ms (18 cycles). When the current is increased to 9000A for the same force of 1.5kN, weld starts to develop after about 40ms (2 cycles). This shows that at a constant force, the rate of weld growth increases with increase in current. This is similar to the results obtained in the experiment in section 6.2.1.1. The same pattern was noticed for the other forces also where the curve converges downward to a

shorter cycle time when the current is increased. It was also noticed that for a constant current, when the electrode force is increased, the time taken for the weld to develop increases. For instance at 1.5kN and 4000A, weld starts to develop after about 360ms (18 cycles) and when the force is increased to 7.5kN and 4000A, the time needed for the weld to develop increased to about 1980ms (99 cycles). This is because at lower force, the resistance for current flow between the sheets is higher than at higher force, which causes high heat to be generated between the sheets to allow the weld to develop faster. Hence at higher force the weld current needs to be increased in order to produce a weld. A similar discussion was also presented for the experiment in section 6.2.2.1.

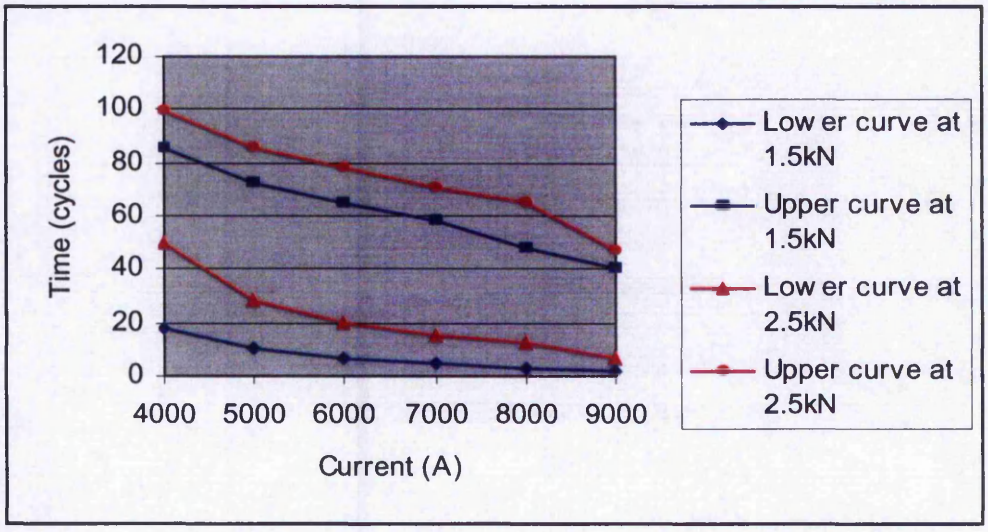

Figure 6.11– Weld lobe curves for 1.5kN and 2.5kN electrode forces

Figure 6.11 shows the weld lobes for two electrode forces of 1.5kN and 2.5kN. The lower curves as already been discussed in figure 6.10 above give the weld times needed to initiate welds using the chosen currents and forces. The upper curves give the weld times for the expulsion limits for the chosen currents and forces. Exceeding these limits would lead to expulsion. The figure 6.11 also shows that the weld lobe is shifted upwards to longer weld time when the electrode force is increased. As already been discussed, when the electrode force increases, the time needed to produce a weld also increases as seen in figure 6.10. Hence the time for expulsion to occur will also increase at a higher electrode force. This explains the movement of the lobe upwards in figure 6.11.

6.2.4 Conclusions of the experiments on the spot welding parameters

The conclusions of the experiments carried out on the important welding parameters that were discussed above can be summarized as below: -

1) weld strength increases with current until expulsion limit is reached
2) weld strength increases with weld time until expulsion limit is reached
3) expulsion due to overheating (high current and longer time) reduces weld strength
4) weld strength reduces with increase in force for the same current and time.
5) weld lobes moves to a longer weld time with increase in force because the time needed to produce a weld and for expulsion to occur for any chosen current increases with increase in force.

From the experiments discussed above, the effects of varying the current, weld time and electrode force on weld formation and also weld strengths were understood. The results of these experiments will be used to correlate with the results from the experiments on the weld monitoring techniques that will be discussed in the following sections.

6.3 Weld development monitoring techniques

6.3.1 Dynamic resistance

The secondary current and secondary voltage measured using the current probe and voltage probe as mentioned in sections 3.1.5 and 3.1.6 in chapter 3 were used to derive the dynamic resistance curve based on the equation 6.3 below:-

$$v_w(t) = i_w(t)R_w(t) + L_w . di_w(t)/dt \quad \text{---------- (6.3)}$$

where $v_w(t)$ = voltage, $i_w(t)$ = current, $R_w(t)$ = resistance and $L_w(t)$ = equivalent inductance between electrodes

Only peak points of the current waveform were taken in order to cancel the inductive component, which is very small and negligible (Asokkumar et al. 1997) i.e.: -

$t = t_1$ (time at peak point) $\quad di_w(t_1)/dt = 0 \quad \therefore R_w(t_1) = v_w(t_1)/ i_w(t_1)$

This is the dynamic resistance method that is widely used by most researchers even though a few used both the peak points of current and voltage and also the instantaneous values of current and voltage (Watney & Nagel 1984). The instrumentation setup used to measure the dynamic resistance during welding is discussed in the next section.

6.3.1.1 Instrumentation setup to measure dynamic resistance during welding

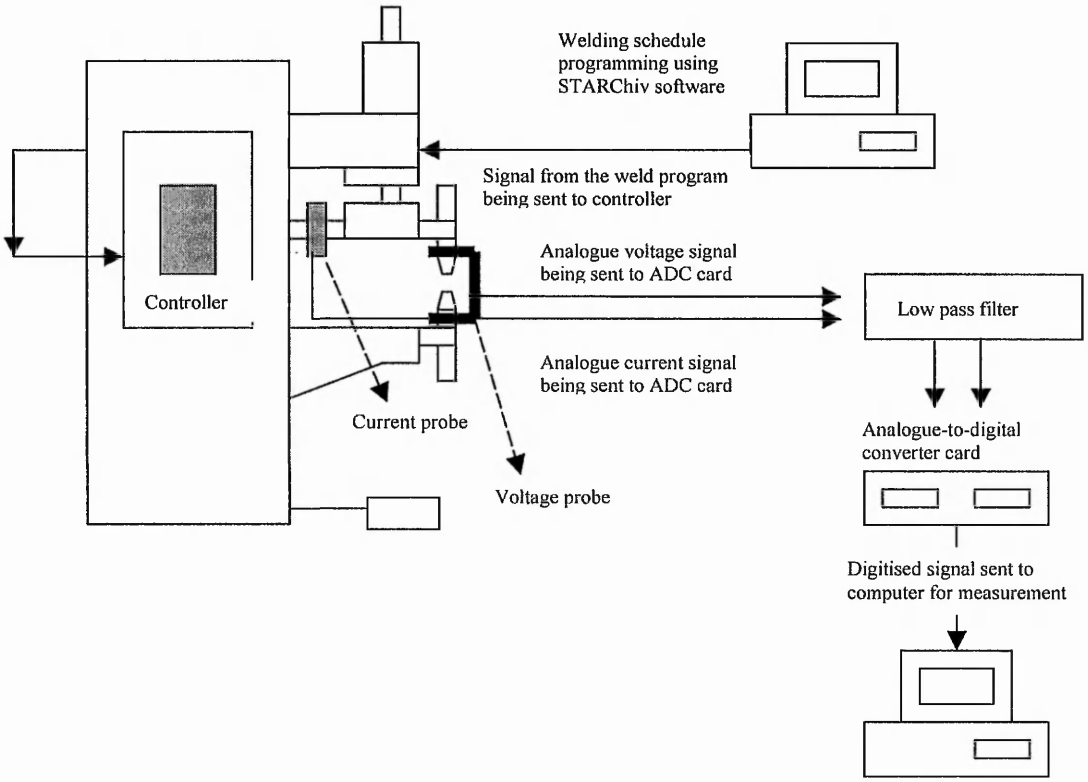

Figure 6.12 –Instrumentation for dynamic resistance measurement

Figure 6.12 shows the instrumentation for measuring the dynamic resistance during welding. The current and voltage signals measured during welding by the current probe and voltage probe are sent via a low-pass filter to the analogue-to-digital converter, which samples these signals at the rate of 1500 samples/sec. After welding has finished the digitized current and voltage waveforms are then fed into a curve fitting program developed using C which computes the peak point of the current waveform and the respective voltage value by means of two third order polynomial equations. Steps below explains the how the resistance points were computed for a 800ms (40 cycle) weld time.

6.3.1.2 Dynamic resistance evaluation algorithm

a) The points that are voltage values, which form the current and voltage waveforms, are fed into the C program as a 2 dimensional array [x][y] where the first column consists of the current waveform points and the second column consists of the voltage waveform points in the y-axis. The time in between these points in both the columns at the x-axis is 0.667ms.

b) The first 4 points from each column are then used to form 3rd order polynomial equations for both the current and voltage waveforms by means of the curve-fitting algorithm.

c) The third order polynomial equation for the current is then differentiated to get a quadratic equation in order to find the maximum and minimum points that represent the time in the x-axis. The time values are then evaluated to see if they fall in between the 2nd and 3rd points. If these values are not in between these points, both the polynomial equations are rejected. The first point in the previous set of points is ignored and another point (5th point) is taken as the fourth point and steps b) to d) are executed again to compute another two polynomial equations. If one of these points falls in between these points, this value represent the time at which the peak point of current occurs.

d) This value is then substituted into both the polynomial equations to get the values of the current and voltage at that time for a half cycle. The current value that is represented by a voltage value will be converted to the current value in term of amperes through a conversion factor. The voltage value is then divided with the current value to get the resistance value for that peak current.

e) The steps mentioned above are repeated for the 40 cycles and 80 resistance points will be obtained; 2 resistance values per cycle or 1 resistance value for each peak current.

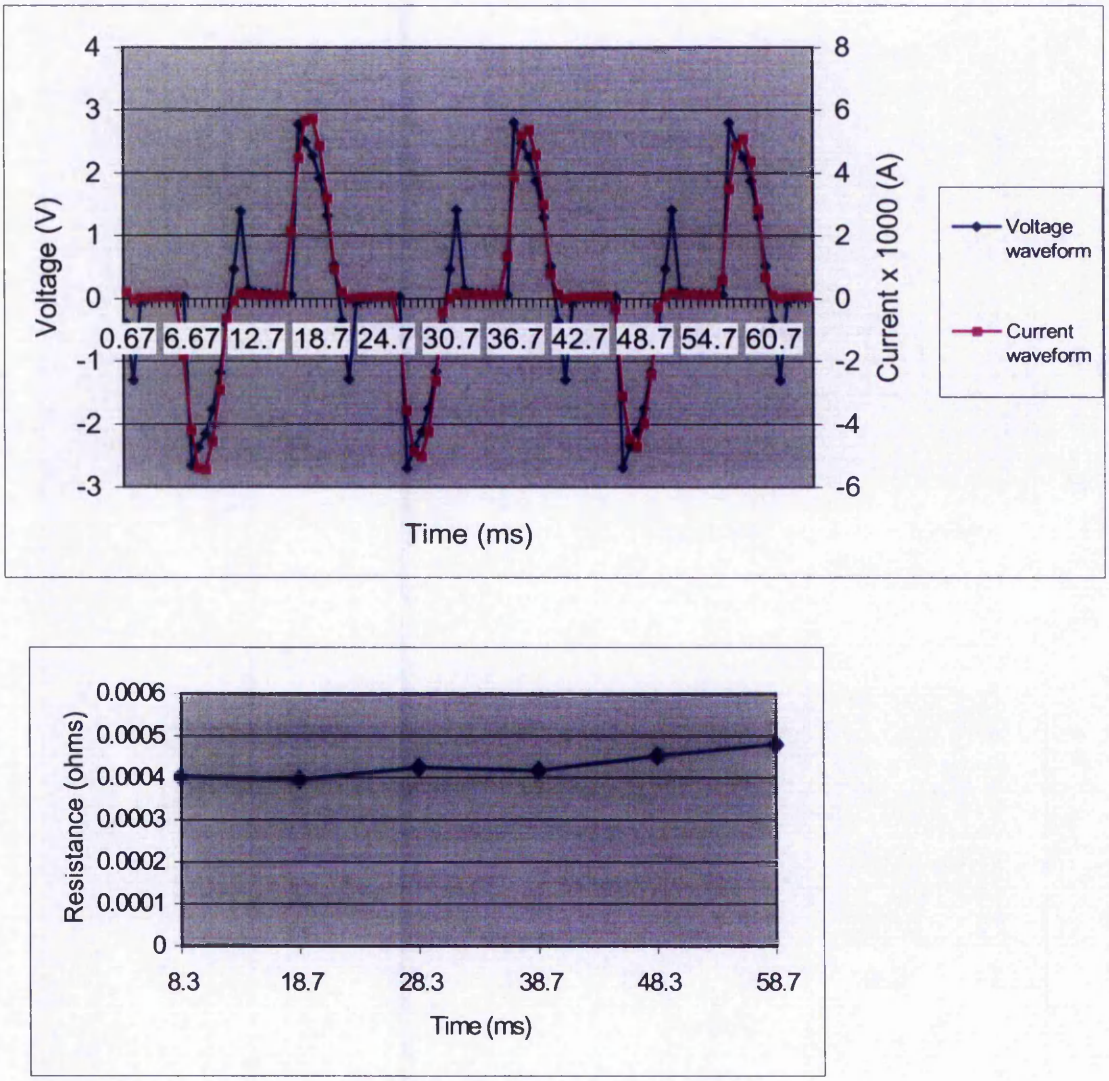

Figure 6.13– The dynamic resistance points

Figure 6.13 shows how the resistance points are computed for the first 6 cycles of the total 40 cycles weld time. Only 6 points were shown for clarity reason. The other 74 points are computed in the similar way to obtain dynamic resistance curve.

6.3.1.3 Interpretation of dynamic resistance curve

Figure 6.14 shows the interpretation on the dynamic resistance curve based on the changes in the curve. The curve is divided into 5 sections (Dickinson & Franklin 1980) :-

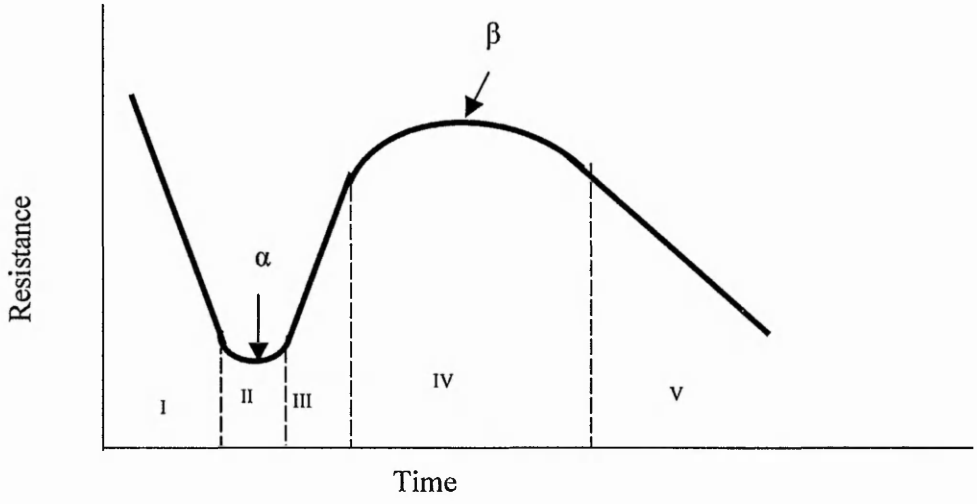

Figure 6.14 – Sections of the dynamic resistance curve

Section I – In this phase presence of impurities and surface contaminants on the surface of sheets to be welded which act as insulators cause an initial high resistance. The breakdown of these impurities due to heating increases the area of current flow causing the resistance to decrease.

Section II – In this phase the breakdown of the surface contaminants causes sheets surfaces to be exposed. Temperature rises due heating reduces the contact resistance between sheets and increases bulk resistance due to increase in resistivity of the bulk material. The reduction in contact resistance due to softening of contact area is balanced by the increase in resistance due to bulk heating at the transistion point α.

Section III - In this phase the heating of the bulk material continues to increase the bulk resistance till melting of sheet metals begin at the end of this section. During melting the contact resistance is zero and bulk resistance is increasing.

Section IV – In this phase the rate of increase in resistance is less than in section III due to the melting which reduced contact resistance to zero and a smaller increase in bulk resistance with the temperature being constant during the phase transformation. Weld starts to grow during this period. Transition point β is the point between increase in bulk resistance and reduction in resistance due to the increase is cross-sectional area at the interface because of the fused metallic bond. Experiments that will be discussed later will show how this β-point is actually used to interprete the achieved weld due to variations in current, time and force.

Section V- In this phase the increase in weld area and mechanical collapse due to softening of the sheet material further reduces resistance

The region of interest is the transition point β in section IV because the position of this point with respect to time indicates the weld development with respect to time.

6.3.2 Cha nges in the dynamic resistance curve for 4 welding currents

For this experiment, 4 welding currents of 4000A, 6000A, 7000A and 9000A were used. The weld time and electrode force were maintained constant at 800ms (40 cycles) and 1.5kN respectively. Electrodes with 6mm tip diameters and mild steel sheets each 2mm thick, were used in this experiment. 10 repetitions were made for each welding schedule.

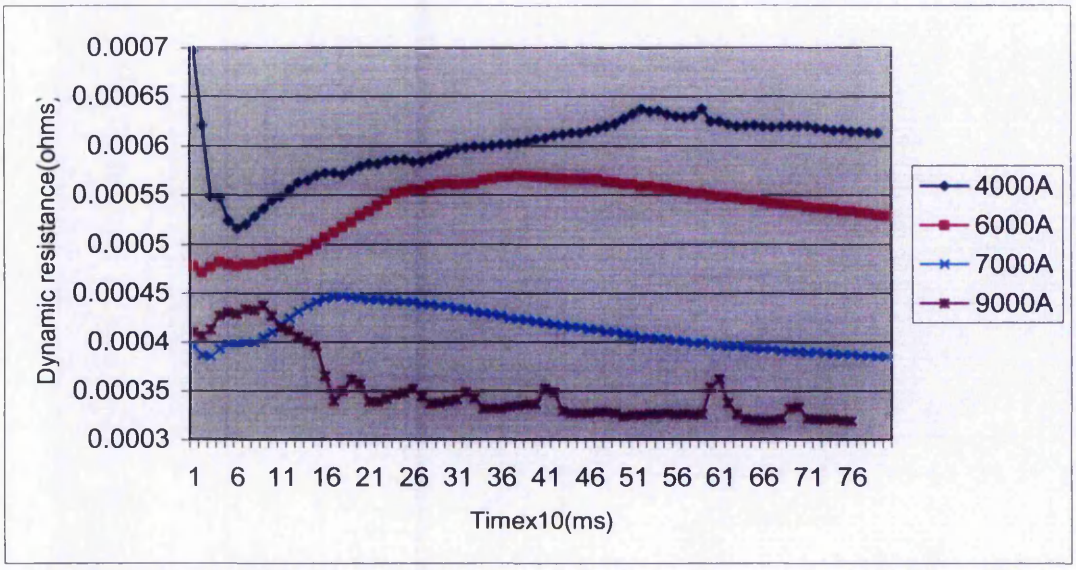

Figure 6.15 - Change in dynamic resistance curves for various welding currents

Current	Average strength	Standard Deviation	99% confidence interval	Heat generation	Average measured weld diameter
4000A	2.49kN	0.100	$2.39 < \mu < 2.59$	0.98kJ	2.54mm
6000A	3.52kN	0.147	$3.37 < \mu < 3.67$	1.95kJ	5.23mm
7000A	5.12kN	0.112	$5.00 < \mu < 5.24$	2.54kJ	6.20mm
9000A	6.68kN	0.163	$6.51 < \mu < 6.85$	4.12kJ	Expulsion

Table 6.8 – Changes in weld strength and diameter due to changes in current

As discussed in section 6.2.1.1, the weld grew stronger with the increase in current. The weld diameters in this experiment were measured using a vernier caliper. At 4000A, the dynamic resistance curve shows a peak about 0.5sec (25th cycle) indicating weld development at this time. However since the weld was developed later in time, the weld cycle ends before the weld is fully developed causing an undersize weld of about 2.54mm to be produced. For 6000A, a peak was noticed about 0.40sec (20^{th} cycle). The weld had enough time to grow about 5.23mm before weld terminates after 0.8sec. For 7000A, a peak was noticed about 0.17sec (9^{th} cycle) a weld diameter of about 6.20mm was achieved. At high current, more heat is supplied and the weld is formed earlier during the weld cycle (Bhattacharya 1972). Heat generation in table 6.8 was seen to increase with increase in current. At 9000A, expulsion occurs causing a rapid drop in the

resistance. Expulsion will increase the area for current flow causing the drop in resistance. Even though the weld strength does not indicate a drop as seen in table 6.8, sparks were developed during welding with this current and traces of molten metal expulsion were seen during testing. The heat values calculated based on equation 1 shows an increase with the increases in current and weld strength. This shows when the current is increased, the heat generation is increased and a stronger weld will be produced. This conclusion also supports the results in table 6.3 that shows the increase in weld strength with increase in current. However the expulsion condition in table 6.3 shows a significant drop in weld strength that was not noticed in table 6.6.

The correlation between the heat generated and the weld strength as shown in table 6.8 was analysed to estimate how both these variables affect each other. The correlation coefficient, r, was calculated based on the equation 6.4 (Freund 1992b):-

$$r = \frac{S_{xy}}{\sqrt{(S_{xx} * S_{yy})}} \quad \text{---------- (6.4)}$$

where x = heat generation variable , y = weld strength variable and S = sums of these variables
The value of r which has a range from –1 to +1 indicates how strong are the two variables related between each other. The determination coefficient r^2 is used to explain the proportion of variance in one variable accounted for by the other variable (Coolidge 2000) .

The significance of the correlation coefficient can be tested using the t test with the formula as below (Coolidge 2000):-

$$t = \frac{r * (N-2)}{\sqrt{(1-r^2)}} \quad \text{---------- (6.5)}$$

where r = correlation coefficent , r^2 = determination coefficent and N = number of samples

The analysis on the heat generated and weld strength were based on the raw data for heat and strength as in appendix C. The calculated r value of 0.942, indicate that there is a stronger positive relationship between the heat generated and the achieved weld strength. A stronger

relationship is assumed if the r value is between +0.5 and +1.0 or –0.5 and –1.0 (Coolidge 2000). The calculated t of 16.64 with 38 degrees of freedom, which is higher than p=0.001 of 3.551 shows significance in the relationship. The r^2 of 0.887 shows that 88.7% of the variance between heat and strength affects each other.

6.3.3 Changes in the dynamic resistance curve for 4 weld times at 6000A and 1.5 kN

In this experiment, 4 different weld times of 200, 400, 800 and 1000 ms (10, 20, 40 and 50 cycles) were programmed in the Starchive program. The current and electrode force were maintained constant at 6000A and 1.5kN respectively. Electrodes with 6mm tip diameters and mild steel sheets with 2mm thick each were used in this experiment. 10 repetitions were made for each welding schedule.

Weld time	Weld strength	Standard deviation	99% confidence interval	Heat generation	Average weld diameter
200ms	-	-		0.79kJ	No weld
400ms	3.21kN	0.48kN	$2.72 < \mu < 3.70$	1.89kJ	2.75mm
800ms	5.01kN	0.08kN	$4.93 < \mu < 5.09$	2.52kJ	5.23mm
1000ms	4.79kN	0.21kN	$4.57 < \mu < 5.01$	3.94kJ	Expulsion

Table 6.9– Change in weld strength and diameter for 4 weld times

Weld was found to increase in size with increase in weld time till the expulsion limit as explained in section 6.2.1.2. The weld diameters in this experiment were measured with a vernier caliper. A similar observation was noticed in this experiment as shown in figure 6.16 below. At 200ms (10 cycles) no weld was obtained since the time was too short for melting to occur. So there was no peak observed as in figure 6.16 within window 1. At 400ms (20 cycles), a β peak was observed in window 1 and the whole cycle ends in window 2 , which shows that weld growth starts at the end of the weld cycle. This would lead to development of undersize welds of about 2.75mm.

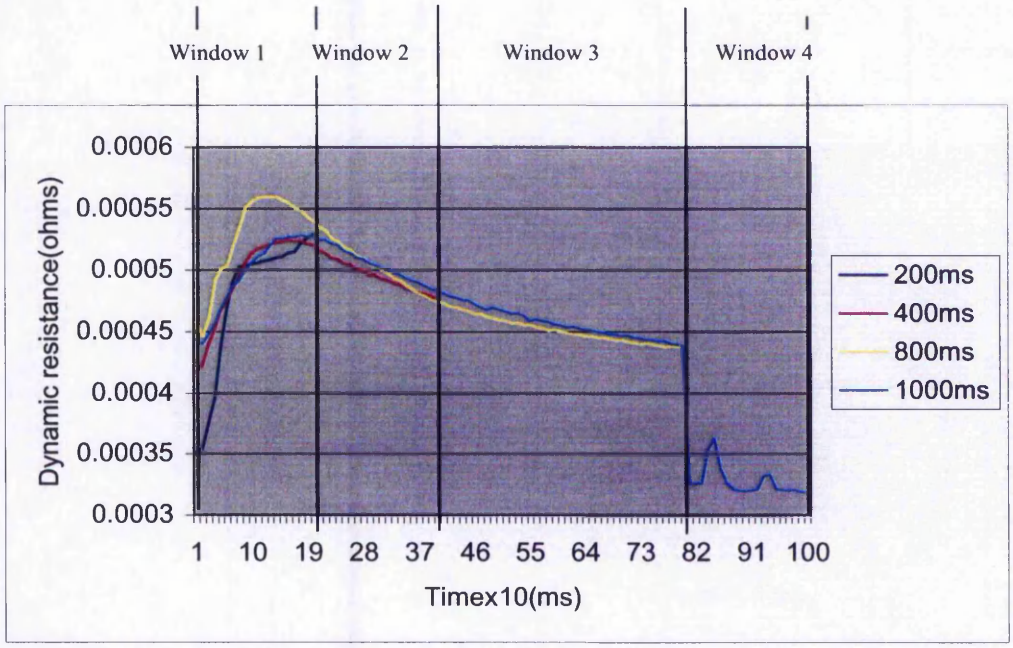

Figure 6.16 – Changes in the dynamic resistance curve for 4 weld times

However as the weld time is increased, weld has sufficient time to grow further to 5.23mm. This could be seen from the β peak developed in window 1 in figure 6.16 and the whole cycle ends only in window 3. At longer weld time as in the case of 1000ms (50 cycles), overheating causes expulsion to occur as seen in window 4. Similar to experiment 6.3.2, traces of metal expulsion as shown in figure 2.10 were noticed when the metal was destructively tested. Expulsion will increase the area for current flow causing a rapid drop in resistance. The heat values calculated based on equation 1 above also increase with increase in weld time and weld strength as seen in table 6.9. This shows the heat generation increases with longer weld time to produce stronger weld. This results also support the results in table 6.3 that shows the weld strength to increase with increase in weld time till expulsion limit. The results in section 6.3.2 and section 6.3.3 are supported strongly by the work done by other authors (Dickinson & Franklin 1980)(Watney & Nagel 1984).

The correlation analysis between the heat generated and the weld strength using the raw values of heat and strength as in appendix C, gave r value of 0.810 which shows there is a strong positive relationship between the heat generated and the weld strength because the value is closer

to +1.0. Positive relationship means increase in one variable would cause an increase in the other variable. The heat that did not produce a weld as in table 6.9 was not taken into consideration during the calculations for r. The calculated t value of 7.276 with a degree of freedom of 28 using equation 6.5, shows significance in the relationship between heat generated and weld strength when tested with lowest possible level of p = 0.001 of 3.674 ($t > p_{0.001} = 3.674$). The r^2 which gives a value of 0.653 shows that 65.3% of the variance between heat and strength are explainable. The r value calculated above took into account the heat and strength during expulsion that occurred in this experiment. The r was calculated again without taking into account the expulsion to study how this affect the r values. The new r gives a values of 0.980 which is better than the r that took expulsion into consideration. The new r^2 of 0.96 shows that 96% of the variance between heat and strength are explainable. The new t value of 21.14 again shows significance in the relationship because the t value rejects the null hypothesis. The results of this analysis states that without taking abnormal conditions such as expulsion into account, the weld strength will increase due to increase in heat generation for longer weld time.

6.3.4 Changes in dynamic resistance curve for 3 electrode tip diameters at 5000A and 1.2 kN

For this experiment, 3 different electrode tip diameters of 6mm, 8mm and 10mm were used. The current, weld time and electrode force were maintained constant at 5000A, 100ms (5 cycles) and 1.2kN respectively. Mild steel sheets each 2mm thick, was used in this experiment. 10 repetitions were made for each welding schedule.

An increase in tip diameter will cause a reduction in current density due to the increase in tip face area as in equation 6.6 below (Holliday et al. 1996):-

$$j = i / A \quad \text{---------- (6.6)}$$

where j = current density(A/mm^2)

i = current (A)

A = area of electrode tip (mm^2)

Electrode tip diameter (mm)	Weld strength (kN)	Standard deviation	99% confidence interval	Heat generated (kJ)
6	4.231	0.215	$4.010 < \mu < 4.452$	2.56
8	2.861	0.185	$2.671 < \mu < 3.051$	2.10
10	2.102	0.262	$1.833 < \mu < 2.371$	1.90

Table 6.10 – Changes in weld strength due to changes in electrode tip diameter

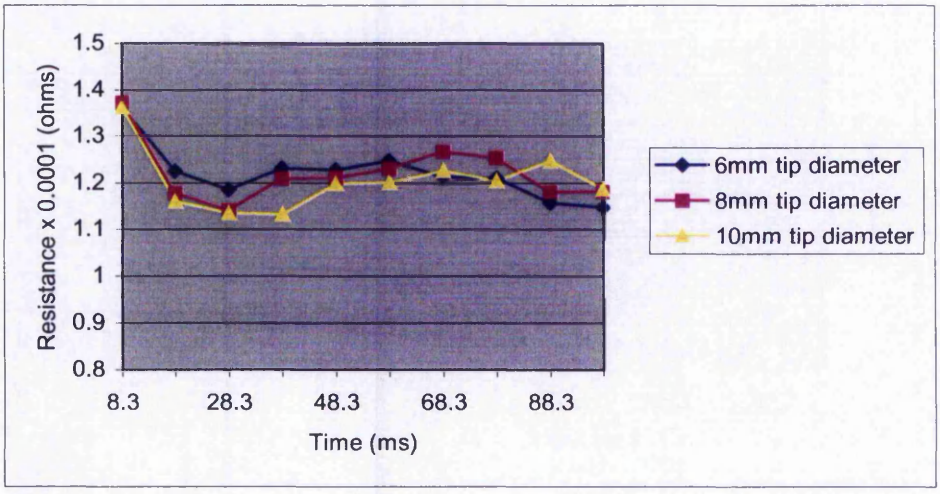

Figure 6.17 – Changes in dynamic resistance due to change in electrode tip diameter

This reduction in current density reduces the heat generation at the weld area. Using a 6mm diameter electrode tip diameter, the resistance β-peak was at 58.7ms. However using a 10mm tip diameter, the β-peak is only noticeable during 88.3ms for the same amount of current and weld time. A reduction in current density when using a 10mm diameter tip, causes a slower rate of weld growth compared to the weld growth rate for a 6mm tip diameter because the resistance peak, which indicates weld development, occurs later in time. Weld strength also was found to reduce with the increase in electrode tip diameter as shown in table 6.10 due to the reduction in the heat generation. Heat generation reduces because the current density reduces with the increase in electrode tip area according to equation 6.6 above.

Test samples	t values at 99%confidence interval
6mm and 8mm	15.27
8mm and 10mm	7.49
6mm and 10mm	19.87

Table 6.11 - T test results for the differences between average weld strengths for different electrode tip diameter

The t test results shown in table 6.11 indicates that all the calculated t values reject the null hypothesis and show significant differences between average weld strengths for different electrode tip diameters. This is because all these t values are $\geq t_{0.005} = 2.878$ for 99% confidence interval. Hence these tests confirm that the increase in tip diameter reduces weld strength to significant difference between them.

The correlation analysis between the heat generated and the weld strength using the raw data as in appendix C gave a r value of 0.889 which shows there is a stronger positive relationship between the heat generated and the weld strength because the value is within +0.5 and +1.0. The calculated t value of 9.987 with a degree of freedom of 28 using equation 6.5, shows the significance in the relationship between heat generated and weld strength when tested with lowest possible level p = 0.001 of 3.674 ($t > p_{0.001} = 3.674$) . The determination coefficient r^2 which gives a value 0.782 however shows that 78.2% of the variance between heat and strength are explainable. The result of this analysis indicates even though electrode deformation due to increase in tip diameter occurs during the welding process, the weld strength and heat generation would still have a positive relationship.

6.3.5 Conclusions on the experiments on dynamic resistance

The conclusions of the experiments carried out on the dynamic resistance curves can be summarized as below: -

a) With increase in welding current at constant time and force, the dynamic resistance β peak occurs earlier during the weld time showing that the rate of weld development increases with increase in welding current till the expulsion limit. The increase in the rate of the weld growth also increases the weld strength till expulsion limit.

b) With increase in weld time at constant current and force, the dynamic resistance covers a wider range in the 'weld time window' with the dynamic resistance β peak occurring earlier in the weld time as in figure 6.16. This shows that the weld had sufficient time to grow with the increase in weld time till the expulsion limit. Further increase in time causes overheating and expulsion. This increase in time also increases the weld strength till expulsion limit where there would be a rapid drop in the resistance as shown in figure 6.16.

c) The use of a larger electrode tip diameter causes the dynamic resistance β peak to occur later in the weld time due to reduction in current density. Reduction in current density reduces heat generation and lowers the rate of weld growth.

Through the experiments carried out on the dynamic resistance curve, the effects of changing the welding current, time and electrode tip diameter on changes in the dynamic resistance curves were understood. The results obtained from these experiments were also found to agree with the results obtained in section 6.2. Similar work carried out by Dickinson(1980) and Asokkumar(1997) supports the results obtained in this section.

6.4 Electrode displacement

Weld growth causes expansion of the material, which creates a force opposite to the welding force (Broomhead & Dong 1990). This force creates a separation between the upper and lower electrode that is proportional to weld expansion (Tsai et al. 1992). A linear-variable-differential- transformer (LVDT) was mounted on the upper arm of the spot welding machine as shown in figure 3.4 of section 3.1.7 to measure the expansion during weld growth by means of the displacement of the upper electrode relative to the fixed lower electrode.

6.4.1 Instrumentation setup to measure electrode displacement

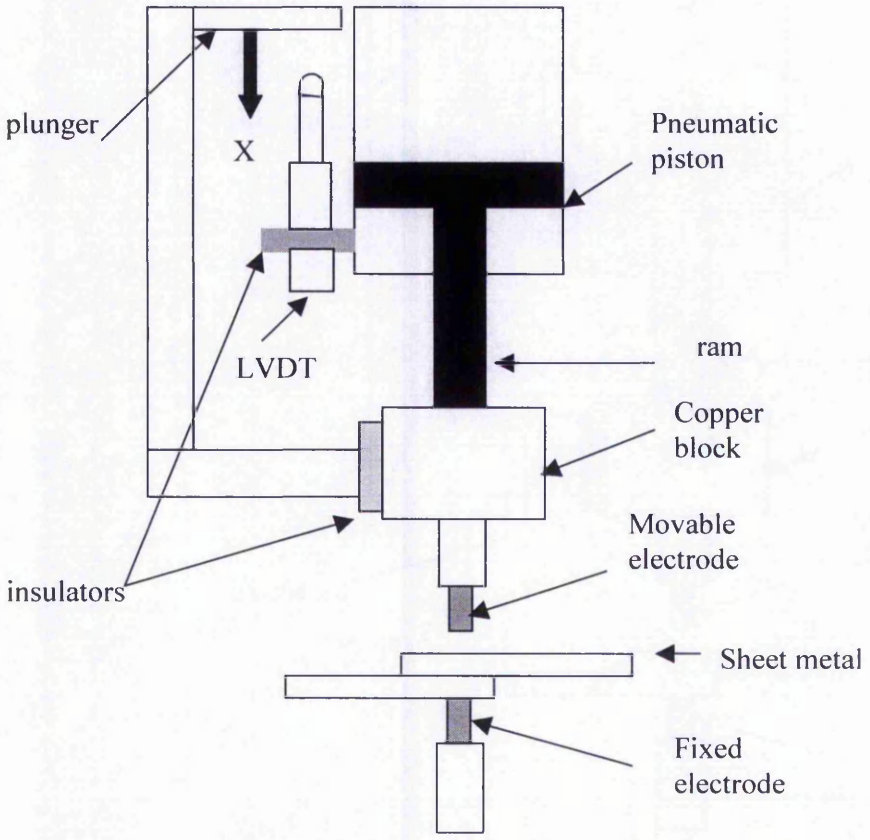

Figure 6.18 – Schematic diagram of the LVDT attachment to the spot welding machine

Figure 6.18 shows a schematic diagram of how the LVDT was fitted to the pneumatically actuated spot welding machine in order to measure electrode displacement during welding.

The plunger and the electrode holder through which the movable electrode is fitted are connected to a copper block. This copper block is connected to the end of the ram that was discussed in section 4.1.3 in chapter 4. When the ram moves downwards due to the movement of the piston, the moveable electrode will come in contact with the sheet metals. During this movement, the plunger will also move downwards in the X direction and come in contact with the LVDT the same time the electrode comes in contact with the metal sheets. Since both the plunger and electrode are connected to the same copper block, movement of the electrode will be equivalent to the movement of the plunger. During welding, the movement of the movable electrode due to material softening and weld expansion will be transmitted by the plunger to the armature of the LVDT so that the LVDT could measure this electrode movement.

6.4.2 Interpretation of the displacement curve

Figure 6.19 below shows a typical electrode displacement curve (Broomhead & Dong 1990):-

In region I – this is the region during the weld cycle. The temperature increase causes the melting of the material and weld growth. Expansion due to weld growth causes the upper electrode to move upwards away from the fixed lower electrode. This increases the separation distance between the upper and lower electrodes, which has an initial separation distance equal to the thickness of the sheets in between them.

In region II – this is the region during the hold cycle when the current is turned off. The weld will cool down under pressure. The weld t ends to contract during c ooling causing the separation distance between the upper and lower electrodes to decrease.

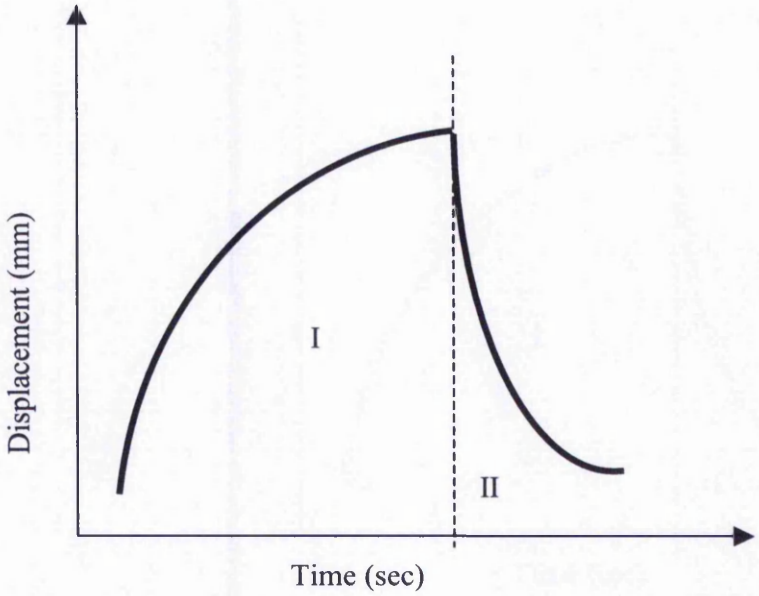

Figure 6.19 – Sections of the electrode displacement curve

Figure 6.20 shows the displacement curve with the current waveform during the weld cycle obtained in this experiment. This figure shows that at constant electrode force, increase in electrode displacement due to weld expansion occurs during the weld cycle.

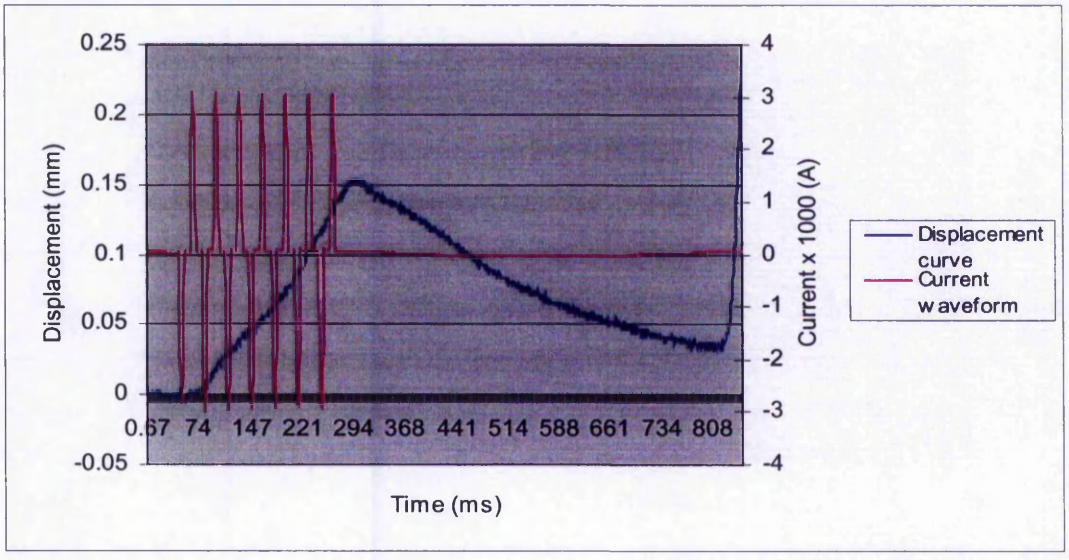

Figure 6.20 –Relationship between displacement curve and current waveform

6.4.3 Changes in the electrode displacement due to changes in current

For this experiment, welding currents ranging from 5000A to 9000A were used. The chosen currents are below the expulsion limit. The weld time and electrode force were maintained constant at 400ms (20 cycles) and 2.4kN respectively. Electrodes with 6mm tip diameters and mild steel sheets with 2mm thick each were used in this experiment. 10 repetitions were made for each welding schedule.

As already discussed in sections 6.1.2, 6.2.1.1 and 6.3.2, weld diameter increases with increase in welding current. This increase in weld expansion was measured in this experiment by means of measuring the upper electrode movement. Table 6.12 shows the displacement of the upper electrode due to weld growth and indentation of the electrode into the metal for 5 welding currents during weld cycle.

Welding current	Average maximum displacement (mm)	Standard deviation (mm)	99% confidence interval	Average indentation (mm)	Average weld diameter (mm)
5000A	0.162	0.00596	$0.152<\mu<0.171$	0.320	No weld
6000A	0.264	0.00759	$0.247<\mu<0.282$	0.349	2.56
7000A	0.453	0.00667	$0.347<\mu<0.461$	0.371	5.11
8000A	0.682	0.04641	$0.629<\mu<0.724$	0.384	6.32
9000A	1.041	0.012542	$0.091<\mu<1.172$	0.396	6.89

Table 6.12– Results of changes in the electrode displacement due to changes in current

Figure 6.21 shows the increase in welding current increases electrode displacement. Electrode displacement increases from 0.162 mm at 5000A to 1.041 mm at 9000A. However the displacement at 5000A is purely due to material expansion since there was no weld developed. The displacements from 6000A to 9000A are due to material expansion and weld expansion since the average weld diameter increased from 2.56mm to 6.89mm. Even though the weld strength values are not given in table 6.12, the measured weld diameters are shown to increase with the

increase in current that obviously means the weld strength is increasing as discussed in earlier experiments. T tests based on equation 6.2 in this chapter were carried out to evaluate the significance of the differences between the average displacement values. Table 6.13 shows the t tests results.

Test samples	t values at 99% confidence interval
5000A and 6000A	32.768
6000A and 7000A	30.983
7000A and 8000A	-21.785
8000A and 9000A	8.584
9000A and 5000A	22.292

Table 6.13– T test results for difference between mean electrode displacements values for various welding currents

The t test results show that all the calculated t values reject the null hypothesis of no difference and show significant differences between average electrode displacement values. This is because all these t values are either $\leq t_{0.005} = -2.878$ or $\geq t_{0.005} = 2.878$ for 99% confidence interval. Hence these tests conform that the increase in welding current increases electrode displacement to significant difference between average displacement values. A similar work (Jou 2003) to this experiment supports the result above.

The true electrode displacement can be obtained from the equation 6.7 below: -

Electrode displacement = Material expansion – Weld contraction – Electrode penetration ---- (6.7) (Waller 1964)

The indentation of the electrode into the sheet metal was found to increase with welding current. The indentation was measured by means of the micrometer similar to the way Hasselman (2002) measured electrode indentations for his work. The thickness of both the metal sheets at the center of the weld was measured using the micrometer. This reading is subtracted from the

thickness of both the metal sheets outside the weld region (≈4.000mm) to calculate the indentation.

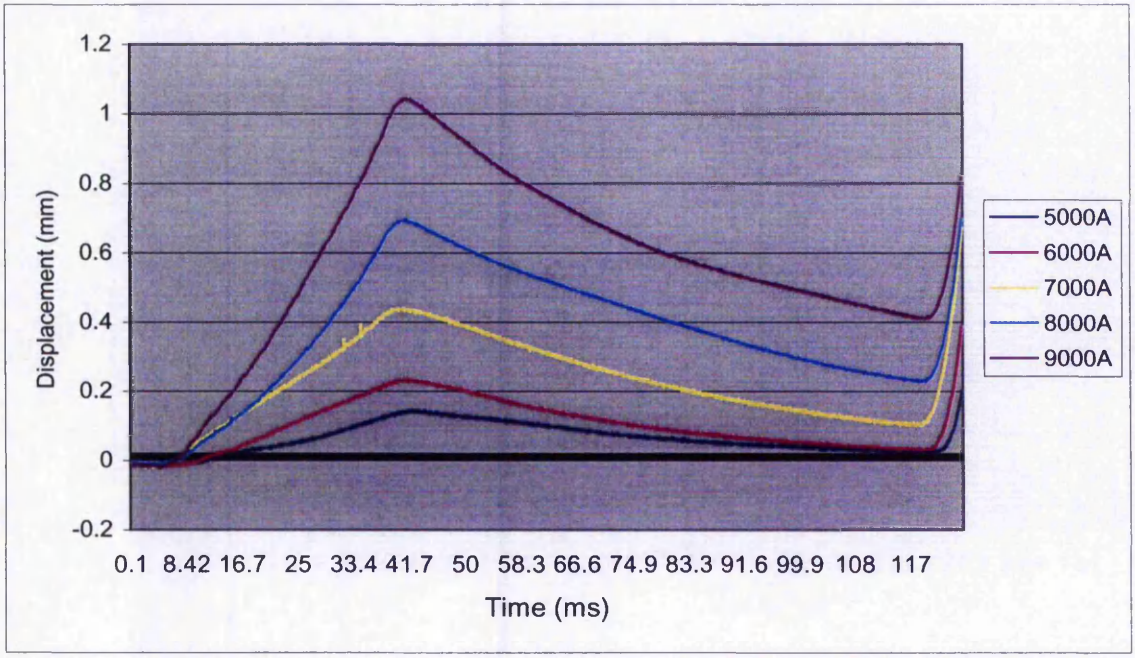

Figure 6.21 – Changes in electrode displacement due to increase in current

The increase in indentation is because a higher current causes the rate of softening of the material to increase (Broomhead & Dong 1990). This phenomenon causes the penetration of the electrode into material to increase at high current.

6.4.4 Changes in electrode displacement due to change in force with constant current (10000A)

Welding current of 10000A and weld time of 400ms (20 cycles) with 3 different electrode forces of 2.4kN, 3.6kN and 4.8kN were chosen for this experiment. Electrodes with 6mm tip diameters and mild steel sheets with 2mm thick each were also used in this experiment. 10 repetitions were made for each welding schedule.

Force (kN)	Average maximum displacement(mm)	Standard deviation	99% confidence interval	Average strength (kN)	Standard deviation
2.4	0.176	0.0072	$0.175 < \mu < 0.177$	1.94	0.10
3.6	0.091	0.0074	$0.091 < \mu < 0.092$	1.07	0.18
4.8	0.040	0.0108	$0.039 < \mu < 0.042$	-	-

Table 6.14 – Changes in the electrode displacement due to change in force

Table 6.14 shows that the electrode displacement reduces with increase in electrode forging force. Changes in electrode deformation was monitored during this experiment. Reduction in electrode displacement is because weld expansion reduces with increase in force due to reduction in heat generation. As discussed in section 6.2.2.1, weld strength reduces with increase in force. Similar results were obtained in this experiment where the weld strength for 3.6kN electrode force is lesser than the weld strength for 2.4kN electrode force and no weld was developed at electrode force of 4.8kN.

T tests were carried out on the average displacement values to determine if they have significant differences.

Table 6.15 gives the results of these tests.

Test samples	t values at 99% confidence interval
2.4kN and 3.6kN	259.727
3.6kN and 4.8kN	-122.445
4.8kN and 2.4kN	-330.602

Table 6.15 – T test results for difference between mean electrode displacements values for various weld forces

The t test results show that all the calculated t values reject the null hypothesis and show significant differences between average electrode displacement values. This is because all these t values are either $\leq t_{0.005} = -2.878$ or $\geq t_{0.005} = 2.878$ for 99% confidence interval. Hence these tests conform that the increase in weld force reduces electrode displacement to significant difference between average displacement values.

6.4.5 Conclusions of the experiments on electrode displacement

The conclusions of the experiments carried out on the electrode displacement during welding below the expulsion limit can be summarized as below: -

a) electrode displacement increases with welding current at constant force and weld time due to increase in weld expansion.
b) electrode indentation increases with increase in current since the rate of softening of material increases at high current
c) electrode displacement reduces with increase in force at constant current and weld time

The results in the experiments support well the results in sections 6.2 and 6.3 and proved that electrode displacement could be used as a reliable method to monitor weld growth during welding. This electrode displacement method will be used later to correlate the results from a piezoelectric force sensor that will be discussed in the next section.

6.5 Electrode force profile

A peizo-electric sensor mentioned in section 3.1.8 was fitted to the frame of the machine for indirect measurement of the electrode force. This section also shows the calibration of the sensor using a load cell.

6.5.1 Theoretical electrode force

The theoretical electrode force profile (AWS 1980) for a spot welding process is as shown in figure 6.22. During the squeeze cycle, electrode force is increased to a preset value by means of pneumatic actuation. The force is maintained at the preset value during weld and hold cycle. Electrode force gradually reduces during the off cycle when the electrodes are released from the welded sheets.

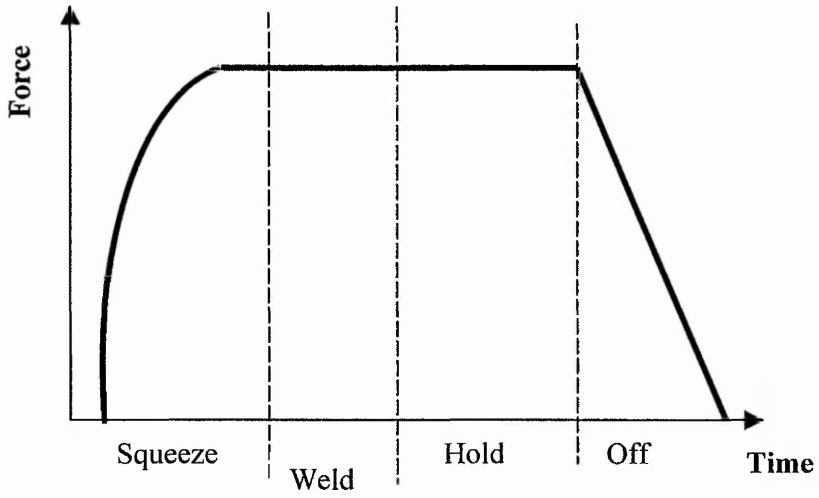

Figure 6.22 – Theoretical force profile

6.5.2 Real force profile

A force profile during experiment shows that the measured force during weld cycle is as shown in figure 6.23. The real profile showed an increase in force during the weld cycle (Tang et al. 2000).

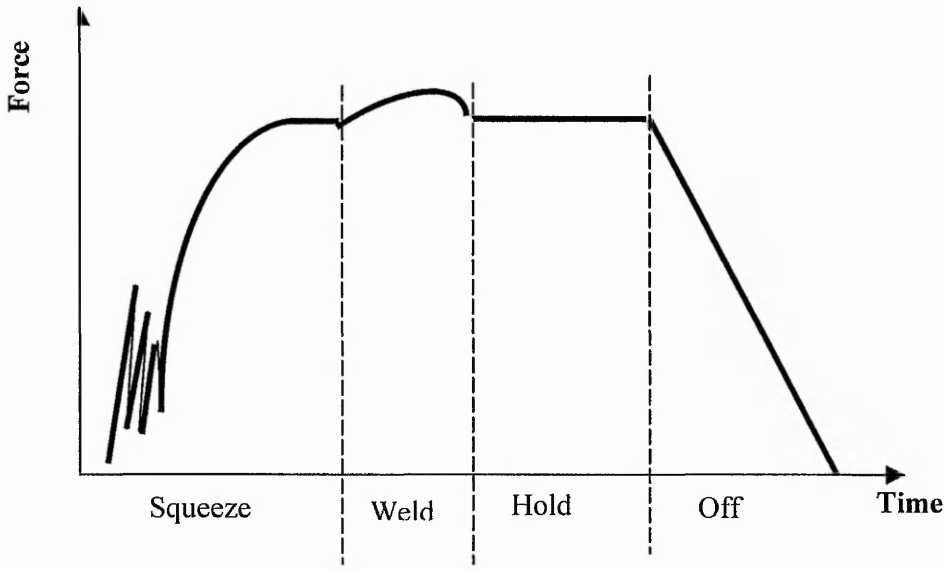

Figure 6.23 – Real force profile

6.5.2.1 Changes in the electrode force profile for 3 pressure settings

The changes in the force profile for 3 preset pressures were investigated by changing the pressures from 2 bar to 4 bar and keeping the current and time constant. Figure 6.24 shows the force profile increases with increase in the preset pressure. This is because at higher pressure, the sheet metals will be pressed harder by the electrodes causing the piezoelectric sensor to record a higher force. ΔF_{max} is the difference in force between the preset force before weld is initiated and the maximum force recorded by the piezoelectric sensor during welding. Table 6.16 tabulates these results.

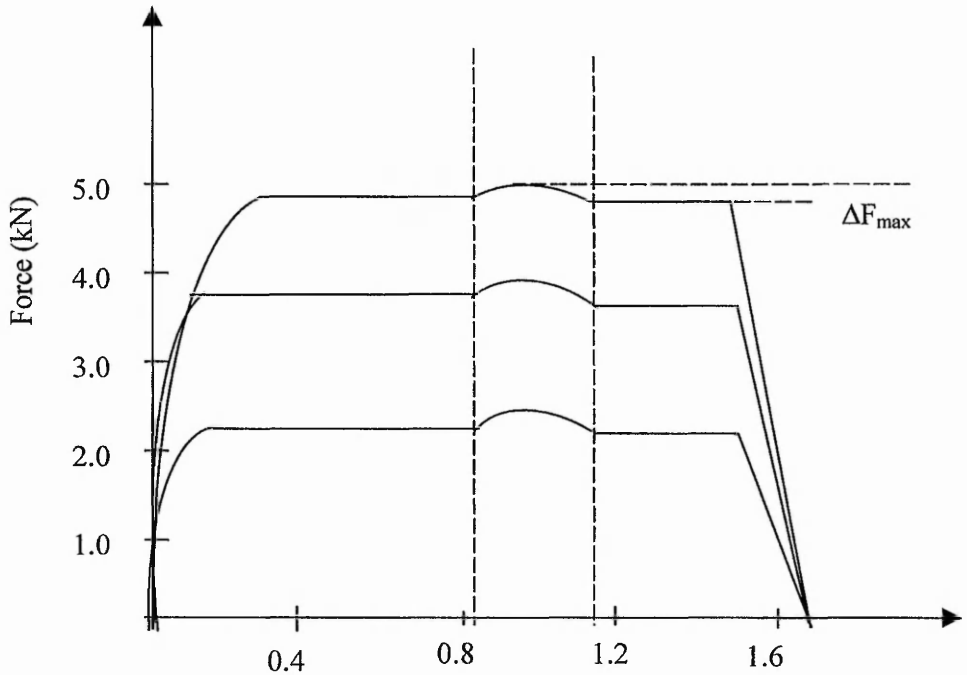

Figure 6.24 – Changes in force profile for different preset pressures

Pressure gauge setting (bar)	Achieved force during squeeze cycle (kN)	ΔF_{max} (kN)	Standard deviation for ΔF_{max} (5 reps)
2	2.4	0.14	0.00694
3	3.6	0.089	0.00748
4	4.8	0.024	0.00612

Table 6.16 – Changes in the force profile due to changes in the pressure setting

The static electrode force for any given pressure can be calculated based on the equation 6.8 (Anon 2000b): -

Force = 22/7 x Diameter^2 x ¼ x Air pressure ---------- (6.8)

For the pneumatic welding machine used in this experiment, the pressure to force conversion is 1 bar is equivalent to 1.2kN for a 125mm diameter pneumatic cylinder.

6.5.3 Weld development and force profile

Figure 6.25 shows the force profile (with and without curve fitting) and the electrode displacement curve obtained in this experiment. Since the force signal has a strong noise during the weld stage, due to electrical-magnetic interference, the trend in the change of the force profile was represented by curve filtering technique. As already seen in figure 6.20, the increase in electrode displacement occurs during the weld cycle and represents the weld growth. Similarly the electrode displacement occurs when the force increases during the weld cycle. This explains that the increase in force during the weld cycle is due to weld expansion. Electrode force constrains the thermal expansion of the weld. When the thermal expansion increases, it suffers from a stronger constraint and creates a larger reaction force. Therefore a force change is expected (Tang et al. 2000).

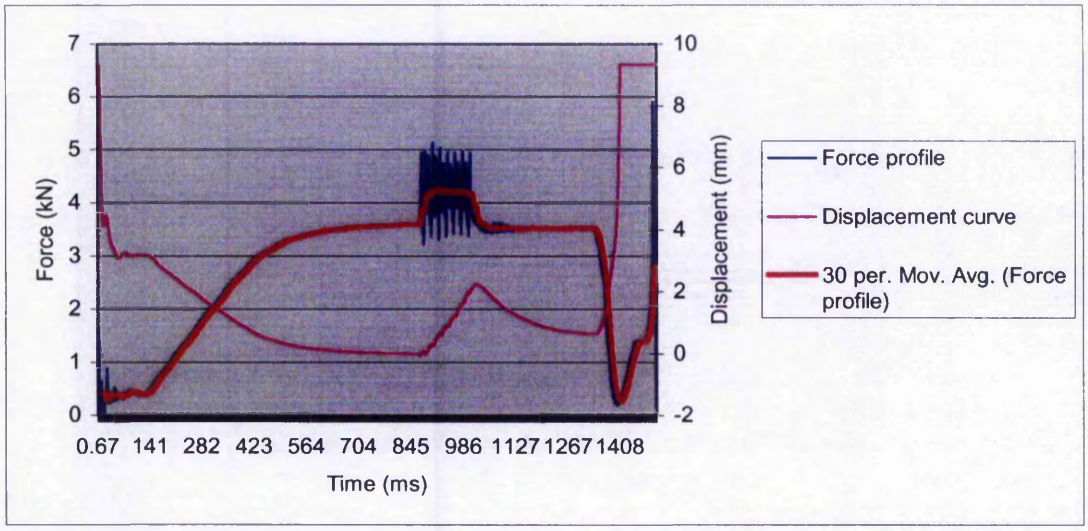

Figure 6.25 – Displacement curve and force profile (with and without curve fitting technique)

6.5.3.1 Changes in force profile due to changes in current

For this experiment, 5 welding currents ranging from 6000A to 10000A were used. The experiment was carried out below the expulsion limit to avoid expulsion. The weld time and electrode force were maintained constant at 400ms (20 cycles) and 2.4kN respectively. Electrodes with 6mm tip diameters and mild steel sheets each 2mm thick were used in this experiment. 10 repetitions were made for each welding schedule.

Current	Average displacement(mm)	Average weld diameter(mm^2)	Average weld strength(kN)	Standard deviation (kN)
6000A	0.0253	1.48	1.01	0.10
7000A	0.0357	2.89	1.20	0.12
8000A	0.0688	5.12	1.98	0.09
9000A	0.0980	6.12	2.20	0.10
10000A	0.1300	6.48	2.56	0.04

Table 6.17 – Experiment on the change in force profile due to increase in current

Table 6.17 shows the obtained results.

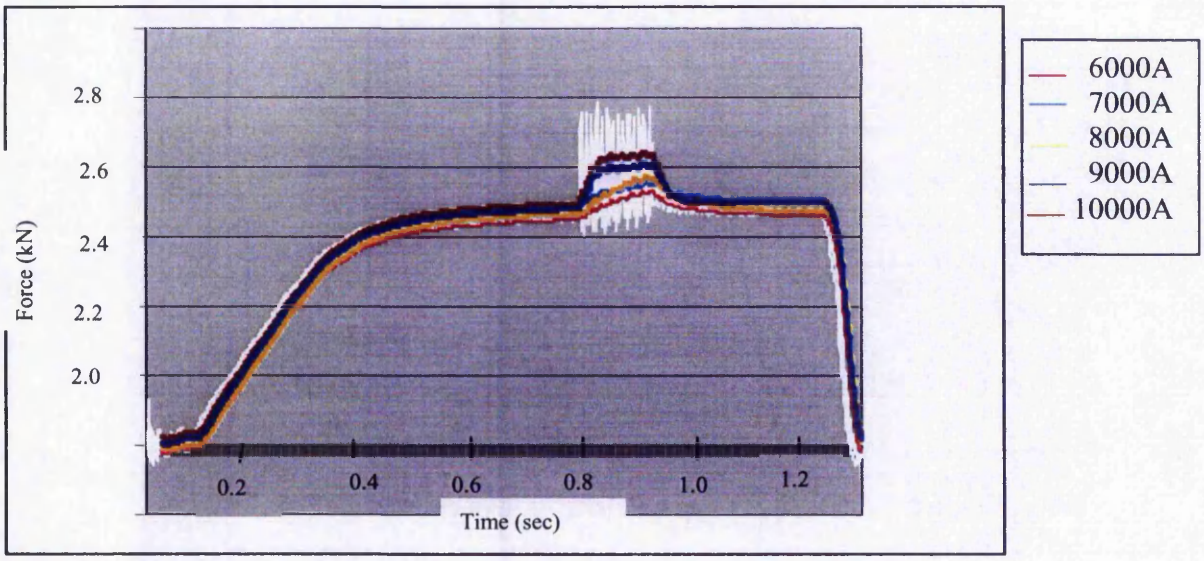

Figure 6.26 – Changes in force profile due to change in current

Figure 6.26 shows the changes in the force profile during the weld cycle for various welding currents.

ΔF_{max} increases with increase in current. This increase in ΔF_{max} is because of the increase in the expansion of the weld and weld growth. The increase in the electrode displacement that directly represents weld expansion supports the observation. Electrode displacement increases from 0.0253mm to 0.1300mm for 6000A to 10000A. When the weld expands, it tends to increase the distance between electrodes causing disturbance in the force equilibrium and create an opposite reaction force due to the constraint from the supplied force. When the expansion is higher, an even higher reaction force is created causing the positive increase in the force signal. A report published by Kistler Instruments AG (Kirchheim & Shaffner 2002) shows the same kind of force profile created using the same piezoelectric sensor used in this study.

6.5.4 Conclusions from the experiments on the electrode force profile

From the experiments carried out on electrode force profile, the following conclusions can be made: -

a) Electrode force increases from the preset force during a weld cycle due to weld expansion

b) ΔF_{max} increases with increase in the weld expansion

c) Force profile increases with increase in pressure.

6.6 Summary of the chapter

The effect of varying the current, time and force to weld strength were investigated in the experiments reported in this chapter. Weld strength was found to increase with the increase in current and time till the expulsion limit is achieved as shown in sections 6.2.1.1 and 6.2.1.2. The t tests in tables 6.4 and 6.5 show significant differences between the average weld strengths achieved for different welding current and weld times. However insignificance difference between weld strengths were obtained due to expulsion because of the drop in the weld strength during this condition. Similarly weld strength was also found to increase with the reduction in force till the expulsion. T test in table 6.7 shows significant differences between average weld strengths for different electrode forces when tested with 95% confidence interval. Experiments on the use of the weld monitoring methods to monitor weld growth were also carried out. The dynamic resistance curve was found to indicate the weld growth based on the β-peak, which is a transition point between the increase in the bulk resistance due to heating of the material and the decrease in resistance due to softening of material during melting and mechanical collapse. The change in the resistance curve agrees well with the results of the experiments on current, time and force. T test carried out in table 6.11 for the achieved average weld strengths for 3 different electrode tip diameters shows the there are significant differences between the average weld strengths for different tip diameters. Weld strength was found to reduce with increase in tip diameter due to reduction in the current density. Electrode displacement was found to increase with increase in current and decrease with increase in force. This is because the weld size was

found to increase with the increase in current and decrease with the increase in force as shown by the results obtained from the weld parameters experiments. Hence both the results from these experiments indicate similarities. T tests carried out in tables 6.12 and 6.14, show significant differences between the average electrode displacements for various welding current and electrode forces. The ΔF_{max} in the force profile was found to increase with the increase in current. It was concluded that this increase is due to weld expansion because the measured electrode displacement that relates well to weld expansion was also found to increase during this experiment as seen in table 6.17. All these results discussed above will later be used to interpret the results that will be obtained from the experiments on the force control during welding which will be discussed in the next 2 chapters.

Chapter 7

INVESTIGATION INTO THE EFFECT OF FORCE CONTROL DURING WELDING ON WELD STRENGTH

In this chapter the results obtained from the forging force control during welding by using 4 force profiles are presented and discussed. Initially 3 constant forging forces were used during welding to study the relationship between force and resistance. Later 4 varying forging force profiles were used for the study. The dynamic resistance curves were used to study the variation during weld cycle for the 3 constant forging forces and the 4 varying forging force profiles. The effects of these variations in resistances for all the 7 types of forging force profiles were studied by calculating the amount of heat generated and measuring the respective weld strengths. The heat generated was calculated using the equation 6.1 in section 6.1.2, for all the results presented in this thesis. Further studies on the changes in the force profile characteristics were also carried out and the resistance changes were investigated, with the aim of developing a force profile that would produce a stronger weld. The t-test was used to test the significance of the difference between means (μ) of sample data as described in section 6.2.1.1. The correlation coefficient r, for sample data was calculated based on the values using equation 6.4 in section 6.3.2.

7.1 Relationship between the dynamic resistance curve and force

The dynamic resistance curve as discussed in section 6.3.1 is one of the methods that is widely used in the spot welding industries (Chien & Kannatey-Asibu 2001). This curve gives

the changes in the resistance, which consists of contact resistance and bulk resistance, during the spot welding process. Resistance change occurs during welding due to the heating of the material, melting once temperature reaches melting point of material and softening of the material and mechanical collapse due to melting (Bhattacharya & Andrews 1974). The explanation of how resistance decreases with the increase in electrode forging force had been discussed earlier in section 2.8.1 in chapter 2. An experiment was carried out to clarify the mentioned relationship by using 3 different forging forces and studying the corresponding dynamic resistance curves. This is presented below.

7.1.1 Changes in the dynamic resistance curve for 3 different electrode forging forces

Three electrode squeeze forces were used in this experiment. The forces were 1.5kN, 2.5kN and 3.5kN. These 3 forces were maintained constant as the forging forces during the weld cycle. The welding currents used were 6000A and 9000A. The weld time of 400ms (20 cycles) and the hold time of 200ms (10 cycles) were programmed in the WS2000 weld timer. The thickness of the sheet metals used was 2mm each and the electrode tip diameter was 6mm. Electrodes with 6mm tip diameters were used in all the following experiments as recommended (Anon 2000b). Each welding schedule was repeated 5 times, and the weld strength values were measured. In all these experiments, the squeeze force was applied through the squeeze force control system as discussed in section 4.3.2. When the required force was reached, the weld cycle was initiated by pressing the footswitch shown in figure 3.1 in chapter 3.

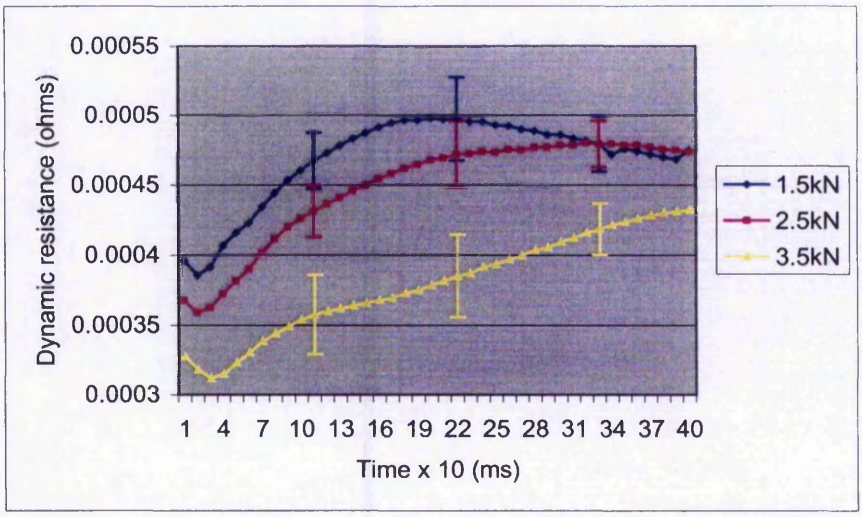

Figure 7.1 – Dynamic resistance curves for 3 different forging forces and 6000A current

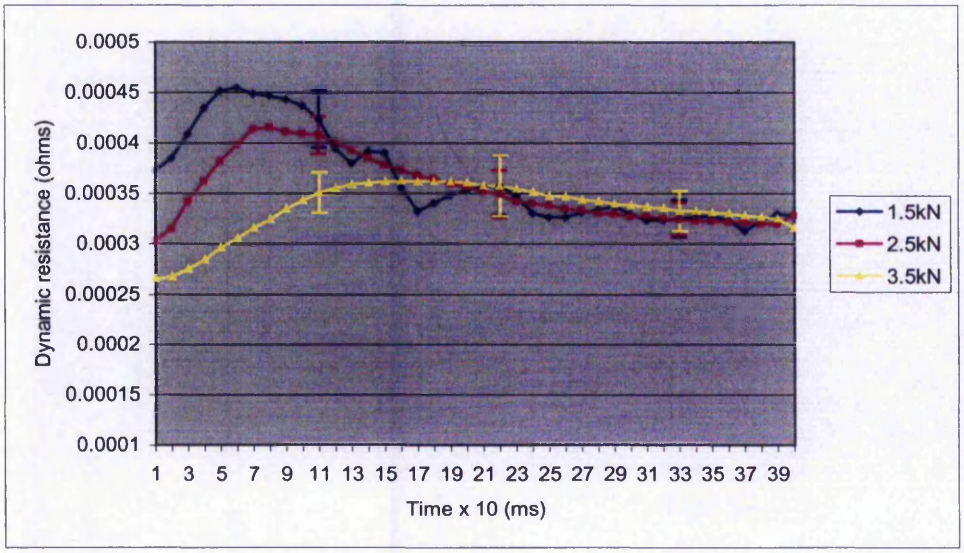

Figure 7.2 – Dynamic resistance curves for 3 different forging forces and 9000 A current

The results of the experiment are shown in figures 7.1 and 7.2 with the error bars indicating variations. Both the figures 7.1 and 7.2 show that the lowest forging force of 1.5kN has the highest average resistance change of the three forces with the peak resistances reaching 0.00049Ω and 0.00046Ω respectively. This could be explained by the contact resistance theory presented is section 2.8.1. A lower force will have a higher contact resistance due to less contact between surface asperities between the two sheets compared to the higher force where the true

contact area is larger due to higher contact between surface asperities (Thornton et al. 1996)(Sari et al. 2002).

Forge force (kN)	Average heat generation (kJ)	Standard deviation	99 % confidence interval
1.5	1.81	0.0102	$1.76<\mu<1.82$
2.5	1.73	0.0080	$1.72<\mu<1.75$
3.5	1.50	0.0089	$1.48<\mu<1.52$

Table 7.1 – Heat generated for 6000A at different forging forces

Forge force (kN)	Average heat generation (kJ)	Standard deviation	99% confidence interval
1.5	3.50	0.0075	$3.48<\mu<3.51$
2.5	3.46	0.0109	$3.44<\mu<3.48$
3.5	3.30	0.0063	$3.28<\mu<3.31$

Table 7.2 – Heat generated for 9000A at different forging forces

7.1.1.1 Discussions on the dynamic resistance change for 3 different forging forces

Due to the highest average resistance in the lowest forging force of 1.5kN, the corresponding average heat generated is the highest as shown in tables 7.1 and 7.2. This is due to the fact that the resistance is proportional to heat as discussed in section 6.1.2. The figures also show the peak of the dynamic resistance curve (β-peak) that was discussed in section 6.3.1.3 in chapter 6, which indicates weld growth. The resistance peak seems to occur earlier for the lower forging force compared to the higher forging force. This can be attributed to the higher rate of heat generation that causes faster weld growth (Hawkins 2000). The high heat generated for the

lower forging force due to the high resistance will also produce a stronger weld compared to the higher force till expulsion limit (Hirsch 1993)

The t-test was used to test the significance of the difference between two means (μ). Table 7.3 shows the results of the t tests that were carried out between the mean heat values, which were given in tables 7.1 and 7.2. The t values satisfy the conditions of $t \leq -t_{0.005}$ or $t \geq t_{0.005}$ where $t_{0.005} = 3.355$, hence the null hypothesis is rejected and the means are found to have significant differences between them. These tests show that the heat generated for different forging forces have significant differences between them with the lowest forging force generating the highest amount of heat.

Current (kA)	Test samples	t value at 99% confidence interval
6000	1.5kN and 2.5kN	13.799
	2.5kN and 3.5kN	42.976
	3.5kN and 1.5kN	-51.206
9000	1.5kN and 2.5kN	6.760
	2.5kN and 3.5kN	28.418
	3.5kN and 1.5kN	-45.678

Table 7.3 – T test results for the difference between mean heat values of the 3 forging forces with different welding currents

7.1.1.2 Discussion on the weld strength changes for 3 different forging forces

Table 7.4 shows that for both the welding currents, a weld that produced the highest average strength was due to the lowest forging force. This result agrees well with the experiment carried out in section 6.2.2 in chapter 6 that shows that the weld strength reduces with increase in

force for the same current and time. This can be due to contact resistance decreasing with increase in forging force, which in turn reduces heat generation for weld development (Thornton et al. 1996).

The test results in table 7.5 show that the t values , reject the null hypothesis and indicate that all the measured weld strengths have significant differences between them. The reason being the t values are either $\leq -t_{0.005} = -3.355$ or $\geq t_{0.005}$ where $t_{0.005} = 3.355$ for the 99% confidence interval.

Current (A)	Force (kN)	Average weld strength (kN)	Standard deviation	Average heat generation (kJ)	95% confidence interval
6000	1.5	5.90	0.190	1.81	$5.507 < \mu < 6.292$
	2.5	4.96	0.146	1.73	$4.655 < \mu < 5.257$
	3.5	2.37	0.351	1.50	$1.645 < \mu < 3.091$
9000	1.5	8.472	0.261	3.50	$7.933 < \mu < 9.010$
	2.5	7.836	0.227	3.46	$7.369 < \mu < 8.303$
	3.5	6.744	0.325	3.30	$6.277 < \mu < 7.412$

Table 7.4 - Weld strengths for the 6 welding schedules

Current (A)	Test sample	t value at 99% confidence interval
6000	1.5kN and 2.5kN	8.770
	2.5kN and 3.5kN	15.234
	3.5kN and 1.5kN	-19.777
9000	1.5kN and 2.5kN	4.112
	2.5kN and 3.5kN	6.167
	3.5kN and 1.5kN	-9.270

Table 7.5 - T test results of the difference between mean strengths for the 3 forging forces with different welding currents

The correlation between the heat generation and weld strength was analysed by using the raw values for heat generation and weld strength and is given in appendix C. The correlation coefficient r was of 0.895 shows that there is a strong positive relationship between the heat generation and weld strength. The positive relationship means increase in heat would cause an increase in strength which is true as in the case of table 7.4. The coefficient of determination r^2, gives 0.8 indicating the variance in heat is accounted by the variance in strength by 80.0%. The t value of 10.599, rejects the null hypothesis of no correlation and shows significant correlation between the heat generated and weld strength, when tested with the minimum possible level of p=0.001 of 3.674 ($t > p_{0.001} = 3.674$) and degrees of freedom of 28.

From the experiment discussed above, the relationship between dynamic resistance and forging forces during the weld cycle of the spot welding process is evident. This inherent relationship between the resistance and force, allows the dynamic resistance to be used as an indicator of the changes in force. The changes in the dynamic resistance curve due to the control of the forging force during the weld will be investigated in the next experiment.

7.2 Changes in the dynamic resistance curve due to force control during weld cycle

The changes in the dynamic resistance curve due to the forging force control during weld cycle were studied using the 4 force profiles A,B,C and D discussed in section 5.3.1. The characteristic of the force profiles as seen in figure 5.10 is an initial force, which then starts to increase or decrease to a different force on the 5th weld cycle (100ms) and ramped at ±0.01kN/ms (1kN/100ms). These force profiles will also be studied by increasing or decreasing the forces at 3 different weld cycles during the weld time and also changing the rate of ramping. The change in the dynamic resistance curves due to the changes in the force profile characteristics will then be investigated.

The 3 cases of changes in the force profile (A,B,C or D) characteristics are given below: -

1) Forging forces increased/decreased at the 5th weld cycle (100ms) for ±0.01kN/ms as shown in figure 5.10 in chapter 5 (case1)
2) Forging forces increased/decreased on the 5th weld cycle (100ms), 15th weld cycle (300ms) and 25th weld cycle (500ms) but keeping the ramping rate constant at ±0.01kN/ms (case2)
3) Forging forces increased/decreased with ramping rates of 0.01kN/ms, 0.005kN/ms and 0.0025kN/ms but the ramp start time is kept constant at 15th weld cycle (300ms) (case3)

The investigation into the changes in the dynamic resistance curve for all the 3 cases is given below.

7.2.1 Changes in the dynamic resistance curve for Case 1

The 4 force profiles A,B,C and D used for this experiment are as discussed is section 5.3.1 and are shown in figure 5.10 in chapter 5. Two different welding currents (5000A and 6500A) were used and the weld time was programmed in the WS2000 weld timer as 800ms (40 cycles). The thickness of the metal sheet used was 2mm each and the electrode tip diameter was 6.0mm. 5 repetitions were made for each welding schedule.

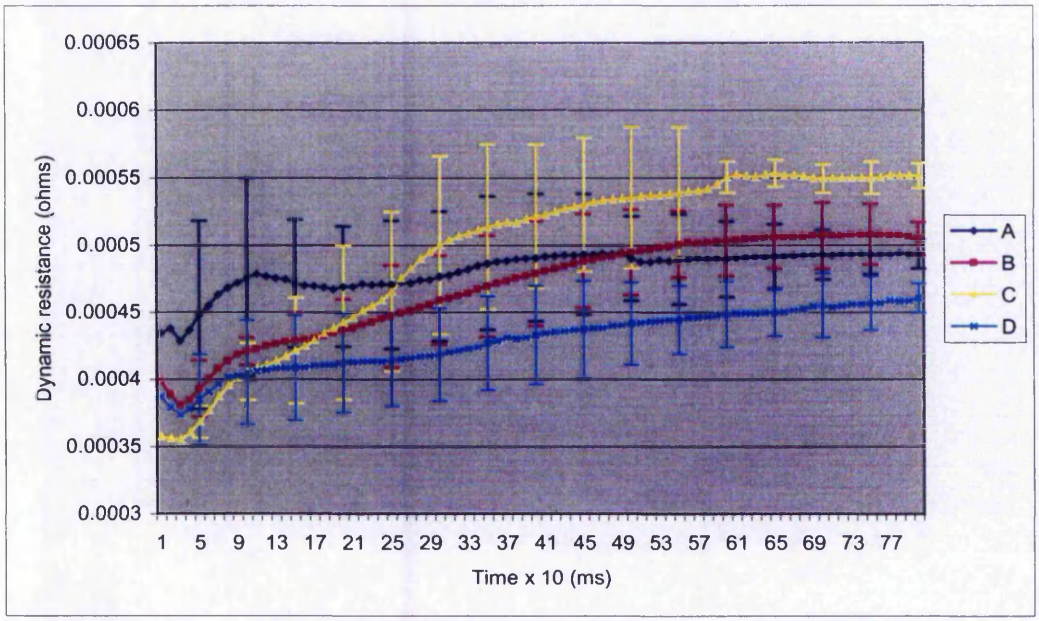

Figure 7.3 – Dynamic resistance curves for 4 force profiles and 5000A current

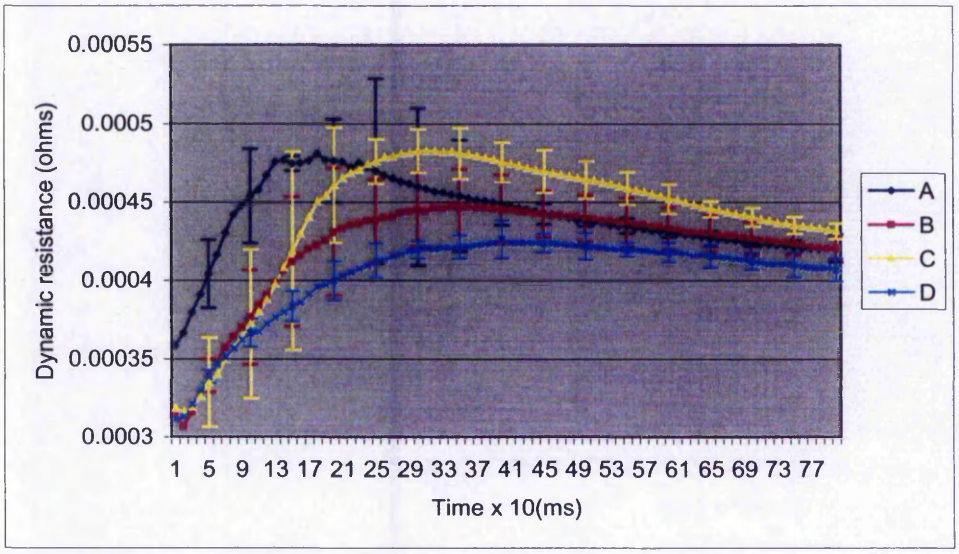

Figure 7.4 – Dynamic resistance curves for 4 force profiles and 6500A current

7.2.1.1 Discussion on the dynamic resistance changes for Case 1

Both figures 7.3 and 7.4 show the average dynamic resistance curves for the four different types of force profiles (A,B,C,D) using welding currents of 5000A and 6500A respectively with the error bars indicating the variations. Figure 7.3 is discussed initially. Comparing the change in dynamic resistance curves for all the four profiles of A, B, C and D, the peak resistance of the resistance curves was found to decrease when the forging force is increased during welding as in the case of the force profile D with a measured resistance of 0.00046Ω. This again relates to the force-resistance relationship. Increasing the force during welding will increase the area through which the current flows causing the resistance to drop (Asokkumar et al. 1997) as already been discussed in section 7.1.1. The peak resistance of 0.00055Ω was noticed for the force profile C could be due to the reduction of the forging force during welding which increases the resistance to current flow. The other observation from figure 7.3 is that since the force profiles B, C and D have an initial forging force value of 2.5kN till 100ms before ramping starts, the dynamic resistance for these 3 profiles are closer to each other till about 100ms. Significant changes in the resistance values were noticed after 100ms. For instance at 300ms, the resistance values for force profile C was about 0.00051Ω, force profile B was about 0.00046Ω and for the force profile D was about 0.00042Ω. This could be due to the changes in forging force that occurs during this period.

The next observation from the figure 7.3 is made by comparing the force profile A and the force profile B. The initial low forging force of 1.5kN creates a high resistance of 0.00047Ω in the case of profile A. However the resistance drops after 100ms, which could be attributed to the change in force. The final resistance values are closer to each other for both the profiles for the same final applied force. Table 7.6 shows the average heat generated for the different force profiles.

Force profile	Average heat generation (kJ)	Standard deviation	99%confidence interval
A	4.74	0.0084	$4.72 < \mu < 4.76$
B	4.70	0.0089	$4.68 < \mu < 4.71$
C	4.96	0.0055	$4.94 < \mu < 4.98$
D	4.29	0.0084	$4.27 < \mu < 4.31$

Table 7.6 – Heat generated for the 4 force profiles and 5000A current

From table 7.6, it can be seen that the force profile C has the highest heat value of 4.96kJ compared to the rest of the profiles. This can be due to the reduction in forging force from 2.5kN to 1.5kN during welding that increases the maximum achieved resistance to 0.00055Ω causing more heat to be generated during welding as seen in figure 7.3. The force profile D has the lowest heat value of 4.29kJ, which could be attributed to the increase in forging force to 3.5kN reducing the maximum resistance during welding to 0.00046Ω causing lower value for heat to be generated for the same welding period.

T tests to evaluate the differences between means were carried out for the set of force profiles of B and D, B and C, B and A, D and C, D and A and finally C and A. Table 7.7 gives the calculated t values.

Test samples	t values at 99% confidence interval
B and D	74.912
B and C	-55.568
B and A	-7.308
D and C	-149.213
D and A	-84.704
C and A	48.995

Table 7.7 – T test results for the difference between mean heat values for the 4 force profiles with 5000A current

Since all these t values are $\leq t_{0.005}$ =-3.355 or $\geq t_{0.005}$ = 3.355, the null hypothesis is rejected and the means are found to have significant differences between them.

The observations made in figure 7.3 apply to figure 7.4 too. Force profile C was found to have the highest peak resistance of 0.00048Ω and the force profile D to have the lowest peak resistance of 0.00043Ω. The resistance values of profiles B, C and D were closer to each other before 100ms due to the same initial applied forging force and vary significantly after 100ms due to the ramping of force. Finally similar to the figure 7.3, comparison of the force profile A and force profile B in figure 7.4 also show an initial high resistance in the former force profile of about 0.00037Ω with the resistance values coming closer to each other at the end of the weld cycle due to the same applied forging force. However compared to figure 7.3, in figure 7.4 all the resistance curves have a significant β-peak which could be due to the use of the high current of 6500A, which accelerates the rate of weld growth for the same welding time. Table 7.8 shows the average heat generated for the different force profiles and 6500A current.

Force profile	Average heat generation (kJ)	Standard deviation	99%confidence interval
A	8.04	0.0055	$8.03 < \mu < 8.06$
B	7.72	0.0207	$7.68 < \mu < 7.77$
C	8.06	0.0089	$8.04 < \mu < 8.07$
D	7.36	0.0055	$7.35 < \mu < 7.38$

Table 7.8 – Heat generated for the 4 force profiles and 6500A current

Similar to table 7.6, table 7.8 also shows that the force profile C has the highest heat value of 8.06kJ compared to the rest of the profiles due to the higher resistance of 0.00048Ω during welding. The force profile D has the lowest heat value of 7.36kJ as the increase in forging force to 3.5kN reduces the maximum resistance to 0.00043Ω causing lower heat value to be generated for the same welding period.

T tests with the null hypothesis of no difference in means were carried out for the same sets of force profiles as for table 7.7 and are presented in table 7.9 below.

Test samples	t values at 99% confidence interval
B and D	37.584
B and C	-33.741
B and A	-33.408
D and C	-149.608
D and A	-195.486
C and A	1.826

Table 7.9 – T test results for the difference between mean heat values for the 4 force profiles with 6500A current

Table 7.9 shows that all the t values except for between C & A (t= 1.826), reject the null hypothesis because these values are $\leq t_{0.005}$ =-3.355 or $\geq t_{0.005}$ = 3.355 for 99% confidence interval. Since t=1.826 is smaller than $t_{0.005}$ = 3.355, the differences between these means were found to be less significant. The t value was found to show that the difference between the means to be significant when tested with 90% confidence interval because the value is greater than $t_{0.1}$ = 1.397.

7.2.1.2 Discussion on the weld strength changes for Case 1

The strengths of the welds for all the 4 profiles and the two welding currents were measured by means of the cross tension test. Table 7.10 shows the average weld strengths achieved by using the force profiles and 5000A weld current. Similarly table 7.11 shows the average weld strengths achieved for the 4 force profiles and 6500A current. Initial discussion on the weld strengths would be based on table 7.10 followed by discussion on table 7.11.

Current (A)	Force profile	Average heat generated (kJ)	Average weld strength (kN)	Standard deviation	95% confidence interval
5000	A	4.74	8.91	0.201	$8.50 < \mu < 9.32$
	B	4.70	9.98	0.255	$9.46 < \mu < 10.51$
	C	4.96	10.83	0.212	$10.40 < \mu < 11.28$
	D	4.29	8.57	0.357	$7.84 < \mu < 9.31$

Table 7.10 – Heat Functions & weld strengths for 4 force profiles and 5000A current

Current (A)	Force profile	Average heat generated (kJ)	Average weld strength (kN)	Standard deviation	95% confidence interval
6500	A	8.04	12.73	0.190	$12.34 < \mu < 13.12$
	B	7.72	12.59	0.335	$11.89 < \mu < 13.28$
	C	8.06	10.89	0.294	$10.29 < \mu < 11.49$
	D	7.36	11.81	0.269	$11.25 < \mu < 12.36$

Table 7.11 – Heat Functions & weld strength for 4 force profiles and 6500A current

When using 5000A, the highest weld strength was achieved for the force profile C with the average strength measuring of 10.83kN as shown in table 7.10. This may be due to the fact that this profile has the highest resistance during welding of 0.00055Ω as shown in figure 7.3 and the highest heat value of 4.96kJ. The lowest strength was achieved for the force profile D with the average strength measuring 8.57kN. This force also has the lowest resistance during welding of 0.00045Ω as shown in figure 7.3 and the lowest heat value of 4.29kJ. With the force profile A, a higher resistance was produced earlier during the weld period compared to the other profiles. However the increase in forging force during welding gives this force profile a similar effect as the force profile D. The strength achieved was about 8.91kN. The means difference test using equation 2 in section 6.2.1.1 was carried out for the set of force profiles of B and D, B and C, B and A, D and C, D and A and finally C and A. Table 7.12 shows the calculated t values.

Test samples	t values at 99% confidence interval
B and D	7.186
B and C	-5.731
B and A	7.368
D and C	-12.171
D and A	-1.855
C and A	14.695

Table 7.12 – T test results for the difference between strength values for the 4 force profiles with 5000A current

The t value of -1.855 is greater than -2.306 (95% confidence interval) and -3.355(99% confidence interval) that shows that these means for the D (2.5kN-3.5kN) and A (1.5kN-2.5kN) force profiles are not very significant due to the overlapping in the confidence intervals of these two profiles as can be seen in table 7.10.

In this case of table 7.11, the highest weld strength was achieved for the force profile A with the average strength measuring 12.73kN. This can be explained as due to an initial high resistance of 0.00037Ω and the high current of 6500A resulting in the increased rate of weld growth due to the increased heat generation. Comparing this result with the strength achieved by the same profile for 5000A, the latter achieved moderate weld strength due to the use of a lower current. The lowest weld strength for the applied current was achieved by the profile C. Even though this profile has the highest heat generation of 8.06kJ, the strength dropped to an average of 10.89kN. This might be due to the occurrence of expulsion that was observed during welding. The use of a high current and reduction of the electrode force during welding causes high heat to be generated due to the higher rate of resistance change as seen in figure 7.4. This in turn will cause the molten metal to be expelled from the molten region (Zhang 1999). The expulsion of material from the weld region will cause loss of material and voids and porosity in the weld (Zhang 1999). Hence this will cause the weld strength to reduce. Expulsion was confirmed due to the traces of metal expulsion as in figure 2.10 when the weld was tested. This profile however

achieved the highest weld strength with the 5000A current as explained above because the heat generated with this current was below the expulsion limit and hence no metal expulsion occurred. The use of 6500A causes the heat generated to exceed the expulsion limit. T test for difference in means was carried out for the same set of force profiles as in table 7.12 and is presented in table 7.13.

Test samples	t values at 99% confidence interval
B and D	4.059
B and C	8.528
B and A	-0.812
D and C	5.162
D and A	-6.246
C and A	-11.754

Table 7.13 – T test results for the difference between strength values for the 4 force profiles with 6500A current

Calculated t values in table 7.13 show that the means for the pair of force profiles of A and B are closer to each other compared to rest of the mean strength values. The value of t= -0.812 which is greater than $-t_{0.025}$ = -2.306 (95% confidence interval) shows insignificant difference between means. All the other t values show that the tested pairs of force profiles have significant differences between them.

The relationship between the generated heats and the measured weld strengths in both tables 7.10 and 7.11 shows that the weld strength increases with the increase in heat generation. The correlation coefficient r calculated based on the raw data for heat and strength as in appendix C, gives a value of 0.781 that shows a stronger positive relationship between the two variables because this value is closer to +1.0. This positive relationship supports the observations in tables 7.10 and 7.11. The r^2 value of 0.611 indicates that the variations in both of these variables affect each other by 61.1%. The t value of 7.713 which rejected the null hypothesis at the lowest possible level of p=0.001 of 3.646 ($t > p_{0.001} = 3.646$) and with 38 degrees of freedom. This

shows a significant correlation between the heat generation and achieved weld strength. However without considering the strength achieved during expulsion and its respective strength as in the case of the previous r, the calculated new value of r gives a value of 0.853. This shows a better correlation between heat and strength can be achieved if the expulsion condition is not taken into account during the calculation of the correlation coefficient. The r^2 gives a value of 0.728 showing both the variables affect each other by 72.8%. This percentage is higher than the percentage (61.1%) achieved when the expulsion data is taken into account.

7.2.1.3 Summary of results for Case 1

The results show that the 2.5kN-1.5kN-force profile (C) produces the highest heat followed by the 1.5kN-2.5kN-force profile (A) during welding for 5000A and 6500A currents. With the 5000A, the 2.5kN-1.5kN-force profile (C) achieved the highest weld strength of 10.83kN. This is because the reduction in forging force to 1.5kN during welding increases the resistance as seen in both figures 7.3 and 7.4, causing more heat to be generated to produce a stronger weld. As in the case of profile A, the initial higher resistance due to lower forging force of 1.5kN would have increased the rate of melting but the increase in force during welding to 2.5kN reduces the resistance causing a reduction in the heat generation. With a 6500A, the same profile C produces the lowest weld strength due to expulsion during welding. The rapid increase in the amount of heat generated due to the reduction in force during welding with profile C would cause the molten metal to be expelled from the weld region when welded with high current. However the increase in forging force to 2.5kN for the profile A has the tendency to reduce the heat generation through reduction in resistance and avoid expulsion at high current. This can be argued as the reason for the highest weld strength of 12.73kN with 6500A, that was produced with the 1.5kN-2.5kN-force profile (A).

7.2.2 Changes in the dynamic resistance curve for Case 2

A further experiment was carried out to investigate the effect of varying the forging force ramping delay time, after the weld cycle was initiated, to the dynamic resistance curve and the

weld strength. Force profile B, being a constant force profile will not be considered in this study. In the previous experiment all the force profiles had a forging force ramping delay time of 100ms or 5 welding cycles. In this experiment 3 different ramping delay times were used; ramping delay at 100ms (5 cycles), ramping delay at 300ms (15 cycles) and ramping delay at 500ms (25 cycles). The current, weld time and hold time were programmed in the WS2000 weld timer as 5000A, 800ms (40 cycles) and 200ms (10 cycles) respectively. The thickness of the metal sheet used was 2mm each and the electrode tip diameter was 6.0mm. 5 repetitions were made for each welding schedule.

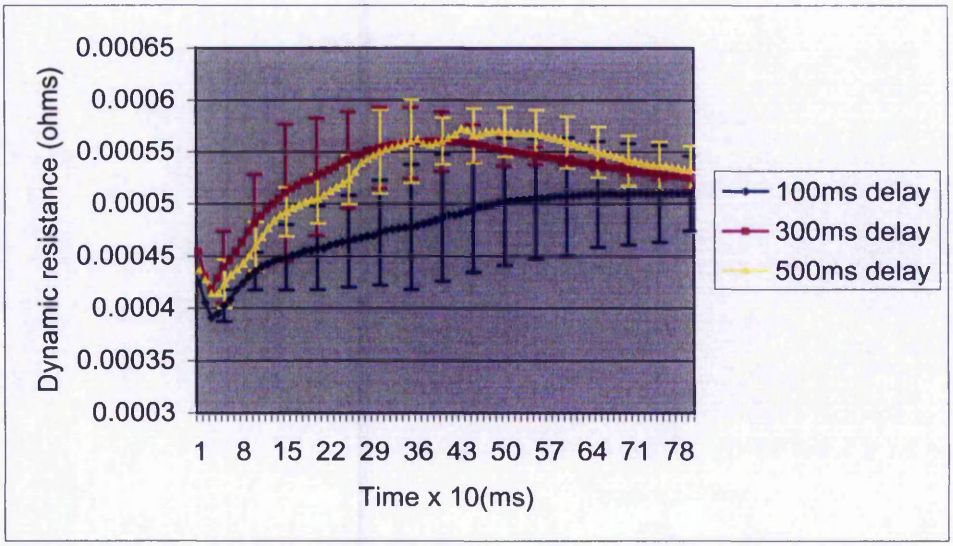

Figure 7.5 – Dynamic resistance curves for 3 ramping delay times for the force profile D

7.2.2.1 Discussion on the dynamic resistance changes for Case 2

Figure 7.5 shows the 3 average dynamic resistance curves due to different ramping delay times for the 2.5kN-3.5kN-force profile (D) with the error bars indicating variations. Initially the resistance values are nearer to each other since the same force value of 2.5kN where applied in all the force profiles before ramping starts. The resistance value starts to drop earlier for the force profile for which ramping starts at 100ms to increase the force to 3.5kN. The delay in the start of ramping actually increases the resistance as seen in figure 7.5. Hence the profile with ramp delay

time of 500ms exhibits a higher resistance of 0.00056Ω than the rest and then drops when ramping starts.

Ramping start time (ms)	Average heat generation (kJ)	Standard deviation	99% confidence interval
100	0.96	0.0071	$0.95 < \mu < 0.97$
300	1.04	0.0084	$1.02 < \mu < 1.06$
500	1.06	0.0084	$1.04 < \mu < 1.08$

Table 7.14 – Heat generated due to 3 ramping delay times for the force profile D

The average heat generated, as shown in table 7.14 indicates that the 500ms ramp delay time actually generates the highest value of 1.06kJ, obviously due to the higher peak resistance of 0.00055Ω produced by this profile. T tests carried out to test for the difference between the means of 100ms and 300ms, 300ms and 500ms and finally 500ms and 100ms are given in table 7.15 below: -

Ramping delays	t values at 99% confidence interval
100ms and 300ms	-16.264
300ms and 500ms	- 3.762
500ms and 100ms	20.330

Table 7.15 – T test results for the differences between mean heat values for the 3 ramping delays for profile D

All t values reject the null hypothesis because these values are $\leq t_{0.005} = -3.355$ or $\geq t_{0.005} = 3.355$ for 99% confidence interval.

The same experiment was carried out on the 1.5kN-2.5kN-force profile (A) with the same force ramping delay times. Figure 7.6 shows the changes in the average dynamic resistance due to 3 force ramping delays for the force profile A with the vertical bars indicating variations. Similar to the discussion above, initial stages up to 100ms in figure 7.6 also shows that the resistance values for the 3 profiles are closer to each other due to the same applied forging force.

Then the resistance values start diverging where the 100ms ramp-start time profile shows resistance of 0.00057Ω and the 500ms ramp-start time force profile shows resistance of 0.00065Ω at 200ms due for force increase. The drop in resistance for the 500ms delay profile might be due to the two reasons of increase in force, which increases the area for current flow, and also faster weld growth. These assumptions were made because the resistance seems to be dropping even before 500ms and resistance change gradually reduces to about 300ms, which shows according to the interpretation of dynamic resistance curve in section 6.3.1.1, the transition β-point or the point of weld formation.

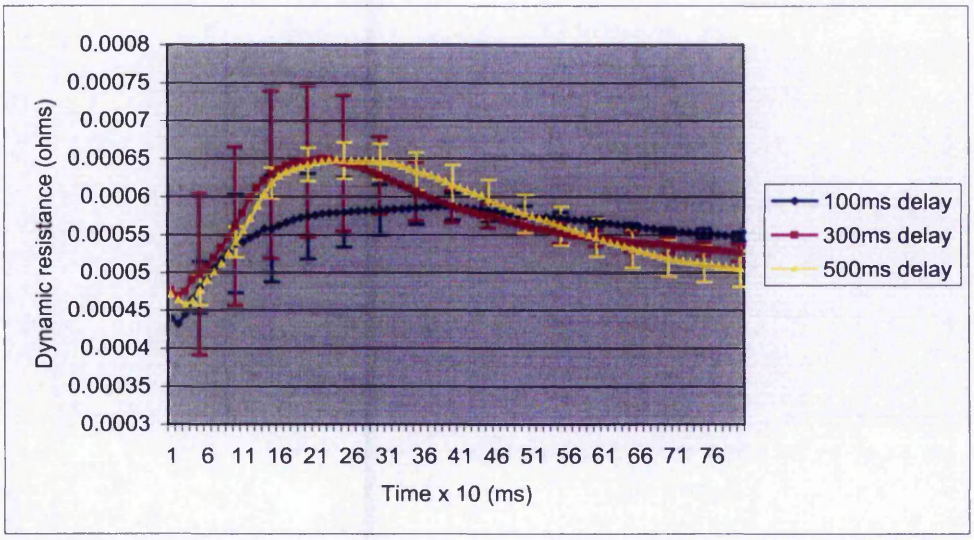

Figure 7.6 – Dynamic resistance curves for 3 ramping delay times for force profile A

The average heat generated for these 3 different delays are shown in table 7.16 below: -

Ramping start time (ms)	Average heat generation (kJ)	Standard deviation	99% confidence interval
100	1.12	0.0045	$1.11 < \mu < 1.13$
300	1.14	0.0084	$1.12 < \mu < 1.15$
500	1.16	0.0055	$1.14 < \mu < 1.17$

Table 7.16 – Heat generated due to 3 ramping delay times for the force profile A

Similar to the results in table 7.14, the results in table 7.16 also indicate that the 500ms ramp delay time force profile generates the highest heat of 1.16kJ and the 100ms ramp delay time force profile produces the lowest heat of 1.12kJ. T tests carried out to check for the significant differences between the means of 100ms and 300ms, 300ms and 500ms and finally 500ms and 100ms are shown in table 7.17 below: -

Ramping delays	t values at 99% confidence interval
100ms and 300ms	-4.693
300ms and 500ms	-4.454
500ms and 100ms	12.586

Table 7.17 – T test results for the differences between mean heat values for the 3 ramping delays for profile A

The t values reject the null hypothesis because these values are $\leq t_{0.005} = -3.355$ or $\geq t_{0.005} = 3.355$ for 99% confidence interval. Hence the tests show that the means have significant differences between them.

Finally the experiment was repeated for the 2.5kN-1.5kN-force profile (C). Figure 7.7 shows the changes in the average dynamic resistance curve for the 3 force ramping down delay times.

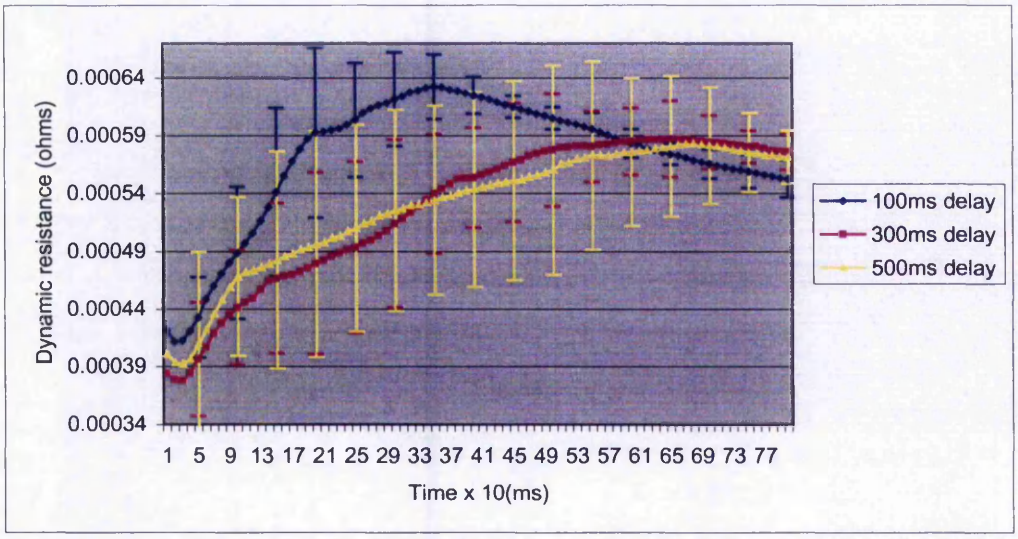

Figure 7.7 – Dynamic resistance curves for 3 ramping delay times for the force profile C

The results obtained for this set of force profiles are opposite to the results discussed above. The 100ms ramp start time force profile is indicating a higher average peak resistance of 0.00064Ω instead of the 500ms ramp start time force profile as for the two experiments above. In both the experiments earlier, the profiles have increasing force profiles that increase the forging force. In this set of profiles the forging force is decreased. Hence the profile that reduces the forging force, earlier in time (100ms) generates a higher peak resistance compared to the profile, which reduces the forging force later (500ms). The profile with the 100ms ramp delay time also shows a prominent β-peak point compared to the other profiles due the higher resistance change. This resistance change will increase the temperature due to heating, resulting in faster rate of melting and softening of material. The drop in the resistance would be generally due to weld growth rather than force change, since force has actually decreased rather than increased as in the previous cases.

In the case of the 300ms and 500ms ramp delay times, the constant forging force of 1.5kN actually increases the resistance for both the profiles. The resistance curves for these profiles are closer to each other until 300ms. After 300ms, the resistance curves seem to be separating with the 300ms profile having a resistance increase of 0.00058Ω and the 500ms profile having a resistance 0.00056Ω due to the force reduction after 300ms.

Studying the average heat generated for these profiles as shown in table 7.18, the 100ms ramp delay time force profile indicates the highest heat generation of 1.11kJ due to the highest peak resistance of 0.00064Ω.

Ramping start time (ms)	Average heat generation (kJ)	Standard deviation	99% confidence interval
100	1.11	0.0071	$1.09 < \mu < 1.12$
300	1.07	0.0071	$1.06 < \mu < 1.08$
500	1.04	0.001	$1.02 < \mu < 1.06$

Table 7.18 – Heat generated due to 3 ramping delay times for the force profile C

T tests carried out on the mean of heat values for 100ms and 300ms, 300ms and 500ms and finally 500ms and 100ms are given in table 7.19.

Ramping delays	t values at 99% confidence interval
100ms and 300ms	8.908
300ms and 500ms	5.469
500ms and 100ms	- 10.909

Table 7.19 – T test results for the differences between mean heat values for the 3 ramping delays for profile C

The t values reject the null hypothesis because these values are $\leq t_{0.005} = -3.355$ or $\geq t_{0.005} = 3.355$ for 99% confidence interval.

The other observation that can be made in figures 7.5 to 7.7 is that the resistance curves are closer to each other at the start and end of the weld cycle. This can be due to the initial force and final force for all the 3 sets of profiles are the same i.e. either force increasing from 2.5kN to 3.5kN or 1.5kN to 2.5kN or force decreasing from 2.5kN to 1.5kN. The ramping of the forces at

3 different times that cause the curves to move away from each other is obvious in the middle section of all the three figures.

7.2.2.2 Discussion on the weld strength changes for Case 2

The cross tension test was used to measure the achieved weld strengths for the 3 sets of force profiles with the 3 ramp delay times and with 5 repetitions, are presented below in table 7.20.

The average weld strengths measured for the force profile D show that the 500ms ramp delay time profile achieves the highest strength of 5.46kN of all the delay times tested. This can be attributed to the higher value of heat (1.06kJ) generated by this profile. The similar trend was noticed in the case of the force profile A too with the 500ms ramp delay time profile achieving higher average strength of 7.48kN due to the high heat generation of 1.16kJ. The opposite trend was noticed for the force profile C with the 100ms ramp delay time force profile achieving higher average strength of 9.55kN rather than the 500ms ramp delay time profile. This can be due to the characteristic of the profile, which reduces the forging force earlier during the weld cycle causing more heat to be generated as shown in table 7.20. This reduction in forging force increases the rate of heat generation causing stronger welds to be developed.

Force profile	Ramping delay (ms)	Average heat generation (kJ)	Average weld strength(kN)	Std.deviation	95% confidence interval
D	100	0.96	4.00	0.180	$3.630 < \mu < 4.374$
	300	1.04	4.93	0.148	$4.624 < \mu < 5.232$
	500	1.06	5.46	0.221	$5.009 < \mu < 5.918$
A	100	1.12	6.69	0.228	$6.219 < \mu < 7.157$
	300	1.14	7.14	0.128	$6.873 < \mu < 7.402$
	500	1.16	7.48	0.400	$6.658 < \mu < 8.302$

C	100	1.11	9.55	0.244	$9.048 < \mu < 10.052$
	300	1.07	8.75	0.264	$8.204 < \mu < 9.292$
	500	1.04	8.23	0.163	$7.891 < \mu < 8.561$

Table 7.20 – Weld strength for 3 force ramp delay times

The significant differences of the mean weld strengths for the 100ms and 300ms, 300ms and 500ms and finally 500ms and 100ms ramping delays for the 3 force profile were tested and the results are given in table 7.21.

Force profiles	Ramping delays (ms)	t values at 99% confidence interval
D	100 and 300	-8.923
	300 and 500	-4.457
	500 and 100	11.453
A	100 and 300	-3.848
	300 and 500	-1.810
	500 and 100	3.836
C	100 and 300	4.976
	300 and 500	3.747
	500 and 100	-10.058

Table 7.21- T test results for the difference between mean strengths for the 3 tested ramping delays

The t values for force profile D seem to reject the null hypothesis because these values are either $\leq t_{0.005} = -3.355$ or $\geq t_{0.005} = 3.355$ for 99% confidence interval. Hence the tests show that the mean strengths have significant differences between them. Next the significant differences of the mean strength for force profile A was tested. Calculated t values show that the first and third values are greater than $t_{0.005} = 3.355$. Hence the null hypothesis is rejected and the mean strengths were found to have significant differences between them. However the t= -1.810 is greater than $t_{0.025} = -2.306$ for 95% confidence intervals respectively indicates that the differences between the means for the 300ms and 500ms ramping delays are less significant. Finally the test was carried out for

the mean strengths of the same pairs of ramping delays as the other two tests but for force profile C. Calculated t values indicates rejection of null hypothesis and indicate that the means have significant differences between them because they are either $\leq t_{0.005}$ =-3.355 or $\geq t_{0.005}$ = 3.355 for 99% confidence interval.

Studying the relationship between the generated heat and the measured weld strength based on the raw data for the heat and strength as in appendix C for the 3 different ramping delays shows that the weld strength increases with the increase in heat generation. The calculated r (correlation coefficient) value of 0.561 shows a positive relationship between the heat and weld strength which supports the observation in table 7.18. The t test shows significant relationship between these two variables because the t value of 4.445 rejects the null hypothesis when tested with the lowest level of p=0.001 of 3.551 ($t > p_{0.001} = 3.551$) and degrees of freedom of 43. The r^2 value of 0.315 shows that the variation of one variable is accounted by the other in only 32% compared to above 60% for the other experiments.

7.2.2.3 Summary of results for Case 2

The results of these experiments indicate that the profiles that increases the forging force at 0.01kN/ms with a delay in the ramp starting time, would increase the resistance and in turn increase the amount of heat generated. As seen in the experiments above, force ramped after 500ms generates a higher heat of 1.16kJ compared to the force ramped after 100ms that generates 1.12kJ heat for force profile A. On the other case, for the profiles where the forging forces are decreased with a delay in the ramp starting time, the resistance is reduced and in turn reduce the amount of heat generated. For instance, in the experiment above, when the forging force is ramped down at 0.01kN/ms to 1.5kN from 2.5kN after 500ms, the amount of heat generated (1.04kJ) seems to be lesser than when the force is ramped down after 100ms (1.11kJ).

7.2.3 Changes in the dynamic resistance curve for Case 3

Experiments in case 3 will investigate the changes in the dynamic resistance curve due to 3 different forging force ramping rates. Profile B will not be used again since it is a constant force profile. The three different forging force ramping rates that will be experimented are: 0.01kN/ms, 0.005kN/ms and 0.0025kN/ms. The current, weld time and hold time were programmed in the WS2000 weld timer as 5000A, 800ms (40 cycles) and 200ms (10 cycles) respectively. The thickness of the metal sheet used was 2mm each and the electrode tip diameter was 6.0mm. 5 repetitions were made for each set of welding schedule. Figure 7.8 shows the 3 ramping rates for the 2.5kN-3.5kN-force profiles (D). Similar ramping rates are used for the 1.5kN-2.5kN force profiles (A) and the 2.5kN-1.5kN-force profiles (C). The forces at constant force region have got an offset of ± 0.01kN in the figure for clarity of each force profile.

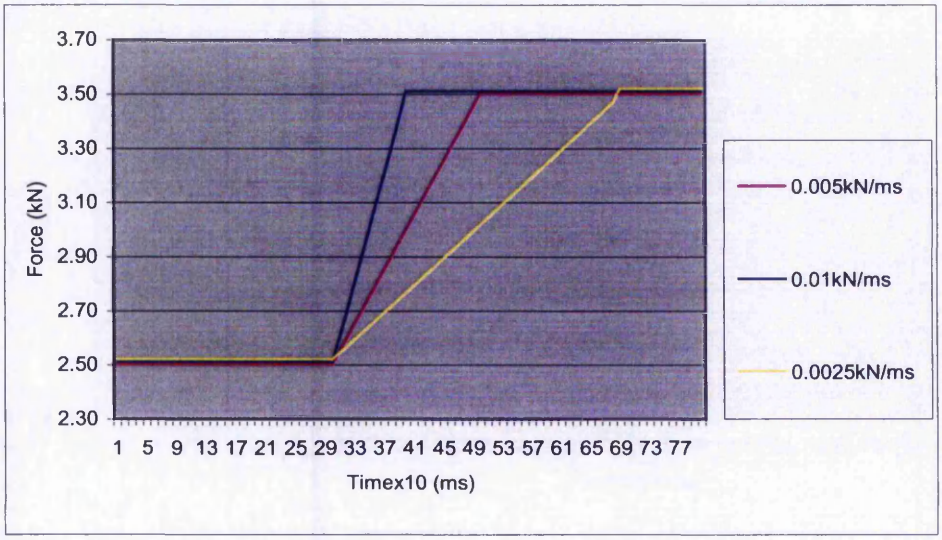

Figure 7.8 – The 3 ramping rates for force profile D

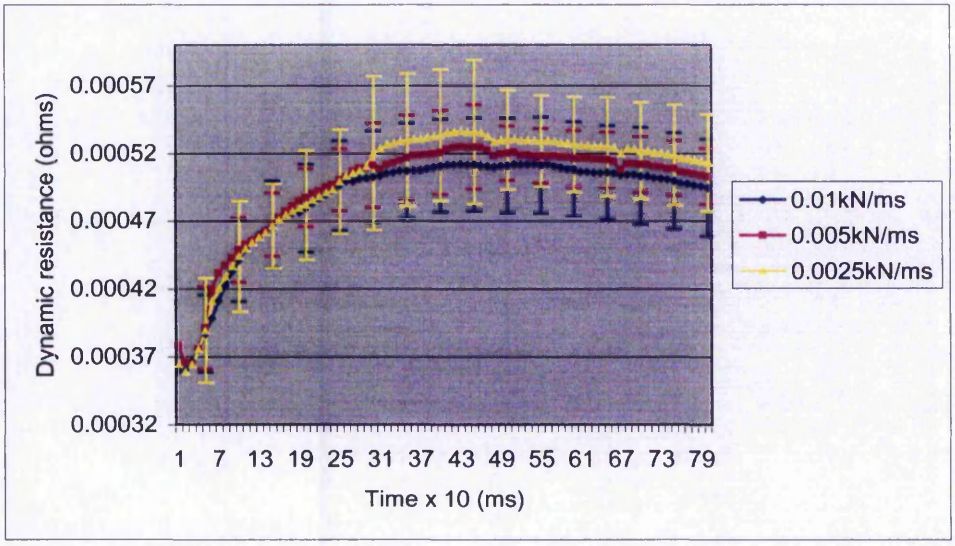

Figure 7.9 – Dynamic resistance curves due to 3 ramping rates for force profile D

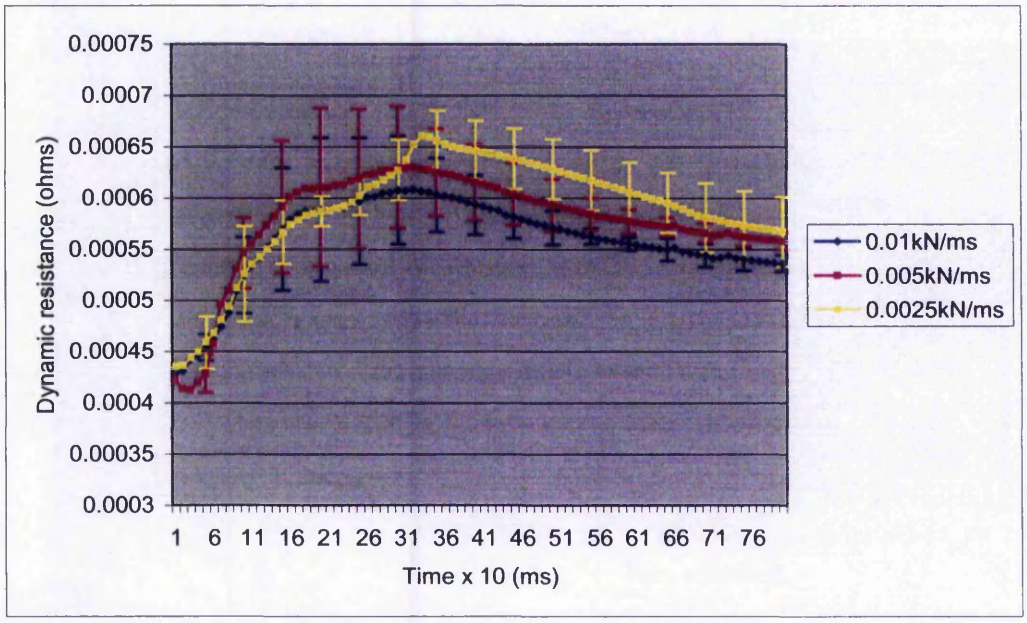

Figure 7.10 – Dynamic resistance curves due to 3 ramping rates for force profile A

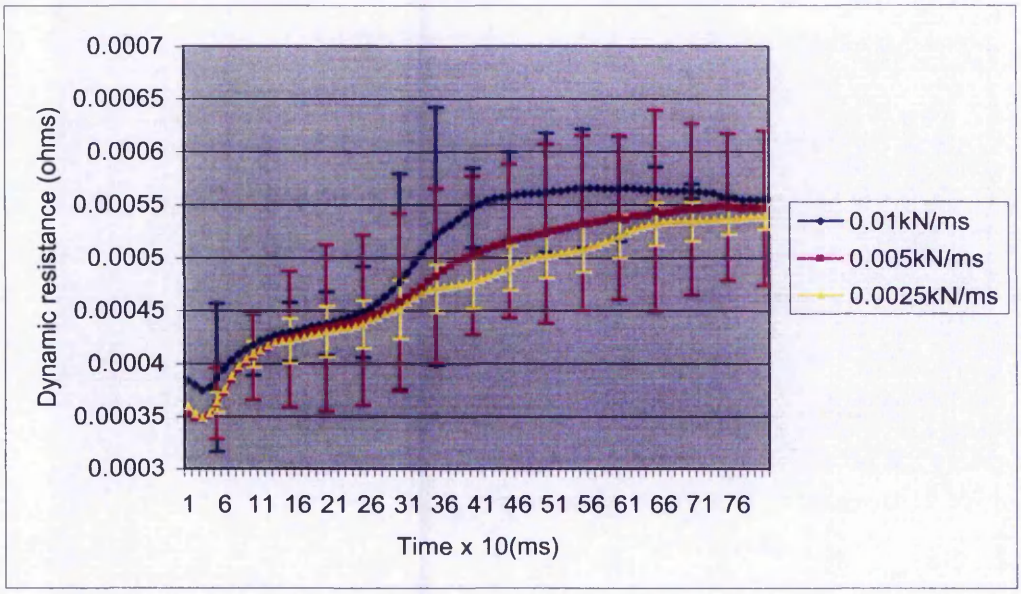

Figure 7.11 – Dynamic resistance curves due to 3 ramping rates for force profile C

7.2.3.1 Discussion on dynamic resistance changes for Case 3

Figures 7.9 to 7.11 show the change in the average dynamic resistance curves for 3 different ramping rates for force profiles D, A and C with error bars to show variations. Figure 7.9 shows that the resistance reduces earlier with the 0.01kN/ms ramping rate. This can be due to the fact that, during this ramping rate, the force is increased to 3.5kN at faster rate of 0.01kN/ms causing an earlier drop in the resistance. A lower ramping rate actually allows the resistance to increase steadily before the resistance drops due to the increase in force. Comparing the curves with 0.005kN/ms ramping rate and 0.0025kN/ms ramping rate, the 0.005kN/ms ramping rate causes the resistance to decrease earlier while the resistance for the 0.0025kN/ms ramping rate continues to increase before decreasing at the end of the weld cycle. Similar observations were noticed in figure 7.10, where the dynamic resistance curve for the 0.01kN/ms ramping rate decreases earlier due to the faster increase in force compared to the 0.025kN/ms ramping rate. Both the figures 7.9 and 7.10 are dynamic resistance curves for force profiles with increasing forces. Figure 7.11 shows the dynamic resistance curves for force profiles with decreasing force i.e. from 2.5kN to 1.5kN. Observation on the 0.01kN/ms ramping curve shows an obvious rapid

increase in resistance after 300ms due to the sudden reduction in the motor torque to decrease the force. This faster rate in force reduction that occurs within 100ms increases the resistance rapidly as seen in figure 7.11. The average dynamic resistance curves for the 0.005kN/ms ramping rate and 0.025kN/ms ramping rate show the similar characteristics as the curves in figure 7.9 and figure 7.10 but in the opposite manner where the 0.005kN/ms ramping rate increases the resistance earlier rather than decreasing due to the characteristic of the force profile. The 0.025kN/ms ramping rate seems to be increasing the resistance steadily due the slower ramping rate.

The other observations on all the dynamic resistance figures are that the resistance values are closer to each other at the beginning and end of the figures and significant variations were observed only in the middle of the figures. This can be due to that for each set of resistance curves on each figure, the force profiles show a significant change in force only in the middle of the force profiles due to 3 different ramping rates with the beginning and ending forces being the same. For example, in the case of figure 7.10, the forces for each profile are the same till 300ms. Then variations occur due to the different ramping rates. Finally all the profiles end with the same for force values again.

The average heat generation for each set of force profile were calculated and are shown in table 7.22 below: -

Force profile	Ramping rates (kN/ms)	Average heat generation (kJ)	Standard deviation	99% confidence interval
D	0.01	4.73	0.0084	$4.71 < \mu < 4.75$
	0.005	4.96	0.0084	$4.94 < \mu < 5.00$
	0.0025	4.98	0.0100	$4.96 < \mu < 5.00$
A	0.01	5.56	0.0084	$5.54 < \mu < 5.58$
	0.005	5.61	0.0071	$5.59 < \mu < 5.62$
	0.0025	5.84	0.0114	$5.81 < \mu < 5.86$
C	0.01	4.98	0.0054	$4.97 < \mu < 4.99$
	0.005	4.67	0.0100	$4.65 < \mu < 4.69$
	0.0025	4.59	0.0070	$4.57 < \mu < 4.60$

Table 7.22 – Heat generation for 3 ramping rates and force profiles

The increasing force-profiles of D and A show that the 0.01kN/ms ramping rate generates the least heat of 4.73kJ and 5.56kJ respectively within the 3 ramping rates. This can be due to the faster ramping rate reduces resistance faster than the other ramping rates as already been discussed in figures 7.9 and 7.10. The reduction in resistance reduces the amount of heat generated for that profile. The 0.0025kN/ms ramping rate generates the highest heat of 4.98kJ and 5.84kJ respectively due to the slower forging force increase, which allows a certain amount of increase in resistance compared to the other two ramping rates. The decreasing force-profile C shows opposite results with the 0.01kN/ms ramping rate achieving the highest heat generation of 4.98kJ compared to the 0.0025kN/ms ramping rate. This may be due to the characteristic of the force profile that reduces the applied forging force at a faster rate. This rapid decrease in force was seen to cause a faster increase in resistance as in figure 7.11. This increase in resistance causes a high heat to be generated. The 0.0025kN/ms ramping rate, which increases the resistance at a slower rate as shown in figure 7.11, generates the lowest heat of all the three decreasing force-profiles.

T tests were carried out on all the 3 profiles to determine the significance of the mean heat values for the 3 ramping rates.

Force profile	Ramping rates (kN/ms)	t values at 99% confidence interval
D	0.01 and 0.005	-43.293
	0.005 and 0.0025	-3.224
	0.0025 and 0.01	44.673
A	0.01 and 0.005	-8.684
	0.005 and 0.0025	-32.949
	0.0025 and 0.01	52.371
C	0.01 and 0.005	59.020
	0.005 and 0.0025	11.442
	0.0025 and 0.01	-66.103

Table 7.23 – T test results for the difference between mean heat values due to 3 ramping rates for 3 different force profiles

Table 7.23 shows the t test results. First test was carried out on force profile D for the means between 0.01kN/ms and 0.005kN/ms, 0.005kN/ms and 0.0025kN/ms and finally 0.00025kN/ms and 0.01kN/ms. The calculated t values show that the first and third t values reject the null hypothesis because these values are either $\leq t_{0.005}$ =-3.355 or $\geq t_{0.005}$ = 3.355 for 99% confidence interval. However the second t value of –3.224 shows insignificant difference between means of the 0.005kN/ms and 0.0025kN/ms ramping rates when tested with 99% confidence interval because the t value is greater than $t_{0.005}$ = -3.355 but rejects the null hypothesis when tested with 95% confidence interval because the value is smaller than $t_{0.025}$ = -2.306.

Next the test as carried out on force profile A. T values show significant difference between the heat generated for the different ramping rates because these values are $\leq t_{0.005}$ =-3.355 or $\geq t_{0.005}$ = 3.355.

Finally the t test was carried out for the same pairs of ramping rates as the other two tests for the force profile C. Again the calculated t values show that the mean heat generated by the 3 different ramping rates have significant differences between them because these values reject the null hypothesis when tested with 95% confidence interval.

7.2.3.2 Discussion on the weld strength changes for Case 3

The average weld strength achieved by the 3 ramping rates above was measured using the cross tension test. Table 7.24 shows the achieved average weld strengths.

Force profile	Ramping rate (kN/ms)	Average heat generation (kJ)	Average weld strength (kN)	Standard deviation	95% confidence interval
D	0.01	4.73	8.35	0.142	$7.963 < \mu < 8.545$
	0.005	4.96	8.40	0.101	$8.188 < \mu < 8.603$
	0.0025	4.98	8.54	0.083	$8.367 < \mu < 8.709$
A	0.01	5.56	10.09	0.192	$9.699 < \mu < 10.489$
	0.005	5.61	10.46	0.130	$10.196 < \mu < 10.732$
	0.0025	5.84	10.54	0.124	$10.287 < \mu < 10.797$
C	0.01	4.98	10.12	0.188	$9.727 < \mu < 10.504$
	0.005	4.67	9.59	0.175	$9.226 < \mu < 9.946$
	0.0025	4.59	9.34	0.156	$9.016 < \mu < 9.660$

Table 7.24 – Achieved weld strengths for 3 force profiles at 3 ramping rates

The force-profiles D and A show that the 0.0025kN/ms ramping rate force profiles have the highest weld strengths of 8.54kN and 10.54kN respectively. This obviously is because of the higher resistances of 0.00053Ω and 0.00065Ω respectively as seen in figures 7.9 and 7.10 and the highest heat generation of 4.98kJ and 5.84kJ respectively generated by these profiles. The strengths for the force-profile C show that the 0.01kN/ms ramping rate achieves the highest weld strength of 10.12kN. This can be attributed due to the characteristic of the profile as already been discussed above that generates the highest heat of 4.98kJ due to the high resistance as in figure 7.11.

Means significance tests were carried out using the t test because the average means for each force profile are closer to each other.

Force profile	Ramping rates (kN/ms)	t values at 99% confidence interval
D	0.01 and 0.005	-0.642
	0.005 and 0.0025	-2.395
	0.0025 and 0.01	2.584
A	0.01 and 0.005	-3.568
	0.005 and 0.0025	-0.997
	0.0025 and 0.01	4.402
C	0.01 and 0.005	4.614
	0.005 and 0.0025	2.385
	0.0025 and 0.01	-7.139

Table 7.25 – T test results for the difference between mean weld strengths due to 3 ramping rates for 3 different force profiles

The test was first carried out on the force profile D. The mean strengths for the 0.01kN/ms and 0.005kN/ms, 0.005kN/ms and 0.0025kN/ms and finally 0.01kN/ms and 0.0025kN/ms are tested. Since the first t value is greater than $t_{0.025}$ = -2.306 for 95% confidence interval and $t_{0.005}$ = -3.355 for 99% confidence interval, the null hypothesis indicates that the means does not have a significant difference between them. However the next two t values show significant differences between means when tested with 95% confidence interval because the values are either greater than $t_{0.025}$ = 2.306 or smaller than $t_{0.025}$ = -2.306, which rejects the null hypothesis but show the mean strengths are less significant when tested with 99% confidence interval.

The test was repeated for force profile A by comparing the means for the same ramping rates as the previous test. The test shows that the first and third t values reject the null hypothesis due to the significant difference between means because the first value is smaller than $t_{0.005}$ = -3.355 (99%) and the third value is greater than $t_{0.005}$ = 3.355 (99%) respectively. The second t value of -0.0997 which is greater then $t_{0.025}$ = -2.306 and $t_{0.005}$ = -3.355 indicates the insignificant difference between means of 0.005kN/ms and 0.0025kN/ms ramping times.

The last t test was carried out on force profile C by comparing the same means as the rest of the tests. The t values show significant differences between means when tested with 95% confidence interval because the t values are either smaller than $t_{0.025} = -2.306$ or greater than $t_{0.025} = 2.306$. However when tested with 99% confidence interval, the second t value of 2.385 shows the difference between the mean strengths are less significant because this value is smaller than $t_{0.005} = 3.355$.

The correlation analysis between heat generation and weld strength was carried out based on the raw data for the heat and weld strength as in appendix C. The r (correlation coefficient) of 0.727 indicates positive relationship between heat and strength as for the other experiments. The t value of 6.923 rejects the null hypothesis and show significance in the relationship when tested with p=0.001 of 3.551 ($t > p_{0.001} = 3.551$) and degree of freedom 43. The r^2 (coefficient of determination) of 0.529 shows that the variation in one variable is accounted by the other variable by 52.9%.

7.2.3.3 Summary of results for Case 3

The study on the 3 ramping rates show that for an increasing force-profile as in the case of the force-profiles A and D, a slower ramping rate would increase the resistance and generates higher heat. This in turn will produce stronger welds. The slower ramping rate of 0.0025kN/ms produced welds of 10.54kN and 8.54kN strength for force profiles A and D respectively, which are stronger than the welds produced by the other ramping rates. As in the case of a decreasing force-profile such as the force profile C; a faster ramping rate seems to create a higher resistance resulting in higher heat output and a stronger weld. The 0.01kN/ms ramping rate produces weld with strength of 10.12kN, which is stronger than the welds produced by 0.005kN/ms and 0.0025kN/ms ramping rates.

Even though some insignificance in the difference between mean strengths were shown in the t test, the comparison between the means between the 0.01kN/ms and 0.0025kN/ms ramping rates always showed significant difference between means at least in the case of 95% confidence

interval as in tables 7.23 and 7.25. Hence it can be concluded there would be a significant difference between the strengths achieved with a faster and slower ramping rate.

7.3 Conclusions of the force profile characteristics study

As mentioned in section 7.2, the force profile characteristics were studied for three different cases. Case1 showed that the force profiles that give the highest weld strengths are the 1.5kN-2.5kN (A) and 2.5kN-1.5kN (C) force profiles as shown in tables 7.10 and 7.11 depending on the welding current used. The characteristics of these profiles are a lower force, which is then increased to a higher force as welding progresses or a higher starting force that is decreased to a lower force as welding progresses.

Case 2 showed that of the 3 profiles studied, the 1.5kN-2.5kN (A) and 2.5kN-1.5kN (C)-force profiles achieve higher weld strengths. However to achieve high weld strengths by using the increasing force profile as the force profile A, the ramping delay should be long such as 500ms as in the case of the experiments in case 2. This is due to a longer delay was found to increase the resistance and generates more heat for stronger weld. For the decreasing force profile such as the 2.5kN-1.5kN-force profile, the ramping delay should be short such as 100ms that was used in the experiments in case 2 to achieve higher weld strengths. A shorter ramping delay was found to increase the resistance rapidly, and hence generates higher weld heat, resulting in improved weld strengths.

The studies in case 3 showed that the 1.5kN-2.5kN-force profile (A) and 2.5kN-1.5kN-force profile (C) achieve higher weld strengths of the 3 profiles experimented as shown in table 7.22. However the characteristic of the force profiles show that for the increasing force profile such as the force profile A, the ramping rate should be slow. For example 0.025kN/ms as used in the experiments in case 3 to achieve high strengths. Experiment results show that a slower ramping rate produces higher heat as shown in table 7.22. In the case of the decreasing force profile, for instance the force profile C, a faster ramping rate for example 0.01kN/ms, as used in

the experiments in case 3, should be used to achieve higher weld strengths. This can be explained as shown in table 7.22, for this profile, a faster ramping rate was found to produce higher heat.

Based on the conclusion of the 3 cases, the guidelines on the optimum force profiles' characteristics to achieve high strengths are specified as: -

a) For increasing force profiles

– use a longer ramping delay and a slower ramping rate. As the experiment result in Case 2 showed, a longer delay before ramping starts would increase the amount of heat generated for weld growth. Hence according to the experiment a ramping delay that is almost half of the total weld cycle would be preferable. This delay would increase the amount of heat needed for weld growth due to the faster of resistance change. A slower ramping rate will also allow the weld to have sufficient time to grow before the increase in forging force constraints the weld region as shown in case 3. Hence the ramping rate should be such that the higher forging force is reached at least an estimated 5 – 10 cycles before the weld cycle finishes so that the cycle ends with a higher forging force. The estimated 5 - 10 cycles before current terminates was assumed to be sufficient for the higher force to forge the weld. This profile should be superior to the profile with no ramping delay and ramping rate or in other words constant force profile because when working nearer to the expulsion limit, the constant force profile could cause expulsion due to its ability to achieve higher heat compared to the varying profile. The increase in the forging force in the varying force profile would reduce the heat generation due to reduction in resistance causing reduction in the rate of weld growth compared to the constant force profile and avoid expulsion. In depth study of this had been carried out in chapter 8 and will be discussed later in that chapter.

b) For decreasing force profiles

– use a shorter ramping delay and a faster ramping rate. As shown in case 2, for this kind of profile, the ramping delay should be short so that the resistance is increased earlier during the weld cycle to increase the heat for weld growth. The minimum ramping delay used in the experiments is 5 cycles. The estimated 5 cycles was assumed to be sufficient for the welding current to burn the surface contaminants and impurities to achieve metallic contact

between sheets before ramping starts. A faster ramping rate will allow the lower forging force to be achieved faster in order to increase the resistance during welding. As shown in case 3, a 0.01kN/ms ramping rate was found to be the fastest rate that could be used to achieve a 1kN force difference in the experiment, due to the inherent inertia and friction in the motor and limitation of the software based controller used in this experiment. The proposed force profile could be superior to a force profile that reduces the forging force at a faster rate without any delay once weld is initiated. This might be due to the possibility that the proposed profile allows a delay for the metallic contact to be formed that will cause a reduction in resistance compared to reducing the force when the contact between sheets are not formed and presence of impurities that could cause expulsion to occur due to the high resistance to current flow.

Based on these guidelines, two force profiles X and Y that will be known as the proposed force profiles will be developed. Experiments will be carried out on these profiles to prove the hypothesis that the profiles developed based on the guidelines above will produce a stronger weld. Further experiments involving the proposed force profiles will be discussed in the next chapter.

Chapter 8

OPTIMIZING FORCE PROFILES FOR IMPROVED WELD STRENGTHS

In this chapter, the development of the proposed force profiles based on the guidelines suggested in chapter 7 will be discussed. 2 profiles (X & Y) are proposed; one for the increasing force and the other for the decreasing force. Each of these will be compared with 2 other test profiles each to evaluate the capability of the profiles to produce stronger welds. These 2 profiles X and Y will then be used to compare the strength developed for forging force control and electrode clamping force (ECF) conditions during welding. The electrode clamping force condition is one that is similar to the pneumatic control system (section 4.3.2), but generated using the servo system. Finally the use of these force profiles to improve or extend the weld lobe will be investigated. The heat generated was calculated using the equation 6.1 in section 6.1.2, for all the results presented in this chapter. The t-test was used to test the significance of the difference between means (μ) of sample data as described in section 6.2.1.1. The correlation coefficient r, for sample data was calculated based on the values using equation 6.4 in section 6.3.2.

8.1 Experiments on the proposed force profiles

Based on the developed guidelines for the proposed force profiles characteristics, two force profiles A (1.5kN-2.5kN) and C (2.5kN–1.5kN) that were discussed in chapter 7 will be used to create the proposed force profiles X and Y as shown in the figure 8.1 below. These two profiles were chosen because of the ability of these profiles to develop stronger welds within the four profiles discussed in case 1 in section 7.2.1. For the increasing proposed force profile X (fig 8.1), a longer ramping start delay of 300ms after the weld was initiated and a slower ramping rate of 0.0025kN/ms were chosen with a total time for the profile of 800ms, equivalent to the total weld

cycle time based on the guideline discussed in section 7.3, in chapter 7. As for the decreasing proposed force profile Y (fig 8.1), a shorter ramping start delay of 100ms and a faster ramping rate of 0.01kN/ms were chosen with the same total time of 800ms that is equivalent to the total weld cycle time based on the guideline in section 7.3, in chapter 7. In order to compare the weld strengths, four more force profiles Xa, Xb, Ya and Yb were developed. These profiles will have one desired characteristic of the proposed force profile and another undesired characteristic. The desired characteristic is the characteristic of the profile that could produce higher strength welds. For example 300ms ramping delay (longer delay) and 0.0025kN/ms ramping rate (slower ramping rate) as in the case for increasing force profile or 100ms ramping delay (shorter delay) and 0.01kN/ms ramping rate (faster ramping rate) as in the case for decreasing force profile. Figure 8.2 below shows profiles X and Y: -

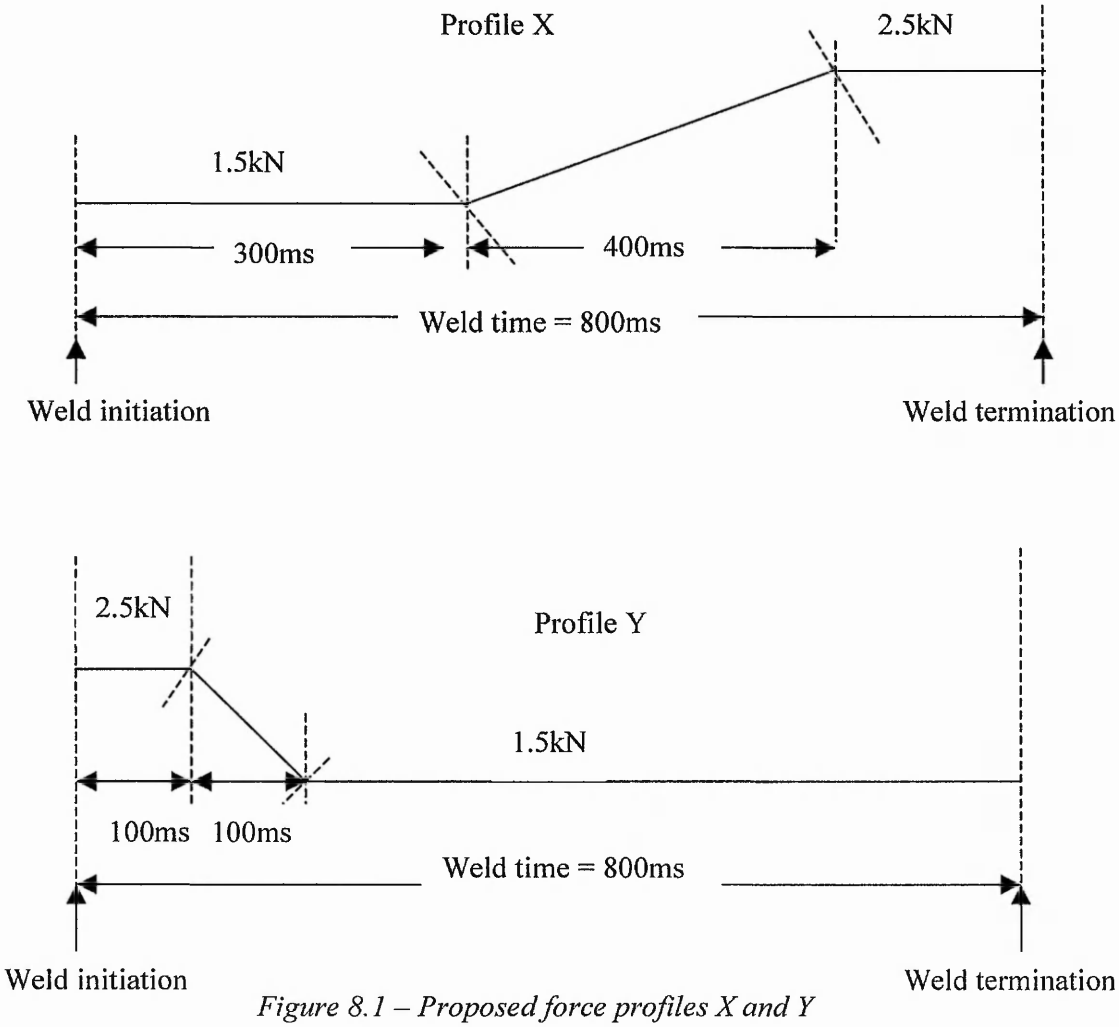

Figure 8.1 – Proposed force profiles X and Y

The undesired characteristic is the characteristic of the profile that produces lower weld strengths. For example 100ms ramping delay (shorter delay) or 0.01kN/ms ramping rate (faster ramping rate) as in the case for increasing force profile and 300ms ramping delay (longer delay) or 0.0025kN/ms ramping rate (slower ramping rate) as in the case for decreasing force profile.

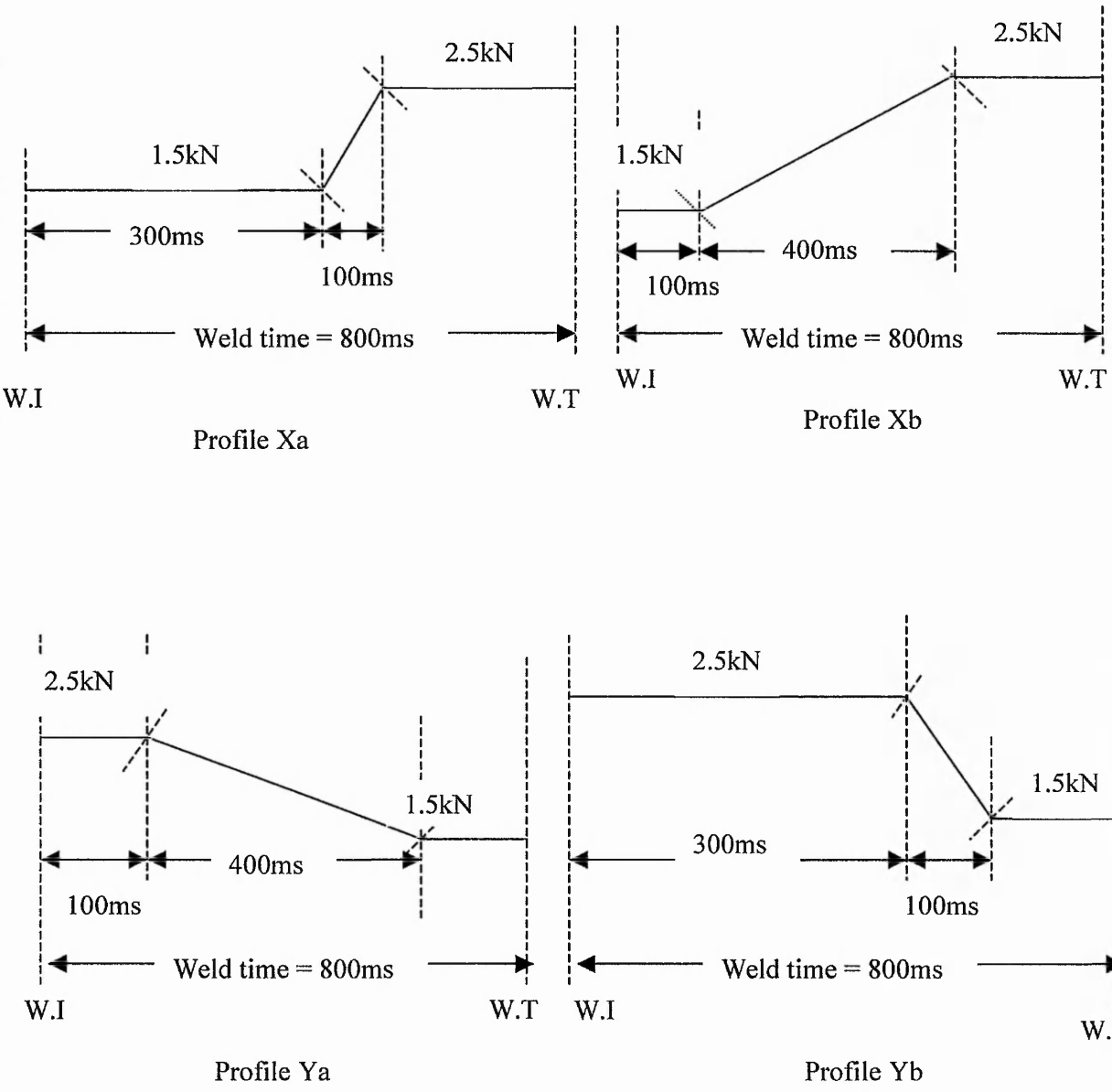

W.I – Weld initiation point

W.T – Weld termination point

Figure 8.2 – Test force profiles Xa, Xb, Ya and Yb

The force profiles Xa, Xb, Ya, and Yb in figure 8.2 are the ones that will be compared with the proposed force profiles X and Y. The increasing profiles Xa and Xb will be compared with profile X. Profile Xa has the desired characteristic where force is ramped after 300ms and an undesired characteristic where the ramping rate is 0.01kN/ms, which is faster. As already been discussed in section 7.2.3, a faster ramping rate of 0.01kN/ms was found to reduce the weld strength for the increasing force profile. Profile Xb has the desired characteristic where the ramping rate is 0.0025kN/ms but the ramping delay is just 100ms which is shorter (undesired). A shorter ramping delay was also found to reduce weld strength for the increasing force profile as seen in section 7.2.2.

The decreasing profiles Ya and Yb in figure 8.2 will be compared with profile Y. The desired characteristic of profile Ya is that the ramping delay is 100ms (shorter) but it has a slower ramping rate of 0.0025kN/ms (undesired). For the decreasing force profile, a slower ramping rate was found to produce a lower strength weld as discussed in section 7.2.3. As for profile Yb, this profile has a faster ramping rate of 0.01kN/ms (desired), but has the undesired longer ramping delay of 400ms. A longer ramping delay was also found to reduce the weld strength for the decreasing force profile as seen in section 7.2.2.

8.1.1 Discussion on the changes in resistance curve for the proposed force profiles

An experiment was carried out with the proposed force profile, profile X together with profile Xa and profile Xb, to study which of these profiles will give the highest weld strength. The experiment was repeated with the profile Y, profile Ya and profile Yb. Two different welding currents of 5000A and 6000A were used. The weld time was kept constant at 800ms(40 cycles) and the hold cycle was maintained as for the previous experiments at 200ms (10cycles). 6mm diameter electrodes and 2mm thick mild steel sheets were used for these experiments. 5 repetitions were made for each force profile.

Figures 8.3 and 8.4 show the change in the average dynamic resistance curves for profile X, profile Xa and profile Xb with the error bars showing 99% confidence interval for currents of 5000A and 6000A respectively. Similarly figures 8.5 and 8.6 show the changes in average dynamic resistance curve for profile Y, profile Ya and profile Yb with 5000A and 6000A current respectively. The error bars in these figures also show the resistance curve for 99% confidence interval.

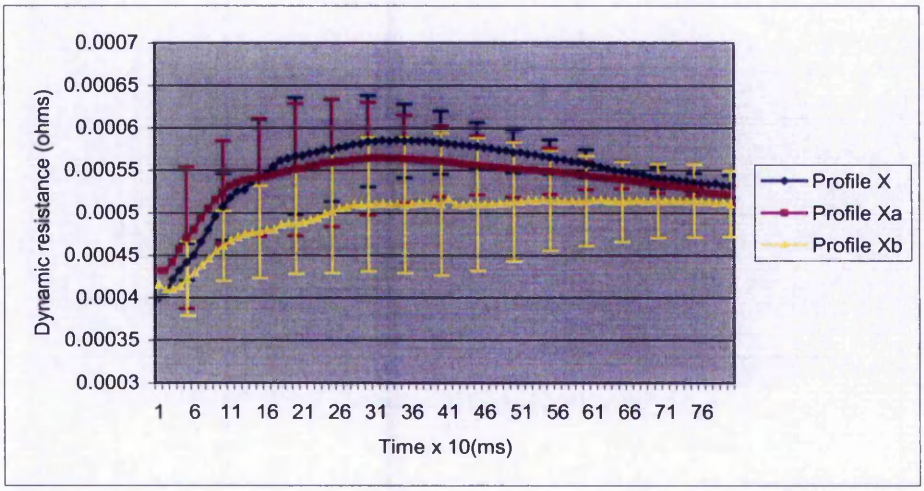

Figure 8.3– Dynamic resistance curves for Profile X, Profile Xa and Profile Xb with 5000A current

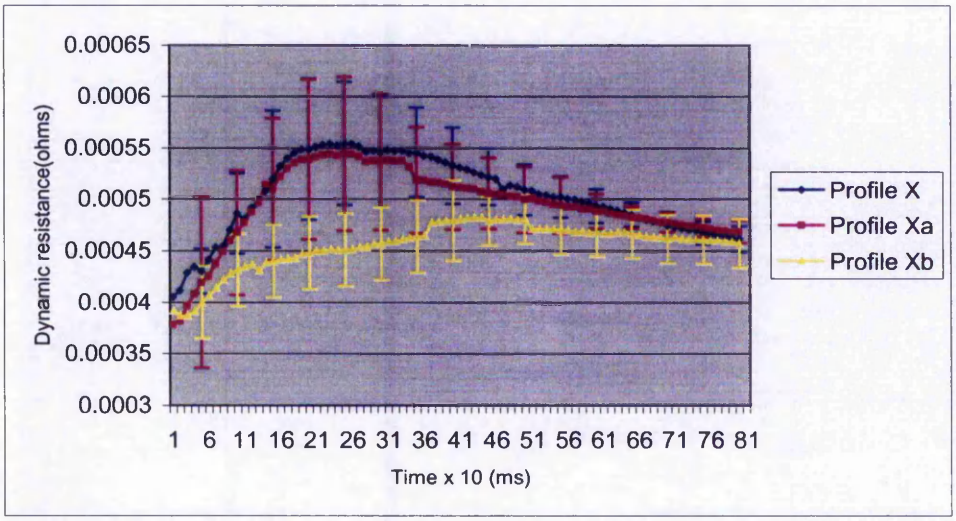

Figure 8.4 – Dynamic resistance curves for Profile X, Profile Xa and Profile Xb with 6000A current

Both figures 8.3 and 8.4 show that the proposed force profile X, has got the highest average peak resistances of 0.00058Ω and 0.00055Ω for 5000A and 6000A currents respectively. The change in dynamic resistance for profile X in figure 8.3 shows a rapid increase in resistance before the change in resistance decrease after 300ms due to the increase in force. Similar behaviour was noticed in figure 8.4, where the dynamic resistance curve for profile X has a higher change in resistance before 300ms and the change in resistance decreases after this period due to the effect of ramping which starts increasing the force to 2.5kN. Profiles Xa and Xb have lower average resistances due to the undesired characteristics of theses profiles. However profile Xa seems to have higher average peak resistance of about 0.00057Ω in figure 8.3 and about 0.00054Ω in figure 8.4 as compared to profile Xb. This can be attributed to the longer delay of 300ms in the force profile before ramping starts, which allows the increase in resistance. The faster rate of ramping (0.01kN/ms) causes the resistance to drop faster, which is more obvious in figure 8.4.

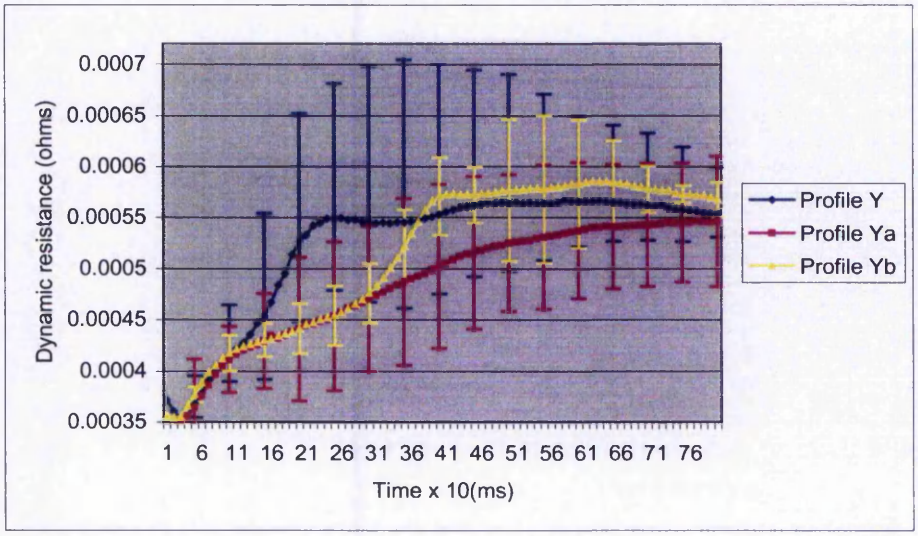

Figure 8.5 - Dynamic resistance curves for Profile Y, Profile Ya and Profile Yb with 5000A current

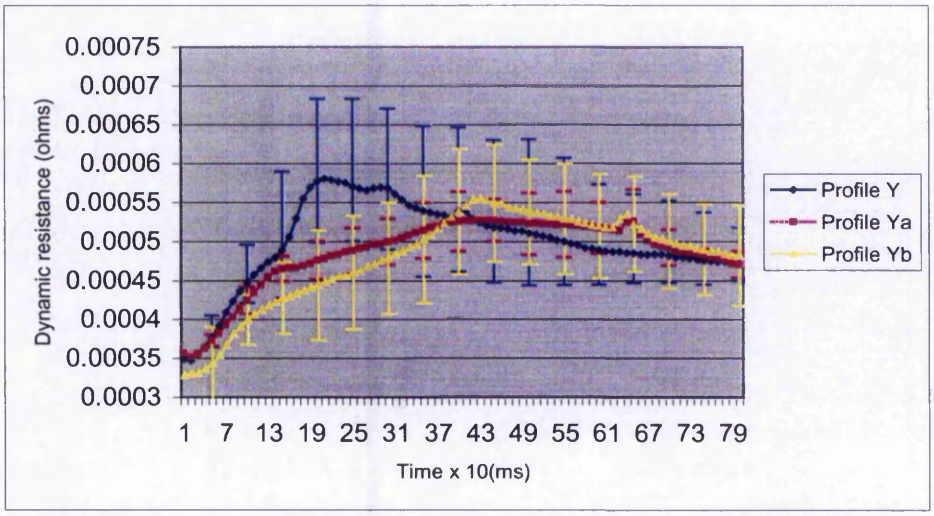

Figure 8.6 - Dynamic resistance curve for Profile Y, Profile Ya and Profile Yb with 6000A current

Figure 8.5 and 8.6 also show that the proposed force profile Y has got the highest average resistances of 0.00055Ω and 0.00057Ω for 5000A and 6000A current respectively. The dynamic resistance curve for this proposed force profile Y in figure 8.5 shows a rapid increase in dynamic resistance till about 240ms. This rapid increase is due to the shorter ramping delay of 100ms and faster ramping rate of 0.01kN/ms to decrease the force to 1.5kN, which happens during the first 200ms. The resistance then starts decreasing most probably due to the increase in weld size that would reduce the resistance to the current flow. It is known that after melting, only the resistance of the bulk material plays the dominant role with the contact resistance becoming zero (Thornton et al. 1996). With just the bulk resistance, no significant increase in resistance is detected after the weld develops. The similar behaviour was also noticed in figure 8.6 for profile Y, where a rapid increase in resistance for the first 200ms occurs. Studying the average dynamic resistance curves for profile Ya and profile Yb, both the figures show that the resistance for profile Yb is lower than resistance for profile Ya till about 300ms.The resistance for profile Yb then increases after 300ms and becomes higher than the resistance for profile Ya. This can be explained due to the characteristics of the profiles as seen in figure 8.2. Profile Ya starts to ramp earlier after 100ms with a slower ramping rate of 0.0025kN/ms than profile Yb which only starts to ramp after 300ms, which causes the resistance to increase for profile Ya. However after 300ms, profile

Yb starts to ramp at a faster rate of 0.01kN/ms to 1.5kN which explains the sudden increase in resistance for this profile after 300ms.

All the four figures seen above show that the proposed force profiles have the highest average peak resistances which indicates the possibility of achieving the highest weld strength. The average heat function for all the dynamic resistance curves and measured average weld strengths are presented below.

8.1.2 Discussion on the heat generation for the proposed force profiles

Table 8.1 shows the measured average heat generation based on the developed dynamic resistance curves.

Welding current (A)	Force profile	Average heat generation (kJ)	Standard deviation	99% confidence interval
5000	Profile X	5.49	0.0084	5.47 <μ< 5.51
	Profile Xa	5.21	0.0055	5.20 <μ< 5.23
	Profile Xb	4.75	0.0054	4.74 <μ< 4.76
	Profile Y	5.43	0.0055	5.42 <μ< 5.45
	Profile Ya	4.97	0.0089	4.95 <μ< 4.98
	Profile Yb	5.02	0.0071	5.00 <μ< 5.03
6000	Profile X	7.91	0.0083	7.89 <μ< 7.93
	Profile Xa	7.70	0.0044	7.69 <μ< 7.71
	Profile Xb	7.20	0.0100	7.18 <μ< 7.22
	Profile Y	7.76	0.0100	7.74 <μ< 7.78
	Profile Ya	7.50	0.0084	7.54 <μ< 7.57
	Profile Yb	7.56	0.0084	7.48 <μ< 7.51

Table 8.1 – Heat generation for the 6 force profiles at 5000A and 6000A currents

Based on table 8.1, it is quite certain now that both the proposed force profiles X and Y will produce stronger welds than the other force profiles at any welding current. This can be explained as both the force profiles generate increased heat compared to the test profiles for both the welding currents. This was clarified by means of the t test.

Welding current (A)	Test samples Force profiles (kN)	t values with 99% confidence interval
5000	X and Xa	57.998
	X and Xb	141.761
	Xa and Xb	130.108
	Y and Ya	100.140
	Y and Yb	111.000
	Ya and Yb	-9.893
	Xa and Yb	54.025
	Xa and Ya	53.964
	Yb and Xb	63.478
6000	X and Xa	45.484
	X and Xb	118.631
	Xa and Xb	91.034
	Y and Ya	54.643
	Y and Yb	45.512
	Ya and Yb	-12.952
	Xa and Yb	34.317
	Xa and Ya	44.760
	Yb and Xb	62.232

Table 8.2 – T test results for the difference between mean heat values for proposed and test profiles with 5000A and 6000A current

Tests were carried out on the mean heat values between profile X and profile Xa, profile X and profile Xb and profile Xa and profile Xb for 5000A as shown in table 8.2. The calculated t values show that there are significant differences between means of the heat generated between profiles

because these values $\geq t_{0.0005}$=3.355 for 99% confidence interval. Similar tests were carried out between profile Y and profile Ya, profile Y and profile Yb and profile Ya and profile Yb for 5000A. The calculated t values again show significant differences between means because these values are either $\leq t_{0.005}$ =-3.355 or $\geq t_{0.005}$ = 3.355 for 99% confidence interval. The t tests were repeated for the mean heat values between profile X and profile Xa, profile X and profile Xb and profile Xa and profile Xb and 6000A. T values show that the null hypothesis is rejected and there are significant differences between means. Similarly mean values between profile Y and profile Ya, profile Y and profile Yb, and profile Ya and profile Yb for 6000A were tested and the t values confirm the significance difference in between means for all these profiles. Through these tests it was confirmed that the proposed profiles X and Y generate higher heat than the test profiles X, Xb, Ya and Yb for both 5000A and 6000A currents.

Comparing profile X and profile Y for 5000A, it was found that profile X seems to have generated a higher average heat of 5.49kJ compared to profile Y, which produces an average heat of 5.43kJ. Similarly comparing profile X and profile Y for 6000A, it was again noticed that profile X generates a higher average heat of 7.91kJ compared to 7.76kJ for profile Y. T tests carried out on both these profile for welding currents of 5000A and 6000A give t values of 13.762 and 39.145 respectively. These t values reject the null hypothesis of no difference between means because these values are $\geq t_{0.0005}$=3.355 for 99% confidence interval. The reason in the differences in heat generated for these profiles could be explained by studying the characteristics of these force profiles. Profile X is an increasing force profile from 1.5kN-2.5kN while profile Y is a decreasing force profile from 2.5kN-1.5kN. This shows that profile X starts from a lower force compared profile Y. Hence the contact resistance for profile X would be higher than profile Y due to the lower force. During welding, profile X maintains the lower force of 1.5kN for 300ms while profile Y takes about 200ms to reach to 1.5kN. So the resistance during this time would be higher in the case of X compared to profile Y. This explains the results for these profiles in table 8.1. Profile Xa shows a higher heat generation (5.21kJ and 7.70kJ) compared to profile Xb (4.75kJ and 7.20kJ) for both the welding currents. This can be explained as due to the delay in the ramping time in profile Xa which starts after 300ms compared to profile Xb where ramping to increase the force to 2.5kN starts at 100ms. According to figures 8.5 and 8.6, it was expected that profile Yb to generate higher heat compared to profile

Ya due to its higher ramping rate of 0.01kN/ms. This was true in both the case of the 5000A and 6000A currents where profile Yb show higher heats of 5.02kJ and 7.56kJ than profile Ya of 4.97kJ and 7.50kJ.

Comparing profile Xa and Yb, both these profiles have the same delay times of 300ms before the force starts ramping and the same ramping rates of 0.01kN/ms. However the difference in these profiles as seen in figure 8.2 is, profile Xa maintains a constant lower forging force of 1.5kN before increasing to 2.5kN while profile Yb maintains a constant forging force of 2.5kN before reducing to 1.5kN force. Since profile Xa maintains a lower force for the same longer delay as profile Yb before the forging force was changed, the heat generated by profile Xa for both 5000A and 6000A currents (5.21kJ and 7.70kJ) were found to be higher than for profile Yb for the same welding currents (5.02kJ and 7.56kJ). Similarly comparing profile Ya and Xb, both these profiles have the same delays of 100ms and ramping rates of 0.0025kN/ms. The difference between these profiles as in figure 8.2 is that profile Ya starts from a higher forging force of 2.5kN and the force is reduced to 1.5kN force after a short delay of 100ms. As in the case of profile Xb, this profile starts from a lower forging force of 1.5kN and the force is increased to 2.5kN force after 100ms. The reduction in the forging force for profile Ya after a short delay was found to produce higher heats of 4.97kJ and 7.50kJ compared to the 4.75kJ and 7.20kJ heats generated by profile Xb due to the increase in forging force after a short delay of 100ms for both welding currents of 5000A and 6000A respectively. Comparison on profiles Xa and Ya shows that profile Xa generates higher heats of 5.21kJ and 7.70kJ for 5000A and 6000A currents respectively compared to 4.97kJ and 7.50kJ as in case of profile Ya for the same welding currents. This can be explained as since profile Xa maintains a lower forging force of 1.5kN for a longer delay of 300ms and reaches the higher force of 2.5kN after 400ms, this profile could produce higher heat due to its higher resistance compared to profile Ya , which starts with a higher forging force of 2.5kN, causing the resistance to be lower than profile Xa and achieves the lower forging force of 1.5kN only after 400ms. Comparing profile Yb and Xb, Yb was found to produce higher heats (5.02kJ and 7.56kJ) compared to Xb (4.75kJ and 7.20kJ) for both the welding currents tested. This can be explained as due to the rapid increase in resistance seen in figures 8.5 and 8.6 for profile Xb due to the reduction in force with a higher ramping rate. While for Xb, the resistance starts to drop after 100ms due to the increase in force.

8.1.3 Discussion on the weld strengths produced by the proposed force profiles

The cross tension test, discussed in section 3.3.2.3, was used to measure the weld strengths for the 6 profiles used in this experiment and are given in table 8.3 below.

Current (A)	Force profile (kN)	Average heat generation (kJ)	Average weld strength (kN)	Std.deviation	95% confidence interval
5000	Profile X	5.49	9.71	0.2038	$9.29<\mu<10.10$
	Profile Xa	5.21	6.80	0.1984	$6.39<\mu<8.21$
	Profile Xb	4.75	5.54	0.2187	$5.08<\mu<5.98$
	Profile Y	5.43	9.21	0.1839	$8.84<\mu<9.59$
	Profile Ya	4.97	6.23	0.1535	$5.91<\mu<6.55$
	Profile Yb	5.02	6.53	0.2902	$5.93<\mu<8.13$
6000	Profile X	7.91	11.89	0.2977	$11.27<\mu<12.50$
	Profile Xa	7.70	11.05	0.3086	$10.41<\mu<11.68$
	Profile Xb	7.20	10.32	0.1882	$9.92<\mu<10.70$
	Profile Y	7.76	11.30	0.1838	$10.91<\mu<11.67$
	Profile Ya	7.50	10.38	0.2338	$9.90<\mu<10.86$
	Profile Yb	7.56	10.54	0.1176	$10.30<\mu<10.78$

Table 8.3 – Weld strengths for 6 force profiles at 5000A and 6000A currents

The measured weld strengths show that the proposed force profiles achieves the highest weld strengths for both the welding currents. The t tests carried out to test the significance of the difference between the average weld strengths are given in table 8.4 below.

Welding current (A)	Test samples Force profiles (kN)	t values with 99% confidence interval
5000	X and Xa	22.877
	X and Xb	31.192
	Xa and Xb	9.541
	Y and Ya	27.817
	Y and Yb	17.442
	Ya and Yb	-2.043
	Xa and Yb	1.717
	Xa and Ya	5.081
	Yb and Xb	6.092
6000	X and Xa	4.380
	X and Xb	9.431
	Xa and Xb	3.453
	Y and Ya	6.917
	Y and Yb	8.330
	Ya and Yb	- 1.056
	Xa and Yb	3.453
	Xa and Ya	3.870
	Yb and Xb	2.218

Table 8.4 – T test results for the difference between mean strengths for proposed and test profiles with 5000A and 6000A current

T test was carried out to test the mean weld strengths between profile X and profile Xa, profile X and profile Xb and profile Xa and profile Xb for 5000A current. The calculated t values show that there are significant differences between the mean strengths of the force profiles because these values are $\geq t_{0.0005}=3.355$ for 99% confidence interval. The test was carried out again for the same pairs of profiles with 6000A current. T values again show significant differences between mean weld strengths. Hence from these tests it can be seen that the profile X produces a stronger weld then both the test profiles (profile Xa and profile Xb) as seen in tables 8.3 and 8.4.

T test was carried out to test the mean weld strengths between profile Y and profile Ya, profile Y and profile Yb and profile Ya and profile Yb for 5000A current. T values show that mean strengths difference between profile Y and profile Ya and profile Y and profile Yb are significant because these values reject the null hypothesis of no difference in means. However the means difference between profile Ya and profile Yb was found to be less significant because the t value of –2.0433 is greater than $t_{0.0025}$ = -2.306 and $t_{0.005}$ = -3.355 for 95% and 99% confidence intervals respectively. The test was again carried out for the same pairs of force profiles and 6000A current. T values again show that mean strengths difference between profile Y and profile Ya and profile Y and profile Yb are significant but the means difference between profile Ya and profile Yb is less significant because the t value of –1.056 is greater than $t_{0.025}$ = -2.306 and $t_{0.005}$ = -3.355 for 95% and 99% confidence intervals respectively. From these tests it can be seen that the profile Y produces a stronger weld then both the test profiles (profile Ya and profile Yb) as seen in tables 8.3 and 8.4 .

Observations on the achieved weld strengths for both the proposed force profiles with 5000A current show that profile X and profile Y, achieve the highest weld strengths of 9.71kN and 9.21kN respectively. A t test was carried out to test the significance of the differences of the two values based on the null hypothesis of no difference. The test that was carried out shows that the t = 4.073 which is greater than $t_{0.005}$ = 3.355 for 99% confidence interval which means that the null hypothesis is rejected and both the averages are not the same. Similarly observations on both the force profiles with 6000A current also show that profile X and profile Y achieve the higher strengths of 11.89 kN and 11.30 kN respectively. The t test gives a value of t=3.76 that is greater than $t_{0.005}$ = 3.355 for 99% confidence interval which again shows that both the averages are different. Hence it can be concluded from the strength results that the proposed force profiles produce stronger welds. The t tests also indicate that profile X produces the stronger weld compared to profile Y and there are significant differences between the means of these profiles even though the achieved strength values are closer.

For the experiments discussed above using force profile X, Y, Xa, Xb, Ya and Yb, correlation between the heat generation and weld strength was analysed using the collected raw data for heat and strength as seen in appendix C. The r (correlation coefficient) was calculated

using equation 4 in section 6.3.2. Value of r = 0.919 shows there is a strong positive relationship between the heat generation and the achieved weld strength in this experiment. Observations in table 8.3, which show that the weld strength increases with the increase in heat generation, support this positive relationship. The test to evaluate the significance of the correlation coefficient was carried out using the t test. T value of 17.785, which is greater than the tested level of significance of $p_{0.001} = 3.460$ ($t > p_{0.001} = 3.460$) at degree of freedom of 58, rejects the null hypothesis and shows significance in the correlation between the heat and strength. The coefficient of determination r^2 gives a value of 0.845 that indicates the variation in one variable is accounted by the other variable by 84.5%.

8.2 Comparison between forging force control and electrode clamping force (ECF) conditions during welding

An experiment was carried out to study the changes in the dynamic resistance curve and achieved weld strength for the forging force control and electrode clamping force (ECF) conditions during welding. During ECF condition (section 4.3.2), the change in forging force is process dependent. The ECF condition would be similar the conventional pneumatic system throughout the weld cycle. Two different currents of 5000A and 6000A were used in this experiment. The weld cycle is 800ms (40 cycles). The two proposed force profiles X and Y were used for force control. The thickness of the sheets used is 2mm and the electrode tip diameter is 6mm. 5 repetitions were made for each condition.

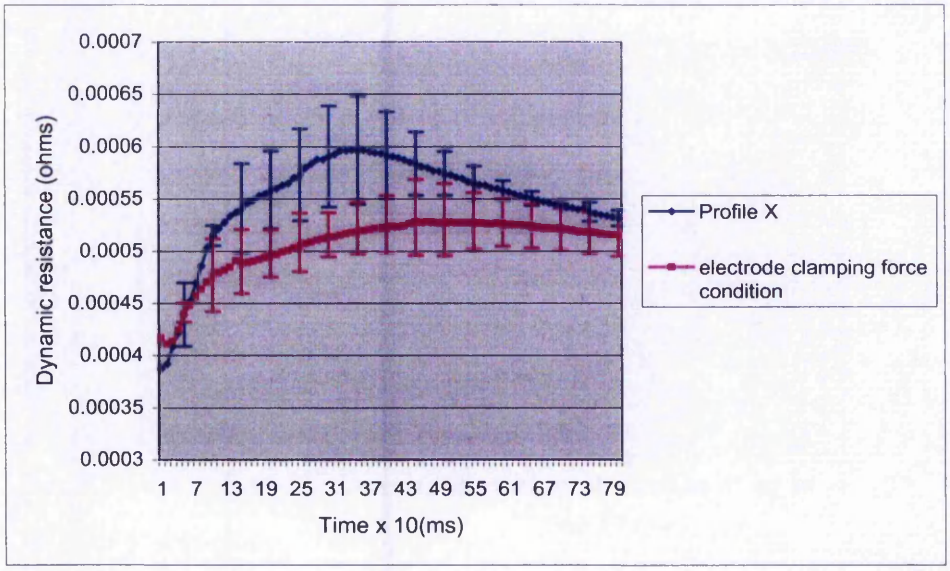

Figure 8.7 – Dynamic resistance for force control(profile X) and electrode clamping force conditions using 5000A current

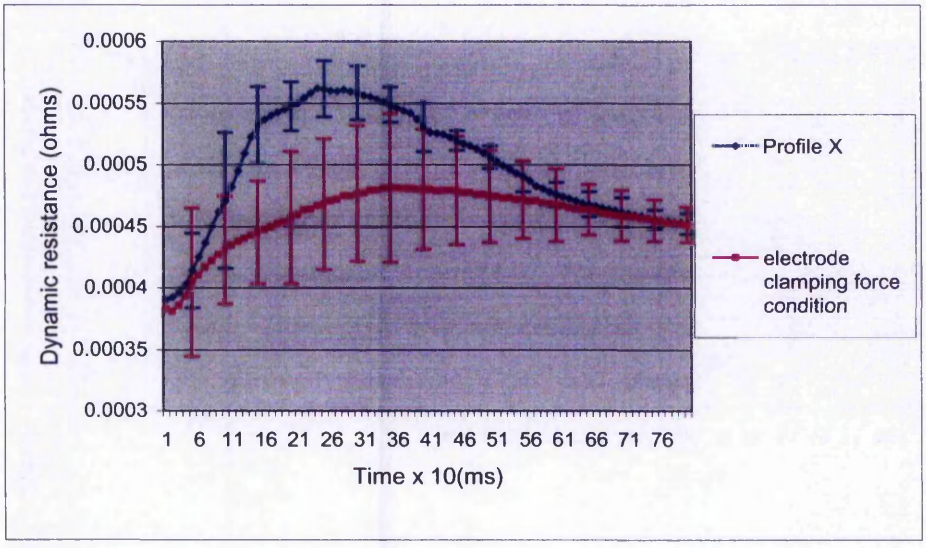

Figure 8.8 – Dynamic resistance for force control(profile X) and electrode clamping force conditions using 6000A current

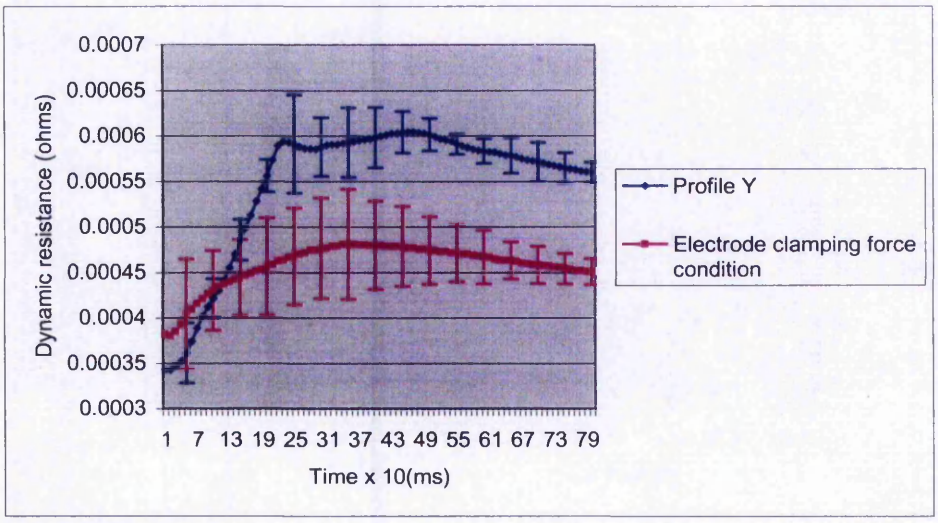

Figure 8.9– Changes in the dynamic resistance for force control(profile Y) and electrode clamping force conditions using 5000A current

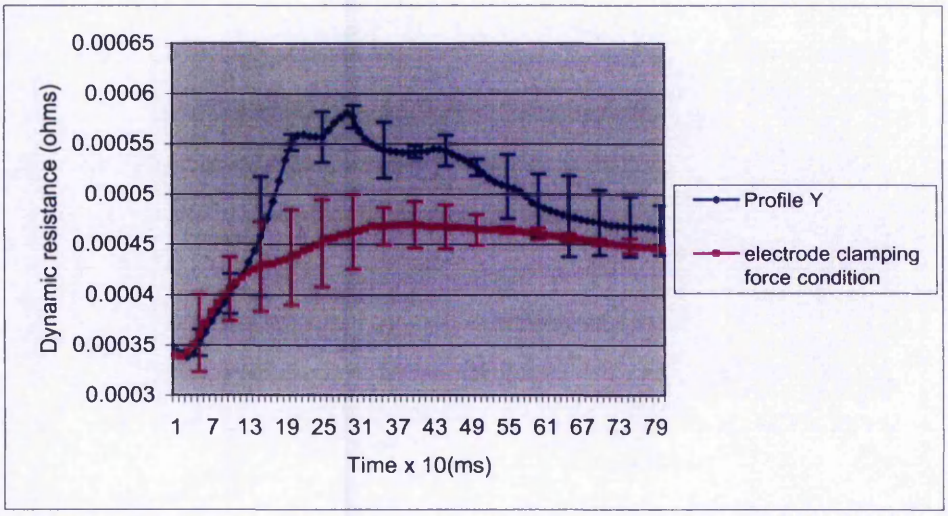

Figure 8.10 – Changes in the dynamic resistance for force control(profile Y) and electrode clamping force conditions using 6000A current

8.2.1 Discussion on the changes in dynamic resistance for forging force control and electrode clamping force (ECF) conditions

Figure 8.7 shows the changes in the average dynamic resistance curves for the forging force control and electrode clamping force condition during welding with 5000A current. The forging force change during welding as recorded by the piezoelectric sensor was due to the weld growth. The error bars show the variations. The force profile used for the force control is the force profile X. The squeeze force of 1.5kN is applied for both the conditions through the squeeze force control system that was discussed in section 4.3.2. The resistance for the ECF condition seems to be lower than the forging force controlled condition as seen in figures 8.7. This could be explained by referring to figure 8.11. Figure 8.11 show the changes in forging force during welding for the ECF condition, along with that for the force profile X with the error bars showing 99% confidence interval. It can be seen that in the ECF condition the forging force increases faster and higher due to softening of the metal and weld expansion (Tang et al. 2000). In the case of the force control condition, the forging force is maintained about 1.5kN for 300ms before the force is increased to 2.5kN, a force which is lower than that recorded in the ECF condition. This explains the differences in the dynamic resistance curves in figure 8.7.

Similar results were noticed in figure 8.8 where the average dynamic resistance for the ECF condition is lower than the controlled forging force condition with force profile X at 6000A. Similar to the explanation for figure 8.11, the lower average dynamic resistance curve for the electrode clamping force condition is due to the weld expansion due to the softening and mechanical collapse that increases the forging force faster than in the controlled condition. The average dynamic resistance curve for the electrode clamping force condition in figure 8.8 shows a significant β-peak compared to the dynamic resistance curve in figure 8.7 due to the high current (6000A). The average dynamic resistance curves for the controlled condition in both the figures show a rapid increase in the change in resistance till about 300ms and then

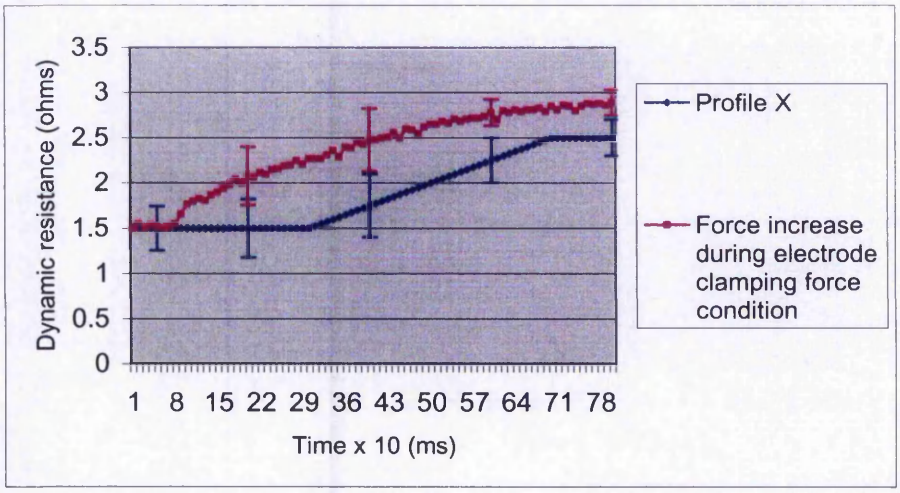

Figure 8.11 - Change in the forces during forging force control (profile X) and electrode clamping force conditions

starts dropping, which indicates the ramping of the force has started. The drop in resistance is more significant in figure 8.8 compared to figure 8.7, due to the use of a higher current. The high current will increase the rate of melting and the increase in the area for current flow due to the increase in the forging force. This faster increase in area will result in a rapid drop of resistance. Since both the conditions start with the same squeeze force, the resistances during the initial stages of the welding are closer to each.

It can be seen from figures 8.9 and 8.10 that the ECF conditions have lower average resistance compared the controlled forging force conditions with force profile Y. Figure 8.12 explains these observations. Figure 8.12 show the changes in forging force during welding for the ECF condition, along with that for the force profile Y with the error bars showing 99% confidence interval. The squeeze forces for both the conditions are the same 2.5kN, which was applied by means of the squeeze force control system discussed in section 4.3.2. During the ECF condition, the forging force increases due to the weld growth during welding. Hence the force as recorded by the piezoelectric sensor could be seen to increase in figure 8.12. However in the controlled force conditions, the chosen force profile reduces the forging force unlike the ECF condition where the forging force is increased during welding. This reduction in forging force during welding will cause the controlled conditions to have higher average resistances than the ECF conditions as seen in figures 8.9 and 8.10. However the use of high current and reducing the

force during welding will increase the risk of expulsion since the molten metal has the tendency to expel from the parent metal during to the lower electrode force (Zhang 1999). This will cause a rapid drop in the resistance as seen in figure 8.10. Similar results have already been discussed in sections 6.2.2.1, 6.3.2, 6.3.3 and 7.2.1.2.

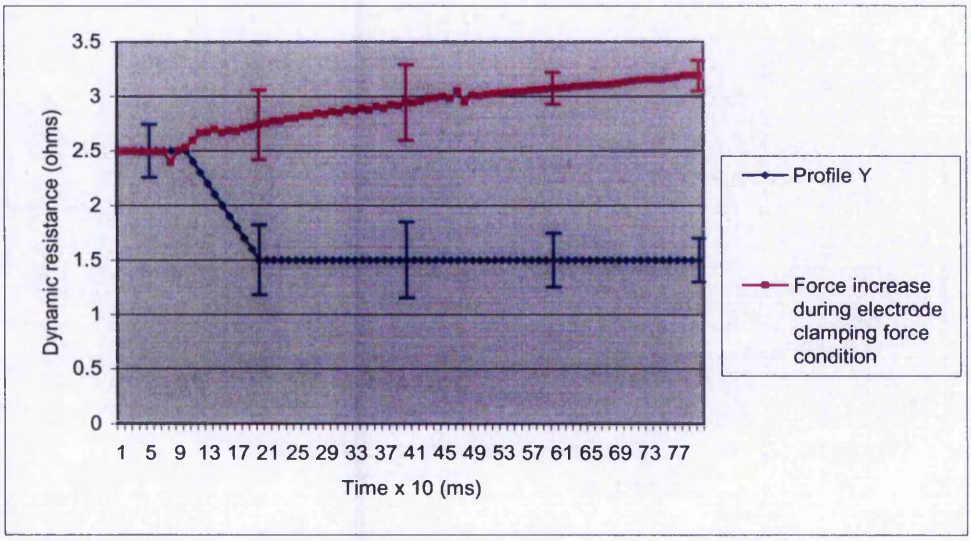

Figure 8.12 - Change in the forces during forging force control (profile Y) and electrode clamping force conditions

Figure	Condition	Average heat (kJ)	Standard deviation	99% confidence interval	t test results for 99% confidence interval
8.7	Force control	5.49	0.0045	5.49 <μ< 5.51	96.412
	ECF condition	5.06	0.0089	5.05 <μ< 5.08	
8.8	Force control	7.74	0.0084	7.72 <μ< 7.76	111.415
	ECF condition	7.13	0.0089	7.11 <μ< 7.14	
8.9	Force control	5.48	0.0054	5.46 <μ< 5.49	263.523
	ECF condition	4.58	0.0054	4.56 <μ< 4.59	
8.10	Force control	7.65	0.0051	7.63 <μ< 7.66	169.060
	ECF condition	6.39	0.0054	6.37 <μ< 6.40	

Table 8.5 – Heat generations for the controlled force and electrode clamping force conditions

The same squeeze forces of 2.5kN cause the resistances during the initial stages of welding to be closer to each other as seen in figures 8.9 and 8.10. The average heat generations for all the figures above are tabulated in table 8.5.

Table 8.5 indicates that the heat generated using the force control is higher than the heat generated for the ECF during welding. This is obviously due to the difference in the resistances as shown in all the figures above. The higher resistance generated during force control causes high heat to be generated during this condition. T test carried out between the means for figure 8.7 rejects the null hypothesis of no difference and shows significant difference between the heat mean values. The t test carried out on heat mean values between force control and electrode clamping force conditions in figure 8.8, shows significant differences between means because the t value is greater than $t_{0.005} = 3.355$ for 99% confidence interval. T tests carried out on figures 8.9 and 8.10, also reject the null hypothesis and show significant differences between means. From these tests it was concluded that the force control during welding produces higher heat compared to the electrode clamping force condition with significant difference between the heats generated during both these conditions. Also it was noticed that the force profile X generates higher heat than the force profile Y for the same welding current as in the cases of figure 8.7 (5.49kJ) & figure 8.9 (5.48kJ) and figure 8.8 (7.74kJ) & figure 8.10 (7.65kJ). The t test carried out on both these profiles for both the welding currents of 5000A and 6000A indicate that the force profile X produces higher heat than the force profile Y with significant differences between the generated heats for both welding currents. This is because the calculated t values of 4.111 and 25.141 for 5000A and 6000A respectively are greater than $t_{0.005} = 3.355$ for 99% confidence interval. The results are similar to the results in table 8.1. Table 8.5 also indicates that the heat generated using the same force profile increase with the increase in current as in the cases of figure 8.7 (5.49kJ) & figure 8.8 (7.74kJ) and figure 8.9 (5.48kJ) & figure 8.10 (7.65kJ). Observations on the heat generated during ECF conditions show the same results as already been discussed in section 6.2.1.1, i.e. for the same applied force, the rate of weld growth increases with increase in current due to the increase in the heat generation (Gould 1987). This could be clarified by comparing the amount of heat generated for figures 8.7 & 8.8 and figures 8.9 & 8.10.

8.2.2 Discussion on the changes in weld strength for forging force control and electrode clamping force (ECF) conditions

The weld strengths achieved by the conditions above were measured by means of the cross tension test with 5 repetitions for each condition. Results of the measured weld strengths are given in table 8.6.

Current (A)	Force profile (kN)	Average heat generation (kJ)	Average weld strength (kN)	Standard deviation	95% confidence interval
5000	1.5 – 2.5 (X)	5.49	9.35	0.1760	$8.99 < \mu < 9.72$
	ECF	5.06	5.36	0.2504	$4.85 < \mu < 5.88$
6000	1.5 – 2.5 (X)	7.74	11.39	0.2355	$10.90 < \mu < 11.87$
	ECF	7.13	9.52	0.2487	$9.01 < \mu < 10.03$
5000	2.5 – 1.5 (Y)	5.48	5.58	0.3579	$4.84 < \mu < 6.31$
	ECF	4.58	2.42	0.2667	$1.87 < \mu < 2.97$
6000	2.5 – 1.5 (Y)	7.65	10.57	0.365	$9.82 < \mu < 11.32$
	ECF	6.39	8.52	0.2391	$8.03 < \mu < 8.01$

Table 8.6 – Achieved weld strengths for the controlled force and electrode clamping force conditions

The results obtained in table 8.6 shows that the force control during welding achieves higher weld strength than the ECF during welding condition. This can be explained as due to the high resistance caused by the use of force profiles during force control as shown from figures 8.7 to 8.10 and the higher heat generation.

Current (A)	Test samples	t test results for 99% confidence interval
5000	Force control with Profile X and ECF condition	29.150
6000	Force control with Profile X and ECF condition	12.208
5000	Force control with Profile Y and ECF condition	15.831
6000	Force control with Profile Y and ECF condition	10.505

Table 8.7 – T test results for the difference between mean weld strengths for controlled force and electrode clamping force conditions

The calculated t value between the mean strengths achieved using force control with force profile X and ECF condition during welding with 5000A current show that the null hypothesis is rejected and both the means have significant difference between them. Similarly the test carried out for the same conditions as the previous test but with 6000A current again shows significant difference between the recorded mean strength values. T tests carried out between the mean strengths achieved using force control with force profile Y and ECF during welding with 5000A and 6000A currents gives t values which are greater than $t_{0.005} = 3.355$ for 99% confidence interval hence the significance between the means differences are conformed. Based on these t tests it was concluded that the force control during welding produces stronger weld compared to the electrode clamping force during welding with significant differences between the measured average strengths. Hence since the ECF condition is an analogy to the conventional pneumatic system, it could be said the forging force controlled servo system would be able to produce stronger welds than the pneumatic system. Table 8.6 also indicates that the force profile X achieves higher weld strength than force profile Y for the same welding current due to the higher heat generated by using this profile. At 5000A the t value based on the t test is 21.132 and at 6000A the t value is 4.221, which indicates that the force profile X achieves higher weld strength than force profile Y with significant differences between the weld strengths. The ECF conditions

show that for the same squeeze force applied, weld strength increases with increase in current due the higher heat generation.

The collected raw data for heat and strength as in appendix C were used to calculate the correlation coefficient r for the heat and strength variables. The r gives a value of 0.89 that shows that there is a stronger positive relationship between the two variables because the value is closer to +1.0. The coefficient of determination r^2 shows that the heat and weld strength are related between each other by 79.0%. The t value of 11.97 which is greater than $p_{0.001}$=3.551 at 38 degrees of freedom reject the null hypothesis and indicate that there is a significant relationship between the heat generated and the achieved weld strength.

8.3 Modifying the lower weld curve using force control

All the experiments that were carried out in chapter 7 and in this chapter were within the weld lobe obtained through ECF condition. The weld lobe that has already been discussed in section 6.2.3 is the region where the ability to produce a weld is possible by using a certain welding schedule that consists of the current, force and weld time. As explained in section 6.2.3, the lobe consists of the lower weld and upper weld curves. The lower weld curve is formed by the set of welding schedules that initiates weld formation. No weld will be formed for any given welding schedule below the lower weld curve.

An experiment was carried to investigate the possibility of using the developed force control to weld below the weld curve that was obtained by ECF condition. Based on figure 6.10 in section 6.2.3, it was noticed that at the ECF condition, weld only starts to develop at 50 cycles when the current is 4000A and applied squeeze force is 2.5kN. In the case of the 4000A and 1.5kN squeeze force, the weld starts to form earlier at 18 cycles. This can be attributed to the use of the lower clamping force, which generated higher heat for faster weld formation as already been discussed in the previous experiments. Hence these two welding schedules would be some of the points that form the lower weld curve. At 40 cycles with 4000A and 2.5kN force, there was no weld developed during welding for the ECF condition because this welding schedule is below the weld curve. The force control will be used to see if a weld can be produced with the welding

schedule of 4000A, 40 cycles and a squeeze force of 2.5kN. The forging force needs to be reduced during welding in order to increase the heat so that a weld can be produced. Hence the decreasing force profile Y will be used for this reason. 5 repetitions were made for each condition.

8.3.1 Discussion on the dynamic resistance changes below the lower weld curve when welded with force control

Figure 8.13 shows the average dynamic resistances for ECF condition with 4000A and 2.5kN squeeze force and the forging force controlled condition with the force profile Y and the same 4000A current. The squeeze forces of 2.5kN for both these conditions were applied using the squeeze force control system that was explained in section 4.3.2. Since with the ECF condition the supplied current is insufficient to produce a weld at the given force, a flat average dynamic resistance line was developed as seen in figure 8.13.

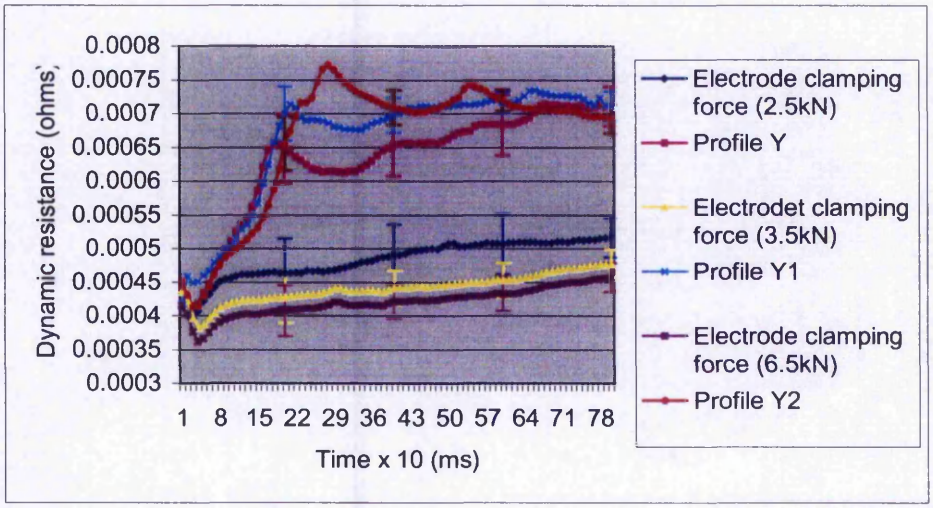

Figure 8.13 – Changes in dynamic resistance curve at force control and electrode clamping force conditions below the lower weld curve

However the decrease in forging force from 2.5kN to 1.5kN using the force control during welding causes the average resistance to increase for the same 4000A. This can cause a weld to

be produced. Referring to the welding lobe in figure 6.10 in section 6.2.3, at the ECF condition, weld starts at the welding schedule of 1.5kN, 4000A and 18cycles(360ms). Hence decreasing the forging force during the controlled condition to 1.5kN for the same current of 4000A and welding for a longer time of 800ms would produce a weld due to the produced higher resistance and longer weld time. The experiment was repeated using 2 new force profiles 3.5kN-1.5kN(Y1) and 6.5kN-1.5kN(Y2) as shown in figure 8.14 below along with profile Y.

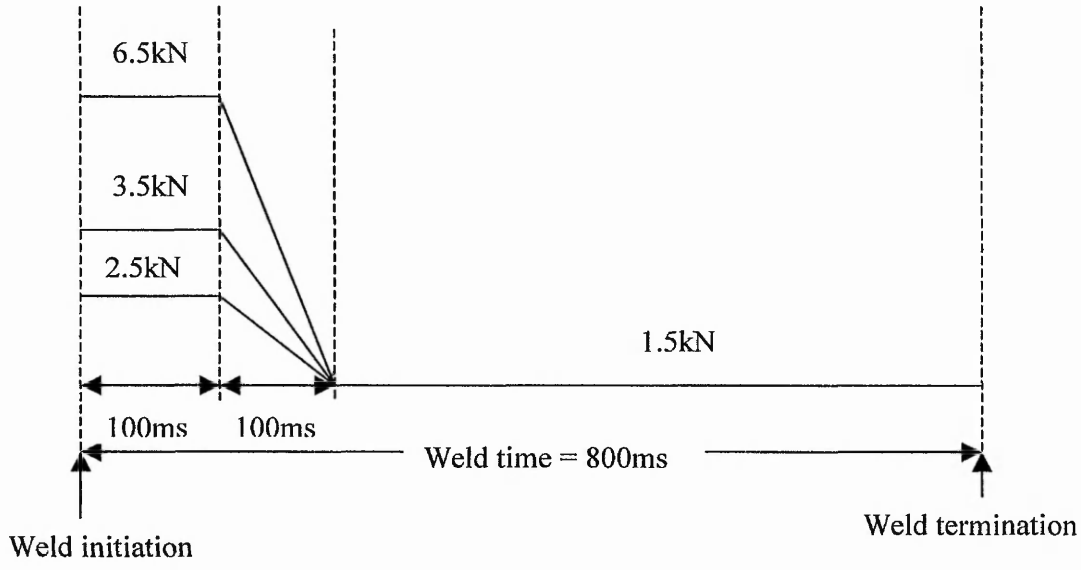

Figure 8.14 – Force profiles Y (2.5kN-1.5kN), Y1 (3.5kN-1.5kN) and Y2 (6.5kN-1.5kN)

Referring to figure 6.10 in section 6.2.3, at the ECF conditions with squeeze forces of 3.5kN and 6.5kN that were applied using the squeeze force control system, weld only starts about 65cycles and 99cycles respectively. Figure 8.13 shows the dynamic resistances for both of these forces at electrode clamping force conditions. Similar to the 2.5kN, these forces also produce flat dynamic resistance lines when welded at 40 cycles and 4000A because no welds were produced for these welding schedules. Comparing all the three dynamic resistances lines at ECF conditions, the dynamic resistance for the 2.5kN squeeze force is highest and the dynamic resistance for the 6.5kN is the lowest. This can be explained based on the concept of contact resistance that has

already been discussed in section 2.8.1. At 2.5kN force, the contact points between the surfaces of the sheets will be less. Hence the resistance for current flow through these contact points will be high that explains the high resistance in the case of the 2.5kN force. As for the 6.5kN squeeze force, the high force will press more of the contact points between the sheet surfaces producing a larger area of contact between surfaces. This will reduce the resistance for current flow as seen in figure 8.14 (Vogler & Sheppard 1993). Similar results for other experiments have already been discussed in section 6.2.1.2 of chapter 6 and section 7.1.1 of chapter 7.

Comparing the dynamic resistance curves for all the three forging force controlled conditions however shows the opposite result to the other condition. The force profile Y2 seems to be having the highest resistance change followed by force profile Y1 and finally the force profile Y having the lowest resistance change. This might be because of the rate at which the controller reduces the motor torque to reduce the forging force. Comparing both the force profiles Y and Y2, the rate at which the force is reduced is for the same time of 100ms. Hence the motor torque is reduced faster in the case of the profile Y2 (0.05kN/ms) compared to the Profile Y (0.01kN/ms) because the motor has to reduce the forging force faster at the same amount of time. This faster reduction of the motor toque increases the rate of resistance change as seen in figure 8.13. This could be the reason for the lower peak resistance of 0.00065Ω for the force profile Y compared to the peak resistance of 0.00077Ω for the force profile Y2. Y1 has an intermediate resistance of 0.0007Ω compared to the peak resistances of Y and Y1 since the forging force was reduced at a rate of 0.02kN/ms.

Squeeze force (kN)	Force profile	Average heat generation (kJ)	Standard deviation	99% confidence interval
2.5	Profile Y	2.99	0.0045	$2.98 < \mu < 3.00$
2.5	ECF condition	2.27	0.0054	$2.26 < \mu < 2.28$
3.5	Profile Y1	3.14	0.0083	$3.12 < \mu < 3.16$
3.5	ECF condition	2.13	0.0084	$2.11 < \mu < 2.15$
6.5	Profile Y2	3.19	0.0084	$3.17 < \mu < 3.21$
6.5	ECF condition	2.07	0.0044	$2.06 < \mu < 2.08$

Table 8.8 – Heat generation for the forging force control *and electrode clamping force conditions with 4000A current*

Table 8.8 shows the average heat generated for the controlled and electrode clamping force conditions using a welding current of 4000A. At the electrode clamping force conditions with squeeze forces of 2.5kN, 3.5kN and 6.5kN, the heat generated is higher for the lower squeeze force of 2.5kN because of the higher resistance of about 0.0005Ω achieved by this force during welding. T test was used to clarify this by calculating the differences between the mean heat values of the 2.5kN and 3.5kN, 3.5kN and 6.5kN and finally 6.5kN and 2.5kN. Table 8.9 gives the results of this test.

Test samples	t test results for 99% confidence interval
2.5kN and 3.5kN	31.348
3.5kN and 6.5kN	14.148
6.5kN and 2.5kN	- 64.202

Table 8.9 – T test results for the difference between mean heat values for 3 squeeze forces

The calculated t values indicate that there are significant differences between the heat values and the 2.5kN squeeze force produces the highest heat of 2.27kJ and the 6.5kN force produces the lowest heat of 2.07kJ. A similar result using 3 different squeeze forces has been presented in section 7.1 of chapter 7. However the use of a lower current of 4000A causes the heat generated to be not sufficient to melt the material during welding. Hence no weld developed for the given squeeze forces and 4000A current.

With the forging force controlled condition, the increase in resistance due to the force control during welding increases the amount of heat generated compared to the electrode clamping force condition. The t tests carried out to find the significance in the differences between the heats generated using force control and without force control for 2.5kN, 3.5kN and 6.5kN is presented in table 8.10 below.

Test samples	t test results for 99% confidence interval
Force control with Profile Y and ECF condition with squeeze force of 2.5kN	229.039
Force control with Profile Y1 and ECF condition with squeeze force of 3.5kN	191.248
Force control with Profile Y2 and ECF condition with squeeze force of 6.5kN	264.103

Table 8.10 – T test results for differences between mean heat values for force controlled and electrode clamping forced conditions

These t values rejects the null hypothesis of no difference in means because these values are greater than $t_{0.005}$ = 3.355 for 99% confidence interval and show that there are significant differences between both the heats generated using the force control and electrode clamping force. A similar result had already been discussed for tables 8.6 and 8.7.

This higher resistance increases the amount of heat generation needed to melt the material and develop a weld. Also it was noticed the force profile which reduced the forging force at a faster rate of 0.05kN/ms (Profile Y2) has an average heat generation of 3.19kJ which is higher than the heat generated by the force profile with a lower force reduction rate of 0.01kN/ms (Profile Y). This can be explained as due to the higher peak resistance of about 0.00077Ω that was observed for force profile Y2 in figure 8.13 with a welding current of 4000A. T test carried out between the mean heat values of the force profiles Y and Y2 gives a t value of –57.300 which is smaller than $t_{0.005}$ = -3.355 for 99% confidence interval hence the significance between the means differences are conformed.

8.3.2 Discussion on the changes in the weld strength below the lower weld curve when welded with force control

The strengths were measured by using the cross-tension test with 5 repetitions for each force profile. Weld strength could not be measured for the electrode clamping force condition because no welds were developed at this condition. The weld strengths given in table 8.11 are the achieved weld strengths during force control.

Force profile (kN)	Average heat generation (kJ)	Average strength (kN)	Standard deviation	95% confidence interval
Profile Y	2.99	2.99	0.1849	$2.61 < \mu < 3.37$
Profile Y1	3.14	3.88	0.2400	$3.39 < \mu < 4.37$
Profile Y2	3.19	3.98	0.1655	$3.64 < \mu < 4.32$

Table 8.11 – Weld strengths for the controlled forging force with 4000A current

Table 8.11 shows that the force profile Y2 achieves the highest weld strength of 3.98kN compared to the force profiles Y and Y1 used in this experiment. This obviously is due to the higher resistance and heat generation achieved during welding by using this profile for the force control as shown in figure 8.13 and table 8.8. T test was carried out to find the difference between the calculated means and is presented in table 8.12.

Test samples	t test results for 99% confidence interval
Profile Y and Profile Y1	-6.508
Profile Y1 and Profile Y2	-0.765
Profile Y2 and Profile Y	8.921

Table 8.12 – T test results for the difference between the mean weld strengths for the 3 force profiles

The only t value that did not satisfy the null hypothesis, which indicates t should either be $\leq t_{0.005}$ =-3.355 or $\geq t_{0.005}$ = 3.355 for 99% confidence interval, is t = -0.765. This shows that the means between the profiles Y1 and Y2 does not have a significant difference between them even though the mean strength for the latter is slightly higher than the former.

To clarify this fact, 5 additional welds were made for each force profile. The new average and standard deviation values for force profile Y1 are 3.97 and 0.295 respectively. The new average and standard deviation values for force profile Y2 are 4.01 and 0.186 respectively. The new t value is –0.256, which again indicates that the means between these force profiles does not show significant differences.

The above discussion shows that by using the force control during welding the lower curve of the weld lobe as shown in figure 6.4 can be modified. As shown in figure 6.10, weld does not start for a 4000A, 2.5kN-welding schedule till about 49-50 cycle. However with the use of a force control, a weld can be produced for the same current at 40cycles. This is also the same for the other two welding schedules with forces of 3.5kN and 6.5kN. The use of the force control during welding actually lowered the welding lobe so that welds can be produced at a shorter weld time of 40cycles for the same amount of current. However this is possible only if the decreasing force profile (profile Y) is used during control. The use of the increasing force profile would not have developed a weld for the same welding current of 4000A because this force further reduces the resistance by increasing the force during welding as seen in the experiments in chapter 7.

Figure 8.15 shows the changes in the lower weld curve for three welding currents of 3000A, 4000A and 5000A. For the electrode clamping force condition weld starts about 90 cycles, 48 cycles and 25 cycles for 3000A, 4000A and 5000A respectively. Figure 8.15 shows the changes in the lower weld curve for three welding currents of 3000A, 4000A and 5000A due to the force control with profiles D, Y and electrode clamping force condition during welding.

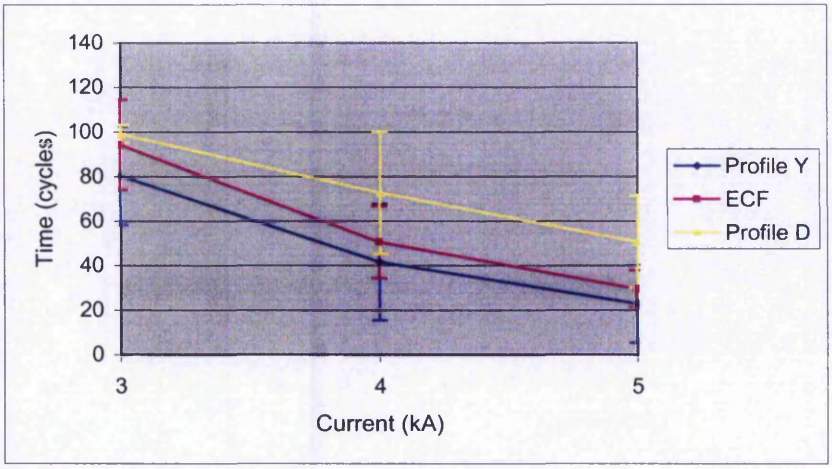

Figure 8.15 – Modification in the lower weld curve due to force control during welding

With the ECF condition weld starts about 90 cycles, 48 cycles and 25 cycles for 3000A, 4000A and 5000A respectively. The weld curve seems to have been modified when the force control is applied. The use of the reducing force profile 2.5kN-1.5kN(Y) has moved the curve downwards to shorter weld time, indicating that weld starts to develop faster than the ECF condition. This can be explained as, the higher resistance produced by this profile as discussed in the experiment above, which increases the rate of melting and weld growth. Hence the new weld cycles with the use of the force profile Y are 80cycles, 40cycles and 22cycles for 3000A, 4000A and 5000A respectively. The use of the increasing force profile of 2.5kN-3.5kN (D) however moves the weld lobe upwards to longer weld time, indicating that the weld starts later compared to the ECF condition. This can be explained as the force profile D tends to reduce the resistance due to the increase in force hence a longer weld time is needed to produce a weld. The weld cycles for the force profile D are 75cycles for the 4000A and 55 cycles for the 5000A. No weld was produced for the 3000A till 99cycles, which is the maximum cycle that can be programmed in the WS2000 weld timer.

8.4 Modifying the expulsion limit using force control

The final experiment was on the use of the force control to avoid expulsion during welding. Expulsion is a phenomenon that has already been explained in section 2.9.1, chapter 2

that occurs due to the tendency of the molten metal to be expelled from the molten region when the force exerted due to weld expansion exceeds the applied electrode force (Tang et al. 2000). Expulsion occurs above the upper weld curve of the welding lobe. In order to avoid expulsion during welding, the force applied by the electrodes need to be increased during welding for currents which would cause expulsion during welding. By increasing the force, the force exerted on the weld is increased and the molten metal could not be expelled from the weld provided the increase in force is greater that the force due to weld expansion as discussed in figure 2.8 in chapter 2. This experiment was carried out on the upper section of the weld lobe with currents, which will produce expulsion at the ECF condition. 5 repetitions were carried out for each condition.

8.4.1 Discussion on the changes in the dynamic resistance curve above the expulsion limit for controlled force and electrode clamping force (ECF) conditions

Figure 8.16 shows the changes in the average dynamic resistance curve that indicate expulsions for two high currents of 9000A and 10000A with force of 1.5kN and welding time of 40 cycles with ECF condition. The error bars indicate variation at 99% confidence interval. A rapid drop in resistance was observed due to the sudden increase in area at the weld region due to the expulsion of the molten metal and the high indentation created by the electrode (Dickinson & Franklin 1980). The figure also shows that the resistance drop occurs earlier for the 10000A current compared to the 9000A current, which can be explained as the rate of energy supplied to cause expulsion increases with increase in current. This would be explained in detail later in this section.

Figure 8.17 shows the changes in average forging force during expulsion at ECF condition for both the welding currents stated above with the error bars showing variations. The force increases during welding before dropping down. This drop in the force can be explained as due to occurrence of expulsion.

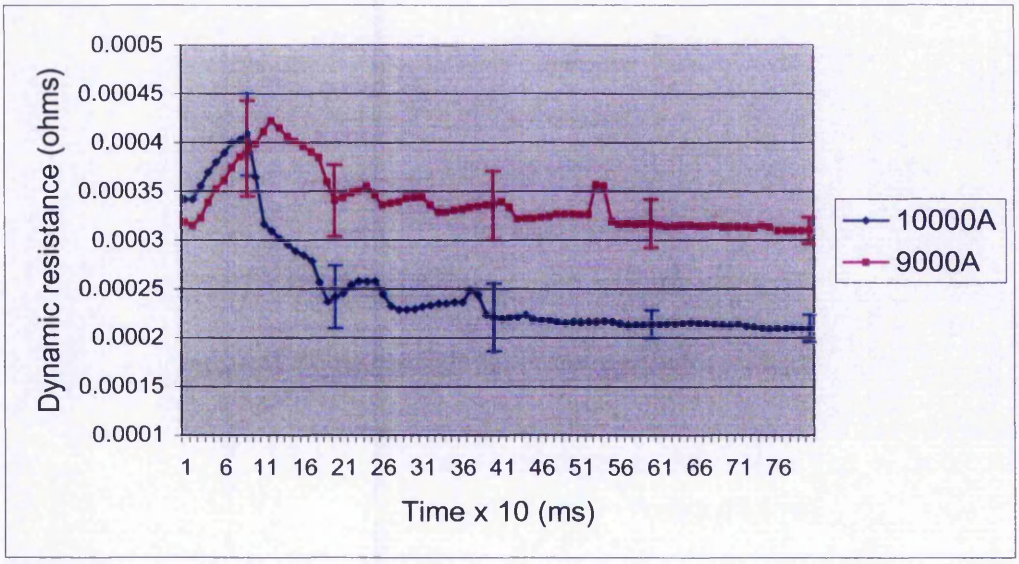

Figure 8.16 – Change in the dynamic resistance curves using ECF (1.5kN) due to expulsion for 2 different currents

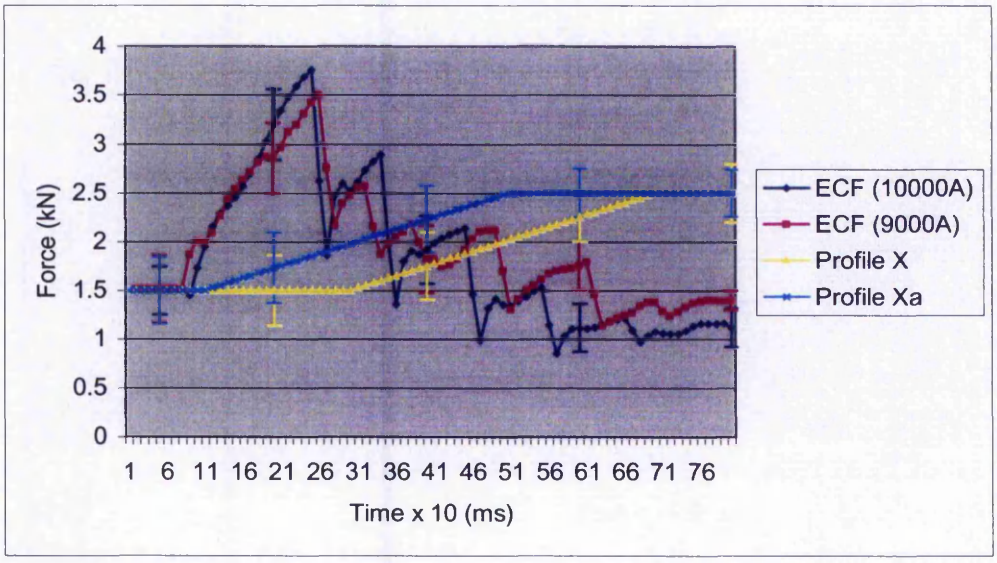

*Figure 8.17 – Forging Force changes during expulsion when **using ECF***

Figure 8.16 also shows the force profile X and one of the test profile (profile Xa), discussed in section 8.4, that will be used to avoid expulsion. The reason for choosing both of these profiles

for this experiment is due to the uncertainty on when the expulsion would occur during welding. Hence profile Xa that starts to increase the forging force after 100ms and profile X that starts to increase the forging force after 300ms were tested to evaluate their ability to constrain the weld growth and avoid expulsion. Figure 8.18 shows the result of this experiment.

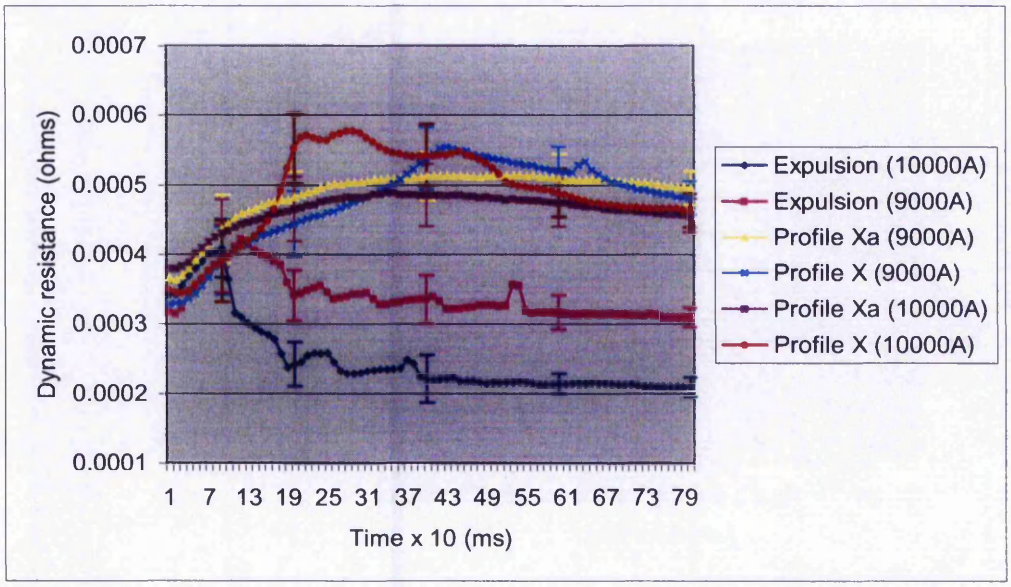

Figure 8.18- Changes in the dynamic resistance curve for force control and electrode clamping force condition at above expulsion limit

Figure 8.18 superimposes the dynamic resistance curves due to expulsion at ECF condition as shown in figure 8.15 with the dynamic resistance curves for the chosen force profiles X and Xa with welding currents of 9000A and 10000A. The figure shows that the dynamic resistances produced by the force profiles are higher than the dynamic resistance during expulsion at ECF condition. The reduction in dynamic resistance during expulsion can be explained as due to the rapid increase in force due to electrode indentation as shown in figure 8.17 and increase in area at the weld region due to expulsion. However the force profiles are maintained at a lower force of 1.5kN for a time before the forging force is increased to 2.5kN to avoid expulsion. Hence the resistance would increase initially and then reduce as forging force starts to increase as seen in figure 8.18. Thus no expulsions were observed with welding was carried out with the forging

force control and using the same 9000A and 10000A current unlike the case of the ECF conditions.

Current (A)	Condition	Average heat generation (kJ)	Standard deviation	99% confidence interval
9000	ECF	11.46	0.0082	$11.44 < \mu < 11.48$
10000	ECF	13.58	0.0044	$13.57 < \mu < 13.60$
9000	Profile Xa	18.99	0.0054	$18.99 < \mu < 19.00$
10000	Profile Xa	22.60	0.0081	$22.58 < \mu < 22.61$
9000	Profile X	22.27	0.0051	$22.26 < \mu < 22.28$
10000	Profile X	25.53	0.0084	$25.51 < \mu < 25.55$

Table 8.13 – Heat generation during forging force controlled and electrode clamping force conditions at expulsion region

Table 8.13 shows the force control during welding produces higher heat compared to the heat generated during ECF conditions. A similar result was also seen in table 8.5. Even though the force control develops high heat compared to the ECF condition, expulsion did not occur as in the case of the electrode clamping force condition due to the increase in force during welding which prevents the molten metal from expelling. Comparing the heat generation for profiles X and Xa , the heat generation for profile X was found to be higher than Xa. Table 8.2 also showed the similar result as table 8.13. This can be explained as due to the longer delay in force ramping of about 300ms, which allows high resistance increase, compared to the 100ms delay in profile Xa before the force increases to 2.5kN.

Current (A)	Test samples	t test results for 99% confidence interval
9000	Profile X and ECF condition	1547.054
	Profile Xa and ECF condition	1187.123
	Profile X and Profile Xa	533.366
10000	Profile X and ECF condition	1689.661
	Profile Xa and ECF condition	1137.509
	Profile X and Profile Xa	472.908

Table 8.14 – T test results for difference in mean heat values for controlled and electrode clamping force conditions above expulsion limit

The t test carried out in table 8.14 shows that all the calculated t values show significant differences between mean heat values because all these values are greater than $t_{0.005} = 3.355$ for 99% confidence interval. Hence it is confirmed that profile X generates the higher heat compared to profile Xa, which is similar to the results in tables 8.1 and 8.2 and force control at the expulsion region generates higher heat without the occurrence of expulsion compared to the ECF condition.

8.4.2 Discussion on the changes in the weld strength above the expulsion limit for controlled forced and electrode clamping force conditions

The weld strengths were measured by using the cross-tension test that was discussed in section 3.3.2.3 with 5 repetitions for each force profile.

Current (A)	Condition	Average heat generation(kJ)	Average Strength (kN)	Standard deviation	99% confidence interval
9000	ECF	11.46	11.43	0.2100	$10.99<\mu<11.86$
10000	ECF	13.58	10.61	0.1159	$10.37<\mu<10.84$
9000	Profile Xa	18.99	12.37	0.1435	$12.07<\mu<12.67$
10000	Profile Xa	22.60	12.84	0.1355	$12.56<\mu<13.12$
9000	Profile X	22.27	13.54	0.1099	$13.31<\mu<13.76$
10000	Profile X	25.53	13.73	0.1596	$13.40<\mu<14.07$

Table 8.15 – Weld strengths for the controlled force and electrode clamping force conditions at expulsion region

Table 8.15 shows the results of the weld strengths achieved due to expulsion during ECF condition and with the forging force control during welding, using profiles X and Xa. First considering the ECF condition where expulsion occurred, the achieved weld strength for 10000A current can be seen to be lower than the 9000A current. Even though the 10000A current produces a higher heat compared to 9000A current, this high heat leads to a massive expulsion with lots of sparks due the molten metal, which expels from the weld region because of overheating. This will cause the weld strength to reduce. Even though expulsion occurred with 9000A current, it might not have been severe compared to as in the case of 10000A current. This is suggested based on the average heat values produced using both these currents in table 8.15. The 9000A current generated an average heat of 11.46kJ while the heat generated using 10000A is 13.58kJ. Hence the weld strength for 9000A was found to be higher than the weld strength for 10000A current. Next discussing the weld strengths for the force profiles, force profile X was found to produce a stronger weld compared to force profile Xa. The similar result had already been discussed in table 8.3 in section 8.1.3. This can be explained due to the higher heat of 22.27kJ and 25.53kJ produced by 9000A and 10000A current respectively for profile X compared to 18.99kJ and 22.60kJ for profile Xa. Even though profile X produces higher strength than profile Xa, sparks were observed during welding with this profile, which shows the developed heats are closer to the expulsion limit. With the use of profile Xa, no sparks were produced for both the currents during welding. The assumed reasons for these as already been discussed above, with the profile Xa, where force increase starts at 100ms, weld growth is under

a continuous increase in forging force that reduces the rate of weld growth and prevents the molten metal from expelling from the weld region. In the case of profile X, force increase only starts at 300ms after weld initiation. Hence the higher heat generated by this profile might have caused a small expulsion before the force increase takes control of the weld growth. Finally comparing the weld strength for controlled force and ECF conditions, similar to the results in table 8.6, table 8.15 also indicates that the use of force profiles during welding at expulsion region produces stronger welds than the ECF condition.

T tests were carried out to evaluate the significant differences between the mean strength values and are presented in table 8.16

Current (A)	Test samples	t test results for 99% confidence interval
9000	Profile X and ECF condition	19.906
	Profile Xa and ECF condition	8.264
	Profile X and Profile Xa	14.474
10000	Profile X and ECF condition	35.370
	Profile Xa and ECF condition	27.966
	Profile X and Profile Xa	9.506

Table 8.16 – T test results for the difference between mean weld strengths for controlled and electrode clamping force conditions at expulsion region

The calculated t values indicate that there are significant differences between the mean strength values for the tested samples because all these values either lesser than $t_{0.005}$ = -3.355 or greater than $t_{0.005}$ = 3.355 for 99% confidence interval.

The correlation analysis for the heat generated and the weld strength gives an r value of 0.88 which shows there is a stronger positive relationship between heat and weld strength because the value is closer to +1.0. The r^2 of 0.774 indicate this relationship between heat and strength affects each other by 77.4%. The t value of 9.803 indicate significance in the relationship between heat and strength because this value is greater than $p_{0.001}$=3.551 with 38 degrees of freedom. Again

calculating r without considering the expulsion conditions as shown in table 8.15 gives a value of 0.95 that shows the correlation between heat and strength would be more precise if abnormal conditions like expulsion is not taken into consideration during analysis. The r^2 value of 0.903 shown that the percentage of variation, which affects both the variables, is higher than the percentage (77.4%) achieved with expulsion taken into consideration. The t value of 12.907 indicate significance in the relationship between heat and strength because this value is greater than $p_{0.001}$=3.922 with 18 degrees of freedom. The values for heat and strength used in the above analysis is shown in appendix C.

The modification of the upper weldability curve using both the force profile X and the test profile Xa as discussed above with welding currents of 9000A, 10000A and 11000A, can be seen in figure 8.19.

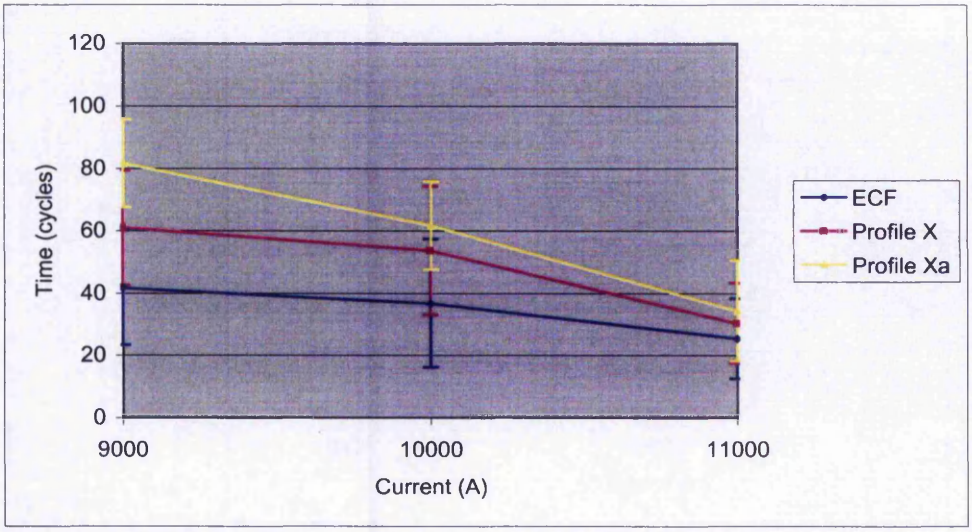

Figure 8.19 – Modification in the upper weld curve due to force control during welding

Experiment was carried out to find the upper weld curve for an ECF condition using a 1.5kN force and welding currents of 9000A, 10000A and 11000A as seen in figure 8.19. The thickness of the sheet used is 2mm. Weld expulsion was found to occur above these welding cycles. The use of the force control during welding was found to have actually moved the weld curve

upwards to a longer weld time. The use of the test profile Xa was found to have moved the upper weld curve to a longer weld time without occurrence of expulsion compared to the force profile X. This might be because the forging force starts to increase earlier about 100ms compared to the force profile X (300ms) causing the weld expansion is under the control of forging force increase for almost the entire weld cycle. The weld curves seems to be converging closer to each other at higher current such as 11000A, might be because the increase in force from 1.5kN to 2.5kN is not sufficient to constrain weld expansion through reduction in heat generation causing the time for expulsion to be closer for both the force controlled and ECF conditions. A larger forging force increase might have to be used in order to increase the time for expulsion to occur at higher welding current. Through the study on avoiding weld expulsion using force control, it was found that the test profile Xa, which starts to increase the force at the 100th ms, was found to be controlling weld expulsion efficiently compared to the force profile X, which starts to increase the force on the 300^{th} ms.

The maximum powers required to cause expulsion for all the 3 conditions in figure 8.19 with the welding currents of 9000A, 10000A and 11000A were calculated based on the maximum resistance before the resistance drops due to expulsion. Table 8.17 shows the obtained results based on 3 repetitions.

Current (A)	Condition	Average power I^2R	Standard deviation	99% confidence interval
9000	ECF	33372	781.13	30230.86 <μ< 36513.14
	Profile X	42400	1352.77	36960.16 <μ< 47839.84
	Profile Xa	49005	855.60	45564.43 <μ< 52445.57
10000	ECF	41148	657.50	38504.03 <μ< 43791.97
	Profile X	48400	1245.2	43392.75 <μ< 53407.25
	Profile Xa	56540	774.5	53425.55 <μ< 59654.45
11000	ECF	43699	945.3	39898.22 <μ< 47500.78
	Profile X	54400	1120.2	49895.40 <μ< 58904.60
	Profile Xa	58740	845.3	55340.84 <μ< 62139.16

Table 8.17 – Maximum power required to cause expulsion during forging force control and electrode clamping force conditions

Table 8.17 shows that for the same welding current, the maximum power required to cause expulsion is higher for profile Xa and lower for the electrode clamping force condition. Hence expulsion would take a longer time to occur with the use of profile Xa compared to the electrode clamping force condition. This was found to be true when referring to figure 8.19. The table also shows for the same condition, the maximum power required to cause expulsion increase with the increase in current.

Current	Test samples	t test at 99% confidence interval
9000	ECF and Profile X	-10.061
	Profile X and Profile Xa	-7.183
	ECF and Profile Xa	-23.489
10000	ECF and Profile X	-8.965
	Profile X and Profile Xa	-9.663
	ECF and Profile Xa	-26.373
11000	ECF and Profile X	-12.708
	Profile X and Profile Xa	-5.354
	ECF and Profile Xa	-20.647

Table 8.18 - T test results for the difference between maximum power to cause expulsion for the forging force control and electrode clamping force conditions

The calculated t values in table 8.18 indicate that there are significant differences between the maximum power for expulsion for the 3 conditions because all these values are lesser than $t_{0.005}$ = -6.965 for 99% confidence interval.

8.5 Summary on the study of the proposed force profiles

8.5.1 Studies on the proposed force profiles

The studies on the proposed force profiles X and Y were found to generate more heat compared to the test profiles Xa, Xb, Ya and Yb. Out of the 2 proposed force profiles suggested, force profile X which increases from 1.5kN to 2.5kN seems to be producing more heat and developing stronger welds compared to the force profile Y which decreases from 2.5kN to 1.5kN. This is because as already discussed in section 8.3; profile X starts with a lower force compared profile Y. Hence the contact resistance for profile X would be higher than profile Y due to the lower force. During welding, profile X maintains the lower force of 1.5kN for 300ms while profile Y takes about 200ms to reach to 1.5kN from a higher value of 2.5kN. So the resistance during this time would be higher in the case of profile X compared to profile Y, causing the heat generated to be higher for the former compared to the latter. Grading the 6 profiles from the profile that produces the strongest weld to the profile that produces the weakest weld, it was found that profile X produces the strongest weld followed by profile Y, profile Xa, profile Yb, profile Ya and finally profile Xb with the weld of the lowest strength as shown in table 8.3. The positive t values on the t test on average weld strengths between X and Y and also between X and Xa, X and Xb, Xa and Xb, Y and Ya, Y and Yb, Xa and Yb, Xa and Ya and finally Ya and Xb and the negative t values on average weld strengths between Ya and Yb as shown in table 8.4 confirmed the grading above.

8.5.2 Comparison between the forging force control and ECF conditions

Study using the forging force control and electrode clamping force conditions during welding showed that the proposed force profiles X and Y under force control produce more heat and developed stronger welds compared to the electrode clamping force condition. Even in this study, profile X was found to develop stronger welds compared to profile Y. Hence it could be concluded that the profile X will be the better force profile that could be used to produce stronger

welds. The use of both the proposed force profiles during welding also was found to widen the weld lobe of the spot welding process. The force profile Y moves the lower weld curve downwards to shorter weld time to produce a weld for a current that will not produce any weld at electrode clamping force condition. The increase in the resistance using this force profile increases the amount of heat so that weld is produced faster during welding. The force profile X moves the upper weld curve upwards and increases the time for expulsion to occur. However in this experiment, one of the chosen test profiles Xa was found to control and avoid weld expulsion efficiently compared to the force profile X that, produces sparks during welding even though profile X gives a higher strength than profile Xa. The characteristics of these profiles that have been discussed in section 8.4 were assumed to be the reasons for these results. From the study on avoiding expulsion, it can be said that expulsion can be stopped automatically during welding if there is an active control of the forging force. The possibility of expulsion can be predicted by monitoring the dynamic resistance curve since the resistance during welding was found to indicate expulsion as in figure 8.16. This will be discussed further in the further work section in chapter 9. Through the results obtained in this chapter it can be concluded that the force control during welding not only affects the weld strength but it also improves the weld strength compared to the conventional electrode clamping force condition that has got no active force control during welding. The use of a force profile similar to profile X that was proven to produce the highest weld strength compared to all the other profiles experimented and current that is below the expulsion limit can be used to produce a weld with reasonable strength faster. Current values nearer to the expulsion limit might increase the risk of expulsion since the welding starts with the lower force and if the forging force is not increased in sufficient time or the increased forging force is not sufficient to constrain weld expansion as in the case for 11000A current in figure 8.19, this would lead to occurrence of expulsion. Force control also widens the weld lobe so that more combinations of welding schedules can be used to produce a weld. Even though all these experiments in this thesis were carried out using mild steel, the force control during welding can also be used to improve the weldability of material like aluminium. Spot welding aluminium was found to be harder due to its high thermal and electrical conductivities (Sari et al. 2002). Hence a higher current and longer weld time needs to be used to produce a weld. With the forging force control during welding, using a lower force and a higher current at the initial stages of welding would increase the resistance hence accelerate the rate of melting to produce a weld at a shorter

time. This would also improve the welding lobe of the aluminium similar the improvement on the welding lobe of the mild steel that was discussed in this chapter. However force control alone was found could not avoid occurrence of expulsion as been noticed in chapter 7 and 8. Hence the conventional current control should also be integrated with the force control to have complete control of the heat input to the weld in order to avoid expulsion completely. This would be described later in the further work section.

Chapter 9

DISCUSSIONS AND CONCLUSIONS

9.1 Discussions

The aim of this project was to investigate and develop a control system for spot welding to achieve improved weld strengths. The use of the conventional pneumatic system to actuate the electrode force made force to be an uncontrollable parameter due to the open loop characteristics of the system. Hence current was used as the control parameter since the heat input needed to produce a weld has a proportional relationship with current (section 2.5). Current control was based on controlling the silicon-controlled-rectifier (SCR) or thyristor firing angle in the primary circuit (Stanway 1992). Force control was almost ignored even when this parameter has equal importance as current when it comes to controlling weld strength due to its uncontrollable characteristics. The electrode force was found to affect the heat input for weld growth indirectly through the resistance (section 2.5). The resistance was found to increase when the force was decreased and vice versa. Hence in this work, force control to vary the resistance and in turn change the heat input to the weld was attempted.

9.1.1 Electrode force as a control parameter

The servo motion control was used to change the electrode actuation system so that electrode is driven by a closed loop system (section 4.2). The servo control system was found to be superior compared to the pneumatic system because other than controlling the electrode in a close loop, it also drives the electrode at a faster speed to have better follow-up with the weld expansion (Arasuna 1999). Servo controlled spot welding machines are available in the market at present, but their usage is only limited. There has been no indication of the ability of these machines to control the forging force during welding. For this project, 4 different controls were

developed in order to control the electrode using the servo control system (section 4.3). They are:- 1) position control, 2) squeeze force control, 3) forging force control and 4) electrode clamping force condition (ECF). The position control system was developed to drive the electrode from a home position to a commanded position closer to the sheet metals that will be welded at a faster speed and then reduce the speed when the electrode is about to come into contact with the sheets to create a 'soft touch' effect. The conventional pneumatic system brings the electrode in contact with the metal sheets with a heavy 'bang' that would cause damage to the electrode tip and the metal surfaces (Tang et al. 2000). This position control also allows the stroke length of the electrode to be varied on-line during the welding process to allow various different components to be welded. The electrode stroke length in a pneumatic system had to be adjusted manually off line in order to weld different components. The evaluation of this system as explained in section 5.1 shows that the system could move the electrode to the desired position with an average overshoot of 0.53mm and with the steady state error of less than 0.0004mm. The second developed control system is the force control during squeeze cycle. The squeeze force in a pneumatic system was found to vary because of leakage in the airline system or friction in the pneumatic system that would cause the required force at the electrode tip not to be attained before the squeeze time finishes. The open loop characteristic of the system initiates the weld cycle after the squeeze cycle ends even if the electrode force did not reach the desired value. This condition would lead to expulsion and bad quality weld. The developed squeeze force control system will ensure that the desired force is achieved before the weld cycle starts. The faster speed of the servo system also was found to achieve the required force faster compared to the pneumatic system leading to a shorter squeeze cycle. The evaluation of this system as in section 5.2 guaranteed that the system could control the electrode force during squeeze cycle with 0% overshoot and average steady state error of 0.02kN. Third control that is the forging force control during weld cycle is described in the next subsection. The fourth system used (ECF) was effectively the second system mentioned earlier, where the squeeze force control was used to achieve the required squeeze force during squeeze cycle. However during the weld cycle, the forging force control was not used and the variation in forging force during welding was entirely process dependent. This is similar to the conventional pneumatic system used in spot welding.

9.1.2 Discussion on the forging force control during welding

Four different force profiles A,B,C and D (section 5.3.1) were used and the force control system during weld cycle was used to control the forging force to follow the given force profile. This force control was first tested without welding to evaluate the ability of the system to control the force according to a given profile. The evaluation showed that the system controlled the electrode force to follow the given force profiles within the ±0.2kN tolerance band. The study on the effect of the forging force control during welding on the heat generation and weld strength was based on the change in the dynamic resistance curve. The dynamic resistance (section 6.3.1) is one of the weld monitoring techniques that is widely used in the industry. An experiment was carried out (section 7.1) to investigate the relationship between resistance and forging force while maintaining constant, the forging force, current and weld time. The results showed that higher forging force leads to lowering of the peak resistance β due to the increase in the area for current flow. This reduction in the peak resistance and the β-peak that occurs much later within the weld cycle reduces the heat generation leading to reduced rate of weld growth. Hence the use of 3 different forging forces, maintained constant during welding, show significant differences between the achieved weld strengths (section 7.1.1.2) with the lowest force achieving highest strength. The results of this experiment indicated the possibility of using the dynamic resistance to compute the heat generation and evaluate the achieved weld strength for different forging forces.

Experiment on the varying forging force control during weld cycles involved two different force profiles; an increasing force profile that increases the forging force during welding and a decreasing force profile that decreases the forging force during welding (section 7.2.1). The decreasing force profile was found to achieve higher weld strength compared to the increasing force profile when a lower current is used. This can be due to the reduction in forging force during welding that increases the resistance (section 7.2.1.1) causing more heat to be generated during welding for the lower welding current. However the same profile causes an expulsion and a drop in the weld strength when a higher current is used because the increase in heat during welding increases the rate of weld growth compared to the case in the lower current, causing molten metal to be expelled from the weld region. Hence in this case the increasing force profile

was found to achieve the highest weld strength. This is because the profile increases the forging force during welding which reduces the heat generation due to drop in resistance. This reduction in heat reduces the rate of weld growth thus avoiding expulsion. The t tests (section 7.2.1.2) show significant differences between the weld strengths achieved by these profiles, adding weight to the argument.

As the objective of the project was to propose a force profile that could achieve improved weld strength; hence detailed studies were carried out on the profiles used in the experiments. As seen in figure 5.10 presented in section 5.3.1, the essential characteristics of these profiles were starting from a certain force and ramping upwards or downwards at a certain ramping rate to another force after a certain delay following weld initiation. Hence the effects of changing the ramping rate and the delay before ramping starts following weld initiation for both the force profiles were experimented as in sections 7.2.2 and 7.2.3. Results show that for the increasing force profile a longer delay before ramping starts would increase the resistance and achieve higher weld strength as shown in section 7.2.2. This longer delay before ramping starts to increase the forging force would increase the resistance causing the heat generation for weld growth to increase. As in the case of the decreasing force profile, a shorter delay before the forging force decreases was found to produce higher resistance and achieves higher weld strength as shown in section 7.2.2. The t tests (section 7.2.2) indicate that the weld strengths produced due to a shorter delay of 100ms and longer delay of 500ms have significant differences between them for both the types of profiles discussed.

While experimenting with different ramping rates using the same delay, for the increasing force profile, a slower ramping rate was found to produce higher heat and achieve stronger weld as shown in section 7.2.3.2. This is because the slower rate of forging force increase would cause the resistance to drop slowly compared to the rapid resistance drop due to a faster ramping rate as seen in figures 7.9 and 7.10 (section 7.2.3). Hence a higher resistance will be produced in the case of the slower ramping rate. An opposite observation was noticed for the decreasing force profile. A faster ramping rate was found to produce higher heat and stronger weld as in section 7.2.3.2. This faster ramping rate to reduce the force during welding would cause a rapid increase in resistance as in figure 7.11 compared to a slower ramping rate. Thus the heat generated will be

higher for the faster ramping rate in the case of the decreasing force profile. The t test carried out on the weld strengths developed for the 3 ramping rates of 0.01kN/ms, 0.005kN/ms and 0.0025kN/ms (section 7.2.3.2), shows that there are significant differences between the weld strengths achieved with faster and slower ramping rates within the confidence interval of 95%. Based on the experiments carried out on the characteristics of the force profiles, the distinct characteristics needed by these two force profiles in order to have the potentials of becoming the optimum force profile were proposed. For the increasing force profile, a longer delay of 500ms and a slower ramping rate of 0.0025kN/ms were chosen because both these characteristics proved to produce stronger weld for this profile. For the decreasing force profile, a shorter delay of 100ms and a faster ramping rate of 0.01kN/ms were chosen to form the profile since they produce stronger weld as discussed above.

Further experiments were carried out on these proposed force profiles named as X and Y to evaluate their potentials to produce stronger welds. For this reason, additional force profiles (Xa, Xb, Ya and Yb) were introduced for each of the proposed force profiles as in section 8.1. The test force profiles were chosen such that they have one desired characteristic similar to the proposed profiles and one undesired characteristic that was found to produce lower strength weld. Experiment carried out with these six profiles and two different welding currents shows that the proposed profiles produces stronger welds compared to the test profiles due to the higher heat generations with these profiles (section 8.1.3). T tests carried out on force profiles X, Xa and Xb for both the welding currents in section 8.1.3, show significant differences between the achieved weld strengths with the proposed force profile X achieving the highest weld strength. Similarly t tests on force profiles Y,Ya and Yb for the same welding currents show significant differences between the weld strength with the force profile Y achieving the highest weld strength. Comparing both the proposed profiles X and Y, profile X was found to have a higher strength weld due to the reason mentioned in section 8.1.2. The 6 profiles were graded from the profile that produces the highest weld strength to the profile that produces the lowest weld strength. The grading shows that profile X achieves the highest weld strength and profile Xb produces the lowest weld strength. The t tests (section 8.1.3) carried out between these profiles for both the welding currents show that the achieved weld strengths have significant differences between them.

9.1.3 Comparison between forging force control and electrode clamping force (ECF) condition

These profiles X and Y were later used to experiment on the force control and the conventional electrode clamping force (ECF) condition during welding. The electrode clamping force condition is such that the variation in the forging force is process dependent. The force profiles will be used for the force control condition. Results indicate that the forging force control condition produces a stronger weld compared to the ECF condition (section 8.2.2). This is because with the force control, a lower electrode force is maintained for a certain amount of time during welding which would cause an increase in resistance and in turn the heat. However in the ECF condition, the melting and softening of material might cause the electrodes to slowly indent into the material increasing the forging force. This increase in force most probably would lower the resistance due to the increase in the contact area causing the heat generation to reduce. The tests carried out (section 8.2.2) conclude that there are significant differences between the weld strengths produces using force control and electrode clamping force condition. Comparison between the profiles X and Y again shows profile X achieving higher weld strengths than profile Y due to reasons mentioned in section 8.1.2. T tests (section 8.2.2) carried out between the average weld strengths of these profiles again showed significant differences between them with profile X achieving higher weld strength. Two conclusions were obtained from this experiment. Firstly the use of force control with a servo controlled spot welding machine would enable improved weld strength compared to the conventional welding with the electrode clamping force. Secondly profile X was identified as the force profile that could achieve the highest weld strength.

9.1.4 Improving welding process using forging force control during welding

Once implementation of both profiles X and Y for the force control during welding was found to produce a stronger weld compared to the electrode clamping force condition, further

experiments were carried out to investigate the possibility of using force control to improve the welding process. Two regions that were considered as the area of study are the upper and lower regions of the weld lobe obtained through ECF condition. According to figure 6.9 (section 6.2.3), below the weld lobe is the no-weld or undersize weld region and above the weld lobe is the expulsion region. The use of the force control to improve the weld strengths in these regions were look at. Based on the knowledge obtained from the experiments carried out on the force profiles, in order to produce a weld below the weld lobe, the resistance needs to be increased to create more heat and initiate weld growth. Hence profile Y, which reduces the force after 200ms of weld initiation was used to create a weld below the weld lobe. Results show that the use of the force control to increase the resistance during welding was able to produce a weld for a current that would not weld under electrode clamping force condition. During ECF condition, the increase in forging force might have reduced the resistance causing the amount of heat generated to be insufficient to initiate melting. With the force control, the forging force is reduced during welding to increase the resistance for the applied current and hence produce sufficient heat to cause the melting of sheet metal. The use of the force control became prominent when the changes in the lower weld curve due to force control was studied as in figure 8.15 (section 8.3.2). The use of the decreasing force profile as profile Y seems to be moving the weld curve downwards to shorter weld time compared to the lower weld curve for ECF condition. This shows the higher heat created by profile Y causes the weld to start developing faster compared to the time needed to produce a weld under the ECF condition. Hence it can be said that the use of the force control allows welds to be formed faster thus reducing the total weld time and that the maximum current needed to produce a reasonable weld is also reduced, which leads to energy saving. Even though aluminium, which is extensively used especially in the automotive industry was not used in this project, the results of the developed forging force control indicates the possibility of improving the weldability of aluminum. As mention in section 8.5, higher current, two to three times that required to weld a comparable steel section, is needed when welding aluminium due to its high thermal and electrical conductivities approximately four times greater than steel (AWS 1984). However, with the forging force control, an initial lower forging force and high welding current should be able to elevate the rate of weld formation and move the lower weld curve to shorter weld time as in the case of the mild steel. This might also reduce the maximum current required to spot weld aluminium.

The final experiment was carried out to study the effect of using the force control in the expulsion region and also to see if it can be used to avoid expulsion and produce better welds. This was another reason for developing the force control. Profile Y was thought not suitable for use in this experiment as this profile increases the heat input during welding. Hence using this profile in the expulsion region would cause massive expulsion that would lead to damage of the electrodes and sheet metal and also endanger the person using the machine. Two force profiles X and Xa as in section 8.1 with different ramping delays were used due to the uncertainty on when expulsion is most likely to occur. Two high currents of 9000A and 10000A that will cause expulsion under ECF condition were used. Results showed that both these profiles managed to avoid occurrence of expulsion when welded with the high currents. Comparing the performance of both these profiles with both the welding currents showed that the use of profile Xa in the force control during welding, welded without creating any sparks. The use of profile X in the force control actually caused some sparks that showed that the heat generated by this profile is closer to the expulsion limit and there is a possibility of expulsion if the current is further increased. This difference in performance could be attributed to the characteristics of the profiles. In profile Xa, force starts ramping about 100ms, which most probably is the time when weld starts to grow. Thus the weld growth will be under a continuous state of increasing force, which would avoid expulsion. However in profile X, high heat is created due to its longer delay and with the use of high current, the rate of weld growth would be even faster. The weld strength analysis in section 8.4.2, showed that the use of profile X achieved the highest strength followed by profile Xa and finally the ECF condition. The t test results in section 8.4.2 show the average weld strength had significant differences between them with the strength for profile X being the highest and weld strength for ECF condition being the lowest. These results have already been discussed earlier (sections 8.1.3 and 8.2.2), which show the profile X achieving higher strength than test profile Xa and the force control during welding achieving higher strength than ECF condition during welding. Again the changes in the upper weld curve were studied to comment on the usage of force control in the expulsion region. As seen in figure 8.19, the use of optimum profile X for force control moved the upper weld curve to longer weld time showing that more time is needed for the same welding currents to cause expulsion compared to the ECF condition. However the force profile Xa seems to have moved the upper curve to the longest weld time compared to the previous two conditions that indicates expulsion takes a longer time to occur

with the use of profile Xa compared to X or the ECF condition. This can be attributed to the mentioned characteristics of the profiles. The other observation in figure 8.19 is that at higher current, the upper weld curves for all the 3 conditions seem to be converging closer to each other and also to a shorter weld time. When current increases, the force due to the weld expansion would also increase, so the increase in force from 1.5kN to 2.5kN might not be sufficient to reduce the heat to suppress the rate of weld growth, causing expulsion to occur earlier. Other alternatives for this problem that were not carried out in this project would be to further increase the electrode force for that certain current to prolong the time for expulsion or reduce the welding current so that the rate of weld growth is reduced. Hence from this study it can be concluded that increasing the forging force could actually avoid expulsion, leading to longer electrode life and also reduce the risk of injury to the operator.

From the discussions above we can conclude that the suggested force profile X can only be used within the weld lobe region to produce stronger welds. Using a current below the expulsion limit with profile X would produce a stronger weld at faster rate because the higher resistance produced due to the combination of a lower forging force and higher welding current. Outside of the weld lobe region, suitable force profiles need to be used depending on the required task; whether to produce a weld at a no weld region or avoid expulsion at the expulsion region. However generally, the use of the forging force control seems to have widened the weld lobe. The advantage of this would be that welds could be developed with shorter weld times and with lower currents, resulting in energy savings. Also the extended expulsion limit allows high currents to be used for improved weld strength, in this weld lobe region.

9.1.5 Correlation Studies

In the studies on the heat and weld strength correlation, all the r values calculated in the experiments for this project show a positive relationship between these two variables, and also show that weld strength will increase when heat increases and vice versa. The correlation coefficient values calculated for the different experiments are given below:-

a) Experiment on changes in the welding current with time and force constant r =0.931

b) Experiment on changes in weld time with current and time force constant and taking expulsion into account r = 0.809
c) Experiment changes in weld time with current and time force constant and without taking expulsion into account r = 0.982
d) Experiment on changes in the squeeze force with constant current and time r = 0.894
e) Experiment on changes in electrode tip diameter for constant current, force and time r = 0.881
f) Experiment on the different force profiles with taking expulsion into account r = 0.781
g) Experiment on the different force profiles without taking expulsion into account r = 0.894
h) Experiment on 3 different ramping delays r = 0.561
i) Experiment on 3 different ramping rate r = 0.727
j) Experiment on the proposed force profiles with their test profiles r = 0.919
k) Experiment on force control and no force control conditions r = 0.889
l) Experiment on force control and no force control conditions at expulsion region with taking expulsion in account r = 0.859
m) Experiment on force control and no force control conditions at expulsion region without taking expulsion in account r = 0.951
n) Combination of all the data with taking expulsion into account r= 0.456
o) Combination of all the data without taking expulsion into account r= 0.48

All the calculated r values except for the last two show a stronger positive relation between the heat generated and the weld strength. Since most of these values are closer to 1 such as 0.8 and 0.9, the relationship between heat and strength can be considered almost linear. The r values vary when expulsion data is included to calculate the relationship; inclusion of expulsion data results in smaller r, compared with the value for r when expulsion data is excluded. The abnormality that occurs through the drop in weld strength during expulsion even though the heat value is increasing causes the correlation coefficient to be lower with the inclusion of the strength data collected during expulsion. The last two r values show a weaker positive relationship between heat and strength. This can be attributed to the reason just given.

9.2 Conclusion of the thesis

1) It is possible to convert electrode force into a control parameter if it is actuated by means of a servo control system instead of the conventional pneumatic system
2) Forging force can be varied during welding by means of different force profiles
3) Heat generation during welding and weld strength varies for different force profiles at constant current and weld time
4) The changes in the force profile characteristics such as ramping delay and ramping rate changes the heat generation during welding and the weld strength.
5) For the increasing force profile, a longer delay before ramping starts and a slower ramping rate would produce higher heat and stronger weld assuming expulsion did not occur during welding
6) For the decreasing force profile, a shorter delay before ramping starts and a faster ramping rate would produce higher heat and stronger weld assuming expulsion did not occur during welding
7) Forging force control during welding produces higher heat and stronger weld strength compared to the ECF condition assuming expulsion did not occur during welding
8) The increasing force profile with a longer delay before ramping starts and a slower ramping rate is the optimum force profile that will produce stronger welds.
9) Forging force control during welding can be used to produce a weld at the ECF's no weld region
10) Forging force control during welding can be used to avoid expulsion at ECF's expulsion region.
11) The optimum force profile can only be used within the weld lobe to produce stronger welds. Using a current below the expulsion limit would produce a stronger weld faster
12) The correlation between heat and weld strength shows both these variable have a almost linear relationship but when abnormal condition such as expulsion is considered, the correlation coefficient becomes lesser.

9.3 Recommendation for further work

9.3.1 F urther investigations on different force profiles

The use of the force profiles to vary the amount of heat supplied during welding by controlling the forging force was found to affect the achieved weld strengths as noticed in chapters 7 and 8. The profiles used in this project are simple profiles that start from one force and was ramped up or down to another force during the welding process. Hence the heating was found to increase for the ramping down profile and decrease for the ramping up profile during the spot welding process. However more complicated profiles such as the pulse-width-modulation or saw-tooth type profiles and their implications to the heating and weld strength were not studied in this project. The fluctuations in the forging force due to the use of these profiles most likely probably would increase and reduce the heating during welding. This action might cause a repetitive heating and cooling action to take place during welding unlike the profiles used in this project that c onsists of only o ne action t hat is h eating t hrough r educing t he forging force o r cooling through increasing the forging force during welding. Hence exploring some of the complicated profiles as suggested might even lead to better knowledge on the effects of controlled heating to weld strengths.

9.3.2 Automatic control of the forging force to avoid expulsion

Through t he experiments c arried o ut in s ection 8. 4, it w as f ound t hat the expulsion could be avoided by controlling the amount of heat supplied to the weld by means forging force control. A control system could be developed to automatically increase the forging force to reduce the heating when expulsion is about to occur. There are no indications of such a system being available in the commercial market at the moment. In order to do this, weld growth should be monitored. The possibility of weld expulsion needs to be identified before it occurs to enable the forging force to be increased. As mentioned in section 8.5, dynamic resistance can be used for expulsion de tection because of the significant c hanges in r esistance o bserved in t he d ynamic

resistance curve due to expulsion. The maximum power that could cause expulsion as discussed in section 8.4.2 can be obtained from the dynamic resistance curve to predict the possibility of weld expulsion during the spot welding process. Relationships need to be developed between the maximum power supplied for welding and the increase in forging force so that the forging force can be automatically increased when the power exceeds the optimum power i.e. the power above, which would cause expulsion. Modelling techniques such as the existing force balance model or statistical model (Zhang 1999) to predict expulsion can be used to develop this relationship. Weld growth monitoring using artificial neural network (ANN) and fuzzy logic had already been used in order to control the current supplied to the weld as mentioned in section 1.2.2 in chapter 1. However there are no publications to-date on any work carried out to control the forging force to reduce the heating and to avoid expulsion during welding with the use of ANN or fuzzy logic. Hence this would be an area that warrants investigation.

9.3.3 Integration of the current control and the force control for better weld control

Integration of the current control to the developed force control could not be carried out in this project due to the unavailability of equipment and high cost. Simultaneous control of both these parameters was thought, would not only allow faster development of weld but also reduce the risk of expulsion. The existing WS2000 weld controller can be integrated with the newly developed forging force control system with a main controller to simultaneously control both these individual systems. The proposed control strategy would be as follows; an initial lower forging force and a higher current to increase the resistance and develop high heat and later followed by an increase in forging force and reduction in current to forge the developed weld under higher force to reduce the heating and also avoid expulsion of molten metal. This simultaneous control would also reduce the total welding time due to the ability of the weld to grow faster. DC inverter is the other suggestion for current control due to its ability to pump more heat to the weld because of its high frequency of 400-2000Hz (Stanway 1992). It is becoming popular and being widely used in the industry nowadays. Its state of the art electronic switching technology allows for better control of the amount of heat supplied to the weld compared to the conventional AC welding (Miyachi 1998). Hence the ability of the

inverter to supply higher heat at a shorter weld time and the usage of the developed forging force control should be able to produce stronger welds at faster weld times. Also with the use of the inverter, the improved feature of the dynamic resistance curve due to its higher frequency compared to the conventional 50Hz frequency enable weld growth monitoring to be more accurate.

References

1) Anon., 1997. Deva Electronic Control Operation Guide, Release 2.3.

2) Anon., 2000a. Harmonic drive, [Online], Available from: http://www.harmonicdrive.de. [Accessed:21-9-2002].

3) Anon., 2002. Ballscrews – Technical Information. Hiwin Technologies, Cat.2002, 2.

4) Anon., 1999. MINT^{tm} for NEXTMove, Programming Guide, Issue 3.2.

5) Anon., 1993. Positioning control system and drives. Parker Hannifin Corp, Cat.1993-1994, A2.

6) Anon., 2000b. Stronghold Spot welding Machine Manual. Issue 1.

7) Arasuna, H., 1999. Spot welding control method and apparatus. US5906755. 1999-05-25.

8) Archer, G.R., 1960. Calculations for temperature responses in spot welds. *Welding Journal*, 39(8), 327-330.

9) Arefin, A.A.S. & Khan,A.J., 1999. 3-dimensional thermal model of resistance spot welding in aluminium. *Proceedings of the ASME heat Transfer Division*, 3, 371-380.

10) Arumugam, A., 2000. Effect of resistance spot welding parameters on electrode deformation. Advances in Manufacturing Technology, *16th National Conference on Manufacturing Research*, London 5-7 September 2000, 285-289.

11) Asokkumar, A., Samuel V.R & Manoharan, S., 1997. Evaluation of the dynamic resistance as quality criterion for resistance spot welding. *Indian Welding Journal*, 24-31.

12) ASME , 1971. Metal handbook – Welding & Brazing. *American Society for Metals*. 8th Edition, 6, 417-.

13) AWS, 1980. Welding handbook. *American Welding Society*. 3rd Edition.

14) AWS, 1984. Welding handbook – Metals and their weldability. *American Welding Society*. 6th Edition, 362.

15) Babu, S.S., Santella, M.L & Feng, Z., 1998. An empirical model of the effects of pressure and temperature on the electrical contact resistance of metals. *Science and Technology of Welding and Joining*, 6, 126-132.

16) Bhattacharya, S. & Andrews, D.R., 1974. Significance of dynamic resistance curves in the theory and practice of spot welding. *Welding and Metal Fabrication*, 296-301.

17) Bhattacharya, S., 1972. Resistance – weld quality monitoring. *Sheet Metal Industries*, 3, 460-466.

18) Brown, J.D., Rodd, M.G. & Williams, N.T., 1998. Application of artificial intelligence techniques to resistance spot welding. *Ironmaking & Steelmaking* , 25(3), 199-204.

19) Broomhead, J.H.W. & Dong, P.H., 1990. Resistance spot welding quality assurance. *Welding and Metal Fabrication*, 58(6), 309-314.

20) Browne, D.J., Chandler, H.W & Wen, J., 1995. Computer simulation of RSW in aluminium : Part 1. *Welding Journal*, 74(10), 339-344.

21) British Standards Institute, BS 1140:1993. British Standard Specification for Resistance spot welding and coated low carbon steel.

22) Cary, H.B., 1989. Modern welding technology. Prentice Hall Publ. 2nd Edition, pp 241.

23) Chang, H.S., Cho, Y.J. & Choi, S.G., 1989. A proportional-integral controller for resistance spot welding using nugget expansion. *Transaction of the ASME*, 111, 332-336.

24) Chang, H.S. & Cho, Y.J., 1990. An iterative learning control system for resistance spot welding process. *Automation of manufacturing processes, ASME, Dynamic System and Control Division*, 22, 129-135.

25) Chen, X., Araki, K. & Mizuno,T., 1998. Modeling and fuzzy control of the resistance spot welding process. *Proceedings of the IEEE International Conference on Intelligent Processing Systems*, 1, 190-194.

26) Chien, C.S. & Kannatey-Asibu, E.Jr., 2001. Investigation of monitoring systems for resistance spot welding. *Welding Journal*, 195-199.

27) Cho, H.S. & Chun, D.W., 1985. A microprocessor based electrode movement controller for spot welding quality assurance. *IEEE Transactions on Industrial Electronics*, 32(3), 234-238.

28) Cho, H.S. & Cho, Y.J., 1989. A study of the thermal behavior of the resistance spot welding. *Welding Journal*, 68(6), 236-244.

29) Chunsheng, W., Fengwu, H., et al., 2002. Electrical-thermal interaction simulation for resistance spot welding nugget process of mild steel and stainless steel. *China Welding*, 11(1), 51-54.

30) Cullison, A., 1993. Resistance weld controller delivers the heat where it's needed. *Welding Journal*, 72(6), 47-49.

31) Coolidge, F.L., 2000. Statistics – A general introduction. Sage Publ. 1st Edition, pp118.

32) David, S.A. & Vitek, J.M., 1989. Correlation between solidification parameters and weld microstructures. *International Materials Review*, 34(5), 213-245.

33) Dickinson, D.W. & Franklin, J.E., 1980. Characterisation of the spot welding behaviour by dynamic electrical parameter monitoring. *Welding Journal*, 89(6), 170-176.

34) Dickinson, D.W., 1981.Welding in automotive industry. *Research Report SG Committee of Sheet Steel Producers*, 19.

35) Dilthey, U. & Dickersbach, J., 1999. Application of neural networks for quality evaluation of resistance spot welds. *ISIJ International*, 39(10), 1061-1066.

36) Dong, P., Victor, M.L. & Kimchi, M., 1998. Finite element analysis of electrode wear mechanism: face extrusion. *Science and Technology of Welding and Joining*, 3(2) , 59-64.

37) Dong, P., 1997. Analysis of resistance spot welding. *30th ISATA*, 209-211.

38) Dorf, R.C. & Bishop, R.H., 1995. Modern Control Systems', Addison-Wesley Publ., 7th Edition, pp 222.

39) Easterling, K.E., 1992. Introduction to physical metallurgy of welding. Oxford: Butterworth-Heinemann. 2nd Edition,

40) Freund, J.E., 1992a. Modern elementary statistics. Prentice-Hall. 8th Edition.

41) Freund, J.E., 1992b. Mathematical Statistics. Prentice-Hall Int. 5th Edition, 522-523.

42) Funk, E.J. & Rice, W., 1967. An analytical investigation of the temperature distributions during resistance spot welding. *Welding Journal*, 64(4), 175-186.

43) Greenwood, J.A., 1961. Temperature in spot welding. *British Welding Journal*, 6, 316-322.

44) Greenwood, J.A., 1966. Constriction resistance and the real area of contact. *British Journal of Applied Physics*, 17, 1621-1632.

45) Greitmann, M.J., 1998. Numerical simulation of the resistance spot welding process using spotwelder. *Mathematical Modeling of Weld Phenomena 4*, 4, 531-544.

46) Gould, J.E., 1987. An examination of nugget development during spot welding, using both experimental and analytical techniques. *Welding Journal*, 66(1), 1-10.

47) Gupta, O.P. & Amitava, D.E., 1998. An improved numerical modeling for resistance spot welding process and its experimental verification. *Journal of Manufacturing Science and Engineering*, 120, 246-251.

48) Guendouze, C., 1995. *Computer assisted generation of parameters for resistance spot welding*. Thesis(PhD). Nottingham University.

49) Han, Z. & Orozco, J., 1989. Resistance spot welding : A heat transfer study. *Welding Journal*, 68(9), 363-371.

50) Haefner, K., Carey, B., Bernstein, B., & Overton, K., 1991. Real time adaptive spot welding control. *ASME Journal of Dynamic Systems, Measurement and Control*, 113, 104-112.

51) Hasselman, T. & Yap, K., 2002. Predictive accuracy of resistance spot welding simulations. *Proceedings of SPIE- International Society for Optical Engineering*, 4753, 904-909.

52) Hawkins, I.L., 2000. Superior quality production s pot welding using adaptive control. *Sheet Metal welding Conference*, 85(12).

53) Hirch, R.B., 1993. Tip force control equals spot welding quality. *Welding Journal*, 72(3), 57-60.

54) Hirsch, R.B.,1998. The effect of tip force on weld quality and electrode life. [Online], Available from: http://www.unitrol-electronics.com/pdf/awspape2color.pdf, pp 1-8. [Accessed: 17-5-2001].

55) Holliday, R., Parker, J.D. & Williams, N.T., 1996. Relative contribution of electrode tip growth mechanism in spot welding zinc coated steels. *Welding in the World*, 37(4), 186-193.

56) Holliday, R., Parker, J.D. & Williams, N.T., 1995. Electrode deformation when spot welding coated steels. *Welding in the World*, 35(3), 160-164.

57) Irving, B., 1996. The search goes on for the perfect resistance welding control. *Welding Journal*, 75(1), 63-68.

58) Javed, M.A. & Sanders, S.A.C., 1991. Neural network based learning and adaptive control for manufacturing systems. *IEEE/RSJ International Workshop on Intelligent Robots and Systems*, 242-246.

59) Jou, M., Li, C.J & Messler, R.W ., 1998. Controlling resistance spot welding using neural network and fuzzy logic. *Science and Technology of Welding and Joining*, 3(1), 42-50.

60) Jou, M., 2003. Real time monitoring of weld quality of resistance spot welding for the fabrication of sheet metal assemblies. *Journal of Material Processing Technology*, 132(1-3), 102-113.

61) Kalpakjian, S., 1995. Manufacturing Engineering and Technology. Addison-Wesley. 3rd Edition, 1182.

62) Kirchheim, A. & Shaffner, G., 2002. Electrode force as an important process variable in the case of resistance spot welding. *Welding and Cutting*, 54(3), 130-131.

63) Kuo, B.C., 1995. Automatic control system. Prentice-Hall. 7th Edition, 708.

64) Li, W., Hu, S.J & Ni.S., 2000. On-line quality estimation in resistance spot welding. *Journal of Manufacturing Science and Engineering*, 122, 511-512.

65) Matsuyama, K., Obert.R & Chun, J.H., 2002. A real time monitoring and control system for resistance spot welding. *Technical paper- Society of Manufacturing Engineers AD02-270*, 1-18.

66) Messler, R.W., 1993, ' Principles of welding: processes, physics, chemistry and metallurgy', New York : Chichester: John Wiley.

67) Milner, D.R.& Apps, R.L ., 1968. Introduction to welding and brazing. Pergamon Press.

68) Miyachi., 1998. Inverters reduce manufacturing costs [Online], Available from : http://www.miyachi1.com/res_tech/pdf/connection-1.pdf, [Accessed : 05-03-2003].

69) Murakawa, H., Kimura, F. & Ueda, Y., 1997. Weldability analysis of spot welding on aluminium using FEM. *Mathematical Modeling of Weld Phenomena 3*, 3, 944-966.

70) Messler, R.W., Jou, Min JR. & Li, C.J., 1995. An intelligent control system for resistance spot welding using neural network and fuzzy logic. *IEEE*, 1757-1763.

71) Messler, R.W. & Jou, M., 1996. Review of control systems for resistance spot welding: past and current practices and emerging trends. *Science and Technology of Welding and Joining*, 1(1), 1-9.

72) Nied, H.A., 1984. The finite element modeling of the resistance spot welding process. *Welding Journal*, 64(4), 175-178.

73) Oldland, P.T., Ramsay C.W, Matlock, D.K & Olson, D.L., 1989. Significant features of high-strength weld metal microstructures. *Welding Journal*, 68(4), 158-168.

74) Rexorth, B., Jan 2003. Life after the chisel. *Design Engineering*, 18.

75) Salvick, S.A., 1999. Using servoguns for automated resistance welding. *Welding Journal*, 78(7) , 29-33.

76) Santella, M.L., Babu, S.S., Riemer, B.W & Feng, Z., 1998. Influence of microstructure on the properties of resistance spot welds. *Trends in Welding Research*, 4(4), 605-609.

77) Sari, H ., Sonmez, H. & Gultekin, N., 2002. The investigation of the relation between resistance components and nugget dimensions in the resistance spot welding of aluminium alloy. *Technical paper-Society of Manufacturing Engineering AD02-247.*

78) Stanwy, J.D., 1992. Technology advances in resistance welding control. *Welding and Metal Fabrication*, 60(4), 159-164.

79) Smallman, R.E., 1992. Modern physical metallurgy. Butterworth Heinemann. 4th Edition, 99.

80) Sohn,I. & Bae,Dongho., 2000. Fatigue life prediction of the spot welded joint by strain energy density factor using artificial neural network. *Key Engineering Materials*, 183(2), 957-962.

81) Sun, X., 2001. PID control gain tuning of a drive position servo system. University of California, 1-6.

82) Tang, H., Hou, H. & Wu, S.J., 2000. Force characterization of resistance spot welding of steel. *Welding Journal*, 79, 175-183.

83) Thornton, P.H , Krause, A.R & Davies, R.G., 1996. Contact resistances in spot welding. *Welding Journal*, 75, 402-412.

84) Tsai, C.L., Dai, W.L & Dickinson, D.W., 1992. Analysis and development of a real time control methodology in resistance spot welding. *Welding Journal*, 70(12), 339-351.

85) Tsai, C.L., Jammal, O.A., Papritan, J.C. & Dickinson, D.W., 1999. Modeling the resistance spot weld nugget growth. *Welding Journal*, 47-54.

86) Vogler, M. & Sheppard, S., 1993. Electrical contact resistance under high loads and elevated temperatures. *Welding Journal*, 72, 231-238.

87) Waller, D.N., 1964. Head movement as a means of resistance spot welding quality control. *British Welding Research Association*, 11(3), 118-122.

88) Watney, D. & Nagel, G.L., 1984. Forms of dynamic resistance curves generated during resistance spot welding. *Sheet Metal Welding Conference*, 85, 12-16.

89) Wei, L., Hu, S.J. & Ni, J., 2000. On-line quality estimation in resistance spot welding. *Journal of Manufacturing Science and Engineering*, 122, 511-512.

90) Wei, P.S. & Ho, C.Y., 1990. Axisymmetric nugget growth during resistance spot welding. *ASME Journal of Heat Transfer*, 112, 309-316.

91) Williams, N.T., Holliday, R.J & Parker, J.D., 1998. C urrent steeping programmes for maximizing electrode campaign life when spot welding coated steels. *Science and Technology of Welding and Joining*, 3(6), 286-294.

92) Wung, P., 2001a. A force based failure criterion for spot weld design. *Experimental Mechanics*, 41(1), 107-112.

93) Wung, P., 2001b. Failure of spot welds under in-plane static loading. *Experimental Mechanics*, 41(1), 100-106.

94) Xihua, Z., Chenyu, W. & Ruobing, Z., 1998. Parameter selecting and quality predicting of spot welding based on artificial neural networks. *China Welding*, 7(2), 81-85.

95) Xu, L., Khan, J.A., Chao, Y.J. & Broach, K., 1999. Numerical study of thermal modeling of resistance spot welding utilizing coupled thermal-electrical-mechanical analysis. *Proceedings of the ASME, Heat Transfer Division*, 3, 395-402.

96) Yagi, T., 2002. Recent trends in the robotization of the Japanese automotive industry. *Industrial Robot*, 29(6), 495-499.

97) Zen Timer, [Online], Available from : http://archive.devx.com. [Accessed: 16-10-2002]

98) Zhang, H., 1999. Expulsion and its influence on weld quality. *Welding Journal*, 78(11), 373-380.

99) Zhang, H., Hu, S.J & Senkara, J., 2000. A statistical analysis of expulsion limits in resistance spot welding. *Journal of Manufacturing Science and Engineering*, 122, 501-510.

100) Zhou, M., Hu, S.J & Zhang, H., 1999. Critical specimen sizes for tensile-shear testing of steel sheets. *Welding Journal*,[Online], Available from: http://www.aws.org/wj/supplement/supplement2.html, 305-313. [Accessed : 19-11-2002]

101) Zhongdian, Z., Yan,L & Lin, W., 1997. Artificial neural network applied to spot welding process modelling. *China Welding*, 6(1), 41-48.

List of publications

1) Aravinthan, A., Sivayoganathan, K., Al-Dabass, D. & Balendran, V., 2001. A Neural Network System For Spot Weld Strength Prediction. UKSIM2001, *Conf. Proc. of the UK Simulation Society*, Emmanuel College, Cambridge, 28-30 March 2001, 156-160, ISBN 1-84233-026-8.

2) Aravinthan, A., Sivayoganathan, K., Al-Dabass, D. & Balendran, V., 2000. Modelling and Simulation of a Spot Welding Process - An Overview. OR42, *42nd Annual National Conference of the UK Operational Research Society*, Cardiff University, 12-14 September 2000.

3) Aravinthan, A., Sivayoganathan, K., Al-Dabass, D. & Balendran, V., 2000. Effect of Resistance Spot Welding on Electrode Deformation. NCMR 2000, *16th National Conf. on Manufacturing Research*, University of East London, 5-7 September 2000.

4) Aravinthan, A., Sivayoganathan, K., Al-Dabass, D. & Balendran, V., 2003. Forging Force Control Models Using Servomechanism. UKSIM2003, *Conf. Proc. of the UK Simulation Society*, Emmanuel College, Cambridge, April 2003, 140-146, ISBN 1-84233-088-8.

APPENDIX A

A function generator was used to supply a 50Hz sine wave with $4V_p$ amplitude and the software timer interrupt used in chapter 4 was used to sample the sine wave at 4 different interrupt times. This test was carried out to evaluate the reliability of the timer interrupt. Figures below show the results of this test.

A.1 Interrupt every 1ms

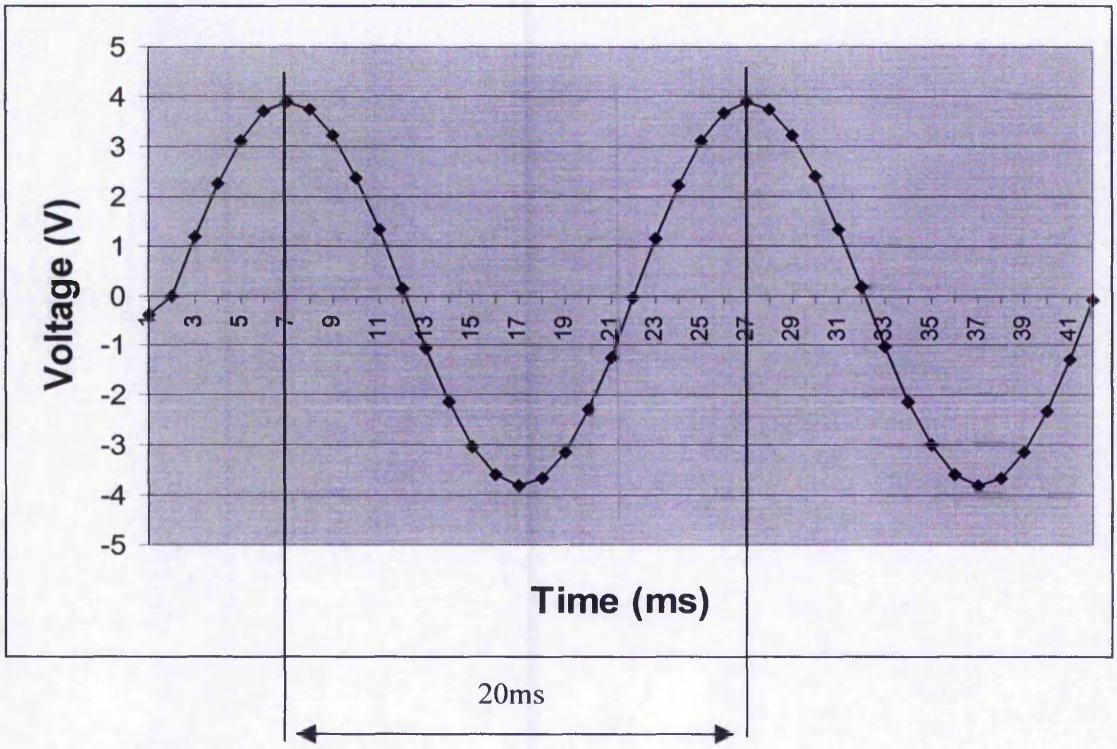

Figure A.1 – 50Hz sine wave sampled every 1ms

Figure A.1 shows a 50Hz and 4V amplitude sine-wave sampled at 1ms. The time from peak to peak is 20ms, which represents a 50Hz sine-wave.

A.2 Interrupt every 2ms

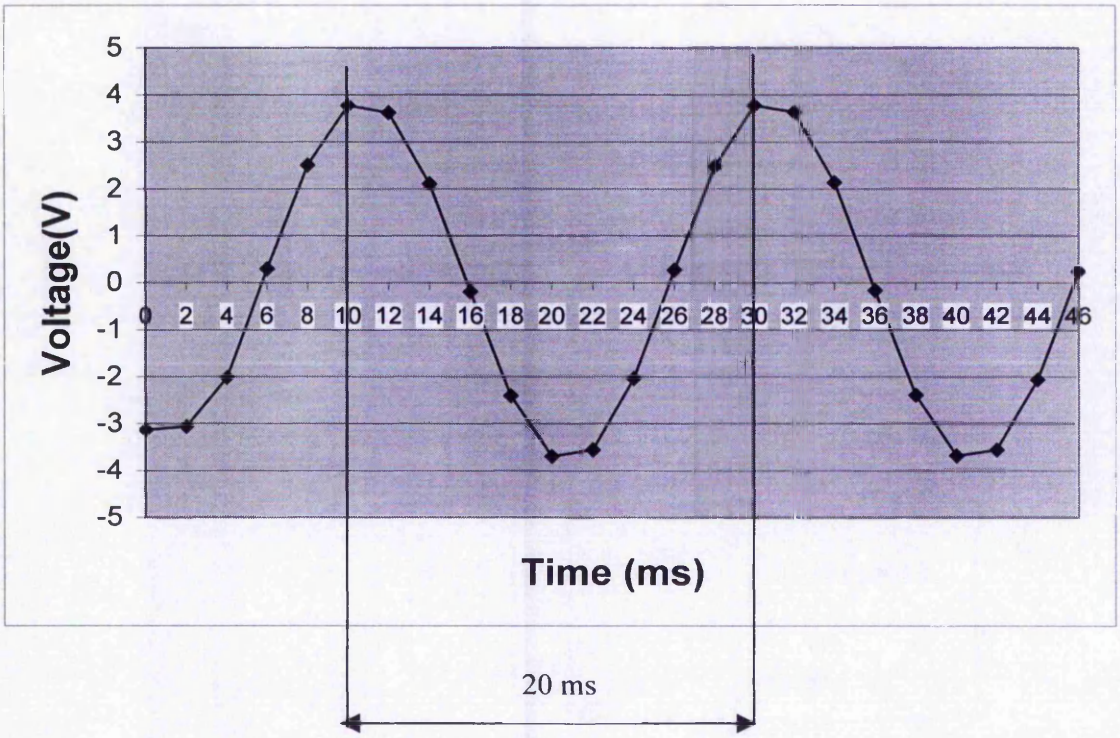

Figure A.2 – 50Hz sine wave sampled every 2ms

Figure A.2 shows a 50Hz and 4V amplitude sine wave sampled at 2ms. The time from peak to peak is 20ms with 10 points sampled every 1 cycle, which represents a 50Hz sine wave.

A.3 Interrupt every 5ms

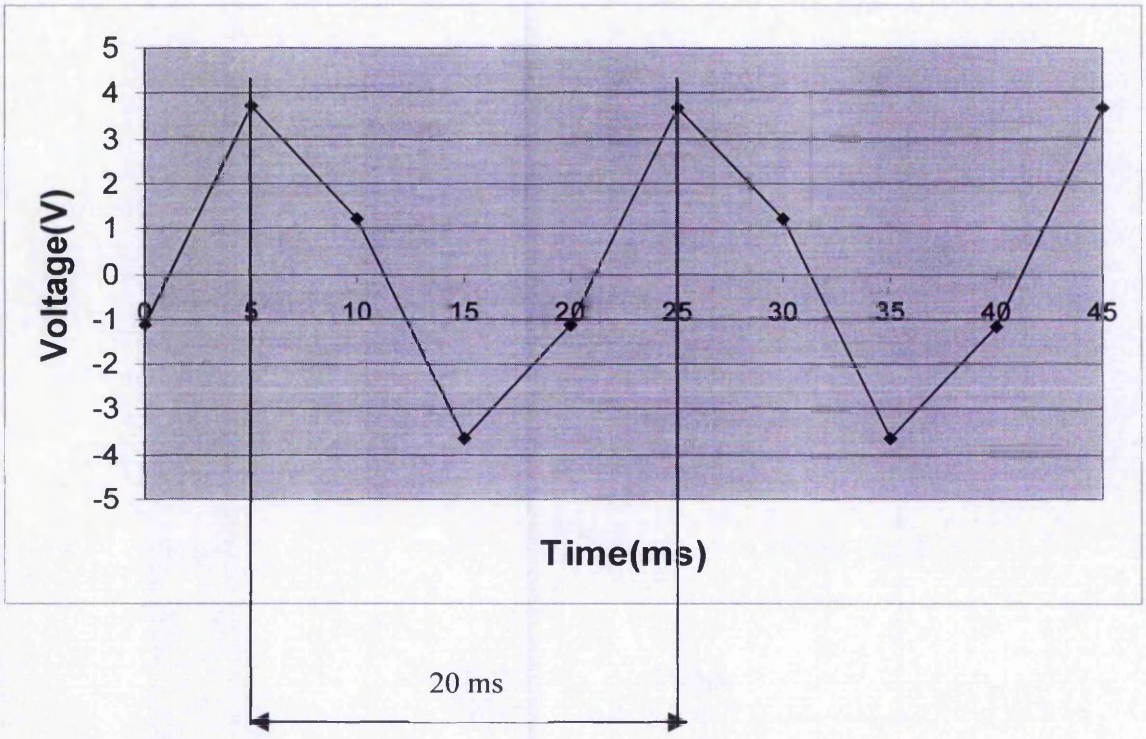

Figure A.3 – 50Hz sine wave sampled every 5ms

Figure A.3 shows a 50Hz and 4V amplitude sine wave sampled at 5ms. The time from peak to peak is 20ms with 4 points sampled every 1 cycle, which represents a 50Hz sine wave.

A.4 Interrupt every 10ms

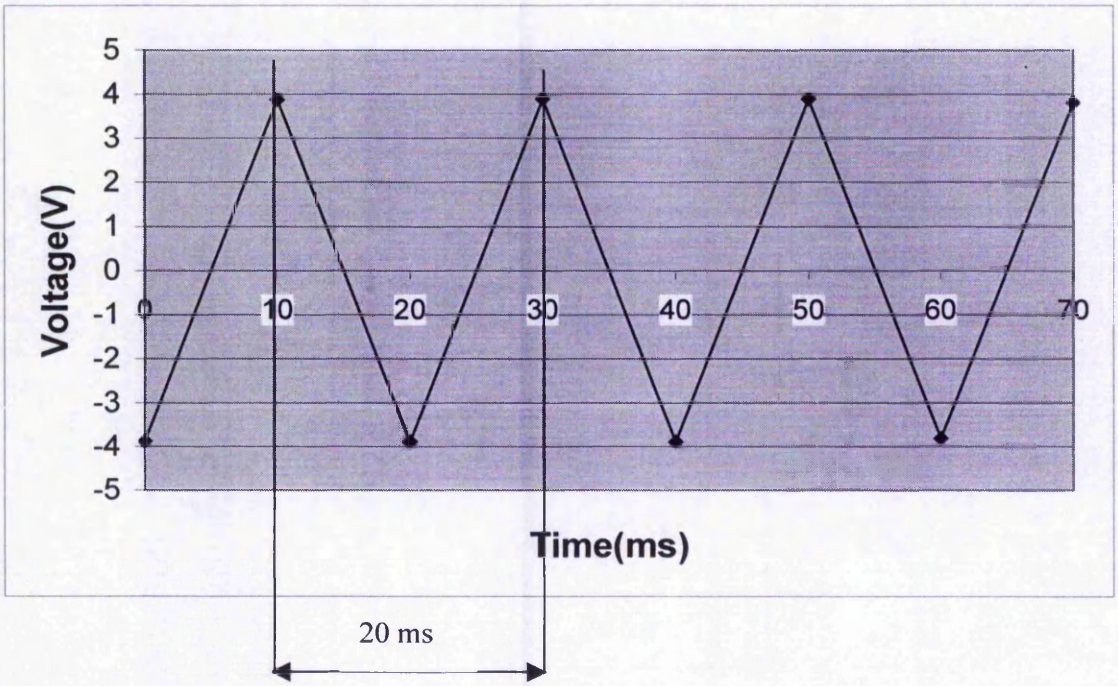

Figure A.4 – 50Hz sine wave sampled every 10ms

Figure A.4 shows a 50Hz and 4V amplitude sine wave sampled at 10ms. The time from peak to peak is 20ms with 1 point sampled every 1 cycle, which represents a 50Hz sine wave. Therefore through this study it was clarified that the timing of the interrupt is reliable and could be applied in the developed control systems

APPENDIX B

Appendix B deals with the repeatability studies carried out on the 3 control systems evaluated in chapter 5 i.e. position control, force control during squeeze force and force control during weld cycle.

B.1 Repeatability study on the position control

Taking 3 repetitions for 5 desired electrode positions tested the repeatability of the position control.

B.1.1 Desired position 600000 counts / 30mm from home position

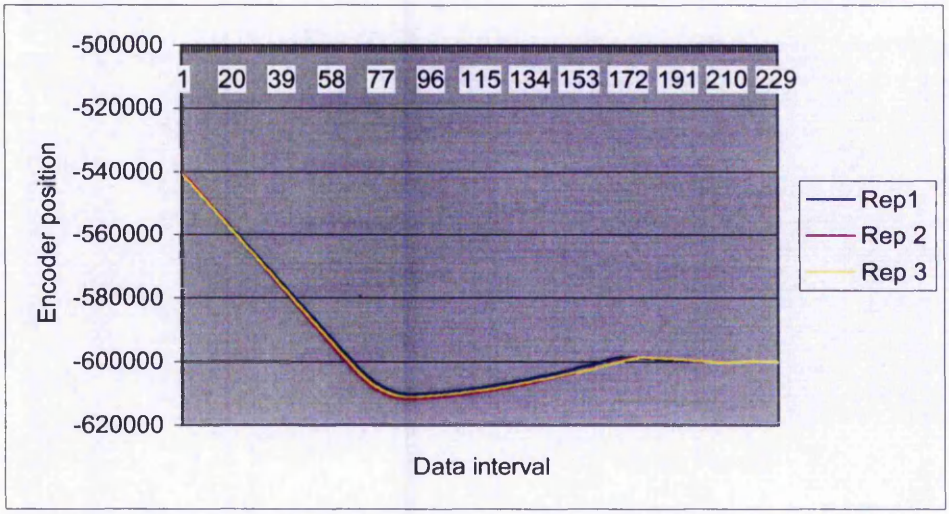

Figure B.1 – Position control for 600000 encoder counts

The average overshoot based on the 3 repetitions is 611156 encoder counts or 30.6mm. The percentage overshoot based on the equation 1 in section 5.3 is 1.8% and the average steady state error is 1 encoder count or 0.00005mm.

B.1.2 Desired position 450000 counts / 22.5mm from home position

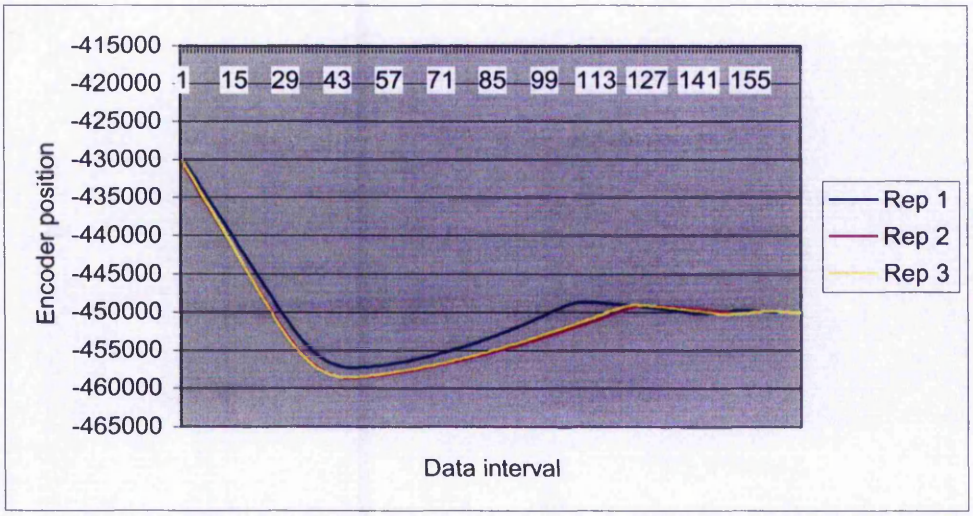

Figure B.2 – Position control for 450000 encoder counts

The average overshoot based on 3 repetitions is 458165 encoder counts or 22.9mm. The percentage overshoot based on the equation 1 in section 5.3 is 1.8% and the average steady state error is 1 encoder count or 0.00005mm.

B.1.3 Desired position 555000 counts / 27.5mm from home position

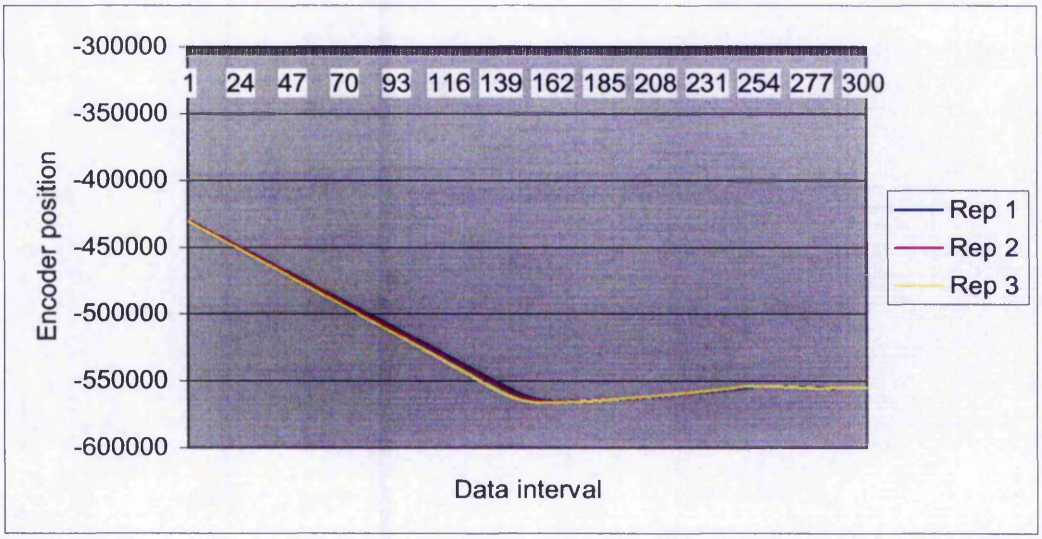

Figure B.3 – Position control for 555000 encoder counts

The average overshoot based on 3 repetitions is 565595 encoder counts or 28.2mm. The percentage overshoot based on the equation 1 in section 5.3 is 2.8% and the average steady state error is 5 encoder count or 0.00025mm

B.1.4 Desired position 632000 counts / 31.6mm from home position

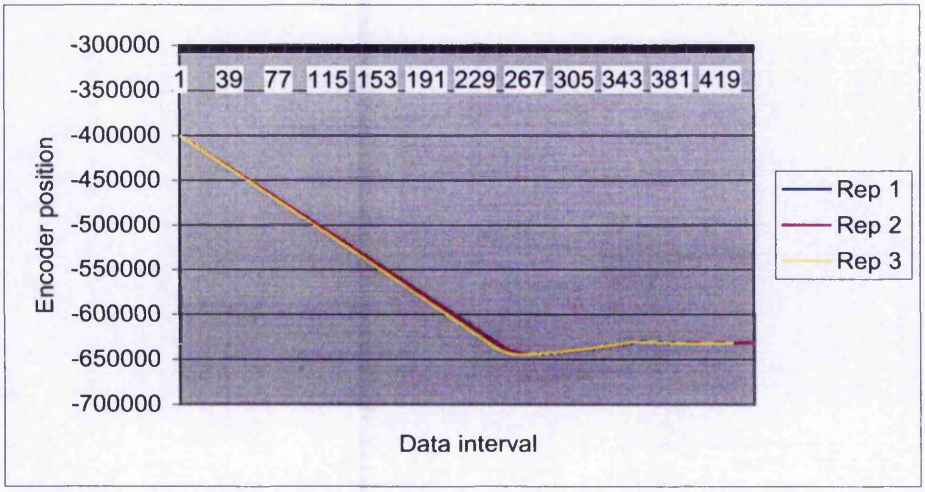

Figure B.4 – Position control for 632000 encoder counts

The average overshoot based on 3 repetitions is 644117 encoder counts or 32.2 mm. The percentage overshoot based on the equation 1 in section 5.3 is 1.9% and the average steady state error is 1 encoder count or 0.00005mm.

B.1.5 Encoder position 463000 counts / 23.15 mm from home position

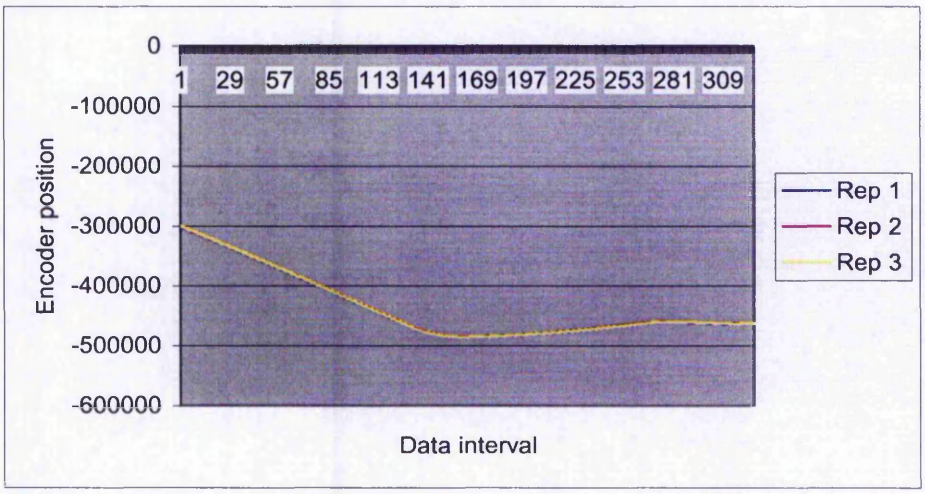

Figure B.5 – Position control for 463000 encoder counts

The average overshoot based on 3 repetitions is 471000 encoder counts or 23.5 mm. The percentage overshoot based on the equation 1 in section 5.3 is 1.7% and the average steady state error is 1 encoder count or 0.00005mm.

From figures B.1-B.5, it was noticed that the developed position control is able to drive the motor so that the electrode moves from the home position to the desired positions with minimal steady state error. All the errors from the figures above are less than 0.00010mm. Since the accuracy of the system is not very critical because it's only going to be used to drive the electrode closer to the metal sheets and will not affect the weld strength during welding the achieved overshoots were assumed acceptable.

B.2 Repeatability study on the force control during squeeze cycle

Table B.1 shows the repeatability study that was carried out on the force control during squeeze for 8 squeeze forces. 5 repetitions were made for each desired force and the results are presented in table below: -

Desired force (kN)	Number of repetition (kN)					Average force (kN)	Std. deviation
	Rep 1	Rep 2	Rep 3	Rep 4	Rep 5		
2.50	2.47	2.49	2.50	2.45	2.46	2.47	0.021
1.80	1.78	1.79	1.75	1.76	1.78	1.77	0.016
3.70	3.66	3.70	3.65	3.67	3.71	3.68	0.026
3.00	2.97	2.96	2.98	2.99	2.99	2.98	0.013
6.30	6.25	6.27	6.30	6.26	6.31	6.28	0.024
4.70	4.66	4.70	4.66	4.68	4.70	4.68	0.020
5.5	5.46	5.45	5.51	5.46	5.50	5.48	0.027
5.0	4.95	4.95	4.96	5.0	5.01	4.97	0.029

Table B.1- Repeatability study on the force control for 8 squeeze forces

Desired force (kN)	Average force (kN)	Standard deviation	99% confidence interval
2.50	2.47	0.021	$2.43 < \mu < 2.51$
1.80	1.77	0.016	$1.74 < \mu < 1.80$
3.70	3.68	0.026	$3.63 < \mu < 3.73$
3.00	2.98	0.013	$2.95 < \mu < 3.00$
6.30	6.28	0.024	$6.23 < \mu < 6.33$
4.70	4.68	0.02	$4.64 < \mu < 4.72$
5.50	5.48	0.027	$5.42 < \mu < 5.54$
5.00	4.97	0.029	$4.91 < \mu < 5.03$

Table B.2 – T test with 99% confidence interval

Table B.2 shows the t test carried out with 99% confidence interval. The study shows the force control is able to apply the required force during squeeze cycles with a confidence interval of 99%.

B.3 Repeatability study on the force control on 5 force profiles

Repeatability studies were carried out on the ability of the force control to follow a given force profile within a tolerance band of ± 0.2kN. 4 repetitions were carried out for each profile.

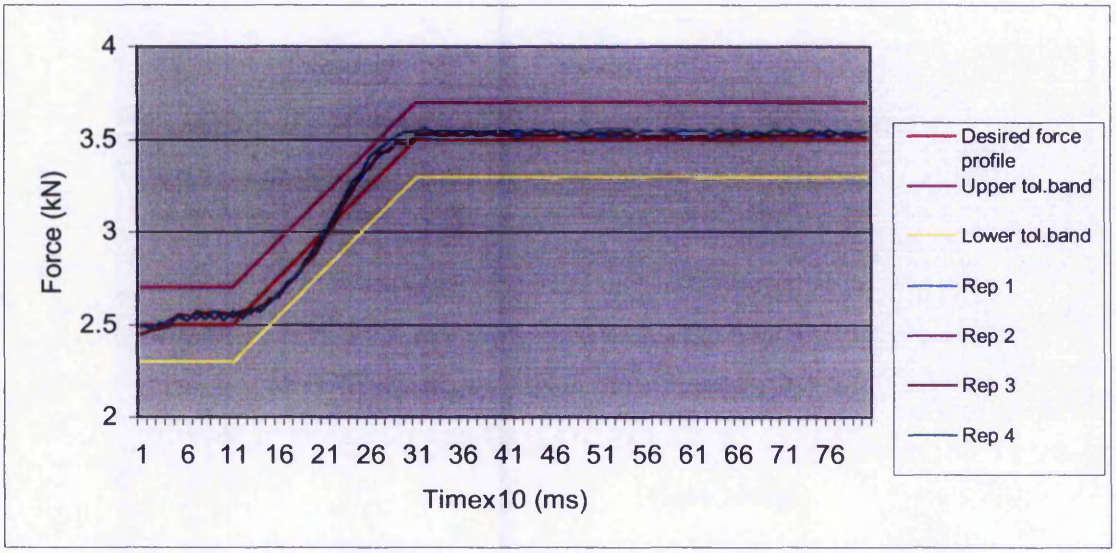

Figure B.6 – Force control for 2.5kN-3.5kN force profile

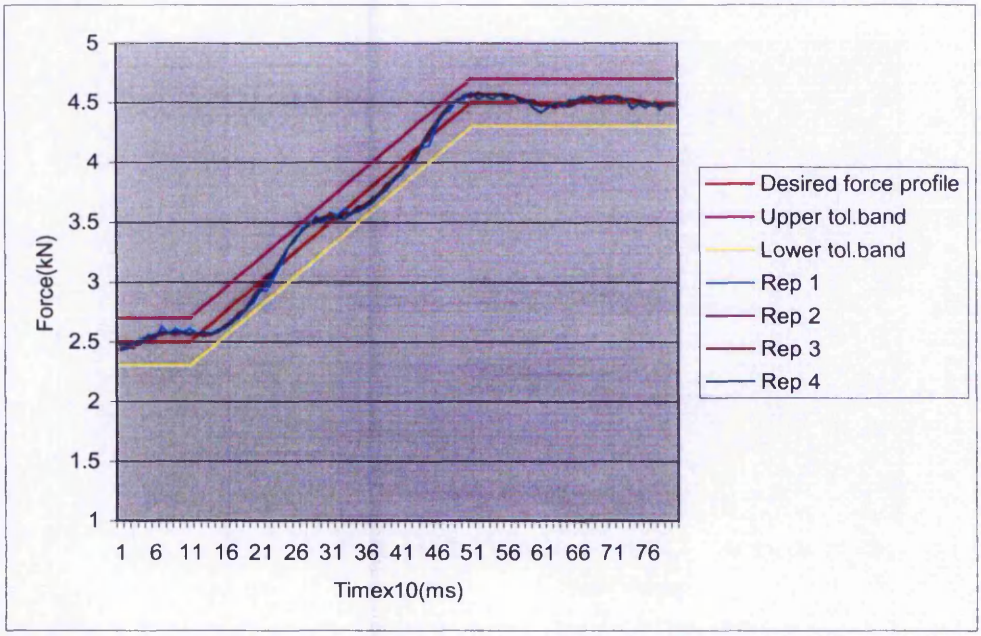

Figure B.7 – Force control for 2.5kN - 4.5kN force profile

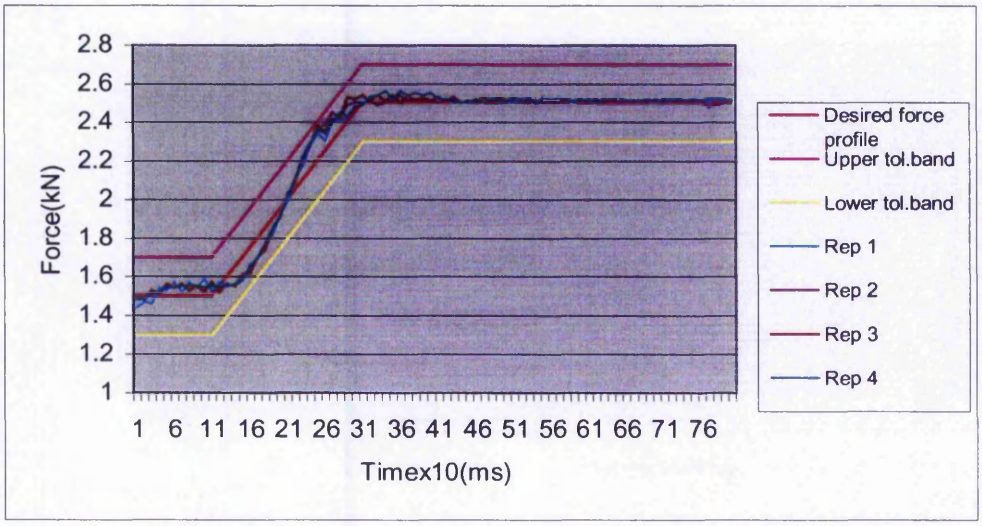

Figure B.8 – Force control for 1.5kN - 2.5kN force profile

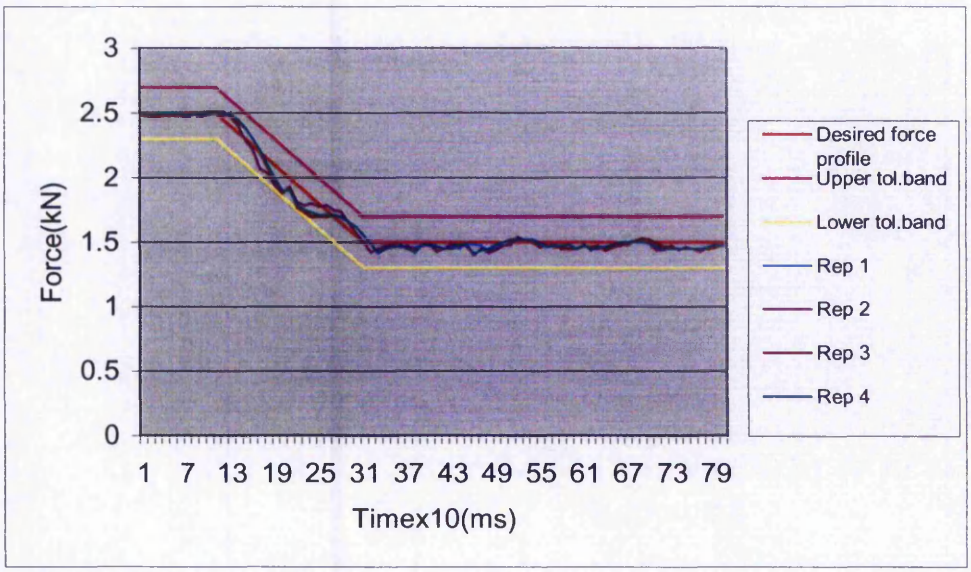

Figure B.9 – Force control for 2.5kN - 1.5kN force profile

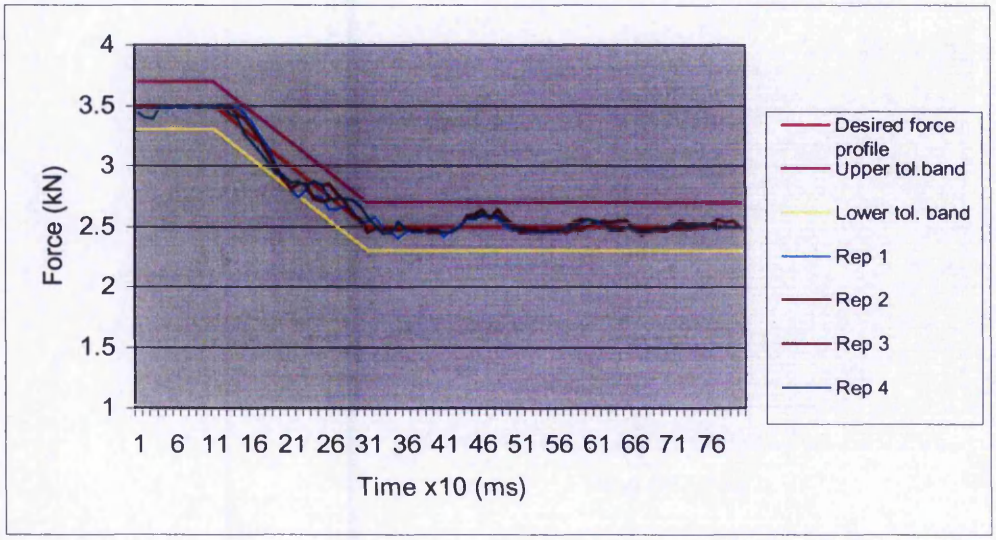

Figure B.10 – Force control for 3.5kN - 2.5kN force profile

Figures B.6 – B.10 show the results of the repeatability study on the force control to follows 5 different profiles. The study shows that the 4 repetitions of the force control for each profile are able to follow the respective force profile within the set tolerance band.

APPENDIX C

This appendix presents all the raw data for the heat generation and measured weld strengths used to calculate the correlation coefficient r in chapters 6,7, and 8.

Heat generation and weld strengths raw data for experiments in chapter 7

Section 7.1

heat	strength
1.79	6.12
1.59	5.12
1.49	2.11
3.46	8.14
3.46	8
1.81	6.2
1.81	5.74
1.74	4.91
1.51	2.89
3.51	8.49
3.45	7.54
1.81	7.12
1.81	5.68
1.74	4.8
1.50	2.5
3.50	8.83
3.47	8.1
3.32	6.58
1.80	5.91
1.73	5.1
1.50	2.34
3.50	8.32
3.45	7.69
3.30	6.97
1.82	6.05
1.72	4.85
1.50	2
3.50	8.58
3.46	7.85
3.32	6.85

Section 7.2.1 with expulsion data

heat	strength
4.73	10.98
4.70	9.88
4.30	8.58
4.96	9.01
8.04	10.68
7.70	12.68
8.04	11.87
7.66	12.98
4.74	10.85
4.69	10.21
4.28	8.03
4.95	8.58
8.05	11.2
7.18	12.4
8.06	11.48
7.37	12.5
4.74	10.58
4.70	10.3
4.28	8.78
4.96	8.98
8.04	10.5
7.74	12.1
8.06	11.58
7.37	12.85
4.73	11.1
4.71	9.7
4.30	8.98
4.95	9.1
8.06	10.98
7.74	12.9
8.05	12.1
7.40	12.7
4.72	10.68
4.72	9.85
4.30	8.5
4.94	8.88
8.03	11.1

7.72	12.85
8.05	12.01
7.40	12.61

Section 7.2.1 without expulsion data

heat	strength
4.73	10.98
4.70	9.88
4.30	8.58
4.99	9.01
7.70	11.68
8.04	11.87
7.36	12.98
4.74	10.85
4.69	10.21
4.30	8.03
4.96	8.58
7.74	12.4
8.06	11.48
7.41	12.5
4.74	10.58
4.70	10.3
4.28	8.78
4.96	8.98
7.74	12.1
8.06	11.58
7.37	12.85
4.75	11.1
4.71	9.7
4.30	8.98
4.94	9.1
7.73	12.9
8.09	12.1
7.40	12.7
7.39	10.68
4.72	9.85
4.30	8.5
4.94	8.88
7.72	12.85
8.05	12.01
7.40	12.61

Section 7.2.2

heat	strength
0.97	3.89
1.03	4.8
1.05	5.2
1.12	6.4
1.13	7.1
1.16	7.5
1.11	9.58
1.06	8.97
1.05	8.2
0.96	4.17
1.05	4.75
1.05	5.45
1.11	6.8
1.14	7.15
1.15	7.67
1.12	9.2
1.08	8.5
1.04	8.42
0.95	4.2
1.04	5.01
1.06	5.67
1.12	6.98
1.12	7.3
1.15	6.85
1.11	9.45
1.07	8.47
1.03	8.15
0.97	3.78
1.03	5.1
1.06	5.3
1.11	6.53
1.14	6.95
1.17	7.45
1.10	9.67
1.07	8.75
1.05	8.35
0.98	3.97
1.05	4.98
1.07	5.7
1.12	6.73
1.13	7.19

1.13	7.93
1.17	9.85
1.12	9.05
1.07	8.01

Section 7.23

heat	strength
4.73	8.45
4.95	8.4
4.98	8.5
5.56	10
5.61	10.3
5.83	10.35
5.00	10.25
4.66	9.47
4.60	9.25
4.74	8.2
4.97	8.38
4.99	8.42
5.55	9.88
5.62	10.58
5.82	10.65
4.99	10
4.69	9.38
4.60	9.37
4.73	8.11
4.97	8.51
4.97	8.55
5.55	10.2
5.60	10.47
5.84	10.49
4.99	9.88
4.68	9.58
4.59	9.43
4.72	8.35
4.96	8.24
4.97	8.64
5.56	10.02
5.60	10.37
5.85	10.59
4.98	10.35
4.67	9.67
4.62	9.12
4.62	8.16
4.74	8.45
4.98	8.58
4.99	10.37
5.57	10.6
5.62	10.63
5.83	10.1
5.00	9.83
4.69	9.52

Heat generation and weld strengths raw data for experiments in chapter 8

Section 8.1

heat	strength
5.48	9.8
4.96	7.01
4.75	5.57
5.43	9.21
5.02	6
5.22	6.93
7.92	12.1
7.70	11.21
7.19	10.58
7.77	11.45
7.55	10.25
7.50	10.56
5.50	9.5
4.97	6.82
4.76	5.22
5.44	9.45
5.03	6.23
5.21	6.63
7.90	11.38
7.70	10.58
7.21	10.47
7.75	11.32
7.55	10.48
7.50	10.46
5.49	9.68
4.98	6.72

4.76	5.45
5.43	9.12
5.02	6.41
5.21	6.45
7.91	12.1
7.70	11.32
7.20	10.68
7.77	11.02
7.56	10.05
7.49	10.23
5.50	9.56
4.96	6.95
4.75	5.65
5.44	8.97
5.01	6.2
5.22	6.13
7.91	11.89
7.71	11.24
7.21	10.38
7.76	11.23
7.57	10.48
7.51	10.1
5.49	10.01
4.96	6.51
4.75	5.8
5.43	9.32
5.02	6.32
5.22	6.51
7.92	11.97
7.72	10.89
7.19	10.6
7.76	11.47
7.56	10.65
7.50	10.23

7.65	10.11
6.90	7.83
5.49	9.14
5.08	5.68
7.74	11.52
7.12	9.2
5.47	5.6
4.58	2.8
7.65	11.1
6.90	7.7
5.50	9.45
5.07	5.5
7.75	11.72
7.12	9.49
5.48	6.01
4.58	2.5
7.64	10.58
6.91	7.46
5.50	9.60
5.06	5.42
7.74	11.34
7.13	9.58
5.47	5.84
4.57	2.10
7.66	10.69
6.91	7.35
5.49	9.28
5.06	5.12
7.73	11.15
7.14	9.89
5.48	5.21
4.59	2.47
7.66	10.4
6.90	7.26

Section 8.2

heat	strength
5.50	9.3
5.06	5.1
7.73	11.2
7.12	9.46
5.48	5.23
4.57	2.25

Section 8.4 with expulsion data

heat	strength
11.46	11.23
11.46	11.29
11.46	11.35
11.47	11.74
11.46	11.55
13.58	10.45

13.58	10.65
13.59	10.52
13.58	10.69
13.57	10.72
19.00	12.32
18.99	12.26
19.01	12.48
19.00	12.56
18.99	12.23
22.60	12.78
22.61	12.95
22.60	12.85
22.59	13
22.59	12.66
22.27	13.5
22.28	13.62
22.26	13.42
22.25	13.46
22.26	13.68
25.53	13.65
25.52	13.78
25.53	13.96
25.52	13.53
25.54	13.72

Section 8.4 without expulsion data

heat	strength
19.00	12.32
18.99	12.26
19.01	12.48
19.00	12.56
18.99	12.23
22.60	12.78
22.61	12.95
22.60	12.85
22.59	13
22.59	12.66
22.27	13.5
22.28	13.62
22.26	13.42
22.25	13.46
22.26	13.68
25.53	13.65
25.53	13.78
25.52	13.96
25.53	13.53
25.52	13.72
25.54	13.72

Heat generation and weld strengths raw data for experiments in chapter 6

Section 6.3.2

heat	strength
1.00	2.35
2.00	3.41
2.59	5.05
4.10	6.68
1.00	2.42
2.01	3.62
2.59	5.14
4.11	6.53
0.99	2.58
2.01	3.69
2.59	5.23
4.10	6.75
0.99	2.59
2.01	3.72
2.59	5.29
4.10	6.84
1.00	2.38
2.01	3.38
2.60	5.1
4.11	6.44
1.01	2.62
2.01	3.29
2.59	5.01
4.11	6.92
1.00	2.38
2.01	3.66
2.59	5.19
4.10	6.8
1.00	2.54

2.01	3.45
2.59	5.24
4.09	6.46
0.99	2.55
2.01	3.44
2.59	4.96
4.10	6.74
1.00	2.46
2.00	3.5
2.59	5.02
4.10	6.62

Section 6.3.3 with expulsion data

heat	strength
1.86	3.22
2.51	5.01
3.95	4.35
1.85	3.1
2.51	4.78
3.95	4.48
1.84	3.25
2.50	4.58
3.95	5.01
1.87	3.36
2.51	5.12
3.96	5.12
1.85	3.15
2.51	5.23
3.96	4.26
1.86	3.15
2.50	4.68
3.96	4.89
1.86	3.25
2.51	4.99
3.95	5.12
1.85	3.31
2.51	5.14
3.95	4.78
1.84	3.28
2.50	5.23
3.95	4.82
1.85	3.14
2.50	5.34
3.95	5.06

Section 6.3.3 without expulsion data

heat	strength
1.86	3.22
2.50	5.01
1.85	3.1
2.50	4.78
1.86	3.25
2.51	4.58
1.86	3.36
2.51	5.12
1.85	3.15
2.51	5.23
1.84	3.15
2.50	4.68
1.87	3.25
2.51	4.99
1.85	3.31
2.51	5.14
1.86	3.28
2.50	5.23
1.85	3.14
2.50	5.34

Section 6.3.4

heat	strength
2.53	4.21
2.08	2.85
1.86	2.05
2.52	4.29
2.07	2.62
1.85	1.89
2.52	4.12
2.07	2.98
1.86	1.95
2.52	4.32
2.08	3.2
1.87	2.2
2.53	4.05

2.08	2.94
1.85	2.25
2.52	4.17
2.08	2.54
1.84	1.68
2.52	4.25
2.07	2.89
1.87	2.12
2.53	4.35
2.07	3.1
1.86	2.24
2.53	4.4
2.07	2.78
1.85	2.1
2.53	4.1
2.08	2.85
1.84	2.25